UNIVERSITY OF CALIFORNIA SAN DIEGO

SAN DIEGO STATE UNIVERSITY

The role of iron in potential algal-bacterial mutualism as related to harmful algae blooms

A dissertation submitted in partial satisfaction of

the requirements for the degree Doctor of Philosophy

in

Chemistry

by

Kyoko Yarimizu

Committee in charge:

University of California, San Diego

Professor John E. Crowell
Professor Ulrich Friedrich Muller

San Diego State University

Professor Carl J. Carrano, Chair
Professor Matthew Edwards
Professor Tom Huxford

2018

The Dissertation of Kyoko Yarimizu is approved, and it is acceptable in quality and form for publication on microfilm and electronically:

_____

_____

_____

_____

_____
Chair

University of California San Diego

San Diego State University

2018

DEDICATION

To my husband

TABLE OF CONTENTS

LIST OF FIGURES

LIST OF TABLES

ACKNOWLEDGEMENTS

First of all, I would like to thank my research advisor Professor Carl Carrano and my thesis committee Professor John Crowell (UCSD), Matthew Edwards (SDSU), Tom Huxford (SDSU) and Ulrich Muller (UCSD) for guiding me through this long journey. Their questions were always challenging yet made me think about what I could do to improve my research.

I would also like to show my deep appreciation to Avery Tatters (USC) for providing me with the *L. polyedrum* strain as well as for helping me set up the algae culture lab. It was one of the most frustrating times for me when I could not keep the cultures alive and in turn, my research could not progress. Without his help, I would not have obtained the *in vitro* data I present in this thesis today.

My research opportunity in CICESE Ensenada, Mexico was one of the most fascinating experiences. With their help, I was able to join in the sample collection during harmful algae blooms as well as processing the interesting data. Beyond science, I have also built many friendships and was able to learn their culture through this collaboration opportunity. Ricardo Cruz-López, thank you so much for working with me throughout my career. I also thank Professor Ernesto García-Mendoza and Helmut Maske for giving me the opportunity to work with them.

From SDSU, I thank Professor Matthew Edwards for helping me and guiding me in how to perform statistical analysis. Professor Steve Barlow for teaching me microscope techniques, Professor Aileen Knowles who was my Master's degree research advisor and has been a life time

coach, Jerry Chiang who is a great friend and gave me a lot of advice on my research, and finally all the Carrano Lab members for being supportive of me.

From Scripps Institute of Oceanography, I thank Melissa Carter and Kristi Speech for collaborating with me to collect monthly sampling from Scripps pier. I thank Professor Katharine Barbeau for giving me advice on iron chemistry and providing us Pacific Ocean samples and Oligotrophic water.

Without funding agencies' supports, I would not have been able to generate all the data I am presenting here. I acknowledge NOAA CSCOR and SDSU Graduate Student Travel Funds for providing me multiple scholarships to attend domestic and international conferences on Harmful Algae. I acknowledge Baja Aqua Farms for supporting me to join the research cruise in Mexico.

Lastly, I cannot say thank you enough to my friends and family members for always believing in me and encouraging me even when I doubted myself. Lastly, a special thanks to my husband, Neal Andrew Holland, who has always been supportive of my career. Without his understanding and support, I could not have done this and would not be here today.

Chapters 3 is in part reprints of the materials published in paper: Yarimizu, K., Polido, G., Gardes, A., Carter, M. L., Hilbern, M., & Carrano, C. J. (2014). Evaluation of photo-reactive siderophore producing bacteria before, during and after a bloom of the dinoflagellate *Lingulodinium polyedrum*. *Metallomics, 6,* 1156-1163.

Chapters 4 is in part reprints of the materials published in paper: Yarimizu, K., Cruz-López, R., Auerbach, H., Heimann, L., Schünemann, V., & Carrano, C. J. (2017). Iron uptake and storage in the HAB dinoflagellate *Lingulodinium polyedrum*. *Biometals, 30,* 945-953.

Chapter 5, in part, has been submitted for publication of the material as it may appear in Frontier, 2018, Yarimizu, K., Cruz-López, and Carrano, C. J. The dissertation author was the primary investigator and author of this paper.

VITA

Education

2018	Doctor of Philosophy in Chemistry, University of California San Diego and San Diego State University
2004	Master of Science in Chemistry, San Diego State University
1996	Bachelor of Science in Chemistry, Ouachita Baptist University

Awards

2017	National Oceanic and Atmospheric Administration Center for Sponsored Coastal Ocean Research (NOAA/CSCOR) scholarship
2017	San Diego State University Graduate Student Travel Fund
2016	International Society for the Study of Harmful Algae (ISSHA) scholarship sponsored by National Oceanic and Atmospheric Administration (NOAA)
2016	San Diego State University Graduate Student Travel Fund
2015	National Oceanic and Atmospheric Administration Center for Sponsored Coastal Ocean Research (NOAA/CSCOR) scholarship
2004	Phi Beta Delta Scholarship, Phi Beta Delta honored student
1995	Ouachita Baptist University student scholarship

Publications

- Yarimizu, K., Cruz-López, R., & Carrano, C. J. (submitted 2018). Iron and Harmful Algae Blooms: Potential Algal-Bacterial Mutualism between *Lingulodinium polyedrum* and *Marinobacter algicola*. *Frontier*.

- Yarimizu, K., Cruz-López, R., Auerbach, H., Heimann, L., Schűnemann, V., & Carrano, C. J. (2017). Iron uptake and storage in the HAB dinoflagellate *Lingulodinium polyedrum*. *Biometals, 30*, 945-953.

- Yarimizu, K., Polido, G., Gardes, A., Carter, M. L., Hilbern, M., & Carrano, C. J. (2014). Evaluation of photo-reactive siderophore producing bacteria before, during and after a bloom of the dinoflagellate *Lingulodinium polyedrum*. *Metallomics, 6,* 1156-1163.

- Javed, R., Yarimizu, K., Pelletier, N., Li, C., and Knowles, A.F. (2007). "Mutagenesis of lysine 62, asparagine 64, and conserved region 1 reduces the activity of human ecto-ATPase (NTPDase 2)." Biochemistry 46: 6617-6627.

Presentation

- Yarimizu, K., et al. (2017) "The role of iron in potential HAB algal-bacterial mutualisms", presented at 9th Symposium on Harmful Algae in the U.S., Baltimore MD, November 11th - 17th 2017.
- Yarimizu, K., et al. (2016) "The role of iron in potential HAB algal-bacterial mutualisms", presented at 17th International Conference on Harmful Algae, Florianopolis Brazil, October 9th -14th 2016.

Posters

- Yarimizu, K., et al. (2015) "The role of iron in algal-bacterial interactions as related to harmful algae blooms", poster presented at 8th Symposium on Harmful Algae in the U.S., Long Beach, November 15th - 19th, 2015.
- Yarimizu, K., et al. (2012) "Detection of photoreactive siderophore biosynthetic genes in the marine environment", poster presented at American Chemical Society, San Diego, March 25th – 29th, 2012.
- Yarimizu, K., et al. (2004) "Enzyme structure and function II" poster presented at IUBMB/ASBMB, Boston, MA, June 12th – 16th, 2004.

ABSTRACT OF THE DISSERTATION

The role of iron in potential algal-bacterial mutualisms as related to harmful algae blooms

by

Kyoko Yarimizu

Doctor of Philosophy in Chemistry

University of California San Diego, 2018
San Diego State University, 2018

Professor Carl J. Carrano, Chair

Phytoplankton blooms can cause acute effects on marine ecosystems either due to their production of endogenous toxins or due to their enormous biomass leading to major impacts on local economies and public health. Despite years of effort, the causes of harmful algal blooms (HAB) are still not fully understood. Our hypothesis is that bacteria that produce photoactive siderophores may provide a bioavailable form of iron to commensally associated phytoplankton, which could in turn affect algal growth and bloom dynamics. Here we report both laboratory-

based studies using binary cultures of the dinoflagellate *Lingulodinium polyedrum*, a major HAB species, with *Marinobacter algicola* DG893, a phytoplankton-associated bacterium that produces the photoactive siderophore vibrioferrin and analysis of field collected data linking seawater iron concentrations, HAB phytoplankton numbers and bacterial populations. Together these results support the notion of a carbon for iron mutualism in some bacterial-algal interactions.

CHAPTER 1. INTRODUCTION

1.1 WHAT ARE HABS?

Phytoplankton are important not only as food source for ultimately all organisms in marine waters but also for their ability to regulate atmospheric CO_2. On the other hand, a few dozen out of the thousands of phytoplankton species, mostly the dinoflagellates, have been found to produce endogenous toxins and therefore to be harmful to the marine environment when the phytoplankton accumulate in sufficient numbers. Such harmful algae blooms (HABs) are frequently observed in the coastal regions of every continent in the world and can directly and indirectly cause acute effects on marine ecosystems, leading to major impacts on local economies and public health. Direct effects caused by HABs, include the killing or sickening of fish, birds and marine mammals upon digestion of toxin producing phytoplankton. Direct human health effects derive from the consumption of shellfish that have ingested toxic phytoplankton. The accumulation of toxin leads to paralysis, diarrhea, and neurotoxic poisoning syndromes that can in some cases be fatal (Anderson 1994; Honner et al., 2012). Indirect impacts of HABs are exemplified by environmental damage caused by hypoxia and anoxia resulting from high biomass accumulation. The consequence is a loss to the tourism and recreation industries. Even blooms of phytoplankton that do not produce toxins can be harmful and cause ecological impacts by the displacement of indigenous species, habitat alteration, or oxygen depletion (Glibert et al., 2005). Major problems are that successful models have not yet been developed to predict

occurrence of these harmful phytoplankton blooms nor have effective means to mitigate their effects emerged.

1.2 HISTORY OF HABS

Some HAB scientists believe that the oldest written record of a HAB was around 1000 years BC, as described in the Bible (Exodus 7:20-21): “the water turned to blood, the fish that were in the water died, and the Egyptians could not drink the water”. Scientists interpret this as a depiction of a dense algal bloom, which produced anoxic conditions and resulted in the indiscriminate killing of both fish and invertebrates (Hallegraeff, 1993). The oldest recorded case of a human fatality caused by a HAB occurred in Poison Cove British Columbia in 1793 when Captain George Vancouver and his crew ate local shellfish, resulting in one death, now known to have been caused by paralytic shellfish poisoning (PSP) (Hallegraeff, 1993). The second oldest recorded human death caused by a HAB appeared in Alaska in 1799 when Alexander Baranof, a Russian fur trader, became ill after eating blue mussels. The event eventually resulted in roughly 100 deaths (Fortuine, 1975). The first recorded HAB incident in California occurred in Sonoma County in 1903 when 12 people became ill and five died after eating California mussels (Lewitus et al., 2012). HABs have been reported worldwide thereafter (Table 1). For example, three consecutive HAB events occurred in 1987 in North America (Anderson, 1994). A bloom in Cape Cod Bay Massachusetts resulted in the death of fourteen humpback whales, one on the North Carolina coast resulted in several people suffering from respiratory problems, eye irritation, diarrhea, and dizziness after eating local shellfish, and one on Prince Edward Island, Canada, caused three deaths and over a hundred patients to suffer from disorientation, vomiting, diarrhea, abdominal cramps, and short-term memory loss after eating local mussels. In California in 1991, the commercial fisheries in Northern California coast were shut down for several weeks due to a

high level of domoic acid detected in Dungeness crabs. It was also recorded that dozens of people experienced gastrointestinal pains and mild neurological symptoms after razor clam consumption. Dead pelicans found during this HAB were dissected, and their guts were found to be packed with anchovies full of toxic diatoms (Horner and Postel, 1993). In California in 2009, a 53 year old woman was taken to an emergency room with bilateral otitis externa and mastoiditis after scuba diving during a HAB (Honner et al., 2012). Table 1 summarizes reported HAB events associated with fatalities in Middle to North Pacific coast. These are just a few examples of HAB events. The unfortunate news is that every coast of every continent is now frequently experiencing HABs.

In recent decades the world's coastal waters are experiencing increased numbers of HABs with continually discovered new HAB species. For example, 22 species of toxic dinoflagellates were recognized in 1984, but this number has been increased to 59 a decade later (Steidinger and Baden, 1984: Burkholder, 1998). Figure 1 compares the reported number of paralytic shellfish poisonings, one of the major results of HABs, in 1970 and 2000. It is apparent that frequency of HAB event is increasing over time.

Table 1 Reported human illness and death by PSPs in Middle to North Pacific coast

Year	Cases	Deaths	Area	Shellfish
Alaska				
1799	150	100	Sitka, Peril Strait	Blue mussels
1934	12	2	Douglas and Admiralty Islands	NR
1944	4	1	Likely Sitka	NR
1947	3	1	Peril Strait	Butter clams
1954	8	1	False Pass	Blue mussels
1962	27	1	Porpoise Island	Littleneck clams
1962	1	1	Hawk Inlet	Blue mussels
1962	1	1	Shelter Bay	Butter clams
1965	4	1	Hawk Inlet	Butter clams
1994	16	1	Kalsin Bay, Kodiak	Blue mussels
1997	9	1	Sturgeon River, Kodiak	Blue mussels, littleneck clams
1999	NR	1	Kodiak	NR
2010	5	2	Juneau and Haines	Cockles, Dungeness, Crab viscera
British Columbia				
1793	4	1	Poison Cove	Mussels, clams
1942	3	3	Barkley Sound	Mussels, clams
1965	4	1	Theodosia Inlet	Cockles
1980	7	1	Health Harbor, Gilford Island	Butter clams
Washington				
1942	9	3	Sekiu, Strait of Juan de Fuca	Mussels, clams
Oregon				
1933	21	1	NR	NR
California				
1903	12	5	Sonoma County	California mussels
1927	103	6	Sonoma, Marin, San Mateo	Mussels
1929	60	4	Sonoma, Marin, San Mateo	Mussels, clams
1936	3	2	Ventura	Mussels
1939	76	8	Santa Cruz, Monterey	Mussels, clams
1943	20	4	Del Norte, Humboldt	Mussels
1944	12	2	San Mateo, Santa Cruz	Mussels
1946	3	1	San Mateo	Mussels
1948	3	1	San Mateo	Mussels
1980	98	2	Sonoma, Marin	Mussels, oysters, scallops

Table 1 continued

Year	Cases	Deaths	Area	Shellfish
Mexico				
1976	7	2	Pacific Mexico	NR
1979	18	3	Mazatlan Bay, extensive fish kill	Oysters, clams
1989	99	3	Gulf of Tehuantepec	Rocky oysters
2001	600	6	Michoacan and Guerrero coasts	NR
2001	101	6	Chiapas, Guerrero coasts	NR

The table was adopted from Lewitus et al. (2012). These are reported human illnesses resulting in death due to paralytic shellfish poisoning (PSP) caused by HAB species in Middle to North Pacific coast of America.

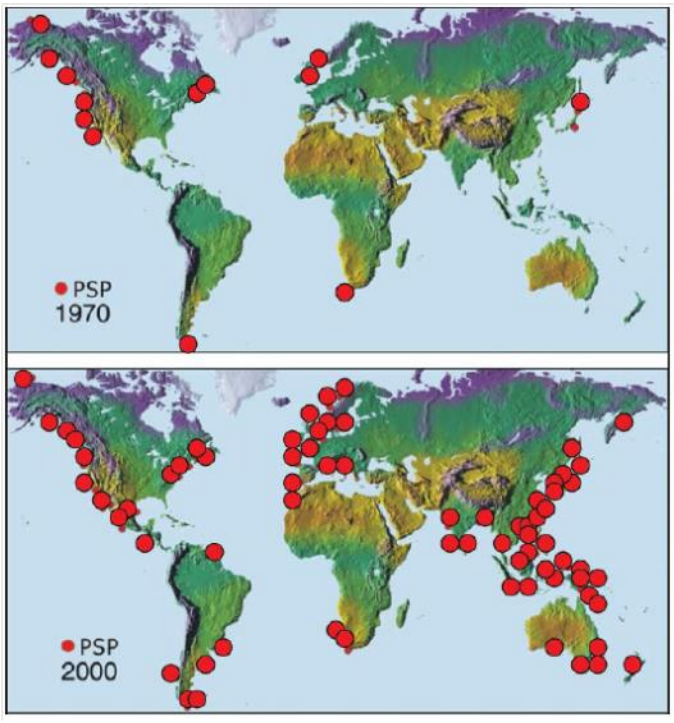

Figure 1 Frequency of Paralytic Shellfish Poisoning caused by HABs in 1970 and 2000
The figure was adopted from GEOHAB (2001) and modified by Glibert (2005). Paralytic shellfish poisoning (PSP) can cause diarrhea, nausea, vomiting, and respiratory paralysis when humans consume shellfish which have been contaminated with HAB species. The reported PSPs are increasing over time.

1.3 WHAT ARE THE CAUSES OF HABS?

Improved tools as well as advanced information technologies to monitor HABs are definitely leading to increased detection of HAB species. However, it seems equally clear that the actual number of such events is also increasing. Whether the factors promoting HABs come from anthropogenic or natural sources is an ongoing debate. Many HAB scientists support natural cause as the dominant factor in increasing HAB's. Roegner et al. (2002) and Tweddle et al. (2010) suggested that oceanographic events such as upwelling, reversal and relaxation of winds, and global climate change may be the major factors initiating phytoplankton blooms. Glibert (2005) suggested that global warming may be the most important factor in increased HABs as climate ultimately controls optimal water condition for algal growth by regulating water temperature, nutrients, and light conditions. Epstein et al. (1993) reported that blooms of optimally warm water species coincided with El Niño events, indicating that global climate change may encourage growth of HAB species. Langlois and Smith (2000) observed that blooms often started offshore and moved to onshore when upwelling winds relax in the dry season. Tweddle et al. (2010) also reported their observation that winds creating upwelling were a factor promoting blooms on the coast of Oregon and that elevated toxin levels were associated with late summer upwelling. On the other hand, some HAB scientists oppose the idea of linking bloom events with climate change, specifically El Niño and La Niña, due to lack of hard evidence: Langlois (2001) questioned the correlation between HABs and ENSO events after monitoring two major HABs on the California coast during a La Niña in 1989 and an El Niño in 1994. Kim et al. (2009) also found no correction between HABs and climate after monitoring chlorophyll mass at Scripps pier during multiple El Niño periods occurring between 1982 and 2000. They observed that only two of the many phenomena, La Niña in 1997 and El Niño in 1998, coincided

with chlorophyll volume. On the other hand there is a sizeable contingent of scientists believing that HABs are mostly a result of human activities. Glibert (2005) suggested that increased nutrient loading, changes in agriculture and aquaculture practices, and overfishing to be the causes of HABs. Since the beginning of the industrial age increased usage of synthetic fertilizers has resulted in an export of phosphorus and nitrate to the coastal zone that has increased more than three-fold (Smil, 2001). Population growth and increased food production also result in an increase in sewage and runoff (Glibert, 2005). Smayda (1998) showed data supporting that increased anthropogenic nutrient loadings were proportional to water column loadings. Hallegraeff (1993) proposed the following four potential explanations for the apparent increase in HABs.

- Increased scientific awareness of toxic species
- Overfishing and an increased utilization of coastal waters for aquaculture
- Eutrophication caused by industrial and agriculture wastes and unusual climatological conditions,
- Transport of dinoflagellate resting cysts in ships' ballast water associated with the movement of shellfish stocks from one area to another

As can be seen, the cause of HABs is not related to a single factor but most likely a combination of many factors originating from both human activity and natural events. The issue is that a model to predict HABs cannot be established until the causes of HABs are well understood.

1.4 TOXINS AND SYMPTOMS

Currently, the toxins produced by HAB species, mostly dinoflagellates, are categorized into five major groups and three additional minor groups (Table 2 and Figure 2). Phytoplankton from the same family may morphologically look alike but their genetic information may differ

through environmental selection favoring one genotype over others (Glibert, 2005). As a result, the toxins produced by phytoplankton from the same family are usually a group of compounds having similar chemical structures and effects. In general, the mechanism of most toxins secreted by symptom-causing HAB species is disruption of electrical conduction between nerve and muscle by toxins bound to the specific membrane receptors. Little is known about the reason that phytoplankton to produce toxins. Some believe that phytoplankton evolved toxin production to defend themselves against predators, i.e. zooplankton, and other grazers, as suggested by observations that predators either swam away from toxin producing phytoplankton, spit out the unpleasant tasting toxic algae, or were gradually paralyzed upon consuming the toxic algae (Anderson, 1994). However, non-toxin producing phytoplankton also form blooms and therefore it is unlikely that toxins serve solely as self-defense (Anderson, 1994).

1.4.1 Amnesic Shellfish Poisoning (ASP)

ASP is caused by the toxin known as domoic acid which is toxin produced by certain marine organisms such as the red alga *Chondria armata* and the diatom *Pseudo-nitzschia* and first reported in 1987 in Prince Edward Island, Canada. The symptoms of illness include nausea, vomiting, abdominal cramps, diarrhea, headache, unstable blood pressure, cardiac arrhythmias and neurological dysfunction, including coma, seizures and memory loss (Pulido, 2008).

1.4.2 Ciguatera Fish Poisoning (CFP)

CFPs are toxins commonly found in coral reef finfish such as barracuda, grouper, and snapper contaminated with toxin producing dinoflagellates and is the most lethal of all currently known toxins produced by phytoplankton. The symptoms are reportedly varied in different oceans and include gastrointestinal, neurological, cardiovascular and other symptoms (Terao, 2000; Lewis et al., 2000). CFP was originally identified in *Gambierdiscus toxicus*, a maitotoxin

producing dinoflagellate. Later, maitotoxins were found to be lipophilic precursors of ciguatoxins produced by herbivorous fish and invertebrates (Yasumoto et al., 1977; Legrand, 1999). Therefore, ciguatoxin and maitotoxin are the two most common toxins associated with CFP. In mice, ciguatoxin and maitotoxin are lethal at 0.45 μg/kg and 0.15 μg/kg intraperitoneally, respectively (Wang, 2008). In adult humans, oral intake of as little as 0.1 μg ciguatoxin can cause illness. Overall CFPs are heat-stable, lipid-soluble, highly oxygenated, and structurally similar to brevetoxins but with higher toxicity (Scheuer et al., 1967; Tachibana et al, 1987; Murata et al., 1990; Lewis et al., 1998).

1.4.3 Diarrhetic Shellfish Poisoning (DSP)

DSP is caused by the toxin known as Okadaic acid which was first isolated from the Japanese marine sponge *Halichondria okadai* in 1976 (Yasumoto et al., 1978). More than 1300 DSP cases were reported in the following five years in the region. Okadaic acid production has now been detected from several marine dinoflagellate genera including *Prorocentrum* and *Dinophysis*. The toxins are lipophilic and heat-stable polyether compounds and cause diarrhea, gastrointestinal distress, nausea, vomiting and, frequently, abdominal pain. These symptoms usually appear from 30 minutes to 12 hours after ingestion of contaminated seafood. However, no deaths related to DSP intoxication have been reported thus far (Yasumoto et al., 1978; Dominguez et al., 2009). Okadaic acid is a specific inhibitor of serine and threonine protein phosphatases 1 and 2A. The reported mouse LD50 by intraperitoneal injection of okadaic acid is somewhere around 200 μg/kg (Takai et al., 1987; Tubaro et al., 2008).

1.4.4 Neurotoxic Shellfish Poisoning (NSP)

NSP is caused by the neurotoxins known as brevetoxins, first isolated from the dinoflagellate *Kerenia brevis* and more recently from other dinoflagellates i.e. *Chatonella*

marina, C. antiqua, Fibrocapsa japonica, and *Heterosigma akashiwo* (Khan et al., 1997; Hallegraeff, et al., 1998). Brevetoxins are tasteless, odorless, and heat and acid resistant. NSPs present symptoms similar to but milder than the symptoms of PSPs and include gastroenteritis and nausea, as well as the neurological conditions of perioral numbness, loss of motor control, and severe muscular pain (Morris et al., 1991; Baden and Adams, 2000). The mouse LD50 is 170 μg/kg body weight intraperitoneally, 94 μg/kg body weight intravenously, and 520 μg/kg body weight orally (Kirkpatrick, et al, 2004). Brevetoxins are depolarizing substances that open voltage gated sodium ion channels in cell walls, leading to uncontrolled sodium influx into the cell (Wang, 2008).

1.4.5 Paralytic Shellfish Poisoning (PSP)

Saxitoxin, one of the most toxic and well studied PSP toxins, can be divided into three subcategories: carbamate compounds, N-sulfocarbamoyl compounds, and decarbamoyl compounds. The three major dinoflagellate genera known to produce PSP toxins are *Alexandrium, Gymnodinium, and Pyrodinium* (Shumway, 1990). Symptoms of PSP include tickling sensations of the lips, mouth and tongue, numbness of the extremities, gastrointestinal problems, difficulty in breathing, and a sense of dissociation followed by complete paralysis, respiratory arrest, and cardiovascular shock or death (Halsetead, 1988). The PSP toxins are heat-stable and water-soluble nonproteinaceous neurotoxins that specifically and selectively bind the sodium channels on excitable cells and block flux of sodium in and out of nerve and muscle cells (Wang, 2008). The mouse LD50 of saxitoxin is 3-10 μg/kg body weight by peritoneal and 263 μg/kg body weight orally (Wang, 2008). The highest level of toxin seen (20,600 mg/100 g shellfish meat!), was obtained from blue mussels harvested from Kalsin Bay, Alaska in May

1994, which was far above the regulatory limit of 80 mg/100 g shellfish meat (Lewitus et al., 2012).

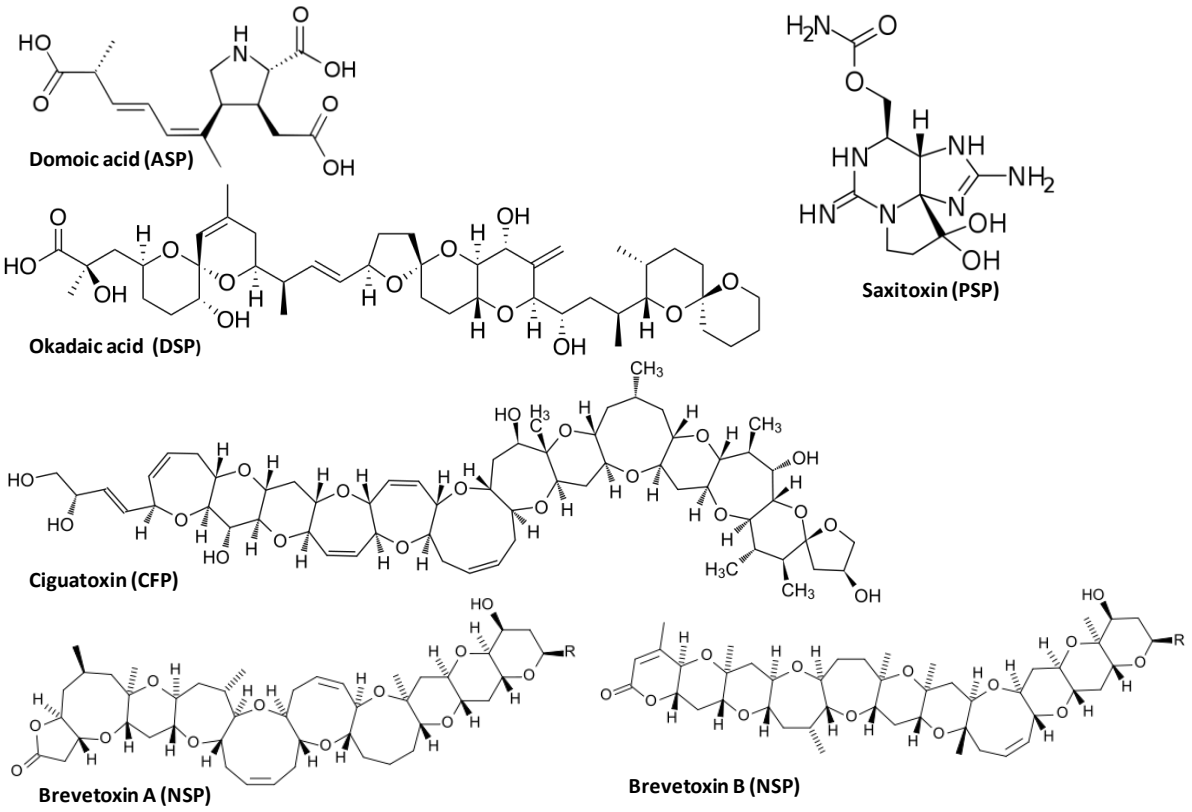

Figure 2 Examples of toxins produced by phytoplankton
The structural example of DSP (Okadaic acid), CFP (Ciguatoxin), ASP (Domoic acid), PSP (Saxitoxin), and NSP (Brevetoxin).

Table 2 Five major and three minor classes of toxins produced by HAB species

Acronym	Type	Major toxins	Human Symptom	Major species
ASP	Amnesic Shellfish Poisoning	domoic acid	nausea, vomiting abdominal cramps diarrhea cardiac arrhythmias neurological dysfunction coma & seizures memory loss	*Chondria armata* *Pseudo-nitzschia*
CFP	Ciguatera Fish Poisoning	ciguatoxins maitotoxins	gastrointestinal neurological cardiovascular other symptoms	*G. toxicus* *P. lima* *P. concavum* *P. hoffmannianum* *O. lenticularis* *O. siamensis*
DSP	Diarrhetic Shellfish Poisoning	okadaic acid	diarrhea gastrointestinal distress nausea & vomiting abdominal pain	Halichondria okadai Prorocentrum spp Dinophysis spp
NSP	Neurotoxic Shellfish Poisoning	brevetoxins	gastroenteritis nausea numbness of perioral area loss of motor control severe muscular pain	*K. brevis* *C. marina* *C.antiqua* *F. japonica* *H. akashiwo*
PSP	Paralytic Shellfish Poisoning	Saxitoxin: • carbamate • decarbamoyl • sulfocarbamyl	numbness of the extremities gastrointestinal breathing issue paralysis respiratory arrest cardiovascular shock death	*Alexandrium* *Gymnodinium* *Pyrodinium*
YTX	Yessotoxin	yessotoxin	not recorded	*P. reticulatum* *L. polyedrum* *G. spinifera*
AZP	Azaspiracid Shellfish Poisoning	azaspiracid	nausea, vomiting, diarrhea, stomach cramps, neurotoxic	*P. crassipes*
PTX	Palytoxin	palytoxin	fever, ataxia drowsiness, weakness of limbs death	*P. toxica* *O. siamensis*

1.5 ECONOMIC IMPACTS CAUSED BY HABS

HABs not only result in severe environmental damages but also economic damages. The current strategy to eliminate further impact on human health caused by HABs is to shut down the affected coastal area during a bloom. This leads to significant layoffs of employees associated with fisheries and tourism: In 1972 in Japan, a bloom of *Chattonella antique* killed 500 million U.S. dollars' worth of caged yellowtail fish in the Seto Island Sea (Okaichi, 1989). While wild fish stocks have the freedom to swim away from problem areas, caged fish appear to be vulnerable to HAB events (Hallegraeff, 1993). In 1991 in Washington and Oregon, the commercial and recreational fisheries were shut down for eight months due to high levels of domoic acid detected in razor clams, which translated into a 20 million U.S. dollars loss (Horner and Postel 1993). In Texas in 2003, a bloom of *Prymnesium parvum* from inland rivers and reservoirs restricted sport fishing and tourism resulting in an estimated 6 million U.S. dollars loss in revenue (Glibert, 2005). Hoagland and Scatasta (2006) evaluated the economic damage caused by HABs in the U.S. per year at 82 million U.S. dollars, which includes four categories: public health, commercial fisheries, recreation and tourism, and monitoring and management. Jin et al. (2008) compared annual landings of soft shell clams, blue mussels, and oysters in New England over the period between 1990 and 2005 and estimated an 18 million U.S. dollar decline in fishery during a 2005 HAB. A one year long closure of the Washington coast due to *Pseudo-nitzschia* blooms caused an estimated loss of 11.36 million U.S. dollars in coastal county incomes due to reduced recreational activity and a 2 million U.S. dollar reduction in incomes due to restricted razor clam harvesting (Dyson and Huppert, 2010). In summary, both economic impact and environmental damage caused by HABs are equally serious and significant.

Since the causes of HABs are not fully understood, models have not yet been established to aid in avoiding HAB damages. Therefore, the current strategy is to reduce their potential damage relies on frequent coastal monitoring and early detection of HAB species and toxin levels. The following are some of the main programs established to facilitate regional ecosystem assessment and management.

U.S. programs:

- ECOHAB (Ecology and Oceanography of Harmful Algal Blooms)
- MERHAB (Monitoring and Event Response of Harmful Algal Blooms)
- PCMHAB (Prevention, Control, and Mitigation)
- Pew Oceans Commission
- U.S. Commission on Ocean Policy
- U.S. Symposium on Harmful Algae
- West Coast Governors' Agreement on Ocean Health (WCGA)

International programs:

- ECOHAB (Ecology and Oceanography of Harmful Algal Blooms)
- EUROHAB (European Harmful Algal Blooms)
- GEOHAB (Global Ecology and Oceanography of Harmful Algal Blooms)
- IOC-UNESCO (Intergovernmental Oceanographic Commission-UNESCO)
- International Conference on Harmful Algae (ICHA)

1.6 HABS IN SAN DIEGO

The coastal water in the Southern California Bight (Santa Barbara to San Diego) has been monitored since the first recorded HAB in the region in 1902 (Torrey, 1902). For Scripps Pier in San Diego (N32°86', W117°25'), twice a week surface chlorophyll monitoring was established

in 1983 and continues today (except between 2000 and 2005) to better understand the link between physical changes in water conditions and biological responses. Historically, HABs have been less frequent in San Diego than in the central and northern parts of California (Price et al., 1991). Six HABs in Southern California were reported in a 30-year monitoring period between 1918 and 1948 (Allen, 1938, 1941), and relatively high chlorophyll concentration was reported at Scripps Pier during El Niño's in 1995 and 1997 as well as a La Niña in 1998. PSP toxin levels exceeded federal alert thresholds in San Diego in 1985, 2006, and 2008 (Lewitus et al., 2012). Kim et al. (2009) summarized two trends from their 18-year monitoring of the pier, 1) chlorophyll concentration at the pier exhibited higher values in more recent years, following the world trend, and 2) compared to other coastal areas, the San Diego coast experiences lower occurrences of HABs likely due to its unique geography. Thus higher chlorophyll concentrations generally coincide with geographic locations associated with shallower depths and strong upwelling winds, while Scripps Pier is located on an inner shelf experiencing weaker upwelling, more favorable winds (Winant and Dorman, 1997; Legaard and Thomas, 2006; Lentz et al., 2008). However HABs at Scripps Pier are still increasing over time and more toxins have been detected in commercial shellfish in recent years although the frequency is still lower than that seen in other coastal areas like Florida which are affected by brevetoxin toxins nearly every year.

1.7 LINGULODINIUM POLYEDRUM AND YESSOTOXIN

L. polyedrum is one of the most common dinoflagellate blooming species at Scripps Pier in San Diego. It is a thecate dinoflagellate belonging to the family *Gonyaulacaceae*. Cells are polyhedral-shaped and range in size from 40-54 μm in length and 37-53 μm in width with double cell walls (Paz et al., 2008). It emits bioluminescence and its life cycle involves vegetative reproduction, temporary cyst formation, and sexual reproduction. It can be found mainly in

temperate and subtropical coastal zones (Lewis and Hallet, 1997). *L. polyedrum* produces yessotoxins (YTXs), a group of polyether toxins which was first isolated in 1986 from the digestive gland of a scallop *Patinopecten yessoensis* during a *L. polyedrum* bloom in Mutsu Bay, Japan (Murata et al., 1987). Since then, worldwide approximately 100 different YTXs and their analogs have been found in other dinoflagellates such as P*rotoceratium reticulatum* and *Gonyaulax spinifera*, and accumulated in mussels (Eiki et al., 2005: Paz et al., 2008). Some YTXs are directly produced by dinoflagellates while others are produced by shellfish metabolism (Paz et al, 2008). Yessotoxin is based on molecular formula $C_{55}H_{82}O_{21}S_2Na_2$, containing a disulfate polyether with 11 adjacent ether rings as in Figure 3; the molecular weight of YTXs ranged between 955 and 1551 mu (Murata et al., 1987; Miles, 2006). The symptoms produced by YTX toxicity in humans are unknown due to the fact that no human intoxication has been reported to this date (Paz et al., 2008). YTXs were also found non-toxic to mice via the oral route but found to be highly toxic via intraperitoneal injection, 100 μg/Kg as a lethal dose (Ogino et al., 1997). YTXs were originally classified as DSPs because they appear and were extracted together with the DSP toxins (Wang, 2008). However, they were later categorized separately since they do not lead to diarrhea nor inhibit protein phosphatases like DSP toxins (Ogino et al., 1997). Although symptoms of YTXs in humans has not been reported, European authorities found YTXs to be potent cytotoxins and established a maximum permitted level in shellfish of 1 mg/kg (EC. Regulation, 2004, L 226, p. 22), several fold higher than other phytoplankton toxins. The precise mechanism of YTXs is for the most part still unknown. Nonetheless, *L. polyedrum* is a toxin producing dinoflagellate and a common bloom species in San Diego. Even though *L. polyedrum* produces only mild toxin, the possibility that it could become acutely harmful under bloom conditions should not be ignored since even non-toxin producing phytoplankton can cause

negative ecological impacts such as the displacement of indigenous species, habitat alteration, or oxygen depletion (Glibert et al., 2005).

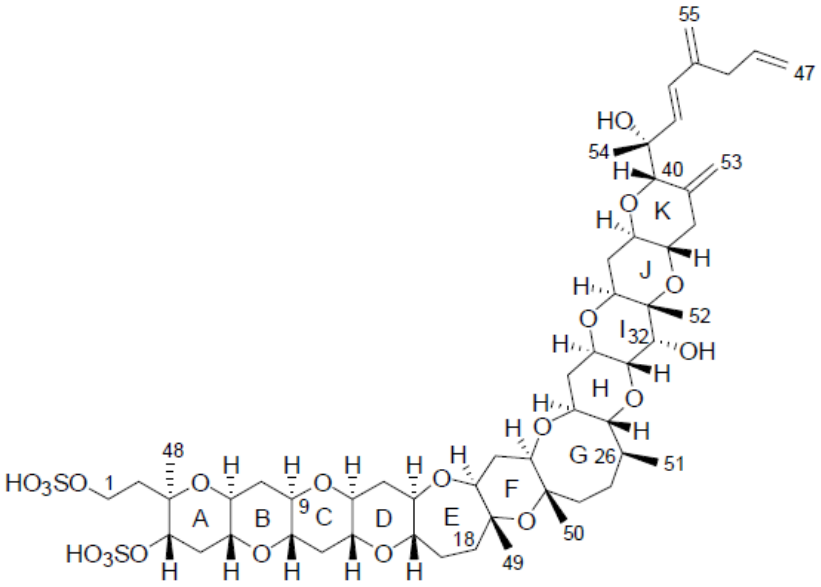

Figure 3 Structure of Yessotoxin
The figure adopted from Paz et al. (2008). Currently, 36 natural derivatives of YTX have been identified and characterized by NMR and liquid chromatography coupled with mass spectrometry (LC-MS).

CHAPTER 2. ALGAL-BACTERIAL MUTUALISM

2.1 PHYTOPLANKTON INTERACTION WITH BACTERIA

While many studies focus on finding the causes of HABs from the perspectives outlined previously, fewer have paid attention to the possible effects that bacterial species that coexist with phytoplankton could contribute to their growth. However, since Bell and Mitchell reported that specific microflora were maintained and microbial activity was altered in the phycosphere (Bell and Mitchell, 1972; Bell and Lang, 1974), an increasing number of studies have suggested that the interactions between phytoplankton and bacteria are in fact very specific and important (Azam and Malfatti, 2007; Amin et al., 2015; Bertrand et al., 2015; Ramanan et al., 2016). It has been postulated that the mutualistic association of some phytoplankton and bacteria is driven by nutrient exchange. While nitrogen and phosphorus are the most often studied nutrients in this regard, the exact interactions involving these nutrients are not well understood (Hallegraeff and Gollasch, 2006). Our hypothesis is that certain bacteria may affect algal growth and bloom dynamics by their control of iron, a trace element known to be growth limiting to phytoplankton in many marine environments (Martin and Fitzwater, 1988; Maldonado et al., 2005; Croot and Heller, 2012).

2.2 IRON IN OCEAN

Iron is an essential element for all living organisms on earth due to its involvement in photosynthesis, respiration, oxidative stress, oxygen storage, and nitrogen fixation. In the ocean,

iron is one of the most important nutrients for phytoplankton and microbes, facilitating their growth through active photosynthesis and respiration processes (Morel et al., 1991; Geider and Laroche, 1994; Wells et al., 1995). The concept that "iron limits phytoplankton growth" has been corroborated by a number of large-scale iron fertilization experiments in High Nitrogen Low Chlorophyll (HNLC) regions, where iron concentration is negligible, and confirmed through shipboard iron enrichment fertilization experiments (Martin and Fitzwater, 1988; Martin et al., 1994; Coale et al., 1996; Boyd et al., 2000). Iron is the fourth most abundant element on the earth. However, its bioavailability in the marine environment is extremely low due to its poor solubility under the mildly alkaline aerobic conditions present in the ocean (Martin and Fitzwater, 1988; Wu and Luther III, 1994). Iron exists on earth in two redox species, Fe(II) and Fe(III), but in the ocean insoluble Fe(III) is the predominant species, forming minerals such as hematite, goethite, pyrite, and oxyhydroxides (Martin and Fitzwater, 1988; Wu and Luther III, 1994; Bruland et al., 1991). In terms of iron concentrations and distributions in ocean, electrochemical methods have been intensively studied for the last decades and it is now known that iron is present in oceans at nanomolar levels (Bruland et al., 1991). In vertical water columns, iron is continuously increased with water depth as exemplified in Figure 3 and Figure 4. The very low iron concentration in surface water is said to be due to primary production in the photic zone (Vraspir and Butler, 2009). A recent study subdivided iron into five fractions or phases of iron: soluble (<0.03 μm), dissolved (<0.22μm), total dissolved (acidified and dissolved <0.22μm), labile (unfiltered), and total (all = acidified, unfiltered) (Wong et al. 2006). The "dissolved iron" was reported as 0.2 to 0.4 nM in the mixed layer in the ocean south of Tasmania, Australia. For horizontal comparison across the surface ocean water, "total iron concentration" offshore in California Current North Pacific was reported to be 0.3 nM while that

on the coast was 100 nM (Martin and Gordon, 1988). In the Atlantic, "total iron concentration" of offshore was reported at a mean of 3 nM while that on the coast was 300 nM (Symes and Kester, 1985).

Additionally, over 99% of soluble iron species in the ocean are complexed with natural organic ligands classified as L1 and L2, which leave a negligible amount of free iron in the ocean (Gledhill and van den Berg, 1994; Rue and Bruland, 1995; van den Berg, 1995). L1 are defined as stronger ligands exemplified by microbial driven siderophores, and L2 are weaker ligands such as cellular products of biogenic particle decomposition (Rue and Bruland, 1997; Macrellis et al., 2001; Hunter and Boyd, 2007). L1 tends to be observed in the upper water column within the top 200 m with constant concentration, whereas L2 is found abundantly in deeper water (Rue and Bruland, 1995, 1997). It has been suggested that a reason for L1 dominating surface to shallow water is that the L1 complexes such as Fe(III)-siderophore may be vulnerable to photochemical degradation (Boye et al., 2001; Barbeau et al., 2003). In fact, photo-reactive marine siderophores such as vibrioferrin have been identified predominantly in surface seawater (Yarimizu et al., 2014).

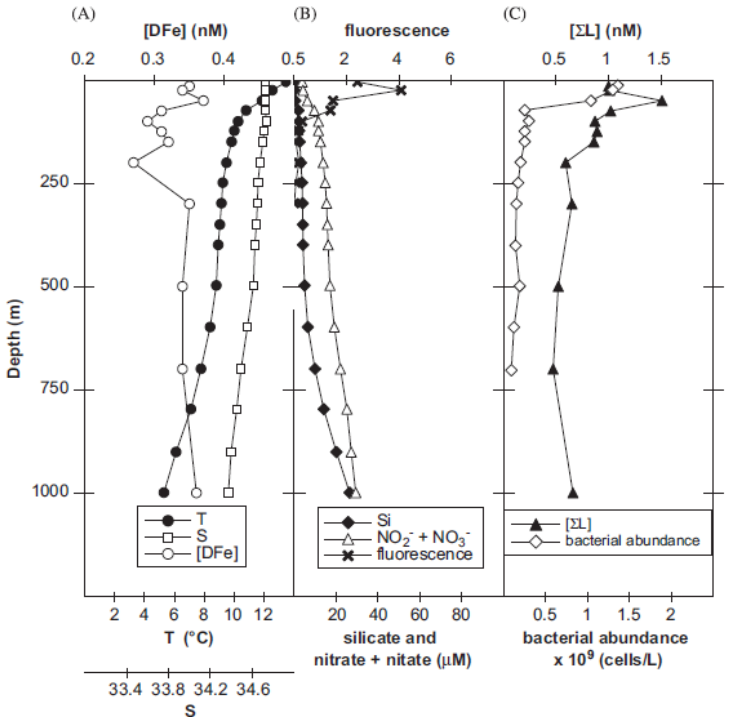

Figure 4 Example of oceanic concentration of fluorescence, nutrients, and bacteria
Figure adopted from Ibisanmi, E., et al. (2011). (A) Iron, temperature, and salinity distributions (B) Nitrate, silicate, and fluorescence distributions (C) Bacterial abundance and vertical distributions of overall iron-complexing ligands.

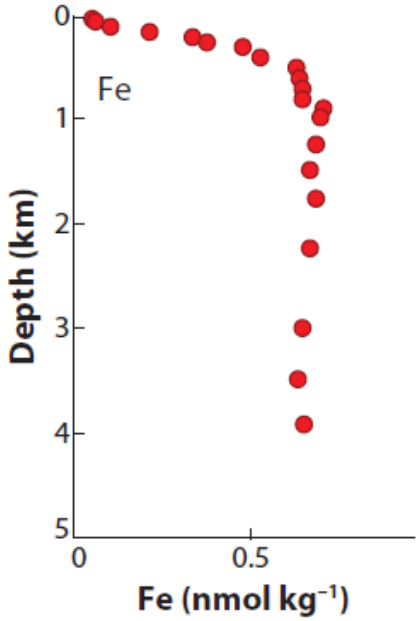

Figure 5 Example of Oceanic iron concentration
Figure adopted from Martin et al. (1989) and modified by Vraspir and Butler (2009).

2.3 IRON ACQUISITION BY BACTERIA

Because of its low bioavailability iron acquisition by both marine bacteria and phytoplankton is a challenge. Many bacteria, however, have evolved sophisticated iron uptake systems based on excreting low molecular weight Fe(III) specific chelating agents known as siderophores. The resulting iron-siderophore complexes are recognized and taken up by specific cell surface receptors. In general, many bacteria produce siderophores during periods of iron starvation, at extracellular iron concentrations below 10^{-6} M (Miethke and Marahiel, 2007).

2.3.1 Siderophores

Since discovery of the siderophore mycobactin in 1949 by Francis Snow et al., several hundred siderophores have been isolated and their structures and transport mechanisms extensively studied (Yamamoto, et al., 1994; Challis and Naismith, 2004; Challis, 2005; Sandy and Butler, 2009). Siderophores were initially categorized into three major classes, catecholates/phenolates, hydroxamates, and carboxylates. Recently, mixed groups of siderophores have been found, leading to a more complex classification (Figure 5). In general, siderophores contain six donor atoms forming a 1:1 complex with Fe(III) with octahedral geometry. Siderophores are hard Lewis bases and thus strongly favor the hard Lewis acid Fe(III) over the softer Lewis acid Fe(II). Their binding effectiveness is pH-dependent. Carboxylate, catecholate/phenolates, and hydroxamate siderophores have pKa values of 3.5-5, 9-12, and 8-9, respectively. This makes, for instance, carboxylate siderophores more efficient in low pH environments where the two other siderophore groups are fully protonated (Miethke and Marahiel, 2007). Thus organisms living in acidic conditions thus prefer carboxylate siderophores for their iron acquisition. Correspondingly hydroxamate and phenolate/catecholate siderophores dominate in more basic environments where their effective binding constants for iron are higher.

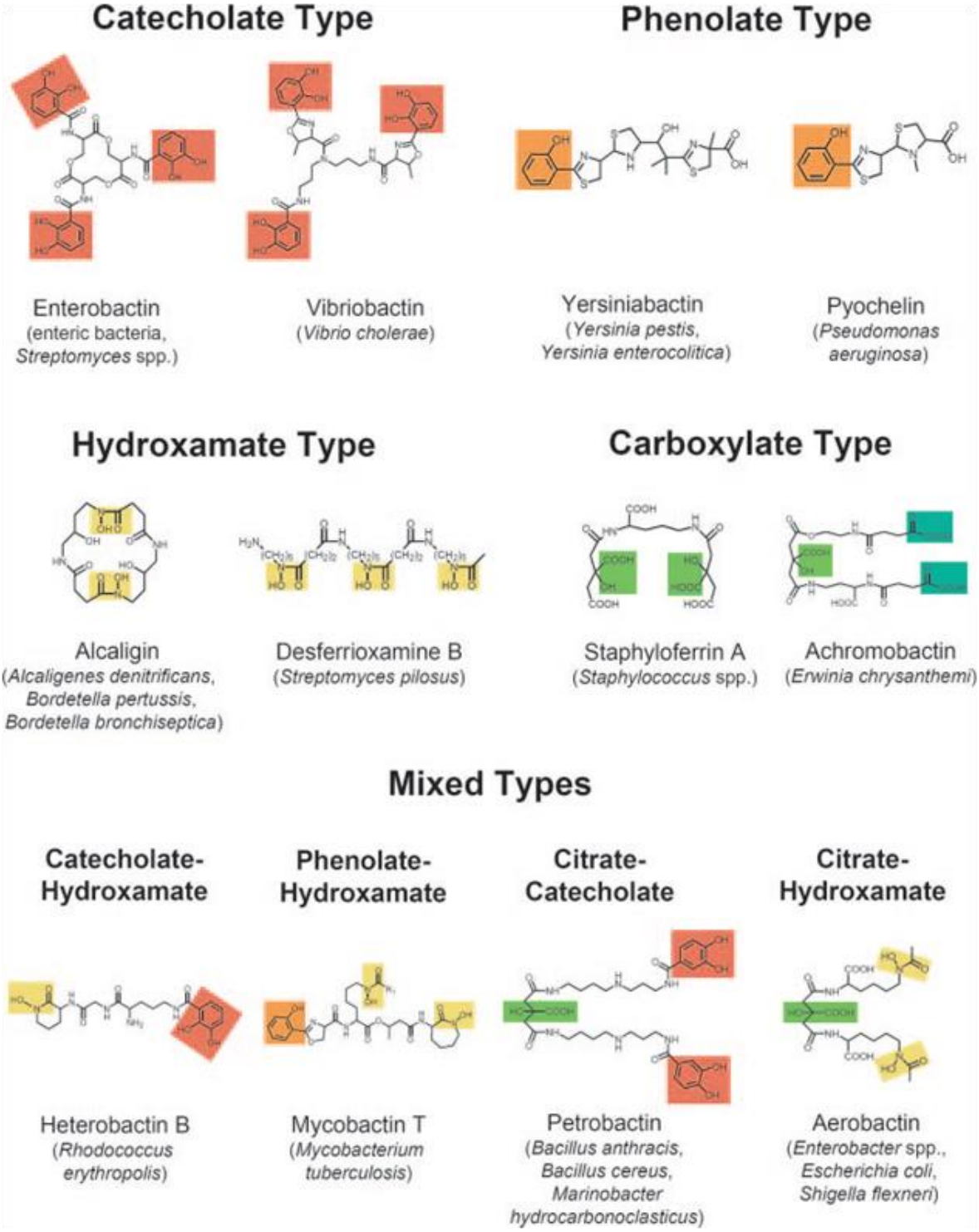

Figure 6 Classes of siderophore
Figure adopted from Miethke and Marahiel (2007).

2.3.2 Marine siderophores

While much research have been done on terrestrial siderophores, the study of marine siderophores is less extensive and only a relatively few structures have been fully elucidated (Vraspir and Butler, 2009). One of the two major attributes that seem to distinguish marine siderophores from those of terrestrial origin is the tendency of the former to contain α- and β-hydroxy acid groups in their iron binding domain The other structural feature dominating the marine siderophores is the inclusion of an amphiphilic moiety with a fatty acid appendage (Barbeau, et al., 2001, 2002; Küpper, et al., 2006). The significance of the α- and β-hydroxy acid groups in marine siderophores is their tendency to make the iron siderophore complex photoactive, first demonstrated for the Fe(III)-aquachelins (Barbeau et al., 2001). The photoactive Fe(III)-siderophore complexes undergo oxidative decarboxylation of the ligand with concomitant reduction of Fe(III) to Fe(II) under near UV photolysis (for example, 300 nm for Fe(III)- aquachelins) (Barbeau et al., 2001). It has been proposed that the transiently released Fe(II) by sunlight-driven dissociation of the Fe(III)-siderophores might be utilized not only by the siderophore producing bacteria themselves but also non-siderophore producing bacteria and other organisms such as phytoplankton (Maldonado et al., 2005; Naito et al., 2008; Amin et al., 2009, 2012).

The siderophore vibrioferrin is one of the representative photoreactive marine siderophores. It was first isolated from *V. parahaemolyticus* in 1992 (Yamamoto et al., 1992; Nishio et al., 1988) and its structure is now fully elucidated (Figure 7). Gene-knockout experiments revealed that vibrioferrin biosynthesis involved an operon containing five genes, pvsABCDE (Tanabe et al., 2003), with its hypothetical biosynthetic pathway as proposed in Figure 8 (Challis, 2005). In this thesis, vibrioferrin was chosen as a model photoreactive

siderophore for a number of reasons. First, it has only relatively weak iron binding properties as it lacks the sixth donor group required to complete the octahedral coordination geometry preferred by Fe(III) (Amin et al., 2009), meaning that more transient Fe(II) would be released into the environment at a faster rate. Second, photolyzed vibrioferrin has no further affinity for iron, while most other photoactive siderophores retain the ability to strongly bind Fe(III) even after photolysis (Amin et al., 2009), leaving more bioavailable iron in the environment. Third, vibrioferrin has been isolated from several different bacteria which are known to be closely associated with HAB species (Amin et al., 2007).

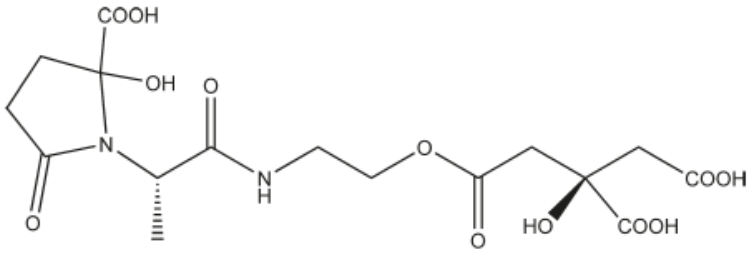

Figure 7 Structure of vibrioferrin siderophore
Figure adopted from Amin et al. (2009).

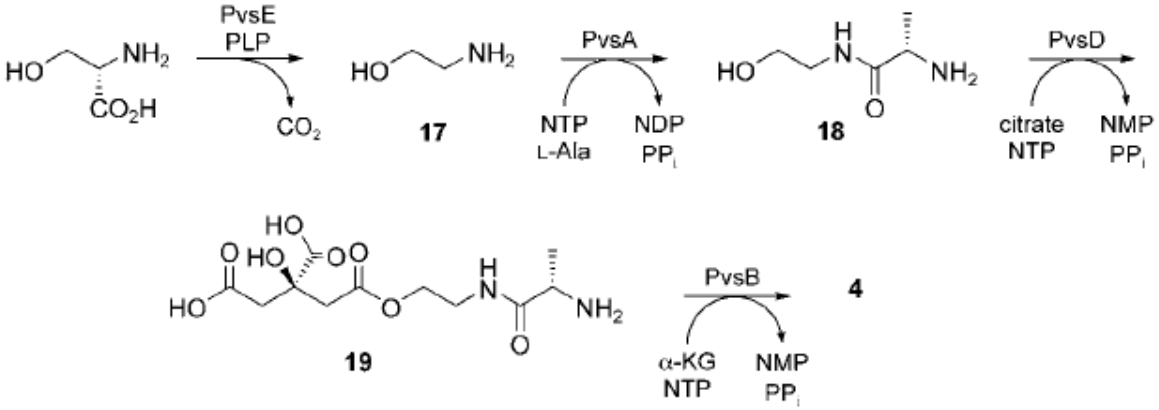

Figure 8 Hypothetical pathway for vibrioferrin biosynthesis
Figure adopted from Challis (2005).

2.3.3 Siderophore biosynthesis

The entire siderophore biosynthetic process is not yet clear, but currently their biosynthesis is categorized into two groups based on involvement or not of nonribosomal peptide synthetases (NRPSs); enzyme complexes that help in assembling amino acids, carboxy acids, and hydroxyl acids to release macrocyclic peptides. NRPS-dependent siderophores are exemplified by many catecholate siderophores enterobactin. NRPS-independent siderophores (NIS) are represented by many hydroxamate and carboxylate siderophores, which rely on other types of enzymes such as monooxygenases, decarboxylases, aminotransferases, acetyltransferases, amino acid ligases, and aldolases. Several NRPS-independent siderophores have been found: aerobactin, rhizobactin, alcaligin, desferrioxamines, vibrioferrin, staphylobactin, anthrachelin and achromobactin (Challis, 2005). Petrobactin is a unique example of a siderophore that is dependent on both NRPSs and NIS synthetases for its biosynthesis (Cendrowski et al., 2004).

2.3.4 Iron uptake by bacteria

The secreted siderophores form complexes with Fe(III) in the surrounding environment. The complex is then either A) taken up by Fe(III)-siderophore specific transporters on the bacterial cell surface or B) undergoes Fe(III)-siderophore reduction to free Fe(II) by ferric reductases on bacterial cell surface. The former mechanism is more widely utilized, as many cell surface receptor proteins for Fe(III)-siderophore complexes have been identified (Figure 9) including FepA for Fe-enterobactin, FhuA for ferrichrome, FhuE for Fe-rhodotorulate and Fe-coprogen, FecA for ferric dicitrate, and Cir and Fiu for linear Fe-enterobactin degradation products (Miethke and Marahiel, 2007). Mechanism A is likely preferred because high affinity receptor proteins on bacterial cell surfaces can increase the rate of Fe(III)-siderophore transport

from the marine environment, where the iron concentration is so dilute (Clarke et al., 2001). These receptors then transport Fe(III)-siderophores from outer membrane to the periplasm against a concentration gradient using energy provided by the TonB complex (TonB-ExbB-ExbD). Fe-siderophore uptake from periplasm to cytoplasm depends on various types of ABC transporters. It is known that bacteria that do not synthesize their own siderophores (so called "cheaters") can still take advantage of xenosiderophores by utilizing the requisite cell surface receptors obtained by horizontal gene transfer (Miethke and Marahiel, 2007).

The outer membrane receptors for iron siderophore complex are only expressed under iron limiting conditions (Braun, 1995 and 1998), typically micromolar in iron (Miethke and Marahiel, 2007). Under high iron conditions the repressor protein Fur binds DNA and negatively regulates transcription of iron transport related genes.

Once Fe-siderophore complexes reach cytoplasm, how free iron is release into the bacterial cells is not completely understood. There are two proposed mechanisms for iron release from siderophores: reduction of Fe(III) to Fe(II) involving ferrisiderophore reductases followed by spontaneous release, or hydrolysis of the Fe(III)-siderophore complex by specialized enzymes to release Fe(II). Whether the iron delivered into cells is immediately used or intermediately stored is also not well known.

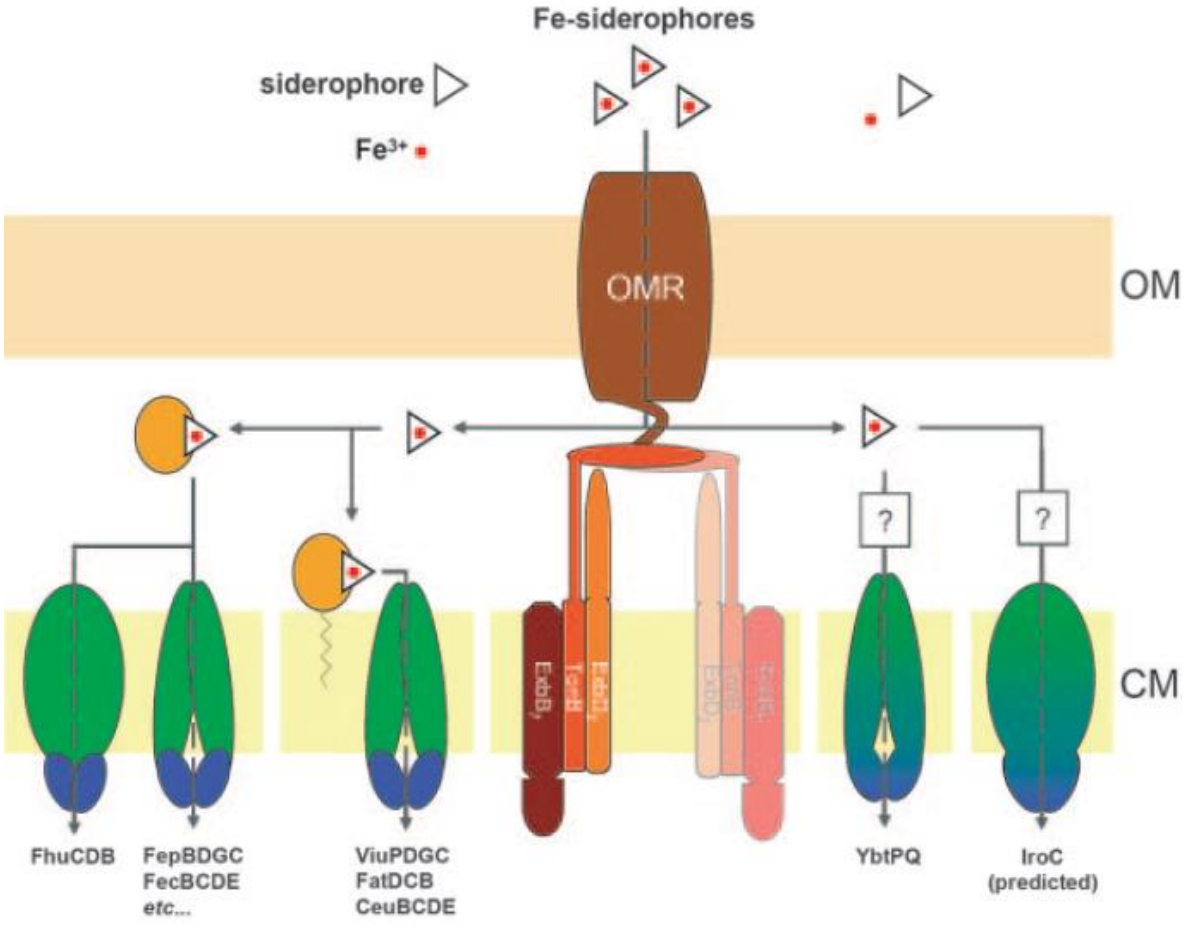

Figure 9 Cellular transport systems for uptake of siderophore-delivered iron in gram-negative bacteria

Figure adopted from Miethke and Marahiel (2007). The color bright orange, green, dark blue represents periplasmic binding proteins, membrane-spanning proteins, and cytoplasmic ATP-binding proteins, respectively.

2.4 IRON ACQUISITION BY PHYTOPLANKTON

As with iron acquisition by bacteria, that by terrestrial plants is also reasonably well understood. The first of the two known basic strategies of iron uptake and storage systems for terrestrial plants are "strategy I plants", seen mostly in dicotyledon, which use a mechanism involving soil acidification followed by induction of Fe(III)-chelate reductase (ferrireductase) and an Fe(II) transporter protein (Moog and Bruggemann, 1994; Robinson et al., 1999). Strategy

II plants", seen predominantly among the monocotyledons and grasses, use iron chelating compounds called phytosiderophores (Römheld and Marschner, 1986). These molecules are functionally, although not structurally, similar to the siderophores produced by bacteria and fungi. In contrast, there is far less knowledge about the corresponding systems in marine plants including phytoplankton.

2.5 PHYTOPLANKTON IRON UPTAKE

2.5.1 Reductive mechanism

One of the possible iron acquisition strategies for phytoplankton is a direct iron reductive mechanism that has been evidenced in some phytoplankton, although not in all. For example, many algae in the class of green algae *Chlorophyta* and diatoms such as *Bacillariophyceae* clearly utilize an initial reductive step with cell surface reductase, identified by conserved genes such as related to FRE2 and FRO2 from *Arabidopsis*. This is then followed either by direct uptake of the reduced Fe(II) via an Fe(II) permease, or reoxidation of the Fe(II) by a multi-copper oxidase, with subsequent transport across the membrane of Fe(III) (Kustka et al., 2007) similar to process found in yeast. The reductive-oxidative pathway seems thermodynamically inefficient; however, its importance on cell surface iron binding has been confirmed with diatom *T. pseudonana* and macro brown algae *Ectocarpus siliculosus* as well as *Macrocystis pyrifera* (Kustka et al., 2007; Böttger et al., 2012; Miller et al., 2014 and 2016).

2.5.2 Non-reductive mechanism

Some phytoplankton do not show signs of using iron reductive mechanisms for their iron acquisition. For example, in one study (Sutak et al. 2012) all five phytoplankton species studied were able to take up both ferric and ferrous iron without a confirmed ferrireductase, suggesting that iron reduction was not a prerequisite for these phytoplankton. In the meantime, some

microalgae evidenced a wide variety of non-reductive pathways, including some based on siderophores or siderophore-like molecules. Others involving transferrin-like proteins (Fontaine et al., 2002) as well as surface binding proteins designated as iron starvation induced proteins, ISIPs (Sutak et al., 2012). The coccolithophores species *Emiliana huxleyi* is one of the well-studied haptophyta representing the use of a non-reductive iron uptake pathway (Hartnett et al., 2012).

2.5.3 Siderophore mediated mechanism

One of the potential non-reductive iron uptake strategies for phytoplankton is via a siderophore-mediated mechanism which can be categorized by the use of either endogenous siderophores or xenosiderophores. Currently, the there is no evidence for the production of endogenous siderophores (with the exception of the cyanobacteria) by phytoplankton (Maldonado, et al., 2005, Raven, 2013). A second option, i.e. the use of existing marine siderophores secreted by other organisms such as bacteria and fungi, may be a possible iron source for phytoplankton. The iron complexed with xenosiderophores may thus be made available by reductive or nonreductive process (Soria-Dengg and Horstmann, 1995; Naito et al., 2008; Hopkinson and Morel, 2009).

2.6 HYPOTHESIS

Although beginning to be understood, much less is known about the iron acquisition strategies that phytoplankton use and how they effectively acquire iron from the low iron concentration environment. Among the marine microalgae, the dinoflagellates appear to be the least studied, likely due to the dearth of genomic data available for these organisms, which typically have very large and complex genomes. Our hypothesis is that there is an iron for carbon mutualism between bacterial producers of photoactive siderophores such as vibrioferrin and

some HAB phytoplankton. To support this hypothesis, here I present a) *in vivo* assays of environmental samples collected from various locations and times, including during bloom seasons, to seek correlations between abundance of iron, phytoplankton numbers, and siderophore producing bacteria and b) *In vitro* studies of *L. polyedrum*, one of the common dinoflagellate bloom species found along the Southern California coast, and *Marinobacter* DG893, a bacterium often found in association with phytoplankton and a producer of the photoactive siderophore vibrioferrin, with respect to their growth rate and iron uptake under various manipulated conditions.

CHAPTER 3. EVALUATION OF PHOTO-REACTIVE SIDEROPHORE PRODUCING BACTERIA BEFORE, DURING, AND AFTER A BLOOM OF THE DINOFLAGELLATE LINGULODINIUM POLYEDRUM

3.1 ABSTRACT

Evidence is increasing for a mutualistic relationship between phytoplankton and heterotrophic marine bacteria. It has been proposed that bacteria producing photoactive iron binding compounds known as siderophores could play an important role such mutualistic associations by sequestering bioavailable iron utilizable by phytoplankton and in exchange receive autotrophically derived dissolved organic matters (DOM). In order to understand the potential photoactive siderophores might be playing in bacterial-algal mutualism or marine biogeochemistry in general, it is important to be able to detect and quantify their presence in various environments. One approach to accomplish that end is to make use of high sensitivity genomics technology (RT-qPCR) to search for siderophore biosynthesis genes related to the production of photoactive siderophores. In this way one can access their "biochemical potential" and utilize this information as a proxy for the presence of these siderophores in the marine environment. In this chapter, we studied the correlation between the presence of bacteria producing one of four photoactive siderophores relative to total bacterial and dinoflagellate numbers from local surface water at the Scripps Pier before, during, and after fall bloom of the

dinoflagellate *Lingulodinium polyedrum*. We believe these findings will aid us in gauging the importance of photoactive siderophores in the marine environment and in harmful algal bloom dynamics in particular.

3.2 INTRODUCTION

Algal blooms are ubiquitous phenomena that have been increasingly observed in the coastal and upwelling parts of the world's oceans (Lewitus et al., 2012; Kim et al., 2009). Even in the absence of toxin production these events often alter the chemical and ecological environment by changing nutrient distribution and the biodiversity of marine ecosystems (Anderson et al., 2012). Consequently these blooms often have immediate acute effects on marine populations and their impact on public health and local economies is large and has been increasing (Lewitus et al., 2012; Honner et al., 2012). Although many physical and biological factors influence bloom dynamics, emerging evidence suggests that bacterial-algal interactions may be contributing to their development and sustenance (Azam and Worden, 2004; Mayali and Azam, 2004; Rooney-Varga et al., 2005; Azam and Malfatti, 2007; Mayali and Franks, 2008). Indeed, some bacterial associates of harmful algal species are clearly important to the physiological welfare of algal cells as evidenced by the fact that many species such as the dinoflagellate *Gymnodinium catenatum* cannot be grown axenically indicating an obligatory requirement(s) that is supplied by bacteria (Green et al., 2004; Bolch et al., 2011). Thus, bacterial-algal interactions are likely to be strongly influenced by the supply of available nutrients. While nitrogen, phosphorous and vitamins have most often been considered in this context, a broad hypothesis that links these bacterial 'symbionts' to the growth of dinoflagellates, diatoms and coccolithophores is in their possible control of the supply of iron.

Iron is an essential nutrient for photosynthesis and respiration in all microorganisms, including phytoplankton and marine bacteria. Despite the fact that iron is the fourth most abundant element on the earth, iron levels in oceanic surface water are extremely low (Martin and Fitzwater, 1988; Bruland et al., 1991; Wu and Luther, 1994). Consequently, iron acquisition from the environment is a significant challenge for microorganisms. The production of organic ligands to complex, solubilize and transport ferric ions is one common strategy used by bacteria to facilitate uptake of iron (Sandy and Butler, 2009). These ligands, known as siderophores, which come in a wide variety of structures, have also been identified as the iron-binding ligands produced by marine bacteria (Tortell et al., 1996; Vraspir and Butler, 2009). One of the characteristic features that seem to distinguish marine from terrestrial siderophores is the near ubiquitous presence of α-hydroxy acid groups in the former which renders their ferric complexes photolabile through a photochemical process such as that shown below, where sid* is the siderophore derived photoproduct (Barbeau et al., 2001 and 2002; Kupper et al., 2006):

$$\text{Fe(III)-siderophore} + h\upsilon \rightarrow \text{Fe(II)} + \text{sid}^* + CO_2 + 2H^+$$

In contrast to marine bacteria, phytoplankton are not known to produce ligands like siderophores or to directly take up bacterial derived ferric-siderophore complexes. However evidence is increasing for a mutualistic relationship between phytoplankton and some marine bacteria and we hypothesize that photoactive siderophores could play an important role in such mutualistic associations through the generation of bioavailable free Fe(II) and/or Fe(III) (Amin et al., 2009).

To understand the potential photoactive siderophores might be playing in algal-bacterial mutualism or marine biogeochemistry in general, it is important to be able to detect and quantify their presence in various environments. Unfortunately, it has been a challenge for researchers to directly measure the quantity of photoactive siderophores due to their low concentration in the

marine environment and their rapid degradation by photochemical reactions. An alternative approach is to make use of high sensitivity genomics technology (RT-qPCR) to search for siderophore biosynthesis genes related to the production of photoactive siderophores. In this way one can access their "biochemical potential" and utilize this information as a proxy for the presence of these siderophores in the marine environment (Gärdes et al., 2013). Here we quantify siderophore biosynthetic genes to act as surrogates for the presence of three photoactive siderophores (petrobactin, aerobactin, and vibrioferrin) in the local sea surface water at the Scripps Pier (La Jolla, CA) before, during, and after a bloom of the dinoflagellate *Lingulodinium polyedrum* during September and October of 2011.

3.3 METHODS

3.3.1 Sampling site

The Scripps Institute of Oceanography (SIO) pier (La Jolla, CA; 32° 53′ N, 117° 15′ W) is a long-term coastal monitoring site in the Southern California Bight. The sampling site is beyond the surf zone and has a bottom depth of 0-2 m with a spring tidal range of 2 m. The site is well known to experience cycles in phytoplankton abundance, such as *Synechococcus sp.* (Tai and Palenik, 2009) as well as larger diatoms and dinoflagellates like *L. polyedrum*, including intense blooms such as that during October 2011.

3.3.2 Chlorophyll and phytoplankton cell counts

Sea surface water samples were collected weekly at Scripps Pier as part of the Southern California Coastal Ocean Observing Harmful Algal Bloom Monitoring Program (http://www.sccoos.org/data/chlorophyll/index.php). Chlorophyll (Chl *a*) values were obtained using standard chlorophyll extraction and analysis procedures outlined by Venrick and Haywayd (1984), in which seawater was filtered through a GF/F filter with approximately 0.7 μm pore size

and then extracted in 90% acetone for 24 hours before reading on a calibrated fluorometer. Abundance of phytoplankton groups and specific species were determined from settling 10 mL of seawater preserved with 4% formaldehyde (Uthermöl, 1958; Sournia, 1978). Cells were identified and counted to lowest taxonomic level with a phase-contrast, inverted light microscope at 200X. The total volume of material counted was 2.5 mL with a detection limit of 400 cells/L.

3.3.3 Sample collection

The surface water was collected from the Scripps Pier at seven time points (Sep 23rd, Oct 2nd, Oct 5th, Oct 9th, Oct 12th, Oct 19th, and Oct 30th) covering before, during, and after the *L. polyedrum* bloom of 2011. At each time point, approximately eight litters of the ocean surface water was collected in acid washed plastic containers. The water samples were immediately filtered through tandem membranes (0.8 μm pore size with 47 mm diameter disc membrane and 0.2 μm pore size with cartridge type membrane) to separate particle-associated bacteria from free-living bacteria. One liter of water sample was passed through each tandem membrane set, however, the samples collected during the peak of bloom easily clogged the membranes and a full 1L could not be filtered. In such occasions, the volume that was able to be filtered was recorded and the final volume was adjusted during DNA extraction to normalize it to 1L extraction. DNA was extracted from each of 0.2 μm and 0.8 μm membranes per protocol in Appendix A (Tillett and Neilan, 2000; Yilmaz and Phlips, 2009).

3.3.4 Quantification of biosynthesis genes by real time q-PCR

The preparation of the degenerate primers for the genes encoding for photoactive siderophore biosynthesis (asbE for petrobactin, iucC for aerobactin, and pvsB for vibrioferrin) was previously described (Gärdes et al., 2013). As it proved impossible to make a single set of degenerate primers that could adequately quantify the *pvsB* gene for both *Marinobacter*

produced vibrioferrin and non-*Marinobacter* produced vibrioferrin, we developed two separate primers designated as pvsB for the former and vibXII for the latter. These primers were used in conjunction with RT-qPCR to quantify the presence of biosynthetic genes for the three photoactive siderophores in the samples per protocol in Appendix B. Additionally, universal bacterial 16S primers were utilized for a Taq-Man assay to estimate total bacterial abundance (Bach et al., 2002: Labrenz et al., 2004). Standards used for quantification were genomic DNA prepared from *Marinobacter algicola DG893, Vibrio splendidus, Marinobacter aquaeolei* and *Vibrio fisherii MJ11* (See Appendix B for combination of standard strain and primer sets). Gene copy numbers of each siderophore biosynthetic gene were determined for both the particle-associated (0.8 μm filter) and free-living (0.2 μm filter) bacterial fractions by RT-qPCR using standard curves. Relative abundance of the genes of interest was determined by comparison to the total bacterial 16S rRNA gene pool. All RT-qPCR were run using an ICycler IQ-5 thermocycler equipped with a multicolor detection system and analyzed by the Bio-Rad IQ-5 Software 2.0. The qPCR and Taq-Man assays of the sample DNA extracts were performed in triplicate and duplicate, respectively. Samples that did not exhibit any background fluorescence including primer-dimer formation were assumed to be inhibited for qPCR, and thus the DNA was further purified using QIAamp DNA Stool Mini Kit (Qiagen, P/N 51504) per protocol in Appendix E.

3.3.5 Phylogenetic analysis of products amplified by RT-qPCR

Representative environment DNA samples amplified by RT-qPCR were selected from beginning, during and end of the bloom time points. The selected PCR amplicons were ensured to have the target melting temperature (Tm). It should be noted that RT-qPCR results from iucC primer set show low signal than that from other primer sets. DNA was cleaned from each

amplicon using 2% agarose gel per and further purified using QIAquick Gel Extraction Kit per Appendix F. The purified DNA from each amplicon was inserted in Promega pGEM-T Easy Vector System I by ligation process and transformed in host organism, Top10 E. Coli competent cells, per protocol in Appendix G and Appendix H. The inserted DNA was sequenced by Microchemical Core Facility (SDSU). The protein sequence of the insert was searched by BLAST. The clone library was constructed from the protein sequences. Using Geneious R6 program, phylogenetic affiliation was established by alignment of the translated clone sequences against previously used known sequences (Katoh et al., 2002). Tree construction was based on amino acid substitution using PHYML with rate optimization as implemented in Geneious R6 (Guindon and Gascuel, 2003). The protein sequences were further analyzed statistically by UniFrac software described in Appendix I and Appendix J (http://bmf2.colorado.edu/unifrac/index.psp).

3.4 RESULTS

3.4.1 Bloom dynamics

As can be seen in Figure 10 presenting dinoflagellate abundance, mainly *L. polyedrum*, increased from less than 50,000 cells/L in the beginning of September to a peak of ca. 150,000,000 cells/L on October 3rd and then declined to below detection levels by the end of October. Diatoms showed a reverse trend in that their abundance was high before and after the *L. polyedrum* bloom and at a minimum when dinoflagellate abundance peaked. The concentration of chlorophyll, which represents an estimate of algal biomass, tracked dinoflagellate abundance. Phaeophytin, which is a pigment derived from the degradation of chlorophyll, was relatively low compared to the chlorophyll yield.

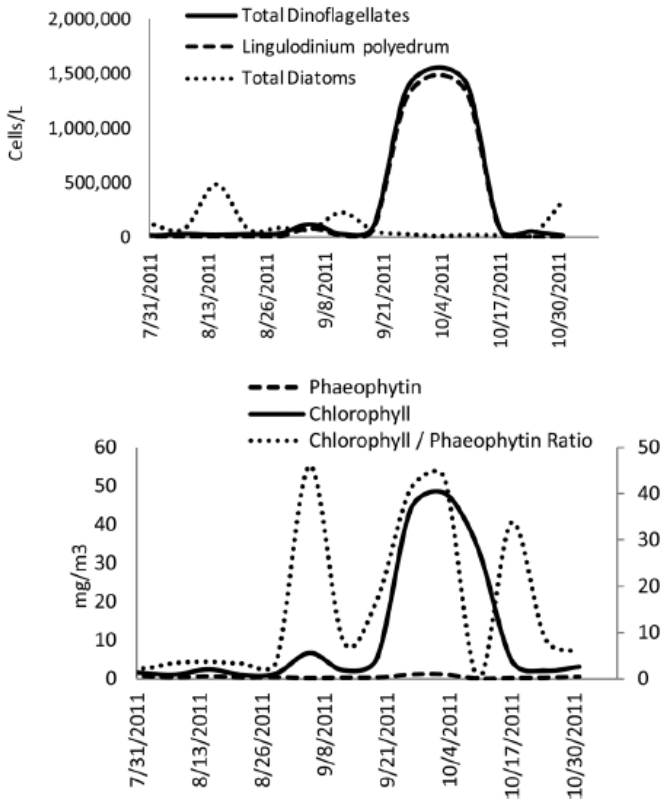

Figure 10 Phytoplankton cell count and chlorophyll concentration during the bloom of 2011 at Scripps pier
Upper panel: Cell numbers *L. polyedrum*, total dinoflagellates, and diatoms by date. Lower panel: Chlorophyll, Phaeophytin and the Chlorophyll/Phaeophytin ratio (mg/m^3) by date.

3.4.2 RT-qPCR

Bacterial numbers (free-living, particle-associated, and total) were determined by Taq-Man PCR assay based on 16S gene copy numbers (Table 3 and Table 4). Free-living bacterial numbers peaked on Oct. 2nd and then declined throughout the remaining sampling period. Particle-associated bacterial numbers on the other hand showed maxima on Oct 2nd (prebloom), Oct 9th (beginning of bloom decline), and Oct 30th (post bloom) with a minimum on Oct 5th at the bloom maximum. It is notable that particle-associated bacteria constituted the majority of the total bacterial numbers at all time points (Figure 11 to Figure 13). However, the relative fraction

of the free living component was largest at the early time points (prebloom) and declined to a very small faction post bloom.

Gene copy numbers for both free-living and particle-associated bacteria producing the photoactive siderophores vibrioferrin (primers pvsB and vibXII) and petrobactin (asbE) are shown in Figure 11 to Figure 13 and Table 5 to Table 10. For all three primers the number of gene copies for the free-living portion of the bacterial producers maximized on Oct 2nd (bloom initiation). For the particle-associated bacteria a different pattern was observed for each of the producers. Thus gene copies of the *Marinobacter* vibrioferrin producers (pvsB primer) showed maxima on Oct 2nd, Oct 9th and Oct 30th and a minimum near the bloom maximum on Oct 5th, while non-*Marinobacter* producers of vibrioferrin (vibX primer) peaked on Oct 2nd and generally declined thereafter. Gene copies of *asbE* from petrobactin producers were more or less constant throughout the study period with a maximum at the end. Overall, gene copy numbers from non-*Marinobacter* vibrioferrin producers constituted the majority of the photoactive siderophore genes detected (ca. 109 copies/L) with the *Marinobacter* vibrioferrin producers approximately an order of magnitude less abundant (108 copies/L) and the petrobactin producers a small minority (106 copies/L). Unfortunately the primers for the gene *iucC* (aerobactin biosynthesis) performed poorly and *iucC* gene copy numbers were below our detection limit at all time points.

Normalizing the gene copy numbers to total bacteria provides an alternate way to look at the data (Figure 14). Here, we see that *Marinobacter* and non-*Marinobacter* producers of vibrioferrin constitute the largest percentage of total bacteria (sum of free-living and particle-associated bacteria) throughout the time points. Comparison of the total photoactive siderophore producers as a percentage of the total bacteria shows they generally track *L. polyedrum* numbers

and maximize at ca. 8.6% of the total bacterial population on Oct 5th, a date near the bloom maximum.

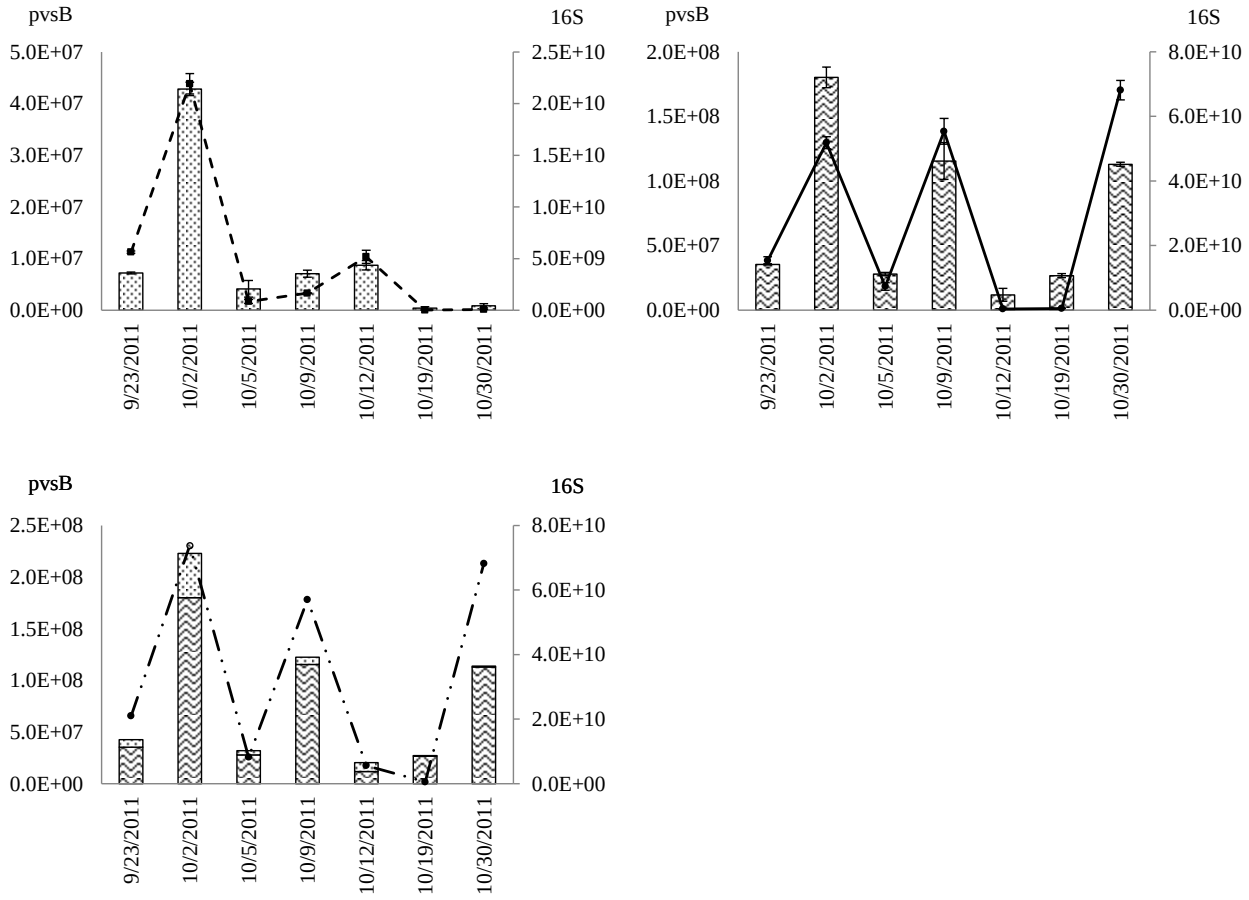

Figure 11 Copy number of *Marinobacter pvsB* gene during the bloom of 2011 at Scripps pier

A) Bar graph shows free-living *Marinobacter* (0.2μm fraction) derived *pvsB* gene copy numbers. Dotted line represents free-living bacterial numbers (*16S* gene copy number from 0.2μm fraction) B) Bar graph shows particle-associated *Marinobacter* (0.8μm fraction) derived *pvsB* gene copy number. Solid line represents particle-associated bacterial numbers (*16S* gene copy number from 0.8μm fraction). Error bars are the average ± one standard deviation of triplicate measurements. C) Total *pvsB* gene copy number and total *16S* gene copy number (dot-dash) are shown.

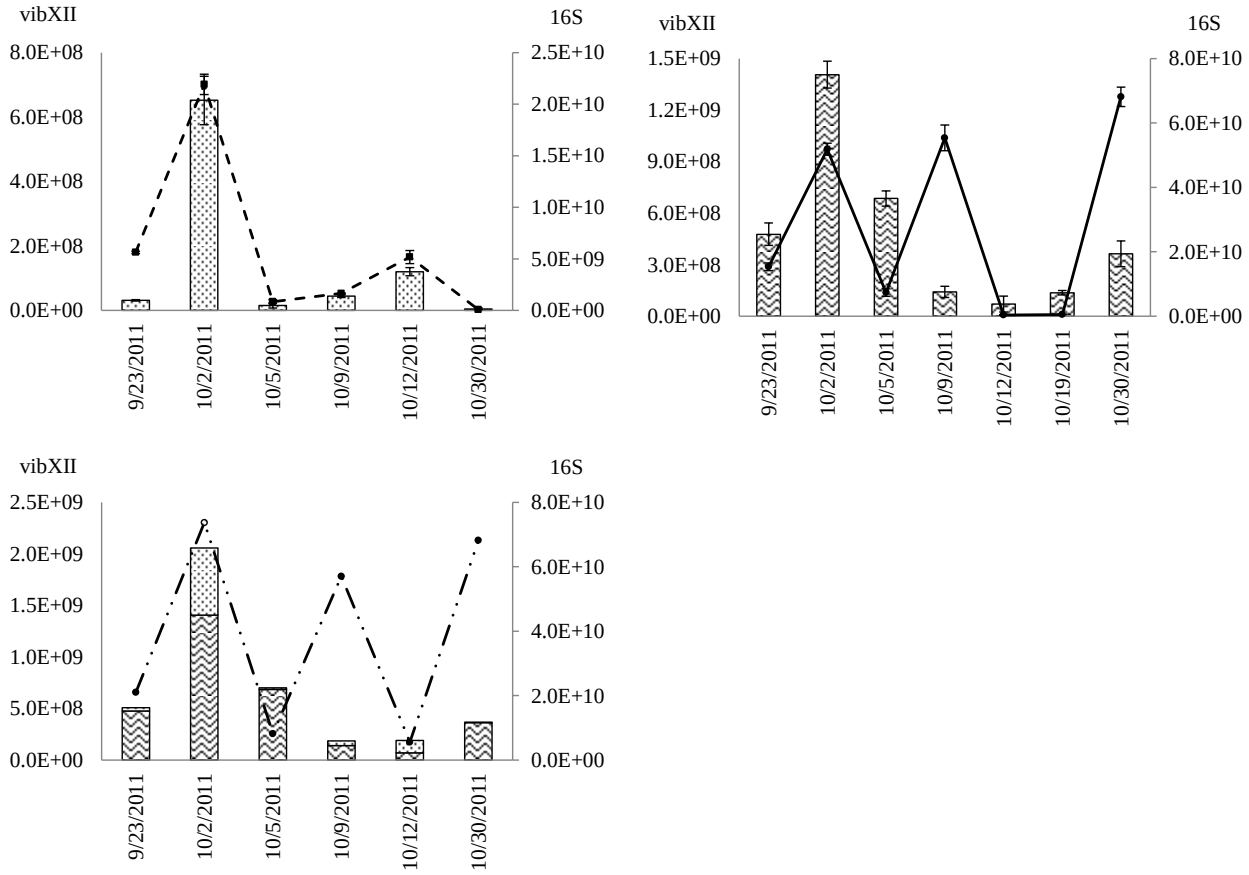

Figure 12 Copy number of non-*Marinobacter pvsB* gene during the bloom of 2011 at Scripps pier

A) Bar graph shows free-living non-*Marinobacter* (0.2μm fraction) derived *pvsB* gene copy numbers. Dotted line represents free-living bacterial numbers (*16S* gene copy number from 0.2μm fraction) B) Bar graph shows particle-associated non-*Marinobacter* (0.8μm fraction) derived *pvsB* gene copy number. Solid line represents particle-associated bacterial numbers (*16S* gene copy number from 0.8μm fraction). Error bars are the average ± one standard deviation of triplicate measurements. C) Total *pvsB* gene copy number and total *16S* gene copy number (dot-dash) are shown.

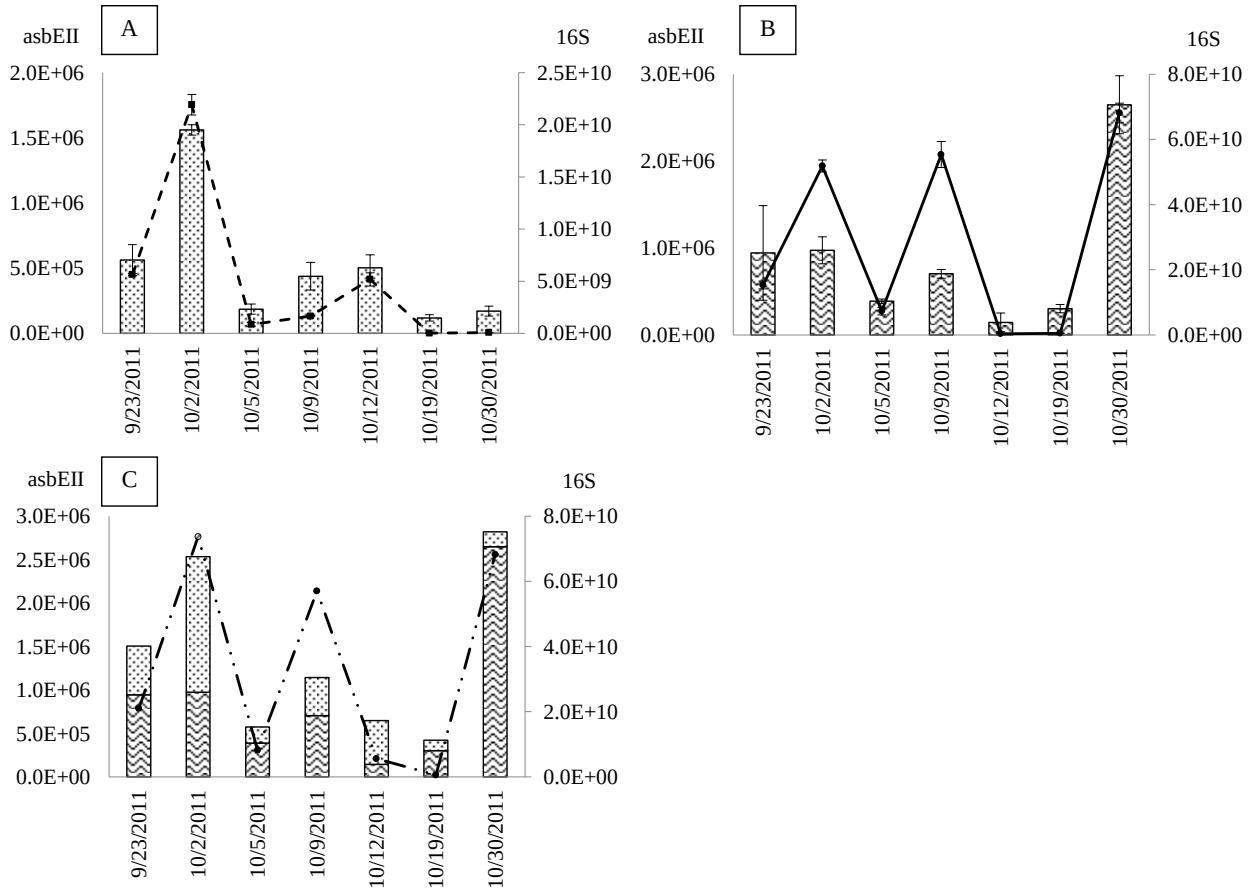

Figure 13 Copy number of *Marinobacter asbEII* gene during the bloom of 2011 at Scripps pier

A) Bar graph shows free-living (0.2µm fraction) derived *asbEII* gene copy numbers. Dotted line represents free-living bacterial numbers (16S gene copy number from 0.2µm fraction) B) Bar graph shows particle-associated (0.8µm fraction) derived *asbEII* gene copy number. Solid line represents particle-associated bacterial numbers (16S gene copy number from 0.8µm fraction). Error bars are the average ± one standard deviation of triplicate measurements. C) Total *asbEII* gene copy number and total 16S gene copy number (dot-dash) are shown.

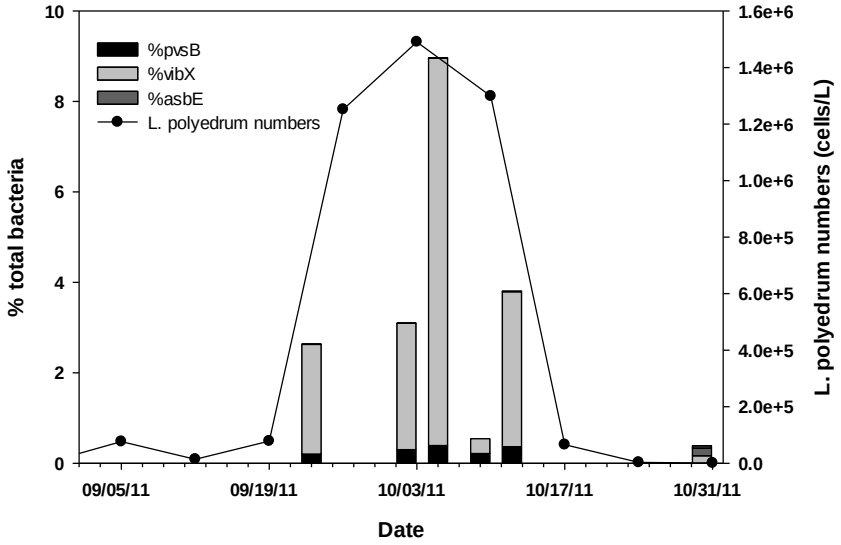

Figure 14 Total siderophore synthesis gene copies and *L. polyedrum* cell counts during the bloom of 2011 at Scripps pier
Bar graph shows the percentage of total siderophore genes i.e. *pvsB* (both *Marinoacter* and non-*Marinobacter* derived) and *asbEII* relative to the total *16S* gene copy number. Line shows *L. polyedrum* numbers.

3.4.3 Phylogeny

Although qPCR requires the use of rather small amplicons (in our case ca. 100-150 bp) which are not ideal for phylogeny studies, as generally speaking the larger the sequences being compared the more accurate the description of diversity, it is still possible to get preliminary data on the community structure of photoactive siderophore producers as a function of bloom dynamics. This data was obtained from clone libraries prepared from our RT-qPCR products. A phylogenetic tree was then constructed from 38 sequences of asbEII related clones and 56 sequences of vibXII related clones. As seen in Figure 15, many of asbEII related sequences are clustered together whereas the group of asbEII and vibXII are rooted at a further point. The phylogenetic tree was consistent with a common ancestor for most of the sequences related to asbEII clones. Similarly, the tree showed a common ancestor among the sequences obtained from vibXII. The two groups, asbEII and vibXII, were further rooted indicating that the two

groups evolved at a later time than the sequences among the groups. In the course of evolution, the protein sequences from two species that have an ancestor in common may have diverged in a variety of ways such as insertions and deletions of amino acids. The sequences often evolve to adapt to a specific environment.

The clone library was constructed from the randomly selected sequences from asbEII and vibXII clones representing three environmental groups or communities i.e. beginning, middle, end of bloom. Each community was statistically analyzed by UniFrac software for similarity and difference from other communities (Lozupone and Knight, 2005: Lozupone et al., 2006). Both environment distance matrix analysis and significance analysis concluded that the community of free-living bacteria from beginning time point was significantly different ($p<0.04$) from all the other communities (either free-living or particle-associated) found at later time points. The cluster environment, Principal Coordinates Analysis, PCA and Jackknife environment analyses all supported this result (Figure 16 to Figure 17).

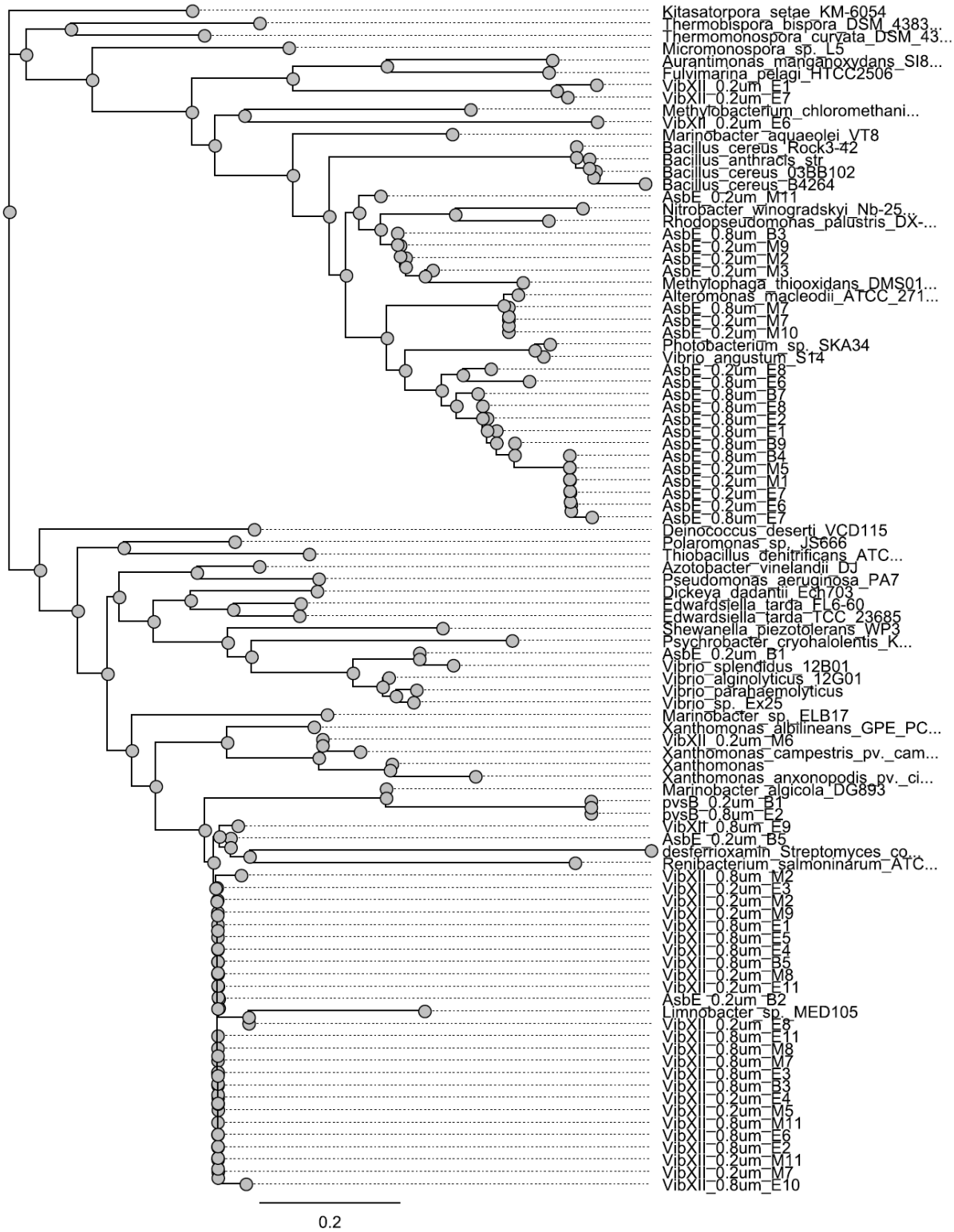

Figure 15 Phylogenetic tree derived from clones obtained by vibXII and asbEII primers
The protein sequences were uploaded to Geneious R6. The phylogenetc tree of asbEII and vibXII was constructed from 38 sequences and 56 sequences which included both samples and references.

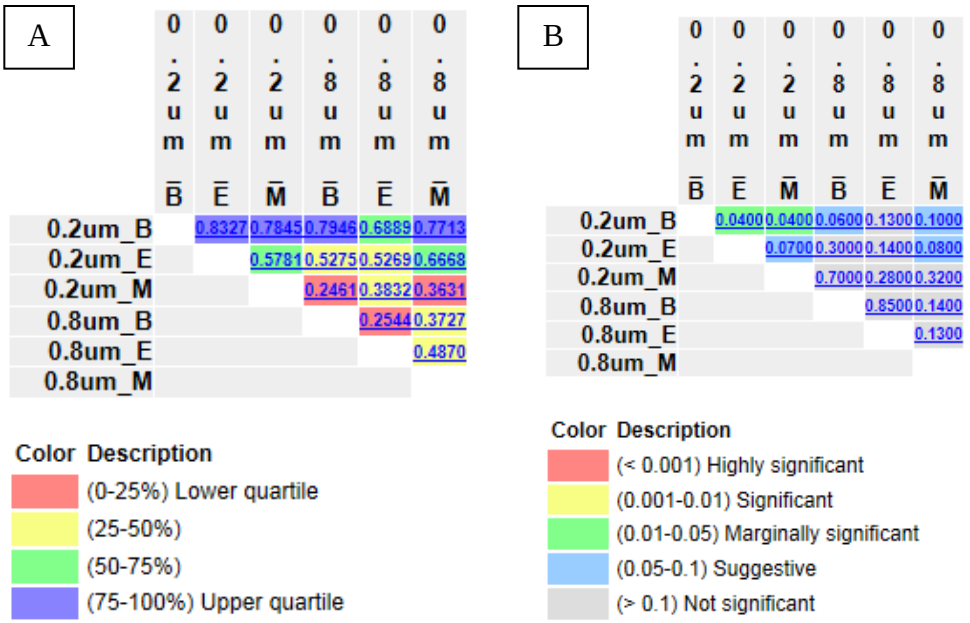

Figure 16 Environment Distance Matrix and UniFrac Significance Test

A: The "Environment Distance Matrix" measures how far apart the environments are in terms of the organisms they share. The distance matrix is colored by quartile: the smallest distance represents most similar pairs by the red color, and the largest distances represents most different pairs by blue color. In this case, any pair of environments with "the free-living bacteria community from beginning of the Red tide" shared less phylogenetic similarity.

B: UniFrac significance analysis measured whether the pattern of each environment differs significantly from each other environment. The parameter of 100 permutations was used and the P-values were corrected for multiple comparisons using the Bonferroni correction. Each p-value was multiplied by the number of pairwise comparisons performed. In this case, the pair of environments, "the free-living bacteria community from beginning of the bloom" and "the free-living bacteria community from middle of the bloom" was marginally significantly different. Similarly, the pair of environments, "the free-living bacteria community from beginning of the bloom" and "the free-living bacteria community of end of the bloom" was marginally significantly different. The rest of any pairs were either suggestively significantly different or not significantly different.

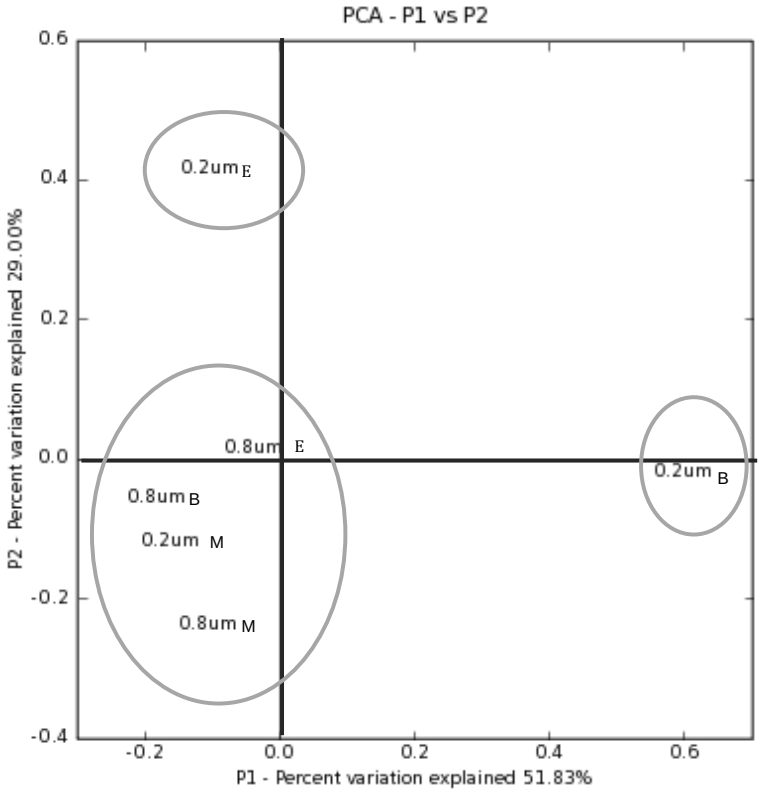

Figure 17 Principal Coordinates Analysis (PCA)
The first principal component (the X-axis) separates the free-living community from beginning of the Red tide from other communities. The second principal component (the Y-axis) separates the free-living community from end of the Red tide from other communities although based on the Unifrac analysis only the former is statistically significant ($p<0.04$).

3.5 DISCUSSION

Using RT-qPCR, we have successfully quantified the biosynthetic genes for the presence of two photoactive siderophores using primers pvsB for *Marinobacter* producers of vibrioferrin, vibXII for non-*Marinobacter* producers of vibrioferrin, and asbEII for petrobactin in the sea surface water during a dinoflagellate bloom at Scripps Pier. The results showed a correlation of dinoflagellate abundance and the total photoactive siderophore producers expressed as a function of total bacterial numbers. All three groups of siderophore producers reached their peak as a percentage of the total bacterial numbers on October 5th at or near the bloom maximum. The non-*Marinobacter* producers of vibrioferrin were by far the most abundant at all time points. More specifically, the relative presence of pvsB, *vibXII*, and *asbEII* to the total bacteria during the time points was between 0.2%-0.4%, 0.3%-8.6%, and 0.002%-0.012%, respectively.

Of particular significance is the predominance of producers of the photoactive siderophore vibrioferrin (VF) throughout the bloom which reached a percentage as high as almost 10% of the total bacterial numbers. In contrast, in a previous study of open ocean sites in the North Atlantic we found that petrobactin producers were dominant (Gärdes et al., 2013). Vibrioferrin is unique among photoactive siderophores in that its photoproduct cannot rebind the released Fe(II) (Amin et al., 2009). In contrast, the photoproducts formed from the photolysis for all the other photoactive siderophores studied thus far including petrobactin and aerobactin have been found to retain the ability to coordinate Fe(III) so that the overall photolysis reaction is actually that shown below (Barbeau et al., 2001 and 2002; Kupper et al., 2006; Abergel et al., 2008):

$$\text{Fe(III)-Sid} + h\nu \rightarrow \text{Sid*} + \text{Fe(II)} \qquad (1)$$

$$\text{Sid*} + \text{Fe(II)} + O_2 \rightarrow \text{Fe(III)-Sid*} \qquad (2)$$

Indeed in some cases the photoproduct (sid*) is actually a better Fe(III) chelator than the parent siderophore (Küpper et al., 2006; Abergel et al., 2008). It has also been shown in the one case where it was studied that the Fe(III) complex of the photoproduct is recognized by the bacteria that produce the parent siderophore and is taken up via the same transport system with equal affinity (Küpper et al., 2006). This observation throws doubt on the ability of these siderophores to provide a bioavailable source of iron to phytoplankton since strong iron binding ability is retained even after photolysis.

FeVF on the other hand not only undergoes photolysis at a faster rate under relatively low illumination conditions compared to other photoactive siderophores, the resulting photoproduct has no significant affinity for Fe(III) (Amin et al., 2009). Thus the photolysis of Fe(III)-VF is an irreversible process that leads to the destruction of the siderophore with the complete release of all of the iron as Fe(II). The latter is likely rapidly oxidized by molecular oxygen ultimately yielding a mixture of soluble and insoluble forms of Fe(III) as in equations 3 and 4.

$$\text{Fe(III)-VF} + h\nu \rightarrow \text{VF*} + \text{Fe(II)} \qquad (3)$$

$$\text{Fe(II)} + O2 \rightarrow \text{Fe(III)}' \rightarrow \text{Fe(III)}\downarrow \qquad (4)$$

where Fe(III)' represents transiently soluble iron hydroxo species and Fe(III)$\downarrow$ represents the increasingly insoluble mineral phases present at equilibrium. This means in practice that under surface illumination conditions bacteria producing VF will see that siderophore rapidly degraded by sunlight with the result of increasing the bioavailability of iron to other organisms including phytoplankton through the formation of soluble Fe(II) and Fe(III)'. Thus with near 9% of the total bacterial population potentially producing VF, large amounts of iron could be constantly recycled into bioavailable forms suitable for supporting phytoplankton growth during the bloom. It is well established through meso-scale iron fertilization experiments that increased

bioavailability of iron can lead to large phytoplankton blooms (Rue and Bruland, 1997; Boyd et al., 2000; Coale et al., 1996).

Finally, analysis of the community structure of petrobactin and non-*Marinobacter* vibrioferrin producers as a function of bloom dynamics yielded the result that the community of free-living bacteria from the beginning time point was significantly different ($p<0.04$) from the other communities. This observation suggests a distinct community of free living photoactive siderophore producers exists whose production of bioavailable iron via photolysis may be involved in bloom initiation. Subsequently a different, and largely particle associated, community thrives during the bloom maximum and decline. Perhaps this community represents a mutualistic iron for carbon arrangement as recently proposed (Gärdes et al., 2013). Clearly further detailed studies will be needed to further address this hypothesis.

3.6 CONCLUSIONS

We studied the correlation between the presence of bacteria producing one of four photoactive siderophores relative to total bacterial and dinoflagellate numbers from local surface water at the Scripps Pier before, during, and after summer bloom of the dinoflagellate *L. polyedrum*. The following are the conclusions obtained from this study.

- Using biochemical techniques such as qPCR to quantify the genes encoding for photoactive siderophore biosynthesis in marine bacteria has great potential to serve as surrogates for the presence of such siderophores in the marine environment.
- Photoactive siderophore producing bacteria are relatively abundant representing 1-9% of the total bacterial population and thus they have the potential to alter the bioavailability of iron in marine environments.

- Vibrioferrin, a uniquely photoreactive siderophore, was by far the most abundant photoactive siderophore produced at all time points.
- The community of photoactive siderophores produced by free living bacteria just prior to the dinoflagellate bloom was significantly different than those found during bloom maximum and decline. This suggests that they could be providing a source of bioavailable iron, which in turn could be involved in dinoflagellate bloom initiation.

We hope these findings will aid us in gauging the importance of photoactive siderophores in the marine environment in general and harmful algal bloom dynamics in particular.

3.7 ACKNOWLEDGEMENTS

This work was funded by NOAA Grants #NA04OAR4170038 and NA08OAR4170669, California Sea Grant College Program Project numbers R/CZ-198 and R/CONT-205 and NSF grant CHE-0924313.

Chapters 3 is in part reprints of the materials published in paper: Yarimizu, K., Polido, G., Gardes, A., Carter, M. L., Hilbern, M., & Carrano, C. J. (2014). Evaluation of photo-reactive siderophore producing bacteria before, during and after a bloom of the dinoflagellate *Lingulodinium polyedrum*. *Metallomics, 6*, 1156-1163.

Table 3 Free-living (0.2 μm membrane) *16S* containing bacteria gene copy number

Time Point	Ct	SQ	Dilution Factor	SQ x Dilution Factor	SQ (filtration correction)	Gene Copy/ L	Mean Gene Copy /L*
2011/7/28	37.05	0.0062	500	3.11	5.31	1.7E+09	1.8E+09
	36.95	0.0067	500	3.33	5.69	1.8E+09	
2011/9/23	35.87	0.0134	500	6.70	17.77	5.7E+09	5.6E+09
	35.92	0.0130	500	6.50	17.24	5.5E+09	
2011/10/2	33.50	0.0620	500	31.00	65.96	2.1E+10	2.2E+10
	33.40	0.0661	500	33.05	70.32	2.3E+10	
2011/10/5	38.31	0.0028	500	1.38	2.22	7.1E+08	8.5E+08
	37.82	0.0038	500	1.90	3.05	9.8E+08	
2011/10/9	32.46	0.1220	20	2.44	4.98	1.6E+09	1.6E+09
	32.37	0.1290	20	2.58	5.27	1.7E+09	
2011/10/12	30.14	0.5470	20	10.94	17.50	5.6E+09	5.2E+09
	30.41	0.4590	20	9.18	14.69	4.7E+09	
2011/10/19	40.20	0.0008	20	0.02	0.03	8.9E+06	1.2E+07
	39.36	0.0014	20	0.03	0.05	1.5E+07	
2011/10/30	36.74	0.0076	20	0.15	0.21	6.9E+07	7.1E+07
	36.65	0.0081	20	0.16	0.23	7.3E+07	

The average dsDNA MW is assumed here to be 650 for marine bacteria. The genome size of free-living bacteria is assumed to be 1.6MB. The average genome mass of free living bacteria is thus 650 x 1.6 MB / (6.022×10^{-23}) = 1.727×10^{-6} ng/genome. For the free living fraction, there are average of 1.8 x 16S rRNA copies per genome. Thus, the gene copy number /mL sample = SQ in ng/mL / (1.727×10^{-6}) /1.8. The Gene copy number was then converted to per L (x1000).

Table 4 Particle associated (0.8 μm membrane) *16S* containing bacteria gene copy number

Time Point	Ct	SQ	Dilution Factor	SQ x Dilution Factor	SQ (filtration correction)	Gene Copy/ L	Mean Gene Copy /L*
2011/7/28	35.24	0.0202	500	10.10	17.25	3.0E+09	2.7E+09
	35.49	0.0171	500	8.55	14.60	2.5E+09	
2011/9/23	33.29	0.0712	500	35.60	94.40	1.6E+10	1.5E+10
	33.46	0.0638	500	31.90	84.59	1.5E+10	
2011/10/2	31.10	0.2930	500	146.50	294.68	5.1E+10	5.2E+10
	31.02	0.3080	500	154.00	309.77	5.3E+10	
2011/10/5	33.92	0.0472	500	23.60	37.96	6.5E+09	7.3E+09
	33.58	0.0591	500	29.55	47.53	8.2E+09	
2011/10/9	27.44	3.1500	50	157.50	306.25	5.3E+10	5.5E+10
	27.28	3.4900	50	174.50	339.31	5.8E+10	
2011/10/12	34.58	0.0308	50	1.54	2.46	4.2E+08	4.0E+08
	34.80	0.0268	50	1.34	2.14	3.7E+08	
2011/10/19	34.24	0.0384	50	1.92	3.27	5.6E+08	5.4E+08
	34.39	0.0349	50	1.75	2.97	5.1E+08	
2011/10/30	26.45	5.9700	50	298.50	409.47	7.0E+10	6.8E+10
	26.54	5.6100	50	280.50	384.77	6.6E+10	

The average dsDNA MW is assumed to be 650 for marine bacteria. The genome size of particle associated bacteria is 3.0 MB. The average genome mass of particle associated bacteria is thus 650 x 3.0 MB / (6.022×10^{-23}) = 3.238×10^{-6} ng/genome. For the particle associated fraction, there are average of 1.8 x 16SrRNA copies per genome. Thus, the gene copy number /mL sample = SQ in ng/mL / (3.238×10^{-6}) /1.8. The Gene copy number was then converted to per L (x1000).

Table 5 Free-living (0.2 μm membrane) *pvsB* containing bacteria gene copy number

Time Point	Ct	SQ	SQ (filtration correction)	Gene Copy /L	Mean Gene Copy /L*
2011/7/28	28.47	0.0281	0.0480	9.9E+06	1.0E+07
	28.43	0.0285	0.0487	1.0E+07	
	28.30	0.0299	0.0511	1.1E+07	
2011/9/23	30.43	0.0135	0.0358	7.4E+06	7.2E+06
	30.56	0.0129	0.0342	7.1E+06	
	30.53	0.0130	0.0345	7.1E+06	
2011/10/2	25.22	0.0940	0.2000	4.1E+07	4.3E+07
	25.07	0.0997	0.2121	4.4E+07	
	25.11	0.0982	0.2089	4.3E+07	
2011/10/5	29.67	0.0180	0.0290	6.0E+06	4.2E+06
	31.22	0.0101	0.0162	3.4E+06	
	31.42	0.0094	0.0151	3.1E+06	
2011/10/9	29.77	0.0173	0.0353	7.3E+06	7.1E+06
	30.15	0.0150	0.0306	6.3E+06	
	29.64	0.0181	0.0369	7.6E+06	
2011/10/12	28.34	0.0294	0.0470	9.7E+06	8.7E+06
	28.82	0.0246	0.0394	8.1E+06	
	28.79	0.0249	0.0398	8.2E+06	
2011/10/19	35.43	0.0021	0.0036	7.4E+05	4.3E+05
	38.39	0.0007	0.0012	2.5E+05	
	37.72	0.0009	0.0015	3.2E+05	
2011/10/30	36.56	0.0014	0.0019	4.0E+05	8.5E+05
	34.11	0.0034	0.0048	1.0E+06	
	33.69	0.0040	0.0056	1.2E+06	

The average dsDNA MW for DG893 is 660.. The genome size of DG893 is 4.41MB. The genome mass of DG893 is thus 660 x 4.41 MB / (6.022×10^{-23}) = 4.833×10^{-6} ng/genome. The gene copy number /mL sample = SQ in ng/mL / (4.833×10^{-6}). The Gene copy number was then converted to per L (x1000).

Table 6 Particle associated (0.8 μm membrane) *pvsB* containing bacteria gene copy number

Time Point	Ct	SQ	SQ (filtration correction)	Gene Copy/ L	Mean Gene Copy /L*
2011/7/28	24.72	0.1130	0.1930	4.0E+07	3.9E+07
	24.78	0.1110	0.1895	3.9E+07	
	24.82	0.1090	0.1861	3.9E+07	
2011/9/23	26.21	0.0651	0.1726	3.6E+07	3.5E+07
	26.26	0.0639	0.1694	3.5E+07	
	26.21	0.0650	0.1724	3.6E+07	
2011/10/2	20.99	0.4550	0.9152	1.9E+08	1.8E+08
	21.17	0.4250	0.8549	1.8E+08	
	21.21	0.4190	0.8428	1.7E+08	
2011/10/5	25.47	0.0857	0.1379	2.9E+07	2.8E+07
	25.66	0.0798	0.1284	2.7E+07	
	25.45	0.0865	0.1391	2.9E+07	
2011/10/9	22.01	0.3120	0.6067	1.3E+08	1.2E+08
	N/A	0.0000	0.0000	0.0E+00	
	22.47	0.2620	0.5094	1.1E+08	
2011/10/12	27.13	0.0463	0.0741	1.5E+07	1.2E+07
	29.58	0.0185	0.0296	6.1E+06	
	27.36	0.0424	0.0678	1.4E+07	
2011/10/19	25.62	0.0810	0.1380	2.9E+07	2.7E+07
	25.89	0.0735	0.1252	2.6E+07	
	25.89	0.0734	0.1250	2.6E+07	
2011/10/30	21.32	0.4020	0.5514	1.1E+08	1.1E+08
	21.39	0.3920	0.5377	1.1E+08	
	21.33	0.4000	0.5487	1.1E+08	

The average dsDNA MW of *DG893* is 660. The genome size of *DG893* 4.41MB. The genome mass of *DG893* is thus 660 x 4.41 MB / (6.022×10^{23}) = 4.833×10^{-6} ng/genome. The gene copy number /mL sample = SQ in ng/mL / (4.833×10^{-6}).The Gene copy number was then converted to per L (x1000). The red highlight is apparent outlier and eliminated from analysis. The red highlight is apparent outlier and eliminated from analysis.

Table 7 Free-living (0.2 μm membrane) *vibXII* containing bacteria gene copy number

Time Point	Ct	SQ	SQ (filtration correction)	Gene Copy/L	Mean Gene Copy /L*
2011/7/28	35.58	0.1210	0.2066	1.2E+08	1.2E+08
	35.31	0.1420	0.2425	1.4E+08	
	36.08	0.0893	0.1525	8.8E+07	
2011/9/23	38.65	0.0189	0.0501	2.9E+07	3.1E+07
	38.39	0.0220	0.0583	3.4E+07	
	38.54	0.0202	0.0536	3.1E+07	
2011/10/2	33.26	0.4880	1.0383	6.0E+08	6.5E+08
	33.22	0.5000	1.0638	6.2E+08	
	32.93	0.5990	1.2745	7.4E+08	
2011/10/5	38.12	0.0260	0.0418	2.4E+07	1.5E+07
	39.25	0.0131	0.0211	1.2E+07	
	39.64	0.0104	0.0167	9.7E+06	
2011/10/9	37.71	0.0333	0.0680	3.9E+07	4.4E+07
	37.39	0.0405	0.0827	4.8E+07	
	37.48	0.0382	0.0780	4.5E+07	
2011/10/12	35.28	0.1440	0.2304	1.3E+08	1.2E+08
	35.47	0.1290	0.2064	1.2E+08	
	35.64	0.1160	0.1856	1.1E+08	
2011/10/19	N/A	0.0000	0.0000	0.0E+00	0.0E+00
	N/A	0.0000	0.0000	0.0E+00	
	N/A	0.0000	0.0000	0.0E+00	
2011/10/30	39.69	0.0100	0.0140	8.1E+06	4.6E+06
	41.76	0.0029	0.0040	2.3E+06	
	41.13	0.0042	0.0059	3.4E+06	

The average dsDNA MW used here was 650 . The genome size of free-living bacteria was assumed to be 1.6MB. The average genome mass of free living bacteria is thus 650 x 1.6 MB / (6.022×10^{-23}) = 1.727×10^{-6} ng/genome. The gene copy number /mL sample = SQ in ng/mL / (1.727×10^{-6}). The Gene copy number was then converted to per L (x1000). The red highlight is apparent outlier and eliminated from analysis.

Table 8 Particle associated (0.8 µm membrane) *vibXII* containing bacteria gene copy number

Time Point	Ct	SQ	SQ (filtration correction)	Gene Copy/ L	Mean Gene Copy /L*
2011/7/28	32.19	0.9360	1.5984	4.9E+08	4.7E+08
	32.23	0.9130	1.5591	4.8E+08	
	32.37	0.8390	1.4327	4.4E+08	
2011/9/23	32.79	0.6490	1.7209	5.3E+08	4.8E+08
	33.25	0.4940	1.3099	4.0E+08	
	32.91	0.6050	1.6042	5.0E+08	
2011/10/2	30.82	2.1300	4.2845	1.3E+09	1.4E+09
	30.71	2.2800	4.5862	1.4E+09	
	30.64	2.3800	4.7874	1.5E+09	
2011/10/5	31.58	1.3500	2.1716	6.7E+08	6.9E+08
	31.63	1.3100	2.1072	6.5E+08	
	31.42	1.4800	2.3807	7.4E+08	
2011/10/9	34.13	0.2890	0.5619	1.7E+08	1.4E+08
	34.45	0.2380	0.4628	1.4E+08	
	34.91	0.1810	0.3519	1.1E+08	
2011/10/12	34.61	0.2160	0.3456	1.1E+08	7.1E+07
	37.46	0.0386	0.0618	1.9E+07	
	34.96	0.1750	0.2800	8.6E+07	
2011/10/19	34.14	0.2870	0.4888	1.5E+08	1.4E+08
	34.39	0.2480	0.4224	1.3E+08	
	34.41	0.2450	0.4173	1.3E+08	
2011/10/30	32.23	0.9110	1.2497	3.9E+08	3.6E+08
	32.07	1.0000	1.3717	4.2E+08	
	32.76	0.6610	0.9067	2.8E+08	

The average dsDNA MW used here was 650. The genome size of particle associated bacteria was assumed to be 3MB. The average genome mass of particle associated bacteria is thus 650 x 3 MB / (6.022×10^{-23}) = 3.238×10^{-6} ng/genome. The gene copy number /mL sample = SQ in ng/mL / (3.537×10^{-6}). The Gene copy number was then converted to per L (x1000).

Table 9 Free-living (0.2 μm membrane) *asbEII* containing bacteria gene copy number

Time Point	Ct	SQ	SQ (filtration correction)	Gene Copy /L	Mean Gene Copy /L*
2011/7/28	34.68	0.0035	0.0060	3.5E+06	3.6E+06
	34.57	0.0037	0.0064	3.7E+06	
	36.02	0.0019	0.0032	1.8E+06	
2011/9/23	39.78	0.0003	0.0008	4.7E+05	5.6E+05
	39.52	0.0003	0.0009	5.3E+05	
	38.95	0.0005	0.0012	6.9E+05	
2011/10/2	36.87	0.0012	0.0026	1.5E+06	1.6E+06
	36.78	0.0013	0.0027	1.6E+06	
	36.79	0.0013	0.0027	1.6E+06	
2011/10/5	40.96	0.0002	0.0003	1.6E+05	1.9E+05
	40.85	0.0002	0.0003	1.7E+05	
	40.19	0.0002	0.0004	2.3E+05	
2011/10/9	40.03	0.0003	0.0005	3.2E+05	4.4E+05
	39.15	0.0004	0.0008	4.9E+05	
	39.04	0.0004	0.0009	5.1E+05	
2011/10/12	39.10	0.0004	0.0007	3.9E+05	5.0E+05
	38.37	0.0006	0.0010	5.5E+05	
	38.32	0.0006	0.0010	5.7E+05	
2011/10/19	42.24	0.0001	0.0002	9.1E+04	1.2E+05
	41.54	0.0001	0.0002	1.3E+05	
	41.40	0.0001	0.0002	1.4E+05	
2011/10/30	41.00	0.0002	0.0002	1.4E+05	1.7E+05
	40.62	0.0002	0.0003	1.6E+05	
	40.07	0.0003	0.0004	2.1E+05	

The average dsDNA MW used here was 650 . The genome size of free-living bacteria was assumed to be 1.6MB. The average genome mass of free living bacteria is thus 650 x 1.6 MB / (6.022×10^{-23}) = 1.727×10^{-6} ng/genome. The gene copy number /mL sample = SQ in ng/mL / (1.727×10^{-6}). The Gene copy number was then converted to per L (x1000). The red highlight is apparent outlier and eliminated from analysis.

Table 10 Particle associated (0.8 μm membrane) *asbEII* containing bacteria gene copy number

Time Point	Ct	SQ	SQ (filtration correction)	Gene Copy/ L	Mean Gene Copy /L*
2011/7/28	35.44	0.0025	0.0042	1.3E+06	1.1E+06
	36.33	0.0016	0.0027	8.4E+05	
	35.59	0.0023	0.0039	1.2E+06	
2011/9/23	37.57	0.0009	0.0023	7.2E+05	9.4E+05
	35.96	0.0019	0.0051	1.6E+06	
	38.14	0.0007	0.0018	5.5E+05	
2011/10/2	36.78	0.0013	0.0026	8.0E+05	9.8E+05
	36.13	0.0018	0.0036	1.1E+06	
	36.26	0.0017	0.0033	1.0E+06	
2011/10/5	37.69	0.0008	0.0013	4.1E+05	3.9E+05
	37.80	0.0008	0.0013	3.9E+05	
	37.95	0.0007	0.0012	3.6E+05	
2011/10/9	36.81	0.0013	0.0025	7.6E+05	7.0E+05
	37.05	0.0011	0.0022	6.8E+05	
	37.07	0.0011	0.0022	6.7E+05	
2011/10/12	38.83	0.0005	0.0008	2.4E+05	1.5E+05
	43.40	0.0001	0.0001	2.6E+04	
	39.47	0.0004	0.0006	1.7E+05	
2011/10/19	38.12	0.0007	0.0011	3.6E+05	3.0E+05
	38.50	0.0006	0.0010	2.9E+05	
	38.75	0.0005	0.0008	2.6E+05	
2011/10/30	33.24	0.0071	0.0098	3.0E+06	2.6E+06
	33.73	0.0056	0.0077	2.4E+06	
	33.59	0.0060	0.0083	2.6E+06	

The average dsDNA MW used here was 650. The genome size of particle associated bacteria was assumed to be 3MB. The average genome mass of particle associated bacteria is thus 650 x 3 MB / (6.022×10^{-23}) = 3.238×10^{-6} ng/genome. The gene copy number /mL sample = SQ in ng/mL / (3.537×10^{-6}). The Gene copy number was then converted to per L (x1000).

CHAPTER 4. IRON UPTAKE AND STORAGE IN THE HAB DINOFLAGELLATE LINGULODINIUM POLYEDRUM

4.1 ABSTRACT

The iron uptake and storage systems of terrestrial/higher plants are now reasonably well understood with two basic strategies being distinguished: Strategy I involves the induction of an Fe(III)-chelate reductase (ferrireductase) along with Fe(II) or Fe(III) transporter proteins while strategy II plants have evolved sophisticated systems based on high-affinity, iron specific, binding compounds called phytosiderophores. In contrast, there is little knowledge about the corresponding systems in marine, plant-like lineages. Herein we report a study of the iron uptake and storage mechanisms in the harmful algal bloom (HAB) dinoflagellate *Lingulodinium polyedrum*. *L. polyedrum* is an armored dinoflagellate with a mixotrophic lifestyle and one of the most common bloom species on Southern California coast widely noted for its bioluminescent properties and as a producer of yessotoxins. Short term radio-iron uptake studies indicate that iron is taken up by *L. polyedrum* in a time dependent manner consistent with an active transport process. Based on inhibitor and other studies it appears that a reductive-oxidative pathway such as that found in yeast and the green alga *Chlamydomonas reinhardtii* is likely. Of the various iron sources tested vibrioferrin, a photoactive and relatively weak siderophore produced by potentially mutualistic *Marinobacter* bacterial species, was the most efficient. Other more stable and non-photoactive siderophores such as ferrioxamine E were ineffective. Several pieces of data including long term exposure to ^{57}Fe using Mössbauer spectroscopy suggest that *L. polyedrum*

does not possess an iron storage system but rather presumably relies on an efficient iron uptake system, perhaps mediated by mutualistic interactions with bacteria.

4.2 INTRODUCTION

Algae are autotrophic, plant-like organisms, most of which live in aquatic environments and all of which lack the typical structure (roots-stem-leaves) and tissues of terrestrial plants. Marine algae are critically important plant-like members of the ocean community which affect not only primary productivity but influence climate by controlling processes such as biogenic calcification, oceanic sequestration of CO_2 and biological release of dimethylsulfide. In addition many microalgae (phytoplankton), including the climatically important diatoms, dinoflagellates and coccolithophores, can form blooms that have occurred with increasing frequency in recent decades. Some of the blooming species have been found to produce endogenous toxins and such harmful algae blooms (HABs) can directly and indirectly cause acute effects on marine ecosystems leading to major impacts on local economies and public health (Lewitus et al., 2012). Direct human health effects derive from consumption of bivalves that have ingested toxic phytoplankton and accumulated toxins leading to paralytic, diarrheic, and neurotoxic poisoning syndromes that can in some cases be fatal (Anderson 1994; Honner et al., 2012). Indirect impacts of HABs include impairment of water quality leading to losses in the tourism and recreational industries. Even blooming phytoplankton that do not produce toxins can be harmful and cause ecological impacts such as the displacement of indigenous species, habitat alteration, or oxygen depletion (Glibert et al., 2005). The economic effects caused by HABs in the U.S. were estimated at $82 million per year in 2006 (Hoagland and Scatasta, 2006). The issue is how these HABs are initiated is not well understood and therefore the current strategy to reduce these

impacts caused by HABs relies on frequent coastal monitoring and early detection of HAB species and toxin levels.

Whether the factors promoting HABs are anthropogenic or have natural sources is an ongoing debate. Some argue oceanographic events such as upwelling, reversal and relaxation of winds, and global climate change are the major factors initiating phytoplankton blooms (Roegner et al., 2002; Tweddle et al., 2010). Others consider HABs the result of human activities such as increased nutrient loading, changes in agriculture, overfishing, and ballast water discharge (Glibert, 2005). Some simply believe that improved tools are leading to increased detection of HAB species (Burkholder, 1998). Nevertheless, HABs are a global threat to living marine resources and human health. While many studies focus on finding the causes of HABs from these perspectives fewer have paid attention to the possible effects that bacterial species that coexist with phytoplankton could contribute to their growth. However, since Bell and Mitchell reported that specific microflora were maintained and microbial activity was altered in the phycosphere (Bell and Mitchell, 1972; Bell and Lang, 1974), an increasing number of studies have suggested that the interactions between phytoplankton and bacteria are in fact very specific and important (Azam and Malfatti, 2007; Amin et al., 2015; Bertrand et al., 2015; Ramanan et al., 2016). It has been postulated that the mutualistic association of some phytoplankton and bacteria is driven by nutrient exchange. While nitrogen and phosphorus are the most often studied nutrients in this regard, the exact interactions involving these nutrients are not well understood (Hallegraeff and Gollasch, 2006). Our hypothesis is that certain bacteria may affect algal growth and bloom dynamics by their control of iron, a trace element known to be growth limiting to phytoplankton in many marine environments (Martin and Fitzwater, 1988; Maldonado et al., 2005; Croot and Heller, 2012).

Iron is an essential element for all living organisms due to its ubiquitous role in redox and other enzymes, especially in the context of respiration and photosynthesis. The iron uptake and storage systems of terrestrial/ higher plants are now reasonably well understood with two basic strategies for iron uptake being distinguished: Strategy I plants, mainly dicotyledons, use a mechanism involving soil acidification and induction of Fe(III)-chelate reductase (ferrireductase) and Fe(II) transporter protein (Moog and Bruggemann, 1994; Robinson et al., 1999). Strategy II plants (in particular, monocotyledons/grasses) have evolved sophisticated systems, similar to those of bacteria and fungi, based on high-affinity, iron specific, binding compounds called phytosiderophores (Römheld and Marschner, 1986). These molecules are functionally, although not structurally, similar to the extensively studied "siderophores" produced by bacteria and fungi.

In contrast, there is far less knowledge about the corresponding systems in marine, plant-like lineages. The Chlorophyta and the Bacillariophyceae are the two best studied groups of algae. Many, although not all, of these marine eukaryotes including the green algae, *Chlamydomonas reinhardtii* and *Tetraselmis suecica* and some of the diatoms clearly involve an initial reductive step involving homologs to the genetically encoded inducible cell surface reductase FRO2 from Arabodopsis (Kustka et al., 2007). This is then followed either by direct uptake of the reduced Fe(II) via an Fe(II) permease or an analog as in the pennate diatom *P. tricornutum* or reoxidation of the Fe(II) by a multi-copper oxidase and transport across the membrane as Fe(III) as in the centric diatom *T. pseudonana* (Kustka et al., 2007). These microalgae are also unique, perhaps because they have been the most heavily studied, in also having a wide variety of non-reductive pathways that have been identified including some based on siderophores or siderophore-like molecules and others involving transferrin-like (Fontaine et al., 2002) or surface binding proteins designated iron starvation induced protein, ISIPs (Sutak et

al., 2012). Among the Haptophyta (coccolithophores) such as *Emiliana huxleyi* a non-reductive uptake path appears probable (Hartnett et al., 2012). A reductive-oxidative pathway and the importance of cell surface binding of iron in the process, has also been confirmed for the macro brown algae *Ectocarpus siliculosus* (Böttger et al., 2012; Miller et al., 2014) and *Macrocystis pyrifera* (Miller et al., 2016).

However among the marine microalgae the dinoflagellates appear to be among the least studied, likely due to the dearth of genomic data available for these organisms which typically have very large and complex genomes. Hence this report presents an in vitro study of the iron uptake and storage systems in the HAB dinoflagellate *Lingulodinium polyedrum*. *L. polyedrum* is an armored dinoflagellate with a mixotrophic lifestyle and one of the most common bloom species occurring along the Southern California coast (Figure 10) widely noted for its bioluminescent properties and as a producer of yessotoxins (Lewitus et al., 2012).

4.3 MATERIALS AND METHODS

4.3.1 Chemicals and reagents

The followings were purchased from Sigma-Aldrich: antibiotics (Penicillin/Streptomycin/Neomycin, P4083-100ML), $^{56}FeCl_3.6H_2O$ (MW270.30, 10025-77-1), sodium azide (NaN_3, MW65.01, S2002-5G), carbonyl cyanide m-chlorophenyl hydrazone (CCCP, MW204.62, C2759-100MG), L-ascorbic acid (ascorbate, MW176.12, A92902-25G), Ethylenediamine-N,N'-bis(2-hydroxyphenylacetic acid) (EDDHA, MW360.36, 1170-02-1). The followings were purchased from Fisher Scientific: $Na_4EDTA.2H_2O$ (MW416.20, BP121-500), 2-Hydroxypropane-1,2,3-tricarboxylic acid (citric acid, MW192.13, A940-500). Other purchased chemicals are as follows: $^{55}FeCl_3$ radionuclide (PerkinElmer, NEZ043), 3-(2-Pyridyl)-5,6-diphenyl-1,2,4-triazine-p,p-disulfonic acid disodium salt hydrate (ferrozine, Acros, MW514.45,

171010010), Sep-Pak® 3cc (200mg) C18 cartridges (Waters, WAT054945). Vibrioferrin (VF) was isolated as previously described (Amin et al., 2007) and desferrioxamine E was a gift of Professor G. Winkelmann, University of Tübingen, Germany.

4.3.2 Algae growth and maintenance

Seawater was collected from local Scripps Pier (N32°86', W117°25', San Diego, CA) and filtered immediately through a 0.22 μm pore size membrane. The filtered seawater was mixed with approximately 0.005% of metal free hydrochloric acid, autoclaved for 30 min, cooled at ambient temperature for 24 hours, and stored in 5°C until use. The pH of the autoclaved seawater was confirmed to be between 8.0 and 8.2 at ambient temperature. *L. polyedrum* strain was isolated from Venice beach California and kindly provided to us by Avery Tatters (University of Southern California). *L. polyedrum* cells were maintained in an autoclaved 1 liter Erlenmeyer flask containing L1 media enriched sterile seawater capped with a ventilation sponge. The cells were grown under 100 μmol photons m^{-2} s^{-1} on a 12 hours alternating light and dark cycle and temperature of 20±2 °C. The upper portion of culture containing healthy *L. polyedrum* cells was diluted 1/5 with L1 enriched sterile seawater every three weeks. Algal growth was monitored by direct cell count using an inverted microscope (Nikon Eclipse TE2000-U, 40X).

4.3.3 Preparation of iron deficient and sufficient *L. polyedrum*

To measure iron uptake only by *L. polyedrum* and to eliminate the possibility of uptake by any associated bacteria, prior to all experiments, the culture containing 10^4-10^5 cells per mL of *L. polyedrum* was treated with 0.1% (v/v) mixed antibiotics for 24 hours. The antibiotics treated culture was gently centrifuged for a few seconds and the pellet was washed three times and re-suspended to the appropriate volume with sterile seawater enriched with either L1 media

with total iron concentration of 1,000 nM $[Fe]_T$ (total added iron concentration) or L1 media without iron to prepare iron sufficient or iron deficient cells, respectively. The cells were incubated under the iron sufficient or deficient conditions for 7-10 days prior to use.

4.3.4 Iron uptake

The details of iron uptake experiments were described in Appendix K to Appendix N. The following are brief summary of experimental procedures. $^{55}FeCl_3$ radionuclide was obtained from Perkin-Elmer. FeEDTA was prepared at molar ratio of EDTA: Fe = 10:1 and ^{56}Fe:^{55}Fe = 140:1. Iron starved axenic *L. polyedrum* culture >10^4 cells/mL was incubated in FeEDTA at 10 μM $[Fe]_T$. Two mL of incubated culture containing roughly 10^4 cells were filtered through a 0.8 μm membrane at each target time-point. Membranes containing cells were washed with 15 mL sterile seawater and placed in scintillation vials. Fifteen mL of Hionic Fluor scintillation fluid was added to each vial and mixed well. The ^{55}Fe taken up was measured on a Beckman-Coulter LS 6500 scintillation counter using the tritium channel. Total iron uptake per cell of *L. polyedrum* was calculated based on specific activity, measured count rates, scintillation counting efficiency, and cell density. It should be noted that the filtered cells were initially washed with titanium (III) citrate EDTA as described in Hudson and Morel (1989) to remove any potentially surface bound iron. However this treatment appeared to damage the cells and thus, all experiments were performed without a titanium wash. For inhibition studies, the following potential inhibitors were added to cultures one hour prior to inoculation with $^{55/56}FeEDTA$: 100 μM ascorbate, 2.5 mM sodium azide and 25 μM carbonyl cyanide 3-chlorohydrazine (CCCP).

4.3.5 Cell surface reductase activity

The experiment was slightly modified from the method described in Shaked et al. (2004). The modified protocol is described in Appendix O. The both iron deficient and sufficient *L.*

polyedrum cultures were incubated with 100 μM ferrozine for 1 hour prior to inoculation with $^{55/56}$FeEDTA. A negative control consisted of 5 mL of seawater containing 10 μM $^{55/56}$Fe, 30 μM EDTA, and 100 μM ferrozine while a positive control was prepared from 5 mL of seawater containing 10 μM $^{55/56}$Fe, 30 μM EDTA, 1 mM L-ascorbate, and 100 μM ferrozine. The samples were incubated under white light for 7 hours. The samples were filtered through 5.0 μm membrane to remove cells. For each sample, 4 mL of the filtrate containing Fe(II)-FZ_3 was passed through C18 Sep-Pak cartridges placed in 15-mL Falcon tube using gentle centrifugation. The column-retained Fe(II)-FZ_3 was washed with 10 mL of sterile seawater mixed with 0.005M HCl and eluted with 5 mL of methanol by gentle centrifugation. The eluant was placed in a scintillation vial, methanol removed by drying in a 44 °C oven overnight, 15 mL of Hionic Fluor scintillation fluid added to the residue and ^{55}Fe(II)-FZ3 measured on a Beckman Coulter LS 6500 scintillation counter using the tritium channel.

4.3.6 Transmission Mössbauer spectroscopy (TMS)

For iron storage studies, *L. polyedrum* was harvested and cultured in for 3 weeks in 1 μM ^{57}FeEDTA enriched sterile seawater. Roughly $5x10^5$ cells were then harvested rinsed thoroughly with sterile seawater and packed into Delrin® Mössbauer sample holders. The Mössbauer spectra were recorded in the horizontal transmission geometry using a constant acceleration spectrometer operated in conjunction with a 512-channel analyzer in the time-scale mode (WissEl GmbH). The detector consisted of a proportional counter and the source consisted of 1.4 GBq [^{57}Co] diffused in Rh and was at room temperature. The spectrometer was calibrated against α-iron at room temperature (RT). For measurements at 77K, samples were placed in a continuous-flow cryostat (Oxford Instruments). Spectral data were transferred from the multi-

channel analyzer to a PC for further analysis employing the public domain program Vinda running on an Excel 2003® platform.

4.4 RESULTS

4.4.1 Algal growth

Growth curves were measured for *L. polyedrum* both under iron sufficient and iron deficient conditions. Optimum growth occurred with a $[Fe]_T$ of 1000 nM. Higher concentrations exerted a toxic effect and substantially decreased growth. Iron deficient conditions ($[Fe]_T$ 0-100 nM) also resulted in a markedly decreased growth rates even in the first generation (Figure 18). Thus while the specific growth rate under iron sufficiency was ca. 500 cells/mL/day, iron deficient conditions resulted in a greatly decreased growth rate of 20 cells/mL/day.

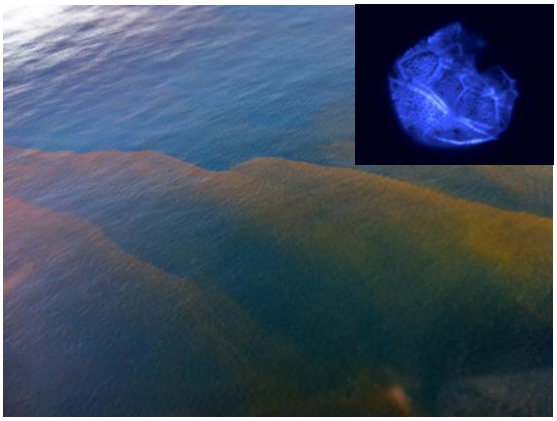

Figure 18 Image of Scripps pier bloom and its bloom species, *L. polyedrum*
L. polyedrum bloom in Scripps Pier in 2011: photo credit for Eddie Kisfaludy © SciFly LLC and Melissa Carter from Scripps Institute of Oceanography. Inset*: L. polyedrum* cell image stained with premixed calcofluor and antifade and photographed with Leica DMRBE microscope at 100X.

4.4.2 Iron uptake

Iron from FeEDTA was taken up by iron deficient *L. polyedrum* in a time dependent manner. The uptake was approximately linear with a rate of 2.0 x 10-3 ng Fe/cell/hr for first 7 hours (Figure 19) and continued, albeit more slowly, over 24 hours. The iron uptake rate by iron

sufficient *L. polyedrum* was similar to that of the iron deficient cells for first 7 hours but appeared to saturate after this point with little or no further uptake over a 24 hr period. The uptake process appeared to be an active one as it was inhibited by a number of metabolic poisons or environmental effects. Thus pretreatment of *L. polyedrum* cells with metabolic poisons, sodium azide or CCCP, resulted in reduction of uptake by approximately 75% and 88%, respectively (Figure 20) while those pretreated with ascorbate or incubated on ice throughout the experiment showed virtually 100% inhibition of iron uptake.

The iron uptake by *L. polyedrum* from various iron sources was also investigated. Iron complexed with either citrate or the siderophore vibrioferrin (VF) were taken up at a much faster rate than that from the iron complex with EDTA while essentially no uptake of iron from either of the highly thermodynamically stable FeEDDHA or ferrioxamine E was seen (Figure 21). Of the various iron sources tested VF was the most efficient. Since VF is known to be a photoactive siderophore the effect of light on FeVF uptake was examined, however unlike the situation seen in *Scrippsiella trochoidea* (Amin et al., 2009), there was no significant difference observed in iron uptake by *L. polyedrum* from FeVF in the light or dark.

When FeEDTA was used as an iron source, it is generally thought that the intact FeEDTA complex is not a biological substrate but rather it merely serves as an iron buffer maintaining a fixed concentration of free soluble Fe(III) at equilibrium while preventing the precipitation of insoluble Fe oxo-hydroxo polymeric species. To test the suitability of this hypothesis, we looked at the iron uptake rate at a fixed concentration of iron as a function of increasing EDTA to Fe ratio. Increasing the EDTA to Fe ratio should increase the concentration of FeEDTA and decrease the concentration of free Fe(III) at equilibrium. Thus if FeEDTA itself is the biological substrate, the uptake rate should increase while if free Fe(III) is the substrate

then uptake should decrease. Upon going from an EDTA/Fe ratio of 1:1 to 10:1 we observe a decrease in the uptake rate (Figure 22) consistent with the idea that FeEDTA is serving simply as an iron buffer and the species actively involved in uptake is free soluble Fe(III). The situation for FeVF iron uptake by *L. polydrum* seems similar as uptake was reduced as the molar ratio of VF to Fe was increased from 1 to 10. This coupled with the fact that there was no increase in iron uptake from FeVF exposed to light as opposed to the dark suggests that the active species is again free soluble Fe(III).

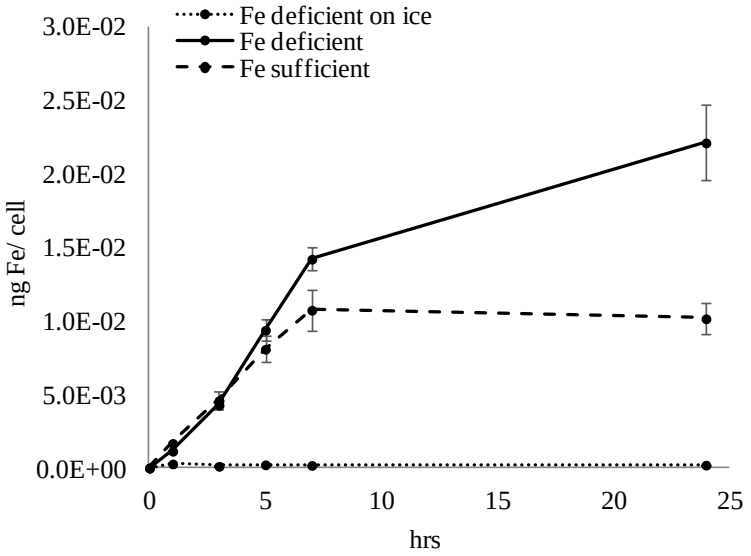

Figure 19 uptake by *L. polyedrum* over 24 hours from 10 µM FeEDTA
The molar ratio was Fe:EDTA = 1:10 where total iron concentration in the culture was 10 µM. The temperature was kept at 20±2 °C except the negative control was remained on ice.

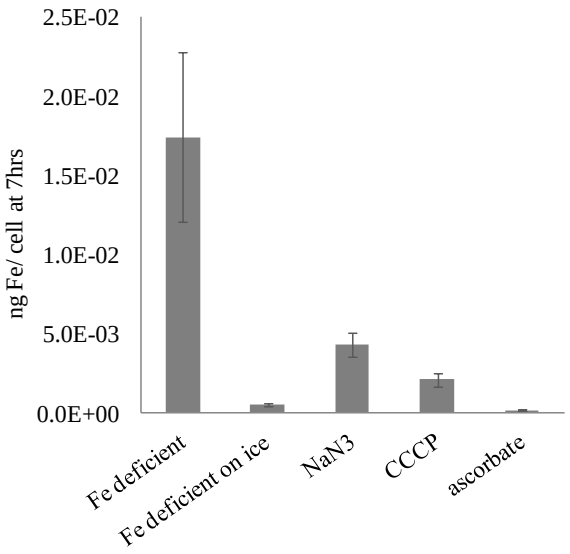

Figure 20 Iron uptake of *L. polyedrum* inhibited by various metabolic inhibitors
Iron uptake of *L. polyedrum* inhibited by various metabolic inhibitors for 7 hours from 10 μM FeEDTA. The iron deficient *L. polyedrum* cells were pretreated with inhibitors NaN_3, CCCP, and ascorbate (for details see text). The temperature was kept at 20±2 °C except the negative control which remained on ice.

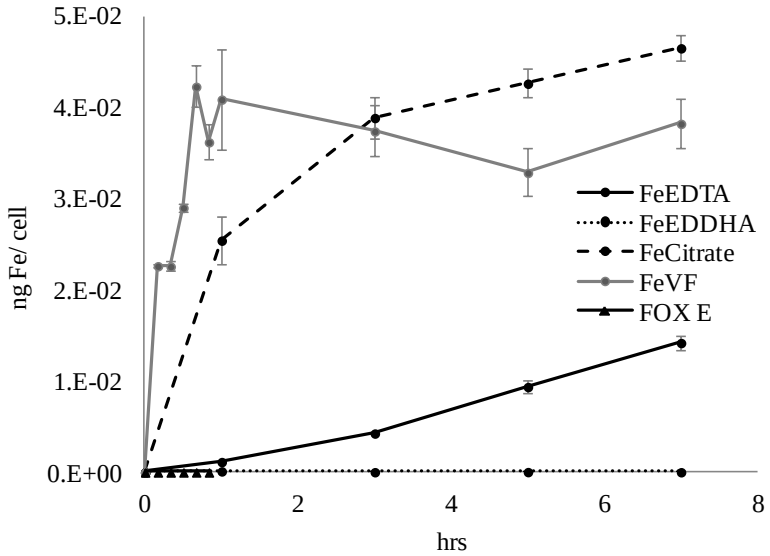

Figure 21 Iron uptake of *L. polyedrum* inhibited from various Fe sources
A) Iron uptake of starved *L. polyedrum* from various Fe sources over 7 hours. The total iron concentration in all solutions was 10 μM. The concentrations of EDTA, EDDHA, and citrate was 100 μM while that of VF was 30 μM and fox E was 10 μM. The temperature was kept at 20±2 °C.

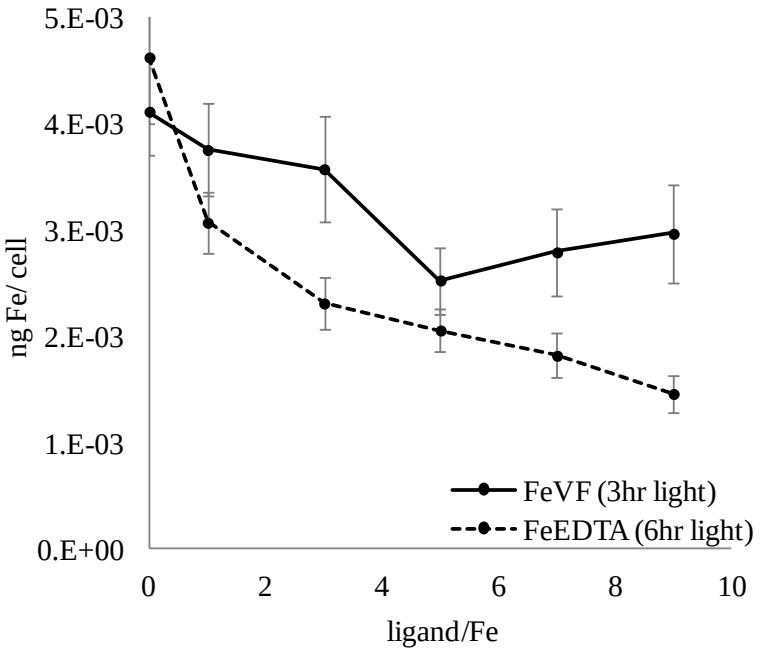

Figure 22 Molar ratio dependent iron uptake from FeEDTA and FeVF by *L. polyedrum*
The concentration of iron was constant 10 µM while that of ligands varied from 10 µM to 90 µM. *L. polydrum* cells were incubated with FeEDTA and FeVF under light. The temperature was kept at 20±2 °C.

4.4.3 Reductase activity

For these experiments *L. polyedrum* cells previously grown under either iron sufficient or deficient conditions were incubated in the presence of 10 µM $^{55/56}$Fe, 30 µM EDTA and 100 µM of the Fe(II) specific chelator ferrozine for 7 hours. Cells were then harvested and the $^{55}Fe(FZ)_3$ complex formed in the supernatant were assayed as previously described (Shaked, 2004; Kranzler, 2011). As can be seen from Figure 23, iron deficient *L. polyedrum* cells were readily capable of reducing Fe(III) in the form of the EDTA complex at a rate of approximately 1.8 x 10-4 ng/cell/hr i.e. commensurate with that of overall iron uptake. Dead cells exhibited no activity indicating that iron reduction was a specific metabolic process rather than a nonspecific one driven by the presence of FZ. Under iron sufficient conditions ferric chelate reduction activity was reduced by over four fold suggesting that the reductase activity is inducible.

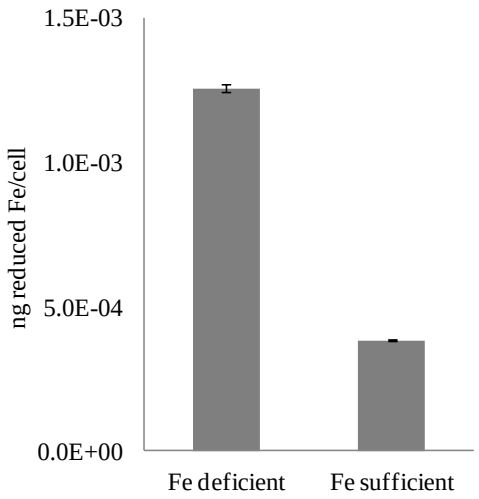

Figure 23 Fe(III) chelate reductase activity for iron deficient and sufficient *L. polyedrum*
Ferrozine, 100 μM, was added to iron deficient and sufficient *L. polyedrum* cultures one hour prior to addition of FeEDTA. The cells were incubated under the condition for 7 hours before analysis.

4.5 DISCUSSION

4.5.1 Cell surface reductase and uptake

In bacteria there are a myriad of uptake systems and acquisition strategies designed to capture iron, many of which are often simultaneously operative in a single organism. These include uptake systems specific for siderophores, or other bound forms of iron (a similar system is also found in strategy II plants) as well as those based on ABC type transporters capable of taking up "free" Fe(III) and other transporters typically more or less specific for ferrous iron (Bauer and Bereczky, 2003; Morrissey and Guerinot, 2009). Model eukaryotes typically adopt iron uptake schemes which involve reduction of Fe(III) to Fe(II) at some point. The first of these mechanisms is a reductive-oxidative pathway such as that found in yeast (Sonier and Weger, 2010). The second is a cell surface reduction/divalent metal permease pathway such as that found in strategy I plants (Weger et al., 2009; Benderliev and Ivanova, 1994; Fisher et al., 1998).

Together the data presented here suggest that iron is rapidly and actively taken up from the media via what is likely a reductive-oxidative pathway similar to that seen in several other

marine algae. However despite some obvious similarities there are also a number of notable differences. Under iron sufficient conditions the uptake process ceases after 7 hours while it continues albeit at a reduced rate, for at least 24 hrs under iron deficient conditions. Additionally while strong cell surface binding appears to be important among many of the marine algae studied (Sutak et al., 2012), it does not appear to be significant for this armored dinoflagellate whose thecal plates are composed mainly of cellulose (data not shown).

Of the various iron sources tested VF, a photoactive and relatively weak siderophore produced by potentially mutualistic *Marinobacter* species (Amin et al., 2009), was the most efficient. Other more thermodynamically stable and non-photoactive siderophores such as ferrioxamine E were ineffective. VF is of particular interest owing to its unique properties. First its Fe(III) complex undergoes rapid photoreduction in the presence of sunlight producing more soluble and bioavailable Fe(II). In addition while most other photoactive siderophores retain the ability to strongly bind Fe(III) even after photolysis the photo-oxidized VF has no further affinity for iron (Amin et al., 2009). Secondly for a proven siderophore it has only relatively weak Fe(III) binding properties as it lacks the sixth donor group required to complete the octahedral coordination geometry preferred by ferric iron (Amin et al., 2009). This leads in turn to a relatively low redox potential (near -350 mV vs. SCE) making its reduction to Fe(II) easily accessible to biological reductants. Finally, VF has been isolated from several different bacteria which are known to be closely associated with dinoflagellates in general and HAB species in particular (Amin et al., 2007). Indeed, during a bloom of *L. polyedrum* at Scripps Pier in 2011, bacteria that had the ability to synthesize VF were found to be by far the most numerous as compared to the other photo-active siderophore producers (Yarimizu et al., 2014). The fact that

VF was the most efficient iron source for *L. polyedrum* is consistent with the hypothesis that mutualistic bacteria may have an important role to play in at least some bloom dynamics.

4.5.2 Storage

The one of the several most obvious conclusions from the TMS long term incubation studies is the lack of an observable ferrous iron pool. In previous in vivo Mössbauer studies by us and others of various bacterial, fungal and algal systems significant amounts of intracellular high-spin ferrous iron octahedrally coordinated by oxygen ligands could be detected (Miller et al., 2014: Miller et al., 2016). However there is no evidence for such species in *L. polyedrum*. Although the overall signal is too weak for detailed analysis, preliminary fits to the data give δ= 0.17 mm/s, ΔEq=0.62 mm/s and Γ=0.42 mm/s. Indeed based on the absorption area in the Mössbauer spectra (Figure 24) we can estimate the total concentration of intracellularly accumulated iron to be >>1 mM (compare for example to similar data shown in Hartnett et al 2012). This very low internal iron concentration even after long term exposure to excess iron is indicative of a lack of iron storage mechanisms such as ferritins or vacuolar based forms. Indeed the severe growth limitation of *L. polyedrum* observed under low iron conditions even in the first generation is also suggestive of a lack of iron storage capability. Given the primarily coastal environment occupied by this dinoflagellate where iron concentrations are expected and found to be relatively high (nM) as compared to the oligotrophic open ocean (pM or less) perhaps an efficient iron storage system is unnecessary.

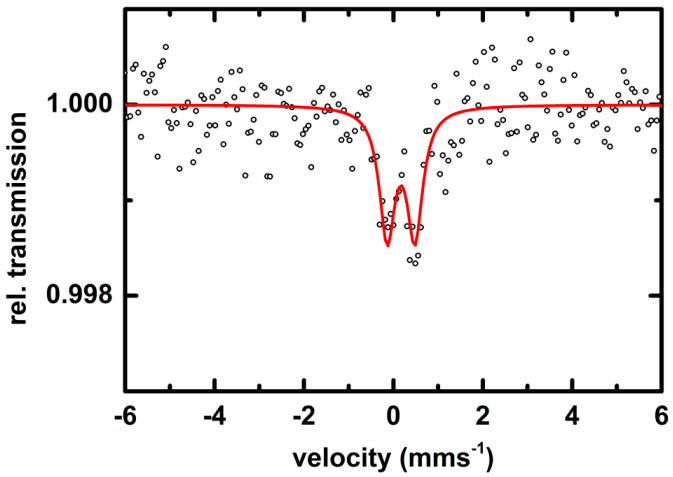

Figure 24 TMS of *L. polyedrum* after 3 weeks incubation in ^{57}Fe enriched growth medium. Data was collected at 77K over 4 days.

4.6 ACKNOWLEDGEMENTS

We thank Avery Tatter (University of Southern California) for providing *L. polyedrum* strain and helping us to set up algae culture laboratory.

Chapters 4 is in part reprints of the materials published in paper: Yarimizu, K., Cruz-López, R., Auerbach, H., Heimann, L., Schünemann, V., & Carrano, C. J. (2017). Iron uptake and storage in the HAB dinoflagellate *Lingulodinium polyedrum*. *Biometals, 30*, 945-953.

CHAPTER 5. IRON AND HARMFUL ALGAE BLOOMS: POTENTIAL ALGAL-BACTERIAL MUTUALISM BETWEEN *LINGULODINIUM POLYEDRUM* AND *MARINOBACTER ALGICOLA*

5.1 ABSTRACT

Phytoplankton blooms can cause acute effects on marine ecosystems either due to their production of endogenous toxins or due to their enormous biomass leading to major impacts on local economies and public health. Despite years of effort, the causes of harmful algal blooms (HAB) are still not fully understood. Our hypothesis is that bacteria that produce photoactive siderophores may provide a bioavailable form of iron to commensally associated phytoplankton, which could in turn affect algal growth and bloom dynamics. This chapter reports a laboratory-based study of binary cultures of the dinoflagellate *Lingulodinium polyedrum*, a major HAB species, with *Marinobacter algicola* DG893, a phytoplankton-associated bacterium that produces the photoactive siderophore vibrioferrin. Comparing binary cultures of *L. polyedrum* with both the wild type and the vibrioferrin minus mutant of *M. algicola* shows that bacteria are necessary to promote dinoflagellate growth and that this growth promotion effect is at least partially related to the ability of the bacterium to supply bioavailable iron via the siderophore vibrioferrin. These results support the notion of a carbon for iron mutualism in some bacterial-algal interactions.

5.2 INTRODUCTION

Phytoplankton blooms are a frequent phenomenon in the coastal regions of every continent in the world. Certain phytoplankton algae occurring in mass proliferations produce

toxins. Such harmful algal blooms (HABs) can, directly or indirectly, impact marine ecosystems with repercussions on local economies and public health (Lewitus et al., 2012). Direct effects on human health are often related to the consumption of shellfish that have ingested toxic phytoplankton, resulting in the accumulation of toxins and, consequently upon human consumption, paralytic, diarrheic, and neurotoxic poisoning which can sometimes be fatal (Anderson 1994: Honner et al., 2012). HABs also have indirect impacts such as impairment of water quality leading to losses in the tourism and recreational sectors. Even phytoplankton blooms that do not produce toxins can be detrimental and lead to ecological impacts such as the displacement of indigenous species, habitat alteration, or oxygen depletion (Glibert et al., 2005). The economic effects caused by HABs in the U.S. alone were estimated at $82 million per year in 2006 (Hoagland and Scatasta, 2006). Current strategies to reduce health-related impacts due to HABs are based on frequent coastal monitoring and early detection of HAB species and toxin levels. Nevertheless, the factors leading to the origins of HABs are still not well understood. Consequently, there is no strategy for their ultimate prevention.

There is an ongoing debate whether the factors leading to HABs are natural or anthropogenic. Oceanographic factors and global climate change including and impacting upwelling, reversal and relaxation of winds may be the major drivers initiating phytoplankton blooms (Roegner et al., 2002: Tweddle et al., 2010). HABs have also been proposed to be the consequence of human activities including eutrophication, changes in land use and agriculture, overfishing, and ballast water discharge (Gilbert 2005). Others consider that better analytics results in increased detection of HAB species (Burkholder, 1998). Nevertheless, HABs are a global threat to human health, fisheries and aquaculture resources. While numerous studies concentrate on the causes of HABs, few have considered that bacterial species coexisting with

microalgae could contribute to their development. However since Bell and Mitchell reported that specific bacterial communities occur and microbial activity was altered in the so-called phycosphere (Bell and Mitchell, 1972; Bell and Lang, 1974), more and more studies suggest that such algal-bacterial interactions are very specific and important (Azam and Malfatti, 2007; Amin et al., 2015; Bertrand et al., 2015; Ramanan et al., 2016; Seymour et al. 2017). A plausible hypothesis suggests that the mutualistic association of some phytoplankton and bacteria is based on nutrient exchange. Nitrogen and phosphorus are the best studied in this regard, although the molecular nature of interactions involving these nutrients is not well understood (Hallegraeff and Gollasch, 2006). Alternatively specific bacteria may affect algal growth and bloom dynamics by their control of iron, a trace element which is often growth limiting to phytoplankton in the marine environment (Miethke and Marahiel, 2007; Maldonado et al., 2005: Croot and Heller, 2012).

Iron is an essential element for all living organisms including phytoplankton and bacteria due to its involvement in photosynthesis and respiration. Despite iron being the fourth most abundant element on the Earth, its bioavailability in the marine environment is extremely low due to its poor solubility under the mildly alkaline aerobic conditions present in the ocean (Martin and Fitzwater, 1988; Wu and Luther III, 1994). To overcome this low bioavailability, bacteria and fungi have evolved sophisticated systems to produce high-affinity iron-chelating compounds called siderophores to acquire, transport, and process this essential metal ion (Sandy and Butler, 2009). The major role of siderophores is to bind mineral phases of iron and to deliver the iron siderophore complex to specific outer membrane receptors on microbial cells. Several hundred siderophores have been isolated and extensively studied with respect to their synthesis, structures and transport mechanisms over the last three decades (Yamamoto et al., 1994; Challis,

2005; Sandy and Butler, 2009: Raymond et al., 2015). While much research has been done on terrestrial siderophores, the study of marine siderophores is less extensive and only a relatively few have been fully elucidated (Vraspir and Butler, 2009). Nevertheless one of the two major attributes that seem to distinguish marine siderophores from those of terrestrial origin is the tendency of the former to contain an α- and β-hydroxy acid group in their iron-binding domain (Barbeau et al., 2001, 2002; Küpper et al., 2006). The significance of the presence of these functional groups in siderophores is in their ability to make the iron-siderophore complex photoreactive. The chelated Fe(III) in such siderophores is reduced in the presence of sunlight via an internal redox process to release Fe(II), a more soluble form of iron (Amin et al., 2009). It has been proposed that sunlight-driven reduction of the Fe(III) would transiently produce Fe(II) which might be utilized not only by the siderophore-producing bacteria themselves but also by non-siderophore producing bacteria and other organisms such as phytoplankton (Maldonado et al., 2005; Naito et al., 2008; Amin et al., 2009, 2012).

While iron acquisition by bacteria is well understood, that of phytoplankton remains less so. There are data to support the possibility of a variety of iron uptake mechanisms being operative simultaneously depending on the species involved. These include an iron-reductive route via a cell surface reductase, a direct xenosiderophore-mediated mechanism and cell surface-enhanced processes (Sutak et al., 2012; McQuaid et al., 2018). However as of yet there are no well documented examples, with some exceptions among the cyanobacteria, where phytoplankton have been shown to produce their own siderophores for iron acquisition (Raven, 2013). Thus how phytoplankton effectively acquire this metal from the low concentration iron environment is still unclear.

Our hypothesis is that algal growth and bloom dynamics may be affected by the increased bioavailability of iron engendered by the presence of photoreactive siderophores produced by mutualistic bacteria. Previously, we studied a bloom of the dinoflagellate, *Lingulodinium polyedrum*, at the Scripps Pier (San Diego, CA, USA) in 2011. *L. polyedrum* is one of the HAB species known to produce Yessotoxins, a group of polyether toxins which can accumulate in shellfish and show high toxicity to mice via intraperitoneal injection (Tubaro et al., 2004). As the first step to search for an association of phytoplankton with specific bacterial photoreactive siderophore producers (producing petrobactin, aerobactin, and vibrioferrin siderophores), we monitored both the population of *L. polyedrum* and the bacterial siderophore producers before, during, and after the 2011 bloom. The results showed that both *L. polyedrum* and the bacterial siderophore producers simultaneously increased and decreased during the bloom period (Yarimizu et al., 2014). At the *L. polyedrum* bloom maximum, the total number of bacterial producers of photoreactive siderophore reached their maximum accounting for roughly 9% of the total bacterial population suggesting that such high abundance of photoreactive siderophore producers could potentially provide bioavailable iron to the phytoplankton in this environment. Furthermore, when the PCR-derived amplicons were sequenced, a phylogenetic tree constructed from the sequencing results showed that the community of siderophore producers in pre-bloom was statistically significantly different than those found during and after the bloom by UniFrac analysis suggesting that this particular bacterial community could be involved in bloom initiation.

As a proof of concept, the present study was performed using laboratory culture data to correlate the association of the vibrioferrin siderophore producing bacterium, *Marinobacter algicola DG893* and the dinoflagellate *L. polyedrum* with iron as a nutrient. It is hoped that

finding an algal-bacterial mutualism based on iron availability may be useful for a more thorough understanding of the mechanisms of HAB formation.

5.3 MATERIALS AND METHODS

5.3.1 Trace iron cleaning procedures

The container cleaning technique was adopted from Bruland and Franks (1979). All plastic and glass containers were washed with pure water and soaked in 3N hydrochloric acid at least for two weeks at ambient temperature. The acid washed containers were rinsed with Milli-Q water and dried in a laminar-flow air bench. For those required sterile condition, acid washed containers were placed in pouch and autoclaved at 121°C for 30 minutes followed by 45 minutes dry cycle. Alternatively, purchased sterile containers Nunc™ Cell Culture Treated Flasks with Filter Caps were used.

5.3.2 Growth media

Of eight sources of natural waters screened, Pacific Ocean oligotrophic water was initially selected for our use due to its extremely small dissolved iron concentration (pM). This was replaced later by Scripps pier seawater because of its easier accessibility and comparable *L. polyedrum* growth patterns observed in the two sources of seawater. Seawater from Scripps pier (32.153°N, 117.115°W, San Diego, CA) was collected (pH 8.2-8.4, 980 mOsm/Kg H_2O, total dissolved iron 3-4 nM) and filtered immediately through 0.22 mm pore size membrane. The filtered seawater was mixed with approximately 0.005% metal free hydrochloric acid, autoclaved for 30 minutes, cooled at ambient temperature for a day, and stored in 5°C until use. The pH of the autoclaved seawater was ensured to be between 8.0 and 8.2 at ambient temperature. L1 nutrient was added to sterile seawater per manufacturer's instruction (L1 media). For those required controlled iron concentration in media, L1 trace element solution without $FeCl_3$ and

Na_2EDTA was prepared in house (Guillard and Hargraves, 1993) and added along with other L1 nutrients (nitrate, phosphate, silicate, vitamins) to sterile seawater (L1-Fe media). Serial dilutions were made on L1 media with L1-Fe media to prepare growth media with target total iron concentrations, $[Fe]_T$.

5.3.3 Artificial Sea Water (ASW)

Solution was prepared in three separate containers, one with 15 g NaCl, 0.75 g KCl, 1 g NH_4Cl in approximately 500 mL water, one with 12.4 g $MgSO_4 \cdot 7H_2O$ in small volume of water, and one with 3.0 g of $CaCl_2 \cdot 2H_2O$ in a small volume of water. The three solutions were mixed and 0.1 g disodium ß-glycerol phosphate was added. The pH was adjusted to 8.0-8.2 and volume was adjusted to 1L. The solution was autoclaved at 121°C for 30 minutes.

5.3.4 Algae maintenance and growth monitoring

L. polyedrum strain was isolated from Venice Beach California and kindly provided to us by Avery Tatters (University of Southern California). *L. polyedrum* cells were maintained in sterile one liter Erlenmeyer flasks containing L1 media and capped with a ventilation sponge. Cultures were exposed to 100 μmol photons $m^{-2} s^{-1}$ on a 12-hour alternating light and dark cycle at a temperature of 20±2 °C (standard growth condition). The upper portion of a culture containing healthy cells was diluted to 1/5 with L1 media every three weeks. Algal growth was monitored by direct cell count using an inverted microscope (Nikon Eclipse TE2000-U, 4x objective). To prepare cells in controlled iron media, cultures containing 10^4-10^5 cells per mL was placed in a 15-mL Falcon tubes and centrifuged for a few seconds to pellet cells which were gently washed three times and re-suspended to an appropriate volume with controlled iron media.

5.3.5 "Axenic" *L. polyedrum* preparation

Non-axenic *L. polyedrum* cells were grown to 10^5 cells/mL in L1 medium. Antibiotics 0.1% (v/v) (Penicillin 5units/mL, Streptomycin 5 μg/mL, Neomycin 10 μg/mL) were added to a non-axenic culture and incubated for 24 hours under the standard growth condition. Antibiotic-treated cultures were placed in 15 mL Falcon tubes and gently centrifuged for a few seconds. The pelleted cells were washed three times and re-suspended with L1 medium containing 0.05% (v/v) antibiotics in a sterile culture flask to appropriate volume. Antibiotics 0.05% (v/v) was added every 3 days to maintain the culture "axenic". The absence of cultureable bacteria in the antibiotic treated *L. polyedrum* was tested by spreading a 10 μL sample of the culture on a marine broth plate (5 g/L peptone, 1 g/L yeast extract, 15 g/L agar in 75% seawater) followed by incubation at 25°C for 2-3 days. The absence of any visible bacterial colonies was considered indicative of an "axenic" culture of *L. polyedrum*.

5.3.6 Bacteria strains and growth monitoring

The model bacterium used was *Marinobacter algicola* DG893 (GenBank code NZ_ABCP00000000.1) since it has been isolated by Green et al. (2004) and well characterized as a producer of the photoactive siderophore vibrioferrin (Amin et al., 2007). The mutant *ΔpvsAB*-DG893 was made as described by Amin et al. (2012) by 872 base pair deletion from the wild type to knock out two siderophore biosynthesis genes, *pvsA* and *pvsB*. To monitor bacterial growth, two methods were used: Optical density at 600 nm was applied to apparently turbid samples which generally contained $\geq 10^7$/mL of bacterial cells. Enumeration of bacteria by serial dilution was applied for samples containing lower numbers of bacteria cells ($<10^7$/mL). For enumeration techniques, serial dilution was made on those samples with sterile seawater, each diluted sample was spread on marine broth plates, and the number of colony forming units

(CFU) recorded from the lowest diluted sample plate. CFU in original sample per mL was calculated by (CFU in diluted sample) / (volume plated in mL) x dilution factor.

5.3.7 Stock bacteria solution

One liter of marine broth was prepared (5 g/L peptone, 1 g/L yeast extract, 15 g/L agar in 75% seawater, pH 8.2, sterile) and dispensed into sterile tubes with a 5 mL volume. A few colonies of bacteria picked from stock plates were transferred into the marine broth tubes and shaken at 25°C for 1-2 days until they reached log phase. The cells were collected by centrifugation, washed three times and re-suspended in sterile medium to an optical density (OD600) of 0.3 (stock bacteria solution).

5.3.8 CAS-dye assay

The method was adopted from Alexander and Zuberer (1991) to detect siderophore production by DG893. Using acid washed glassware, the following stock solutions were prepared: 10 mM HDTMA in water, 2 mM CAS in water, 1 mM $FeCl_3.6H_2O$ in water, 50 mM piperazine anhydrous buffer (pH5.6), and 0.2 M 5-sulfosalicylic acid in water. CAS solution was prepared by pouring a mixture of 15 mL of CAS and 3 mL of $FeCl_3.6H_2O$ slowly into 12 mL of HDTMA followed by addition of 50 mL of piperazine. The final volume was adjusted to 200 mL with water. CAS shuttle solution was prepared by adding 20 μL of 5-sulfosalicylic acid to every mL of CAS solution (used within one day of preparation). Samples to be tested were centrifuged to remove particles and 0.5 mL supernatant was mixed with 0.5 mL of CAS shuttle solution followed by incubation in the dark at ambient temperature for 10 minutes. A color change from dark purple to clear red indicated siderophore production.

5.3.9 Materials and reagent

The following materials were purchased from Sigma-Aldrich: Chrome azurol S (CAS, C-1018, MW605.28), antibiotics (Penicillin/Streptomycin/Neomycin, P4083-100 mL), peptone (P-1265), iron(III) chloride hexahydrate ($FeCl_3 \cdot 6H_2O$, 10025-77-1, MW270.30), manganese(II) chloride tetrahydrate ($MnCl_2 \cdot 4H_2O$, 13446-34-9, MW197.91), hexadecyltrimethylammonium bromide (HDTMA, H6269-100G, MW364.45), 1,4-diazacyclohexane, diethylenediamine **(**Piperazine, P45907-100G**,** MW 86.14), 5-sulfosalicylic acid (390275, MW218. 18), zinc sulfate heptahydrate ($ZnSO_4 \cdot 7H_2O$, 1088830500, MW287.54), cobalt(II) chloride hexahydrate ($CoCl_2 \cdot 6H_2O$, 8025400010, MW129.83), copper(II) sulfate pentahydrate ($CuSO_4 \cdot 5H_2O$, 209198-5G, MW249.69), sodium molybdate dehydrate ($Na_2MoO_4 \cdot 2H_2O$, 331058-5G, MW241.95), selenous acid (H_2SeO_3, 211176-10G, MW128.97), nickel(II) sulfate hexahydrate ($NiSO_4 \cdot 6H_2O$, 227676-100G, MW262.85), sodium orthovanadate (Na_3VO_4, 450243-10G, MW183.91), potassium chromate (K_2CrO_4, 216615-100G, MW194.19), salicylaldoxime (SA, 84172-100G). The following materials were purchased from Fisher Scientific: trace metal-free hydrochloric acid (Optima, A466-250), yeast extract (BP9727-500), agar (BP1423-500), Casamino Acids (BP1424-500), Nunc™ Cell Culture Treated Flasks with Filter Caps (12-565-57), ethylenediaminetetraaceticacid, tetrasodium salt dihydrate ($Na_4EDTA \cdot 2H_2O$, BP121-500, MW416.2), boric acid (AAJ67202A1). Other materials were purchased as follows: 0.22 μm filter membrane (Millipore, MillexGV, SLGV033RS), L1 medium kit (Bigelow, MKL150L), pure water (Barnstead water system, 18.2 mΩ). Vibrioferrin (VF, MW434.35) was isolated and purified in house according to Amin et al. (2007).

5.4 RESULTS

5.4.1 Seawater selection

Natural seawater was collected from local Scripps pier in December 2014, January 2015, and February 2015 as well as from San Diego Bay (32.65°N 117.19°W) in February 2015. Natural water was also collected from Ensenada Bay (31.86°N -116.66°W) in January 2015. Oligotrophic water was collected by Professor Katharine Barbeau (Scripps Institute of Oceanography) from local open-ocean in September 2011 and kindly provided to us. Artificial seawater (ASW) was prepared in house and also made from a purchased kit, Coralife Marine Saltwater Aquarium Salt Mix, per manufacturer's instruction. These eight sources of seawater were compared for pH, osmolality, and total iron concentration (Figure 25). The pH was between 8.0 and 8.2 for all seawater. The osmolality was between 980 and 1040 mOsm/Kg H_2O for all seawater except that of in-house ASW was 635 mOsm/Kg H_2O. $[Fe]_T$ of Scripps water was between 3 nM and 4 nM while that of Ensenada bay water was 8 nM. Oligotrophic water was initially selected for our experimental use due to its negligible amount of $[Fe]_T$. Later, Scripps seawater replaced oligotrophic water for two reasons, easier accessibility and comparable *L. polyedrum* growth observed in the two sources of seawater.

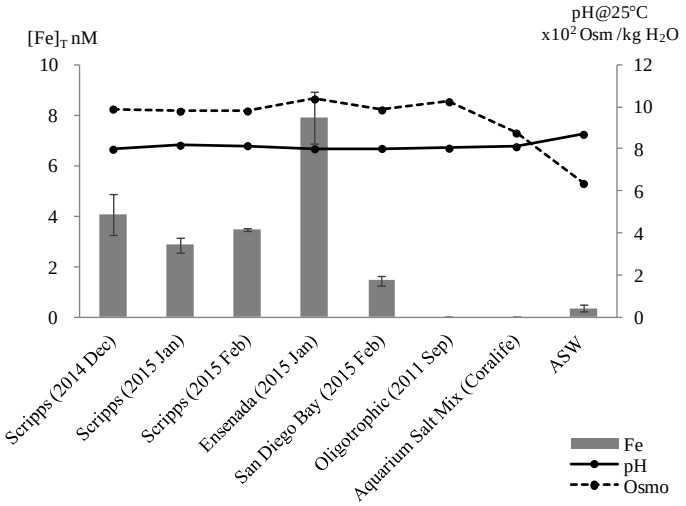

Figure 25 Seawater screening: pH, osmolality, and total iron concentration
Natural water was collected from 6 different sources and articifical sea water was prepared from two different methods. The seawater was compared for pH, osmolality and total iron concentration.

5.4.2 Bacterial growth

The growth of DG893 and mutant *ΔpvsAB*-DG893 in L1 media containing different total iron concentrations $[Fe]_T$ (1,000, 100, 10, and 0 nM) was monitored (Table 11). All media were divided in two parts, one maintaining [EDTA] at 10,000 nM (L1 nutrient level) with variable $[Fe]_T$, and the other reducing [EDTA] along with $[Fe]_T$ to maintain molar ratio of Fe: EDTA of 1:1. All media were prepared with and without sterile Casamino acids. In each media, ca. 10^6 cells/mL of DG893 or mutant *ΔpvsAB*-DG893 was added and shaken in dark at 30°C. The bacterial growth in each media was monitored for 5 days by optical density at 600 nm. Neither WT DG893 nor the mutant grew in simple seawater or L1-Fe media without a carbon source (Figure 26). Addition of iron to seawater or L1-Fe media also did not maintain growth (Figure 27). However upon addition of Casamino acids, both DG893 and the mutant grew and their growth increased with increasing $[Fe]_T$ in media (Figure 28). There was no remarkable difference in growth pattern between DG893 and the mutant, consistent with the report by Amin et al. (2012). In summary, both DG893 and mutant require carbon source to grow to a detectable level in seawater medium.

Table 11 DG893 and mutant *ΔpvsAB*-DG893 growth monitoring matrix

The same matrix was set up for mutant *ΔpvsAB*-DG893.

ID	L1-Fe -EDTA	[EDTA] nM	$[Fe]_T$ nM	Casamino Acids, mg/mL	DG893 stock µL
1	+	10,000	1,000	-	100
2	+	10,000	100	-	100
3	+	10,000	10	-	100
4	+	1,000	1,000	-	100
5	+	100	100	-	100
6	+	10	10	-	100
7	+	-	-	-	100
8	-	-	-	-	100
9	+	10,000	1,000	10	100
10	+	10,000	100	10	100
11	+	10,000	10	10	100
12	+	1,000	1,000	10	100
13	+	100	100	10	100
14	+	10	10	10	100
15	+	-	-	10	100
16	-	-	-	10	100

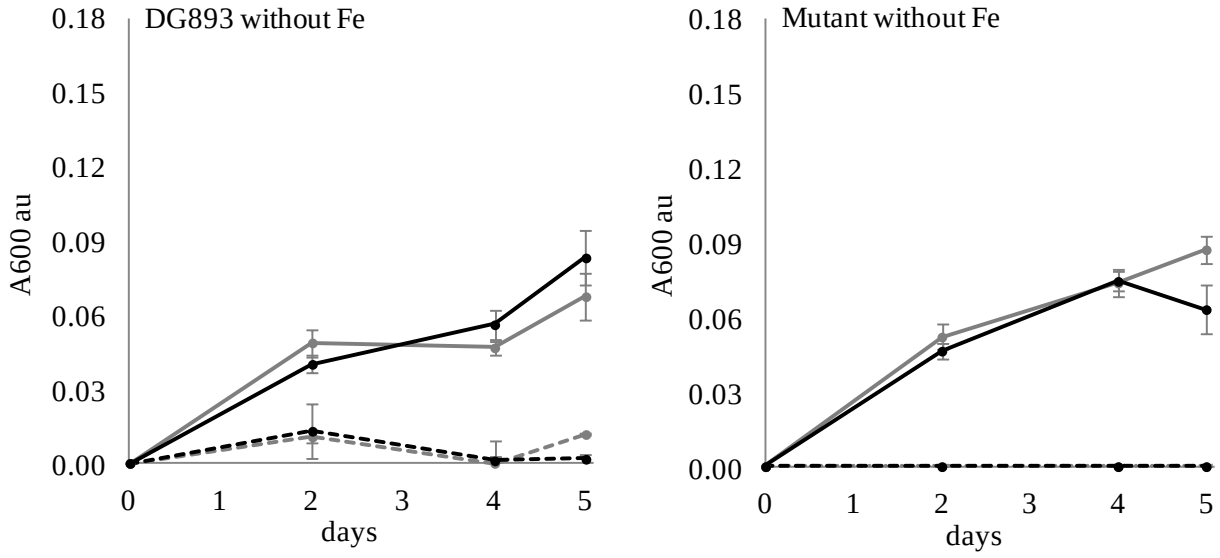

Figure 26 Bacterial growth in media without Fe

The bold lines represent media containing 10 mg/mL Casamino acids. The dotted lines represent media without Casamino acids. The grey lines represent L1-Fe media. The black lines represent plain seawater.

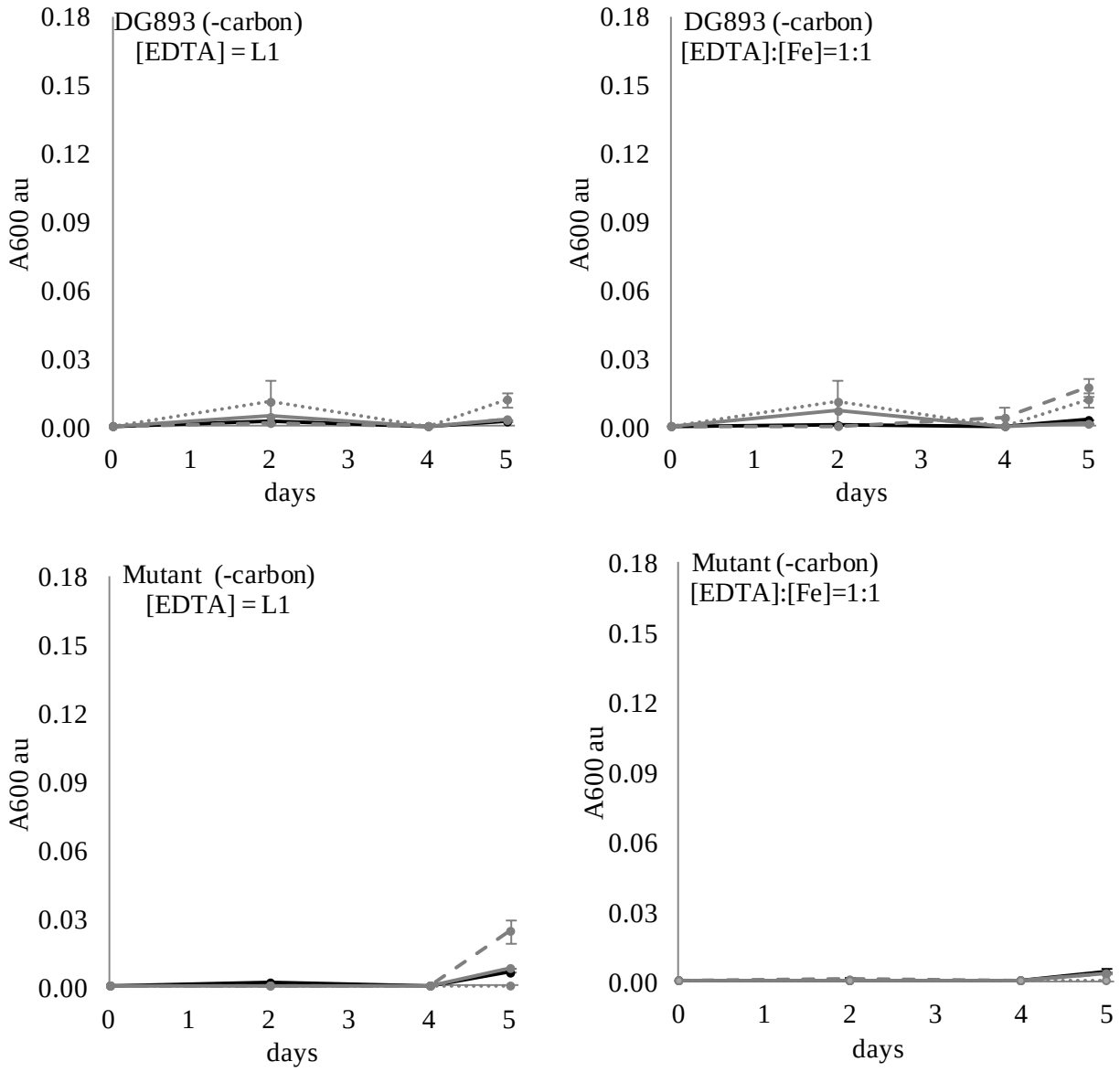

Figure 27 Bacterial growth in media with Fe without Casamino acids
DG893 and mutant were incubated in L1 media containing different $[Fe]_T$. The black bold line, grey bold line, grey wide dotted line, and grey narrow dotted line represent L1 media with 1,000 nM, 100 nM, 10 nM, 0 nM $[Fe]_T$, respectively. The left two panels contained 10,000 nM [EDTA] in media with variable $[Fe]_T$. The right two panels contained reduced [EDTA] along with $[Fe]_T$ to maintain their molar ratio at 1:1.

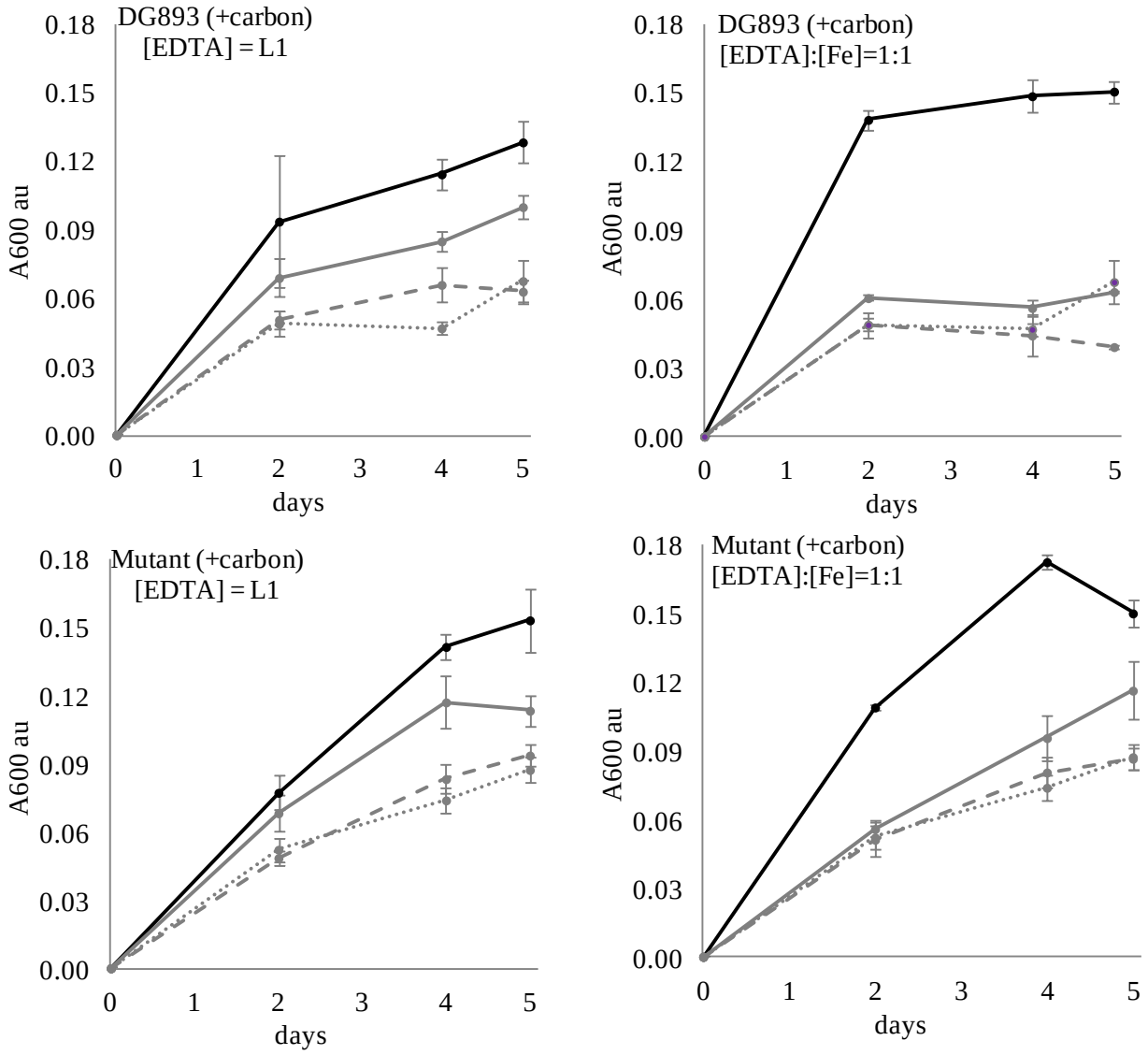

Figure 28 Bacterial growth in media with Fe and Casamino acids
DG893 and mutant were incubated in L1 media containing 10 mg/mL Casamino acids and different $[Fe]_T$. The black bold line, grey bold line, grey wide dotted line, and grey narrow dotted line represent L1 media with 1,000 nM, 100 nM, 10 nM, 0 nM $[Fe]_T$, respectively. The left two panels contained 10,000 nM [EDTA] in media with variable $[Fe]_T$. The right two panels contained reduced [EDTA] along with $[Fe]_T$ to maintain their molar ratio at 1:1.

5.4.3 Siderophore production and total iron concentration $[Fe]_T$

The ability to produce the siderophore vibrioferrin (VF) by DG893 but not by the mutant was confirmed by the CAS-dye assay. Since siderophore biosynthesis is generally turned on under low iron concentrations and turned off under high (Braun, 1995 and 1998; Miethke and

Marahiel, 2007) WT was grown in L1 media containing various $[Fe]_T$ with 0.3% Casamino acids at 30°C in dark for 24 hours to find the approximate $[Fe]_T$ under which DG893 produces VF. The WT did not produce VF in the media with $[Fe]_T \geq 10$ μM but did so with a $[Fe]_T$ of 1 μM or less (Figure 29). The mutant *ΔpvsAB*-DG893 did not show signs of siderophore production under any of the conditions tested. The results suggest that under normal seawater conditions, where $[Fe]_T$ is estimated to be nM to pM, that siderophore biosynthesis in DG893 is likely turned on.

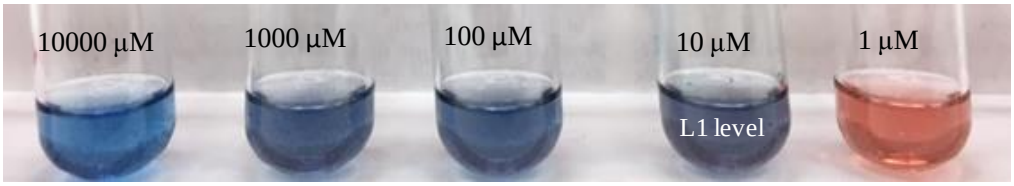

Figure 29 Siderophore production by DG893 in media with various $[Fe]_T$

5.4.4 Axenic culture preparation

The difficulty in preparing and maintaining axenic cultures of many marine algae has been reported in the past (Green et al., 2004; Jauzein et al., 2015; Liu et al., 2017). In fact, Lupette et al. (2016) noted that completely axenic cultures of a model green algal species could not be maintained despite the use of antibiotic treatment protocols. We were partially successful in our efforts to prepare axenic *L. polyedrum*. Initially, non-axenic *L. polyedrum* cultures containing 10^5 cells/mL were treated with antibiotics (1% v/v Penicillin 50 units/mL, Streptomycin 50 μg/mL, Neomycin 100 μg/mL) for 24 hours under the normal growth conditions. The treated cells were washed and re-suspended with sterile L1 media and while the "axenicity" of the culture at this point was confirmed, bacterial colonies reappeared after only a few days (Figure 30). An attempt was made to keep 1% antibiotics in the culture longer than 24 hours, however, dinoflagellate cells began to disintegrate after 2 days suggesting that 1%

antibiotics must be removed from the culture within 24 hours. The fact that the negative control and sterile L1 medium without phytoplankton cells remained bacteria-free for weeks ruled out a possibility of culture contamination. We believe that the antibiotics are most likely eliminating only free-living bacteria leaving attached bacteria unaffected. The next effort of preparing axenic cultures was made by immediate dilution of antibiotic-treated cultures. The rationale of this attempt was to minimize attached bacteria on *L. polyedrum* cells by dilution. The antibiotic treated *L. polyedrum* culture was diluted 200-fold with sterile L1 medium and incubated under standard growth conditions. The diluted culture remained bacteria-free for the first 10 days, however microbial growth was observed on the 12^{th} day as the number of *L. polyedrum* cells also increased. Although this dilution method suggested that the culture stayed bacteria free for up to 10 days, the *L. polyedrum* cell count was too dilute to be useful for further study. The next attempt at axenic culture preparation was made with three sequential antibiotic treatments. The non-axenic culture was treated with 1% antibiotics for 24 hours, washed three times, and re-suspended with sterile L1 medium. The cells were allowed to recover under normal growth conditions for a day and then again treated with 1% antibiotics. This procedure was repeated three times. This procedure also failed as the dinoflagellate cells began to disintegrate. Finally, using a similar procedure but reducing the concentration of antibiotics to 0.1% for the first treatment and adding 0.05% subsequently every 2-3 days resulted in *L. polyedrum* cultures without visible cell damage that appeared to be free of free-living bacteria for more than a month.

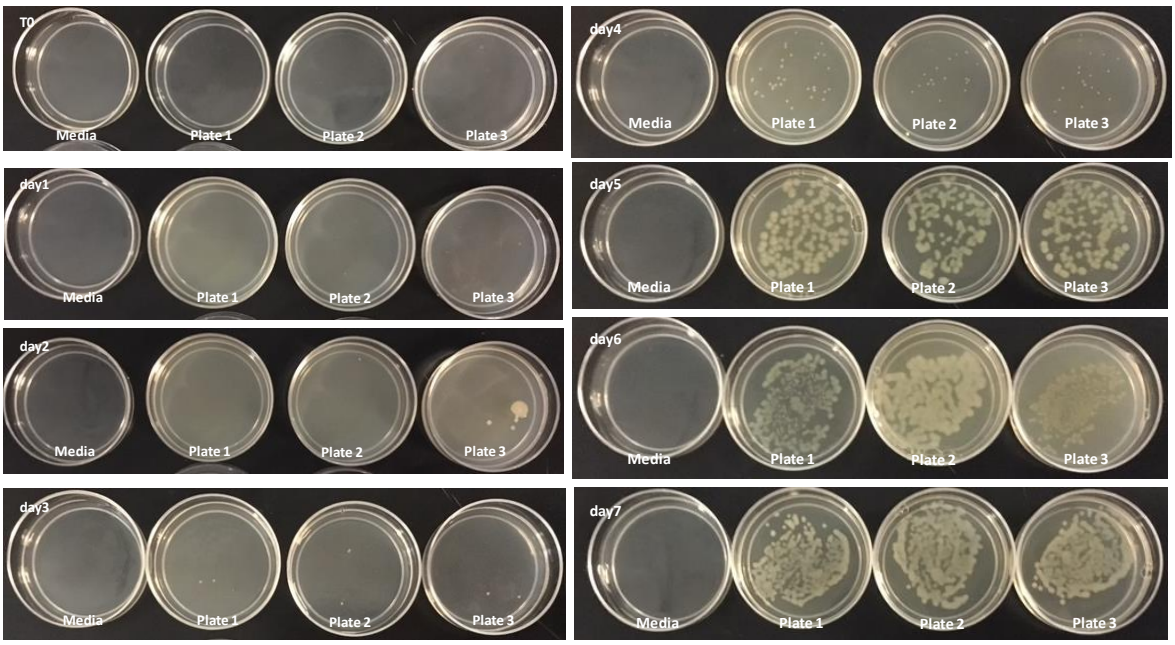

Figure 30 Sterility test of *L. polydrum* culture after treated with 1% antibiotics
Approximately 10^5 cells/mL non-axenic *L. polyedrum* were treated with 1% (v/v) antibiotics for 24 hours, washed, and re-suspended with sterile L1 media to the original volume. The sterility test was performed by spreading 10 µL of culture on a marine broth plate and incubated at 25°C for 2-3 days. The sterility of the culture was confirmed a day after antibiotics treatment, however microbial was detected on 2nd day and after.

5.4.5 *L. polyedrum* growth screening

A matrix containing thirty cultures of *L. polyedrum* in L1 medium containing different numbers of DG893 cells in the initial inoculum (10^7, 10^6, 10^5, 10^4, 10^3, 0 CFU/mL) and different $[Fe]_T$ (10^4, 10^3, 10^2, 10^1, and 0 nM) was set up. The same matrix was set up with the mutant *ΔpvsAB*-DG893. Bacterial growth was monitored by enumeration of bacteria by serial dilution and phytoplankton growth was monitored by direct cell counts under the microscope. Regardless of the starting bacterial cell number, both DG893 wild type and mutant grew in all the binary culture matrices over 28 days to eventually reach a bacterial population of ca. 10^5 CFU/mL. The group of media containing 1,000 nM $[Fe]_T$ showed the greatest growth of *L. polyedrum* regardless of the starting bacterial inoculum (Figure 31). The group of media containing ≤10 nM

$[Fe]_T$ showed very slow *L. polyedrum* growth regardless of starting bacterial inoculum. No significant differences in *L. polyedrum* growth co-cultured with DG893 or the mutant were observed, which left a question as to whether VF secreted by DG893 would have a significant effect on *L. polyedrum* growth. It was speculated that under these growth conditions, the amount of VF being produced by DG893 was insufficient to see detectable changes in *L. polyedrum* growth. This was later confirmed (*vide infra*) when excess VF artificially added to the culture produced pronounced *L. polyedrum* growth. Finally, the growth pattern of axenic *L. polyedrum* was similar to that of a non-axenic culture. This observation left open another question as to whether DG893 and *L. polyedrum* were commensally associated. However this also was confirmed by experiments described below where after subsequent culturing the "axenic" *L. polyedrum* ceased to grow while binary *L. polyedrum* DG893 kept growing exponentially (Figure 32).

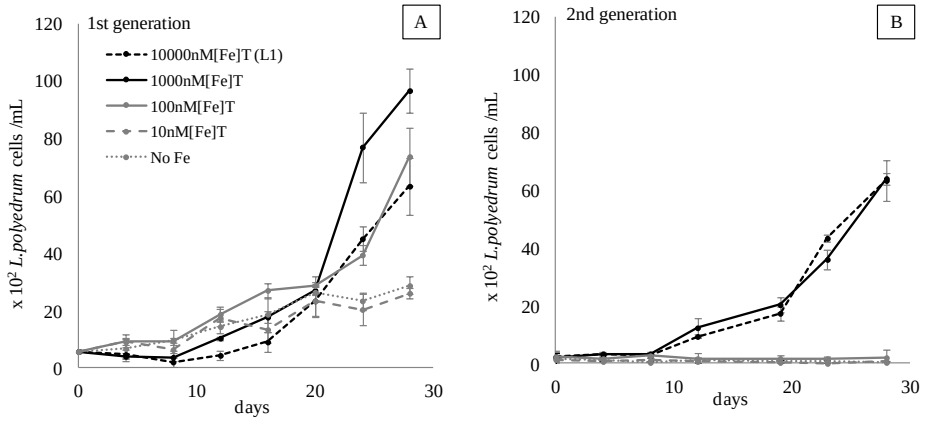

Figure 31 *L. polydrum* co-cultured with a starting inoculum of DG893 at 10^3 cells/mL in media with various $[Fe]_T$

A) 1st generation growth of *L. polyedrum* in the presence of DG893. The starting inoculum of DG893 was 10^3 cells/mL which reached 10^5 cells/mL after 28 days incubation under the standard growth conditions. A similar pattern was observed in all other groups: i.e. media containing a starting inoculum of DG893 of 10^7, 10^6, 10^5, 10^4, 10^3, 0 cells/mL and $[Fe]_T$ of 10^4, 10^3, 10^2, 10^1, or 0 nM. B) 2nd generation growth of *L. polyedrum* in the presence of DG893. After 28 days the cultures in panel A were diluted to a *L. polyedrum* concentration of 10^2 cells/mL with appropriate media and incubated under the standard growth condition for an additional 28 days.

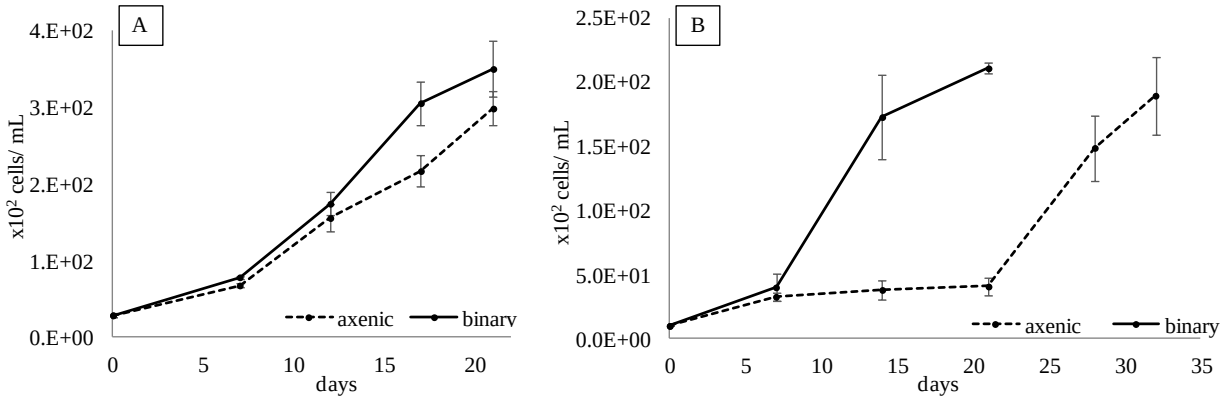

Figure 32 Rescue of *L. polyedrum* by addition of DG893
A) 1st generation of *L. polyedrum* growth maintained in L1 media either "axenic" or co-cultured with DG893. B) Growth of *L. polyedrum* in the 2nd subculture either "axenic" or co-cultured with DG893. After the 2nd subculture of "axenic" *L. polyedrum* was incubated under the standard growth conditions for 21 days, an inoculum containing approximately 10^2 cells/mL of DG893 was added and incubation continued for an additional 14 days.

5.4.6 Subsequent batch culture growth of *L. polyedrum* in DG893 binary culture

L. polyedrum grown in L1 media containing various $[Fe]_T$ and DG893 (Figure 31 A) for 28 days were diluted with appropriate media to adjust *L. polyedrum* to 10^2 cells/mL in the 2nd subsequent batch culture. The *L. polyedrum* growth in this 2nd subsequent culture was monitored for another 28 days under each growth condition. The result showed that the 2nd subsequent batch culture *L. polyedrum* in the higher two $[Fe]_T$ (10,000 and 1,000 nM) maintained their exponential growth while those in the lower three $[Fe]_T$ did not grow (Figure 31 B). Although the cells under the latter conditions did not completely die out, the few cells that survived had their swimming activity under the microscope clearly reduced.

5.4.7 Axenic *L. polyedrum* culture and rescue

The growth of "axenic" and binary cultures of *L. polyedrum* with DG893 in L1 was compared over several subsequent batch cultures. No significant difference in growth was observed in the 1st culture, however, a clear difference was observed in the 2nd subsequent batch

culture of *L. polyedrum* with and without DG893. While *L. polyedrum* with DG893 grew fully in both the 1st and 2nd subsequent batch cultures, "axenic" *L. polyedrum* ceased to grow (Figure 32). When DG893 was added to the 2nd subsequent "axenic" batch culture, *L. polyedrum* cells began to regrow exponentially demonstrating that DG893 could rescue "axenic" *L. polyedrum*.

5.4.8 Non-axenic *L. polyedrum* growth and rescue

The non-axenic *L. polyedrum* was maintained in L1 medium and assumed to contain not only siderophore-producing bacteria but also other unknown bacteria. The non-axenic culture was divided in two parts, one diluted to 1/5 with L1 medium and other diluted to 1/5 with L1-Fe medium (batch subculture 1). When the cell count reached approximately 10^4 cells/mL, both cultures were further diluted with appropriate medium. Therefore, one culture maintained $[Fe]_T$ at L1 level throughout the subsequent batch cultures while the other contained successively reduced $[Fe]_T$. The *L. polyedrum* growth was monitored for 28 days for each subculture. After the 6th subculture where $[Fe]_T$ in the medium was estimated to be 2 nM, *L. polyedrum* stopped growing completely (Figure 33). On 29th day of the 6th subculture, an iron supplement to give a $[Fe]_T$ of 5850 nM was added to the culture and growth was continued to be monitored for additional 28 days. The results indicate that the *L. polyedrum* culture which stopped growing under 2 nM $[Fe]_T$, could be rescued by addition of iron after 28 days (Figure 34).

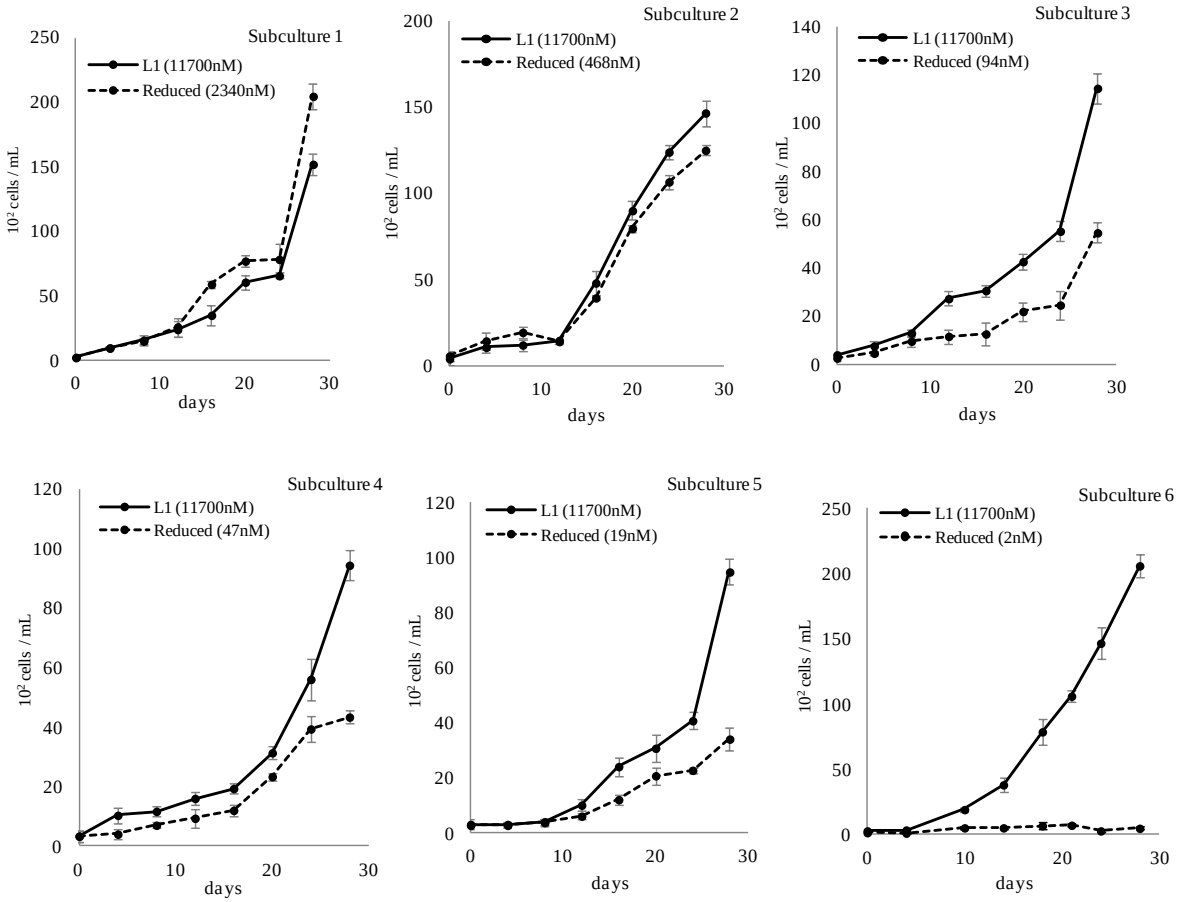

Figure 33 Non-Axenic *L. polyedrum* growth in L1 media and reduced $[Fe]_T$ in 6 generations
One culture was maintained at a $[Fe]_T$ at L1 level throughout the generations while the other contained subsequently diluted $[Fe]_T$ over the generations.

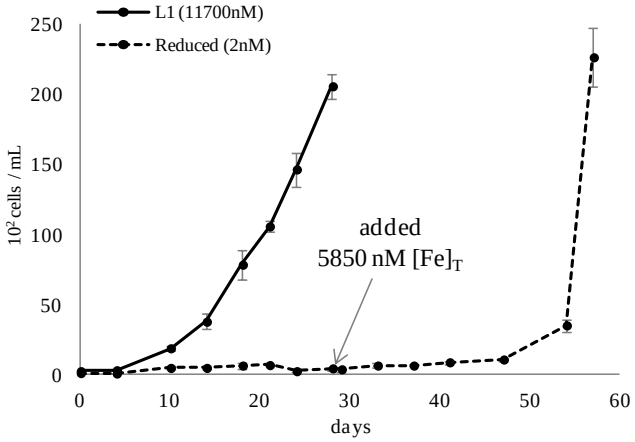

Figure 34 Iron starved non-Axenic *L. polyedrum* growth rescued by iron addition
The iron deficient culture contained 2nM $[Fe]_T$. 5850 nM $[Fe]_T$ was added to the iron deficient culture on day 28 which rescued *L. polyedrum* growth.

5.4.9 *L. polyedrum* growth in DG893 supernatant

Earlier it was stated that when *L. polyedrum* was co-cultured with either DG893 or the mutant *ΔpvsAB*-DG893, little difference was observed in its growth pattern. We speculated that this may have been due to the small amount of VF produced by the equilibrium population of DG893 in the binary culture. To test this idea, samples of the supernatant of the media from the WT DG893 grown under ideal conditions and containing detectable amounts of VF by CAS-dye assay, as well as the mutant *ΔpvsAB*-DG893 which did not, were added to *L. polyedrum* cultures and there growth was compared. It should be noted that we while traditionally grow DG893 and the mutant in marine broth containing Casamino acids these were found to be toxic to *L. polyedrum* cells (Table 12). In this experiment, we instead used ASW with succinic acid (at from 0.001% to 0.1%) as a carbon source (pH 8.2) to grow DG893 and the mutants prior to their supernatant being added to *L. polyedrum* cultures (Table 13, Table 14, Table 15). *L. polyedrum* growth was enhanced the most by the addition of the DG893 supernatant. The mutant supernatant also showed a slightly positive effect on *L. polyedrum* growth compared to media without bacterial supernatant, however the degree of growth was not as large as that induced by the DG893 supernatant (Figure 35). These results suggest that VF has potential influence on *L. polyedrum* growth, but that other extracts from bacteria (vitamin B_{12}?) may also have a potential effect on their growth. Further experiments were performed using purified VF itself. When VF at 57.11 μM was directly added to a *L. polyedrum* culture in L1 media containing 100 nM $[Fe]_T$, *L. polyedrum* reached cell counts approximately 1.5 times as large as those in media without VF (Figure 36).

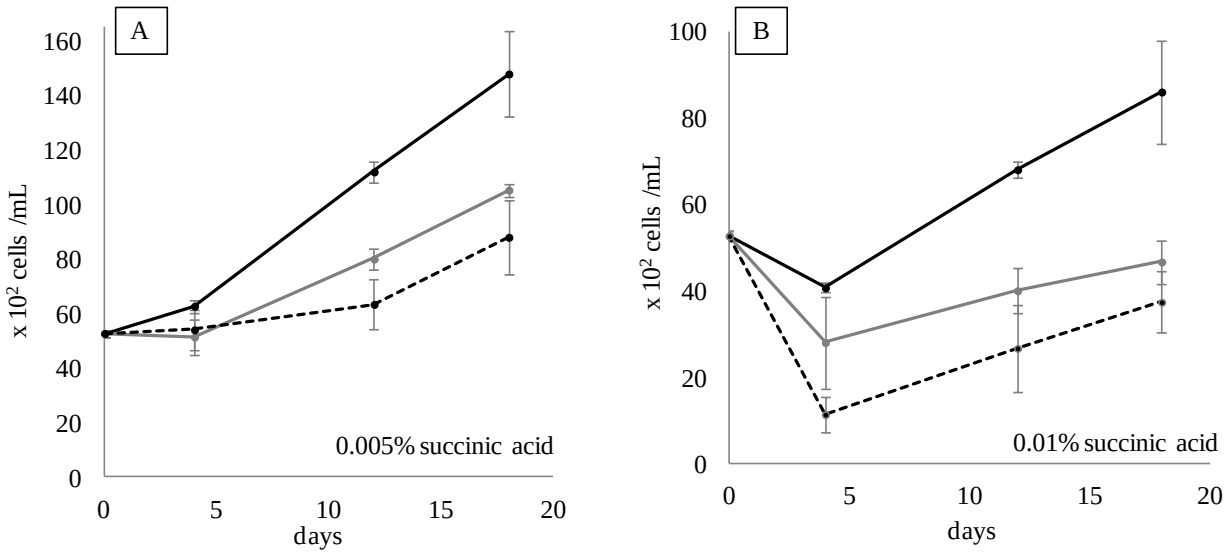

Figure 35 *L. polyedrum* growth in media with DG893 supernatant, mutant supernatant, and without bacterial supernatant

The black lines, grey lines, and dotted lines represent *L. polyedrum* growth in media with DG893 supernatant, with mutant supernatant, and without bacterial supernatant, respectively.

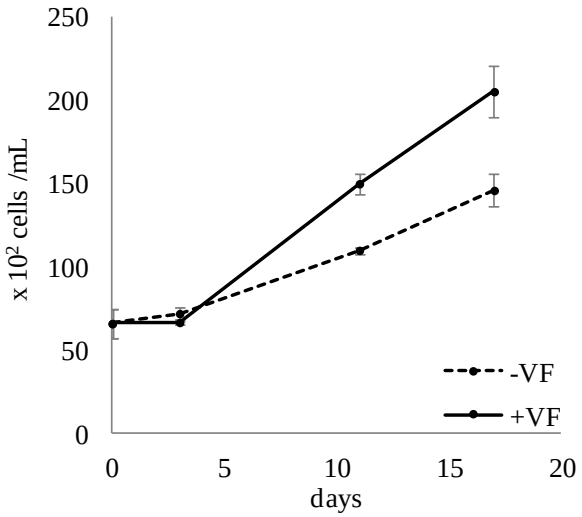

Figure 36 *L. polyedrum* growth in L1 media with 100 nM $[Fe]_T$ with and without VF

Purified VF (57.11 μM) was added directly to a *L. polyedrum* culture in L1 media with 100 nM $[Fe]_T$.

Table 12 *L. polyedrum* cell counts in L1 media containing carbon additives

Casamino Acids or succinic acid ranging from 0.001% to 0.1% was simply added to *L. polyedrum* culture and the cell survival was monitored. The cells died out in media containing ≥0.01% Casamino Acids. The cells survived in media containing 0.001% Casamino Acids, however, DG893 was hardly grown in the condition. The cells survived in all conditions tested with succinic acid.

ID	1	2	3	4	5	6	7
water	Scripps	Scripps	Scripps	Scripps	Scripps	Scripps	Scripps
media	L1	L1	L1	L1	L1	L1	L1
carbon	Casamino 1mg/mL (0.1%)	Casamino 0.1mg/mL (0.01%)	Casamino 0.01mg/mL (0.001%)	Succinate 1mg/mL (0.1%)	Succinate 0.1mg/mL (0.01%)	Succinate 0.01mg/mL (0.001%)	NA
pH	8.1	8.1	8.1	8.1	8.1	8.1	8.1
day 0, cells/mL	6,000	6,000	6,000	6,000	6,000	6,000	6,000
day 2, cells/mL	0	0	6,800	10,400	8,700	11,600	7,800
day 4, cells/mL	0	0	12,300	11,100	13,100	12,900	13,100

Table 13 VF production by DG893 in L1 media with controlled $[Fe]_T$ and succinic acid

DG893 was shaken in the media containing different amount of $[Fe]_T$ and succinic acid at 30°C for 2 days. CAS-dye assay was performed on 2nd day and all matrices resulted in negative on siderophore production.

ID	1	2	3	4	5	6	7	8	9
water	Scripps	Scripps	Scripps	Scripps	Scripps	Scripps	Scripps	Scrips	Scripps
media	L1-Fe	L1-Fe	L1-Fe	L1-Fe	L1-Fe	L1-Fe	L1-Fe	L1-Fe	L1-Fe
Fe, nM	100	100	100	100	10000	10000	10000	10000	1000
succinic acid	1 mg/mL (0.1%)	0.1 mg/mL (0.01%)	0.01 mg/mL (0.001%)	0 mg/mL (0%)	1 mg/mL (0.1%)	0.1 mg/mL (0.01%)	0.01 mg/mL (0.001%)	0 mg/mL (0%)	1 mg/mL (0.1%)
pH	8.1	8.1	8.1	8.1	8.1	8.1	8.1	8.1	8.1
CAS-dye@day2	-	-	-	-	-	-	-	-	-

Table 14 VF production by DG893 in L1 media with controlled $[Fe]_T$ and concentrated succinic acid

DG893 was shaken in the media containing either 100 nM or 10000 nM $[Fe]_T$ with higher concentration of succinic acid at 30°C for 2 days. CAS-dye assay was performed on the 1st and 2nd day and all matrices resulted in negative on siderophore production.

ID	1	2	3	4	5	6 (control)
water	Scripps	Scripps	Scripps	Scripps	Scripps	Scripps
Fe, nM	10000	10000	100	100	100	100
media	L1-Fe	L1-Fe	L1-Fe	L1-Fe	L1-Fe	L1-Fe
carbon	Succinate 50mg/mL (5%)	Succinate 20mg/mL (2%)	Succinate 10mg/mL (1%)	Succinate 5mg/mL (0.5%)	Succinate 1mg/mL (0.1%)	Casamino 5mg/mL (0.5%)
pH	7.4	7.9	7.9	7.9	7.9	8.0
CAS-dye 24hr	-	-	-	-	-	+
CAS-dye @48hr	-	-	-	-	-	+

Table 15 VF production by DG893 in ASW with succinic acid
DG893 was shaken in ASW containing 0.1-1% succinic acid at 30°C for 2 days. CAS-dye assay was performed on 1st and 2nd day. All matrices resulted in positive on siderophore production by 48 hours incubation.

ID	1	3	4 (control)
water	ASW	ASW	ASW
media	L1-Fe	L1-Fe	L1-Fe
carbon	Succinic acid 10mg/mL (1%)	Succinic acid 1mg/mL (0.1%)	Casamino acid 1mg/mL (0.1%)
Fe, nM	0	0	0
pH	8.13	8.07	7.98
CAS-dye @24hr	-	-	+
CAS-dye @48hr	+	+	+

5.4.10 DG893 growth in *L. polyedrum* supernatant

"Axenic" *L. polyedrum* cells were resuspended in L1 media containing 100 nM, 1,000 nM, 10,000 nM $[Fe]_T$ and incubated under the standard growth conditions for two days to collect their organic extracts (Table 16). The *L. polyedrum* cultures were divided in two parts, one of which was filtered through a 0.22 μm membrane to collect only organics and the other was kept without filtration to keep phytoplankton cell debris. The *L. polyedrum* supernatant with and without cells was added to the stock DG893 containing 0.3% Casamino Acids, and the mixture shaken at 30°C for several days. The control was prepared in the same manner without *L. polyedrum* supernatant and cells. In the media containing 1,000 nM and 10,000 nM $[Fe]_T$, DG893 growth was enhanced by the presence of *L. polyedrum* supernatant and was even more pronounced with the supernatant containing cell debris (Figure 37). In media with 100 nM $[Fe]_T$, only a subtle difference was observed in DG893 growth with and without *L. polyedrum* supernatant.

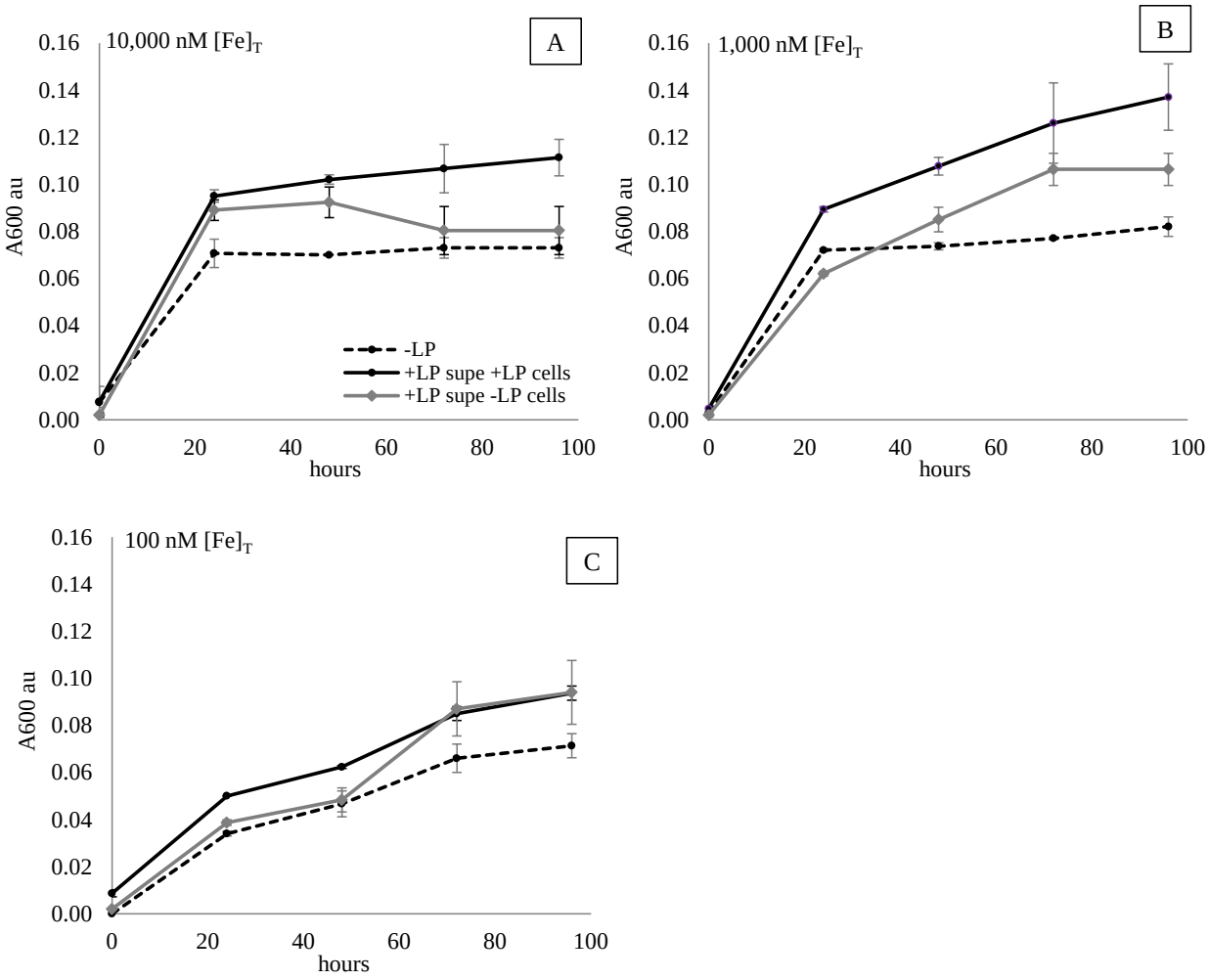

Figure 37 DG893 growth in media containing different $[Fe]_T$ with and without presence of *L. polyedrum* supernatant and cell debris

The black lines are DG893 growth in *L. polyedrum* supernatant with their cell debris, the grey lines are DG893 growth in *L. polyedrum* supernatant without their cell debris, and the dotted lines are DG893 without *L. polyedrum*.

Table 16 Sample matrix *L. polyedrum* growth in media with DG893 supernatant, mutant supernatant and without bacterial supernatant

L. polyedrum growth was compared in media with DG893 supe, with mutant supe, and without bacterial supe. DG893 and mutant was grown in L1-Fe enriched ASW containing succinic acid at 10 mg/mL (pH 8.0) for two days at 30°C in shaker. CAS-dye assay confirmed positive result on DG893 confirming VF production and negative on mutant. These bacterial solution was filtered through 0.22 μm membrane and the filtrate was added to *L. polyedrum* culture in L1 media with 100 nM $[Fe]_T$ to final succinic acid concentration at 0.1-0.001%.

	1	2	3	1'	2'	3'
water	Scripps	Scripps	Scripps	Scripps	Scripps	Scripps
media	L1-Fe	L1-Fe	L1-Fe	L1-Fe	L1-Fe	L1-Fe
Fe, nM	100	100	100	100	100	100
succinic acid	0.1mg/mL (0.01%)	0.1mg/mL (0.01%)	0.1mg/mL (0.01%)	0.05mg/mL (0.005%)	0.05mg/mL (0.005%)	0.05mg/mL (0.005%)
bacteria supe	DG893	mutant	NA	DG893	mutant	NA
CAS-dye	+	-	-	+	-	-
pH	8.31	8.38	8.40	8.42	8.41	8.39

5.5 DISCUSSION

Before proceeding to a discussion of the results presented here it is important to operationally define what we mean by $[Fe]_T$ and "axenic" cultures. Here we used the term total iron concentrations $[Fe]_T$ to mean the total analytical amount of iron added to culture and includes all phases of iron present in the solution. This is different from the total dissolved iron concentration which we routinely measure for environmental seawater samples (and which is approximately 2-6 nM for Scripps Pier water for example) as determined by cathodic stripping voltammetry (CSV). Total dissolved iron in such environmental samples are processed by filtration through a 0.22 μm membrane followed by acidification. As a result, total dissolved iron in a sample is much lower than the total analytical iron concentration. We use this operational definition as it is not possible to measure total dissolved iron in culture media using the CSV method because equilibrium between the various iron oxo/hydroxo species potentially present in seawater at pH 8.2 is reached only extremely slowly and thus concentrations of total dissolved iron are constantly changing over the time course utilized in these experiments. Using a straight

forward expression of total analytical iron concentration is thus a potentially more reproducible approach with which to compare the effects of iron on bacterial and algal growth in a laboratory setting.

Secondly we use the term "axenic" in quotation marks for describing cultures of *L. polyedrum*, to mean the absence of any observable *cultureable* bacteria based on the absence of visual bacterial colonies when cultures were placed on solid media and incubated for several days. We were only partially successful making the culture "axenic" by treating the culture with low concentration of antibiotics and sequential addition of the antibiotics to the culture over extended times. Using this method the culture appeared to remain bacteria free for at least a month. However when the sequential addition of antibiotics to the culture was stopped, bacteria growth was observed to return within a few days. Thus clearly the cultures were not truly axenic. Nevertheless our main concern was that the dominant species of bacteria growing in our binary culture should be DG893 and that "axenic" cultures should contain insignificant numbers of unknown bacteria. We confirmed the former by qPCR and the latter was further supported by presence of few if any bacteria seen via DAPI staining. To our knowledge, there is at present no general protocol for preparing a completely axenic culture *of L. polyedrum* hence our use of the operational definition of "axenic" described here.

We initially investigated conditions under which the bacterium *Marinobacter* DG893 and the dinoflagellate *L. polyedrum* could grow independently. As expected, in the absence of an added carbon source DG893 could not grow in natural unamended seawater or in L1 supplemented ASW irrespective of the iron concentration. In the presence of an adequate artificial source of carbon however bacterial growth was controlled by the available concentration of iron. Under idealized conditions, both DG893 and the VF null mutant reached a

final concentration of around 10^5 CFU/mL independent of the initial inoculum. However even *without any externally added carbon source* DG893 grew well in the presence of *L. polyedrum* indicating that the dinoflagellate leaked enough dissolved organic carbon (DOC) to fully support the growth of the bacterium. The notion that DG893 could utilize *L. polyedrum* as a carbon source was further supported by the observation that growth of DG893 was stimulated when it was incubated in the media containing the supernatant from a filtered *L. polyedrum* culture which contains non-specific organics secreted from *L. polyedrum*. These may possibly include dimethylsulfoniopropionate (DMSP) a labile carbon and sulfur source known to "leaked" from dinoflagellates (Caruana and Malin, 2014).

In the case of both "axenic" and nonaxenic cultures of the photosynthetic dinoflagellate *L. polyedrum*, iron proved to be a growth limiting nutrient. Thus maximum growth occurred at total iron concentrations of 100-1000 nM while higher concentrations proved toxic and lower concentrations (0-10 nM) were growth limiting. In the first culture, both "axenic" and non-axenic cultures grew equally well. However, their growth showed a remarkable difference in the second batch subculture. Here the non-axenic *L. polyedrum* culture continued to grow exponentially in although now only at the higher $[Fe]_T$. When the iron concentrations were kept high, *L. polyedrum* cultures continued to thrive up to at least 6 subcultures. However when the iron concentrations were allowed to be reduced by dilution in subsequent subculturing, the growth gradually ceased. Poorly growing subcultures in low iron media could however be rescued by the addition of additional iron to the culture. Remarkably "axenic" *L. polyedrum* subcultures ceased to grow regardless of $[Fe]_T$ but could be rescued by the addition of DG893. These results emphasize the importance of both bacteria and iron to *L. polyedrum* growth.

Our results further suggest that the *L. polyedrum* growth promoting effects of the bacterium *Marinobacter* DG893 were in fact not unspecific but at least partially related to its production of the photoactive siderophore vibrioferrin. Thus only the supernatant of DG893 that contained sufficient amounts of vibrioferrin facilitated *L. polyedrum* growth. While the addition of the supernatant from a culture of the VF null mutant of DG893 also improved grow of *L. polyedrum* the effect was much less than that from the WT. This observation was further confirmed by direct addition of purified VF into the *L. polyedrum* culture which growth increased 1.5 times more than those without VF. These results imply that the presence of the siderophore vibrioferrin clearly influences *L. polyedrum* growth, but that other factors such as vitamin B12 (Cruz-Lopez and Maske, 2015) provided by bacteria may also be important in promoting this apparent bacterial-algal mutualism.

Here we have focused on a bacteria that produces the photoreactive siderophore, vibrioferrin. Vibrioferrin was chosen for more detailed study for a number of reasons. First vibrioferrin has been isolated from several different bacteria which are known to be closely associated with HAB species (Amin et al., 2007) and we found that bacteria that had the ability to synthesize vibrioferrin were by far the most numerous as compared to the producers of other photoreactive siderophores which we followed during the bloom of *L. polyedrum* at Scripps Pier in 2011. We initially supposed that vibrioferrin was a good candidate for a siderophore that could provide bioavailable iron for both the bacterial produces and their algal partners as it is the most rapidly photolyzed of the photoactive siderophores tested and that photolyzed vibrioferrin has no further affinity for iron. This feature is unusual in that most other photoactive siderophores retain the ability to strongly bind Fe(III) even after photolysis (Amin et al., 2009). However we have recently showed that while vibrioferrin was the best source of iron for *L. polyedrum* of the ones

we tested (Yarimizu et al., 2017), it was not due to its photolysis since iron uptake from VF was the same in the dark as in the light. We therefore attribute its ability to provide bioavailable iron to the dinoflagellate to its relatively weak iron binding properties (with respect to other more traditional siderophores) as it lacks the sixth donor group required to complete the octahedral coordination geometry preferred by Fe(III) (Amin et al., 2009). This in turn leads to a less negative reduction potential (within falls within the biological range) so that the iron can readily be released from it by the cell surface reductases known to be present in *L. polyedrum.*

As a final note, while this laboratory study strongly supports a carbon for iron mutualism between the dinoflagellate *L. polyedrum* and *Marinobacter* DG893 as previously proposed (Amin et al, 2009), it is unclear at present how, or indeed if, such a mutualism will operate in the field. To this end we have collected data from several field studies involving both HAB and non-HAB bloom events and are currently searching for relationships between phytoplankton, vibrioferrin producing bacteria, and available iron. We hope that both these laboratory and field studies will complement each other and advance our knowledge of the potential role of bacterial-algal interactions in understanding the mechanisms of HAB formation.

5.6 AKNOWLEDGEMENTS

We thank Avery Tatter (University of Southern California) for providing *L. polyedrum* strain and helping us to set up algae culture laboratory. We thank Professor Michael Latz (Scripps Institute of Oceanography) for providing us reference *L. polyedrum*. We also thank Professor Katharine Barbeau (Scripps Institute of Oceanography) for providing us Pacific Ocean oligotrophic water and advice on iron measurement techniques. The National Science Foundation grant to CJC (CHE-1664657) is gratefully acknowledged for partial support of this work.

Chapter 5, in part, has been submitted for publication of the material as it may appear in Frontier, 2018, Yarimizu, K., Cruz-López, Carrano, C. J. The dissertation author was the primary investigator and author of this paper.

CHAPTER 6. POTENTIAL ROLE OF IRON AND VIBRIOFERRIN SIDEROPHORE DURING A *GYMNODINIUM CATENATUM* BLOOM IN THE GULF OF CALIFORNIA AND *CHATTONELLA MARINA* BLOOM IN BAJA CALIFORNIA PACIFIC

6.1 ABSTRACT

Phytoplankton blooms can cause acute effects on marine ecosystems due to their production of endogenous toxins and their enormous biomass leading to major impacts on local economies and public health. Despite years of effort, the causes of harmful algal blooms are still not fully understood. Our hypothesis is that bacteria that produce photoactive siderophores may provide a bioavailable source of iron for phytoplankton which in turn could stimulate algal growth and regulate bloom dynamics. Here we correlate iron concentrations, phytoplankton cell counts, bacterial cell abundance, and copy numbers for the photoactive siderophore vibrioferrin biosynthesis gene in water samples taken from blooms of the dinoflagellate *Gymnodinium catenatum* in Gulf of California in January 2015 and 2017, and from a Raphidophyceae *Chattonella marina* bloom in off the Pacific coast of northern Baja California in March 2017. Our results suggest that free-living siderophore producing bacteria likely play an important role in controlling phytoplankton populations.

6.2 INTRODUCTION

Phytoplankton blooms are a frequent phenomenon in the coastal regions of every continent in the world. Some of the blooming species have been found to produce endogenous

toxins and are consequently called harmful algae blooms (HABs), which can both directly and indirectly cause acute effects on marine ecosystems that have major impacts on local economies and public health (Lewitus et al., 2012). Direct human health effects derive from consumption of shellfish that have ingested these phytoplankton and accumulated their toxins, leading to paralytic, diarrheic, and neurotoxic poisoning syndromes that can in some cases be fatal (Anderson 1994; Honner et al., 2012). Indirect impacts of HABs include impairment of water quality leading to losses in the tourism and recreational industries. Even bloom forming phytoplankton that do not produce toxins can be harmful and cause ecological impacts such as the displacement of indigenous species, habitat alteration, and oxygen depletion (Glibert et al., 2005). The economic effects caused by HABs in the U.S. were estimated at $82 million per year in 2006 (Hoagland and Scatasta, 2006). The current strategy to reduce the health impact caused by HABs relies on frequent coastal monitoring and early detection of HAB species and their toxin levels. However the issue of how these HABs are initiated is still not well understood and therefore there is no strategy for their ultimate prevention.

Whether the factors promoting HABs are anthropogenic or have natural sources is an ongoing debate. Some argue oceanographic events such as upwelling, reversal and relaxation of winds, and global climate change are the major factors initiating phytoplankton blooms (Roegner et al., 2002; Tweddle et al., 2010). Others consider HABs the result of human activities such as increased nutrient loading, changes in agriculture, overfishing, and ballast water discharge (Gilbert, 2005). Still, others believe that improved tools are the primary reason for the increased detection of HAB species (Burkholder, 1998). Nevertheless, it is clear that HABs are a global threat to living marine resources and human health. While many studies have focused on isolating the causes of HABs from these perspectives, fewer have paid attention to the possible

effects that bacterial species who coexist with phytoplankton could contribute to their growth. However, since Bell and Mitchell (1972) reported that specific microflora were maintained and microbial activity was altered in the so-called phycosphere (Bell and Mitchell, 1972; Bell and Lang, 1974), an increasing number of studies have suggested that the interactions between phytoplankton and bacteria are very specific and important (Azam and Malfatti, 2007; Amin et al., 2015; Bertrand et al., 2015; Ramanan et al., 2016; Seymour et al. 2017). Indeed, it has been postulated that the mutualistic association of some phytoplankton and bacteria is driven by nutrient exchange. While nitrogen and phosphorus are the most often studied in this regard, the exact interactions involving these nutrients are not well understood (Hallegraeff and Gollasch, 2006). Our hypothesis is that certain bacteria may affect algal growth and bloom dynamics through their control of iron, a trace element known to be growth limiting to phytoplankton in many marine environments (Martin and Marahiel, 1988; Maldonado et al., 2005; Croot and Heller, 2012).

Iron is an essential element for all living organisms including phytoplankton and bacteria due to its involvement in photosynthesis and respiration. Despite iron being the fourth most abundant element on the Earth, its bioavailability in the marine environment is extremely low due to its poor solubility under the mildly alkaline aerobic conditions present in the ocean (Martin and Fitzwater, 1988; Wu and Luther III, 1994). To overcome this low bioavailability, bacteria and fungi have evolved sophisticated systems to produce high-affinity iron chelating compounds called siderophores to acquire, transport, and process this essential metal ion (Sandy and Butler, 2009). The major role of siderophores is to bind mineral phases of iron and to deliver the iron siderophore complex to specific outer membrane receptors on microbial cells. Several hundred siderophores have been isolated and extensively studied with respect to their synthesis,

structures and transport mechanisms over the last three decades (Yamamoto et al., 1994; Challis, 2005; Sandy and Butler, 2009: Raymond et al., 2015). While much research has been done on terrestrial siderophores, the study of marine siderophores is less extensive and only a relative few have been fully elucidated (Vraspir and Butler, 2009). Nevertheless one of the two major attributes that seem to distinguish marine siderophores from those of terrestrial origin is the tendency of the former to contain a α- and β-hydroxy acid group in their iron binding domain (Barbeau et al., 2001, 2002; Küpper et al., 2006). The significance of the presence of these functional groups in siderophores is in their ability to make the iron siderophore complex photoreactive. The chelated Fe(III) in such siderophores is reduced in the presence of sunlight via an internal redox process to release Fe(II), a more soluble form of iron (Amin et al., 2009). It has been proposed that sunlight-driven reduction of the Fe(III) would transiently produce Fe(II) which might be utilized not only by the siderophore producing bacteria themselves but also non-siderophore producing bacteria and other organisms such as phytoplankton (Maldonado et al., 2005; Naito et al., 2008; Amin et al., 2009, 2012).

While iron acquisition by bacteria is well understood, that of phytoplankton remains less so. There are data to support the possibility of a variety of iron uptake mechanisms being operative simultaneously depending on the species involved. These include an iron reductive route via a cell surface reductase, a direct xenosiderophore-mediated mechanism and cell surface enhanced processes (Sutak et al. 2012). However as of yet there are no well documented examples, with some exceptions among the cyanobacteria, where phytoplankton have been shown to produce their own siderophores for iron acquisition (Raven, 2013). Thus how phytoplankton effectively acquire this metal from the low concentration iron environment is still unclear.

Our hypothesis is that algal growth and bloom dynamics may be affected by the increased bioavailability of iron engendered by the presence of photo-active siderophores produced by mutualistic bacteria. An important component for the evaluation of this hypothesis is the ability to measure the presence or absence of such siderophores in the marine environment. However the direct quantification of photoactive siderophores in seawater is very difficult due to their extremely low concentrations and their rapid degradation by photochemical reactions. The siderophore vibrioferrin for example has a half-life of less than 7 min in sunlight illuminated seawater. Our approach has been an indirect one that uses highly sensitive molecular biology technology (RT-qPCR) to search for genes involved in the biosynthesis of photo-active siderophores from seawater derived DNA. RT-qPCR can detect as few as 20 gene copies (Bach et al., 2002; Labrenz et al., 2004) which is thousands of fold lower detection limit than obtainable by HPLC for example. Measuring biosynthesis gene copies in the marine environment does not directly represent siderophore concentrations but rather only quantifies the density of bacteria that carry photoactive siderophore biosynthesis genes, which may or may not be transcribed. Nevertheless in most oceanic regimes where the iron level is extremely low, it can be strongly argued that siderophore biosynthesis should typically be "turned on" and bacterial derived siderophore production should thus be highly active (Johnson et al., 1994). We have in several cases confirmed this presumption (unpublished results) validating its role as a siderophore proxy.

Using this technology and approach we have recently studied a bloom of the dinoflagellate, *Lingulodinium polyedrum*, at the Scripps Pier (San Diego, CA, USA) in 2011. *L. polyedrum* is one of the HAB species known to produce Yessotoxins, a group of polyether toxins which can accumulate in shellfish and show high toxicity to mice via intraperitoneal injection

(Tubaro et al., 2004). As the first step to search for an association of phytoplankton with specific bacterial photoactive siderophore producers (producing petrobactin, aerobactin, and vibrioferrin siderophores) we monitored both the population of *L. polyedrum* and the bacterial siderophore producers before, during, and after the 2011 bloom. The results showed that both *L. polyedrum* and the bacterial siderophore producers simultaneously increased and decreased during the bloom period (Yarimizu et al., 2014). At the L. polyedrum bloom maximum, the total number of bacterial photoactive siderophore producers reached their maximum accounting for roughly 9% of the total bacterial population suggesting that such high abundance of photoactive siderophore producers could potentially provide bioavailable iron to the phytoplankton in this environment. Further when the PCR derived amplicons were sequenced a phylogenetic tree constructed from the sequencing results showed that the community of siderophore producers pre-bloom was statistically significantly different than those found during and after the bloom by UniFrac analysis suggesting that this particular bacterial community could be involved in bloom initiation.

The chapter provides new environment data from two blooms of dinoflagellate *Gymnodinium catenatum* in the Gulf of California in 2015 and 2017 as well as a bloom of Raphidophyceae *Chattonella marina* in Baja California Pacific Ocean in 2017. *G. catenatum* is specially becoming a major HAB species in Gulf of California and happen to be seen every winter since 2015. It is a paralytic shellfish toxin (PST) producer and is preferably found in temperate and tropical waters in the world (Hallegrae and Fraga, 1998). This study assayed water samples collected from these three blooms to seek for correlation of phytoplankton, siderophore producing bacteria, and iron concentration. Here we specifically focused on producers of a single photoactive siderophore, vibrioferrin. Vibrioferrin was chosen for more detailed study for a

number of reasons. First it has only relatively weak iron binding properties as it lacks the sixth donor group required to complete the octahedral coordination geometry preferred by Fe(III) (Amin et al., 2009). More importantly photolyzed vibrioferrin has no further affinity for iron while most other photoactive siderophores retain the ability to strongly bind Fe(III) even after photolysis (Amin et al., 2009). In addition, vibrioferrin has been isolated from several different bacteria which are known to be closely associated with HAB species (Amin et al., 2007). Finally we found that bacteria that had the ability to synthesize vibrioferrin were by far the most numerous as compared to the other photo-active siderophore producers we followed during the bloom of *L. polyedrum* at Scripps pier in 2011.

6.3 MATERIALS AND METHODS

6.3.1 Study sites

Study site 1 - Gulf of California *Gymnodinium catenatum* bloom of 2015: The study site is located in the northwestern region of the Gulf of California, San Felipe, (México, 30.9ºN - 31.1ºN and 114.6ºW - 114.8˚W). The dinoflagellate bloom of *G. catenatum* was observed in the middle of January 2015 most intensively on the northwestern coast of the Gulf. Of the 22 points located in an area of 25 km parallel to the coast and 11 km offshore, four points with distinctive differences in Chlorophyll *a* concentrations were our interest: Station 4 (SF4: 31.00575°N - 114.64435°W) at surface, station 8 (SF8: 30.9454°N - 114.65455°W) at surface and 15 m depth, and station 7 (SF7: 30.93085°N - 114.70435°W). On January 17th and 18th, 2015 at the peak of *G. catenatum* bloom, the water samples were collected from these four points (Figure 38).

Study site 2 - Gulf of California *Gymnodinium catenatum* bloom of 2017: Exactly two years later, another *G. catenatum* bloom occurred in the Gulf of California at Puertecitos, far south of San Felipe (Figure 38). The research cruise could not be operated at the bloom peak due

to the storm, and thus the water sample collection was performed after the bloom peak, February 4, 2017, from five stations: station 1 (30.19757°N – 114.35792°W) at surface and 10 m depth, station 2 (30.20913°N - 114.35904°W) at 10 m depth, station 3 (30.22226°N - 114.36083°W) at surface and 10 m depth, station 4 (30.24557°N - 114.36303°W) at surface, and station 5 (30.25880°N - 114.36251°W) at 10 m depth.

Study site 3 - Baja California Pacific Ocean *Chattonella marina* bloom of 2017:

This was a 4-day research cruise in the Pacific Ocean along the coast to offshore of Ensenada Mexico to the United States boarder on March 23 - March 26, 2017 (Figure 39). Of 50 stations originally planned to study, some were withdrawn during the cruise due to logistics reasons and others were eliminated from analysis due to the error during sample processing. As a result, the total of 22 stations with two depths, surface and Deep Chlorophyll a Maximum (DCM) detected with a SBE 19 plus V2 SeaCAT Profiler CTD (Sea-Bird Scientific, Bellevue, WA, USA), were analyzed for this study. During the cruise, a bloom of *C. marina* bloom was observed within a small diameter of station 31.

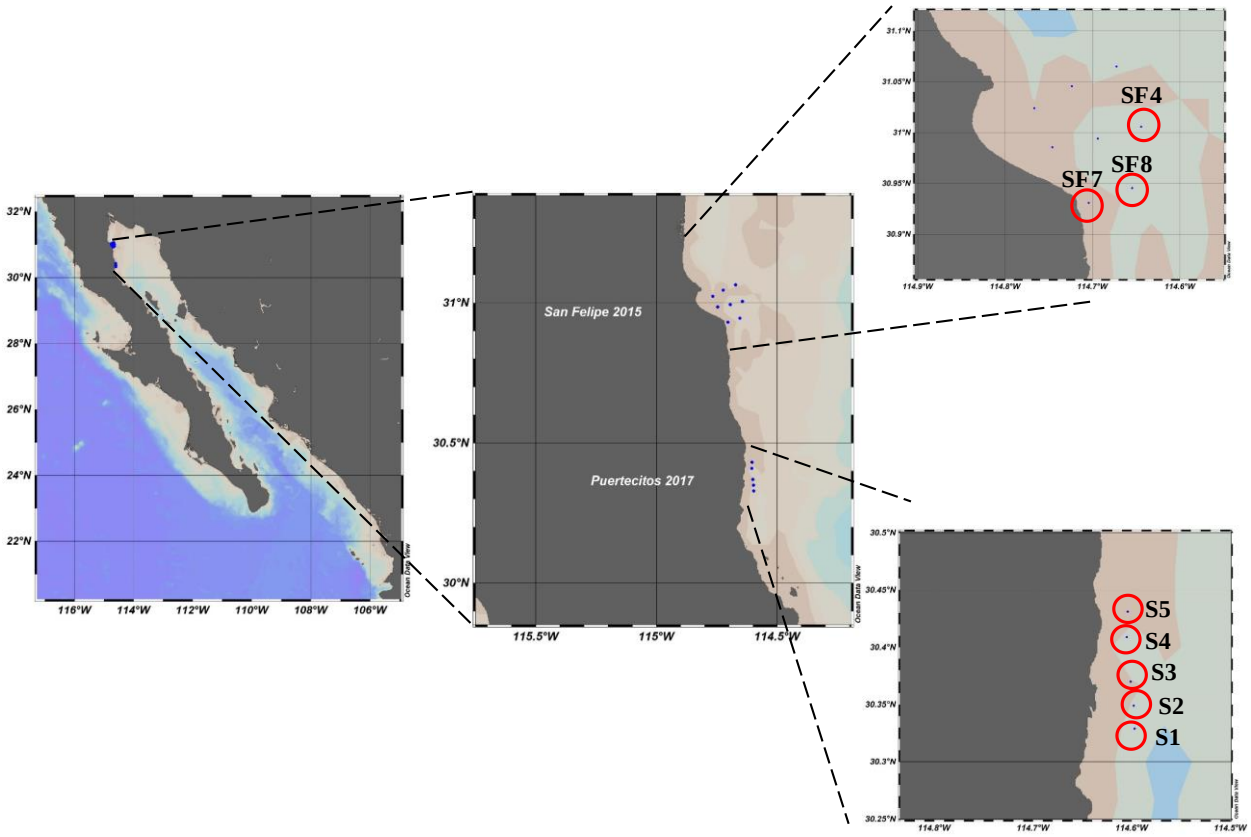

Figure 38 Station map of cruise at Gulf of California during *G. catenatum* bloom in January 2015 and February 2017

The bloom occurred in northern part of the Gulf in 2015 (San Felipe) while 2017 bloom was in southern part of the Gulf (Puertecitos)

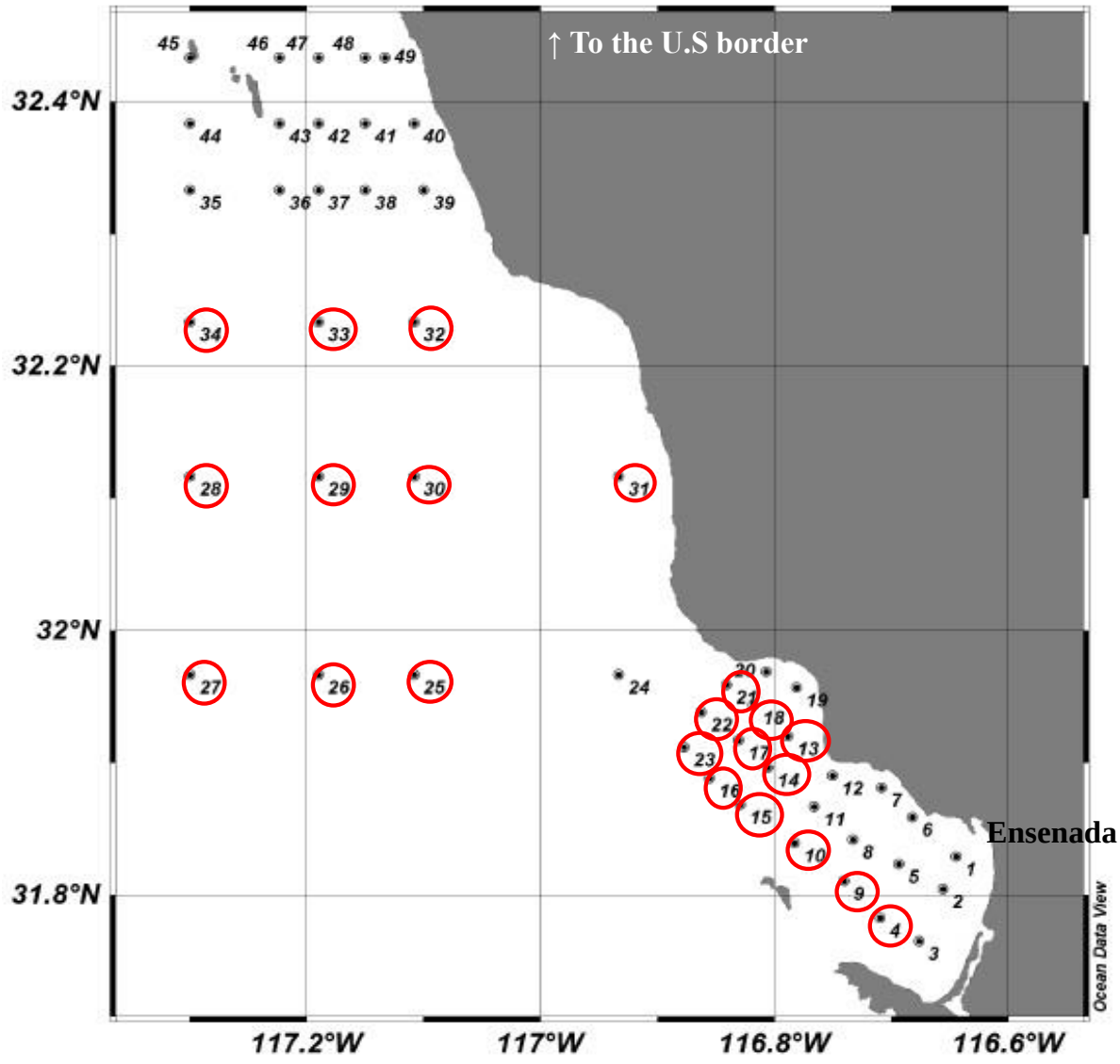

Figure 39 Station map of cruise at Baja California Pacific Ocean during *Chattonella marina* bloom in March 2017

6.3.2 Sampling

The location was determined by real-time monitoring using a Sea Soar and Moving Vessel Profiler and sampling depths were determined based on pressure triggered by an auto-fire module mounted on the rosette for the Niskin casts. The water samples were collected using a trace metal rosette with Teflon-coated Niskin bottles deployed on non-metallic hydroline. For

phytoplankton cell count analysis, the water samples were placed in dark plastic bottles and fixed with a Lugol-acetate solution per Utermöhl technique (Utermöhl, 1958; Sournia, 1978). For measuring chlorophyll *a* (Chl *a*) concentration, the water samples were filtered through 25 μm diameter GF/F filters and the membrane were stored in -20˚C storage until analysis. For analysis of siderophore producing bacteria, one liter of water samples were collected in acid washed Nalgene bottles (VWR 16058-189) and immediately filtered through tandem connected 0.8 μm and 0.2 μm pore size polyvinylidene fluoride membranes using a pressure less than 3.3 kPa to avoid cell disintegration. The membranes were stored in liquid nitrogen until DNA extraction was performed. In theory, 0.8 μm and 0.2 μm pore-size membranes separate bacteria associating with eukaryotic phytoplankton from free-living bacteria. For measuring total iron concentration, 100 mL of the 0.2 μm filtered water from each station was acidified by adding 200 μL of concentrated trace metal grade hydrochloric acid immediately after filtration. The acidified samples were stored at -20°C until the iron assay was performed.

6.3.3 Chlorophyll *a* and phytoplankton cell count

The samples collected for phytoplankton cell count analysis were placed in dark plastic bottles and fixed with a Lugol-acetate solution per Utermöhl technique (Utermöhl, 1958; Sournia, 1978) was used to count and identify phytoplankton cells. The phytoplankton sediment was analyzed to count the cell numbers and identify the species under a LEICA DMI3000B (Leica Microsystems, Germany). The method of quantification of Chlorophyll *a* (Chl *a*) and other phytoplankton pigments was adopted from Heukelem and Thomas (2001) and modified by Almazán-Becerril and García-Mendoza (2008). The extraction and pigment quantification of particulate material was performed by high performance liquid chromatography (HPLC) using a Agilent 1260 instrument equipped with a Zorbax Eclipse XDB-C18 reverse-phase column (150

mm length x 4.6 mm internal diameter and 3.5 μm size particles). This method has been validated with 16 pigment standards (DHI, Inc., Sweden) as described in Almazán-Becerril and García-Mendoza (2008).

6.3.4 DNA extraction

Details of DNA extraction procedure is provided in Appendix A. Briefly, the membranes that filtered the sample seawaters were treated for DNA extraction using a slightly modified XS buffer method (Tillett and Neilan, 2000; Yilmaz and Phlips, 2009). Each membrane was placed in an autoclaved Eppendorf tube and soaked in 1 mL buffer containing 0.1M TrisHCl (pH7.4), 0.02M EDTA (pH8.0), 0.8M ammonium acetate, 1% (w/v) SDS, 1% (w/v) potassium ethyl xanthenate, and 6.25 mg/mL RNase A. The bacterial cells were lysed by incubating the tubes in a 70˚C water bath for 30 min with frequent vigorous vortexing followed by incubation on ice for 15 min. The membranes were removed from the tubes, and the cell debris was discarded after centrifuging the cell lysate at 14,000 rpm for 10 min. The supernatant was transferred into a new autoclaved tube and mixed with 1 mL of molecular biology grade isopropanol for 10 min at room temperature. The precipitated DNA was collected by centrifugation at 14,000 rpm for 10 min at 4˚C. The collected DNA was washed with 1mL of 70% cold ethanol twice, dried to remove ethanol in a 40ºC incubator for 30 min, and resuspended in 100 μL of 30 mM TE buffer (pH8.0) for storage at -20˚C until analysis. In many cases, the initial assay of the extracted DNA via RT-qPCR exhibited no sign of a fluorescence signal for the 16S rRNA gene indicating presence of inhibitory substances in the environmental samples interfering with the assay, which has been reported in several studies in the past (Bach et al., 2002; Yarimizu et al., 2014). Therefore all the extracted DNA samples from 0.8 μm membranes were further purified using

QIAamp DNA Stool Mini Kit (Qiagen, P/N 51504) according to the manufacturer's recommendations.

6.3.5 Primers

The target gene of interest is *pvsB* which is the enzyme involved in the last step of vibrioferrin siderophore biosynthesis (Challis, 2005). Two sets of degenerate primers designated pvsB and vibXII, both encoding for the *pvsB* gene, were previously designed by sequence alignment from dozens of bacteria known as vibrioferrin producers (Appendix B). The primer designated pvsB was designed to hybridize the *pvsB* gene from *Marinobacter* species while the vibXII primer amplified the *pvsB* gene from *non-Marinobacter* species. Two separate degenerate primer sets were necessary as we could not find a single set that could adequately quantify both *Marinobacter* and non-*Marinobacter pvsB* (Gärdes et al., 2013). Nevertheless the PCR amplicons from both the pvsB and vibXII primer sets detect the same *pvsB* gene and hence report on the presence of vibrioferrin biosynthesis.

6.3.6 Detection of siderophore synthesis gene by RT-qPCR

The procedure is summarized in Appendix B. The DNA standard for use with primer pvsB was extracted from *Marinobacter algicola DG893* (GenBank code NZ_ABCP00000000.1) while that for use with vibXII was extracted from *Vibrio splendidus* (GenBank code NZ_AJZL00000000.1). Using RT-qPCR we constructed the standard curve from these genomic DNA covering the concentration range of 0.0002 ng/μL to 200 ng/μL. Each PCR sample was prepared in triplicate by mixing 12.5 μL SYBR Green (Bio-Rad, P/N 1725120), 3 μM each primer, 2 μL DNA sample or standard, and water to a final 25 μL volume. The standards and samples were assayed for *pvsB* gene detection by fluorescence signal using ICycler IQ-5 thermocycler equipped with a multicolor detection system as previously described (Gärdes, et

al., 2013). The temperature program was consisted of an initial incubation at 95˚C for 5 min followed by 45 cycles of 95˚C for 10 s and 60˚C for 1 min. The melt curve was collected by an additional temperature program which increased 0.5°C per 30 s for 71 cycles between 60°C to 95°C. The assay results were analyzed by Bio-Rad IQ-5 Software 2.0. The reliability of dataset was monitored by examining the linearity of standard curve with a correlation coefficient of 0.99 or above being required for acceptance. Comparing the fluorescence signal from standards and samples, the sample starting quantity, the amount of DNA containing *pvsB* gene in ng/µL, was obtained.

6.3.7 Theoretical bacterial cell count

The following procedure was adopted (Labrenz et al., 2004; Degen et al., 2006: Ritalahti et al., 2006) to calculate gene copy number of *Marinobacter* based *pvsB* in environmental samples.

$$gene\ copy\ per\ L = DNA\ conc.\left(\frac{ng}{\mu l}\right) \text{ x } \left(\frac{1\ g}{10^9\ ng}\right) \text{ x } \left(\frac{1\ mol\ bpDNA}{660\ g\ DNA}\right)$$

$$\text{x } \left(\frac{6.022 \text{ x } 10^{23}\ bp}{mol\ bp}\right) \text{ x } \left(\frac{1\ copy}{genome\ bp}\right) \text{ x } \left(\frac{number\ of\ target\ gene}{1\ genome\ of\ standard}\right) \text{x } CF$$

DNA conc. is starting quantity (SQ) of sample DNA containing *pvsB* gene in ng/µL obtained by RT-qPCR. *CF* is concentration factor and *genome bp* is genome length of standard *DG893*, (4,413,003 bp). The average MW of one DNA base pair is assumed to be 660 g/mon. The number of *pvsB* copies in the standard *DG893* genome is one. The same equation was used to obtain non-*Marinobacter* based *pvsB* gene copy numbers using standard genome size of *Vibrio splendidus* of 5,282,500 bp and one *pvsB* gene copy per genome. Estimation of bacterial cell number from gene copy number was obtained from the following equation where the average

copy number of *pvsB* gene and *16s rRNA* genes is assumed to be 1.0 and 1.8, respectively (Biers et al., 2009).

$$bacterial\ cell\ number\ in\ L = \left(\frac{gene\ copy\ number}{L}\right) \text{ x } \left(\frac{1\ genome}{number\ of\ target\ gene}\right)$$

6.3.8 Determination of total dissolved iron concentration $[Fe]_{diss}$

The total dissolved iron concentration was measured by anodic stripping voltammetry in a dedicated trace metal clean hood in triplicate via Fe standard addition (Bruland et al., 1991; Abualhaija and van den Berg, 2014; Buck et al., 2012). All implements including pipettes were acid washed prior to use. Salicylaldoxime (SA: ≥ 98%, Fluka) was prepared at 4 mmol/L in HPLC grade methanol. Borate-ammonium buffer was prepared at 1.5 mol/L of boric acid (≥99.99%, Alfa Aesar) in 0.4N trace metal grade ammonium hydroxide. Dissolved Fe standard (atomic absorption standard solution) was purchased from Aldrich and diluted to 1 µM with 0.01N HCl. The seawater samples from each station were filtered through 0.22 µm membrane and 100 mL of filtrate was acidified by adding 200 µL of concentrated metal free HCl and stored at frozen for a week. A day before assay, acidified sample was mixed with 7.5 mM borate-ammonium buffer, was adjusted to pH 8.2 with NH_4OH, was incubated at ambient temperature for 2 hours, was mixed with 5µM salicylaldoxime solution, and was equilibrated at ambient for 24 hours. The Controlled Growth Mercury Electrode (CGME) system was purchased from BioAnalytical Systems (BASi) and coupled to a BASi Epsilon 2 Voltammetric Analyzer. Total dissolve iron concentration was determined by triplicate reading of sample peak height at around -450 mV obtained from 10 mL sample placed in Teflon cells as compared to five-point iron standard created from 10 µL increment addition of 1 µM Fe standard. The parameters used were: 45sec deposition time, stir during deposition, 10 seconds quiet time, without purge, 0 mV initial

potential, -850 mV final potential, 10 μA full scale, 6 mV step E, 35 ms pulse width, 50 mV pulse amplitude, 1m sec sample period.

6.3.9 Statistical analysis

All statistical analyses were done using SYSTAT ver 12. Prior to analyses, all data were examined for normality and equality of variances. The dataset on vibrioferrin gene copy number were statistically assessed for significant differences and similarity in areas. All data were then examined for normality and homoscedasticity using graphical interpretation of residuals. Multiple Pearson's correlations was used to determine if ocean nutrient variables (i.e. Fe, NO_3, NO_2, NH_4, PO_4, SiO_2) were correlated with one another. Following this, independent linear regressions were used to examine the relationships between iron and each of the categories (abundance of *G, catenatum*, free-living and attached *Marinobacter* VF producers, free-living and attached non-*Marinobacter* producers, free-living and attached total bacteria).

6.4 RESULTS

6.4.1 Gulf of California *G. catenatum* bloom of 2015

This study analyzed water samples collected from Gulf of California on January 17th 2015, the peak of *G. catenatum* bloom. The main purpose of this study was to examine the relationship between the abundance of *G. catenatum* and vibrioferrin producing bacteria with respect to their concentration during a bloom. The estimated *G. catenatum* cell count was 3000, 34100, 9300, and 9300 cells/L for station SF4, SF7, SF8, and SF8 (15 m depth), respectively, implying that SF7 was the core of the bloom and SF4 was far from the bloom. This was supported by the Chl *a* analysis showing that the water from SF7 contained the highest pigment concentration (6.18 μg/L) and that from SF4 was the lowest (3.12 μg/L). Consistent with *G. catenatum* population, the water from SF4 contained much lower concentration of both total

bacteria and VF producing bacteria compared to the other three sites. The reason for the low abundance of *G. catenatum* as well as bacteria at SF4 is likely due to the location of SF4 which was not only far from the bloom core but also far away from the coast. Next, the core of the bloom (SF7) and the station located closer to the core but slightly away from the coast (SF8) were compared. Interestingly, the water from SF7 having the highest abundance of *G. catenatum* cell was found to contain lesser amount of total bacteria and VF producers while the water from SF8 contained lower *G. catenatum* cell and higher bacterial cell counts (Figure 40). A various reasons for this observation, increased *G. catenatum* with decreased bacterial number near the bloom core, could be considered such as timing of the sampling (night of the bloom peak day for this study), species specific interaction, location specific interaction, and seasonal effect. However, further study with a larger sample size will be necessary to make any conclusions. Another observation from this cruise was that the non-*Marinobacter* based VF producing bacteria, which are primarily *Vibrio* species, were several orders of magnitude more abundant than that from *Marinobacter* based at all four sites (Figure 41). Additionally, the VF producing bacteria were predominantly found on the 0.8 μm filters suggesting that VF producers were possibly associated with phytoplankton during the *G. catenatum* bloom (Figure 41). The reason for the high concentration of attached non-*Marinobacter* VF producer during this cruise was not known and further studies were needed to conclude. This cruise however, collected brief information on *G. catenatum* and VF producer to initiate a study on algae-bacterial relationship.

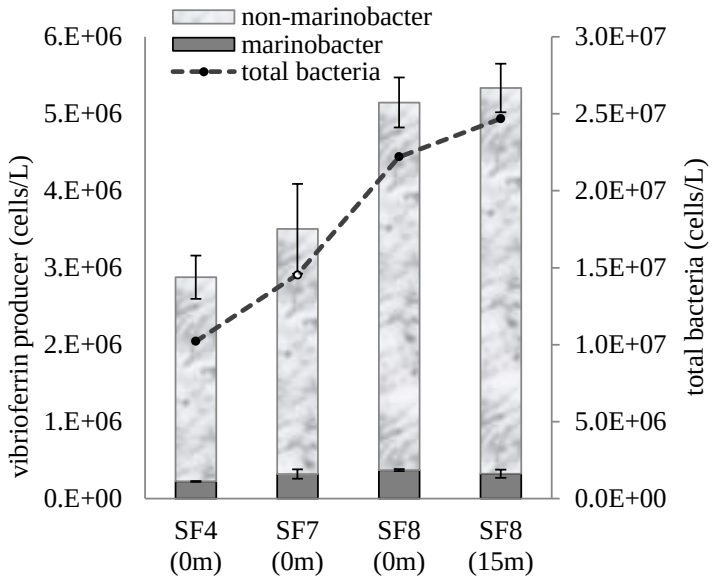

Figure 40 Estimated population of vibrioferrin producing bacteria cell (*Marinobacter* and *non-Marinobacter*) and total bacteria cell from the four study sites at Gulf of California during *G. catenatum* bloom (January 17th, 2015)

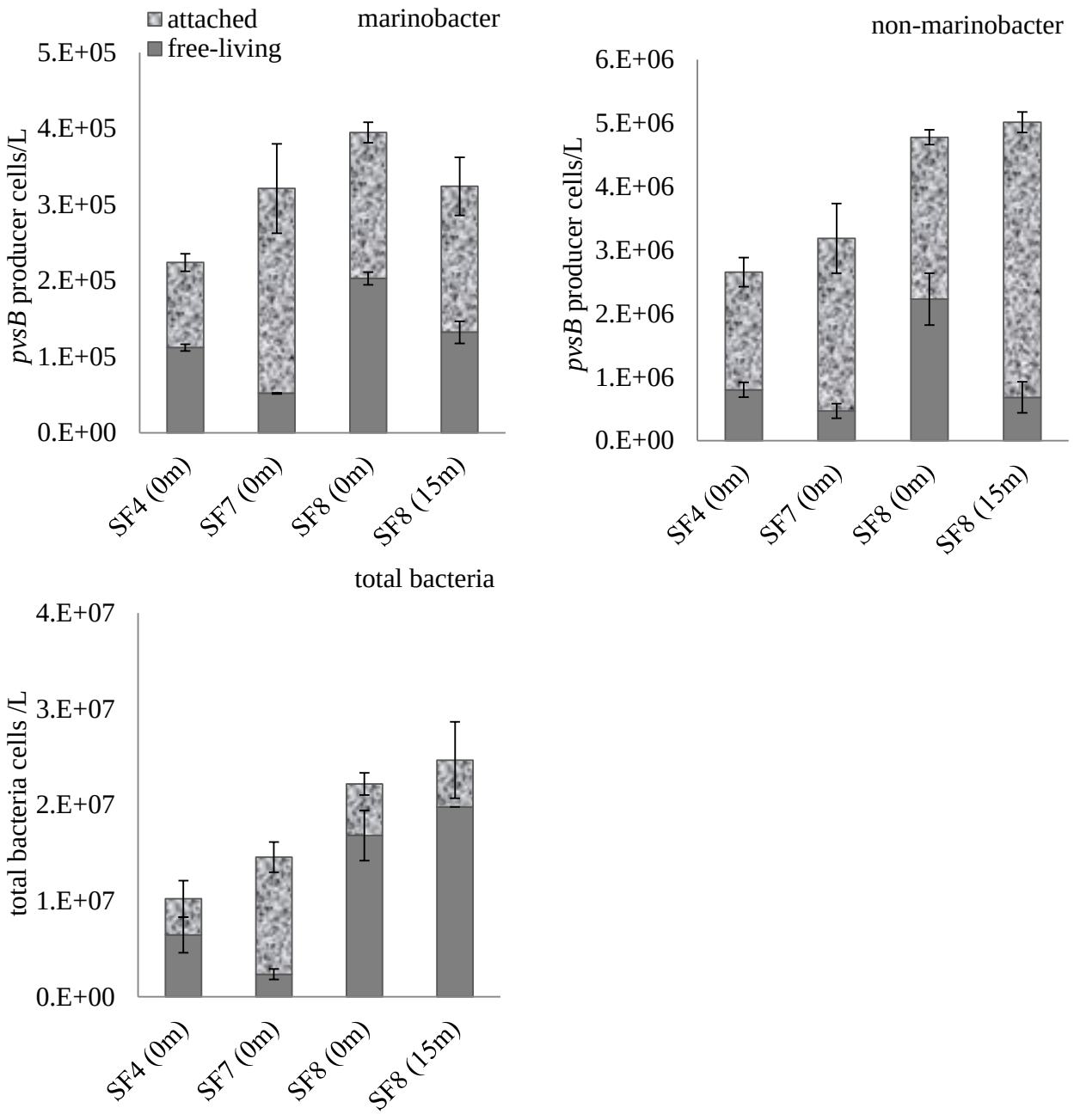

Figure 41 Distribution of free-living and attached bacteria during *G. catenatum* bloom at Gulf of California in January 2015

Table 17 Summary of bacterial cell number per liter of seawater collected from Gulf of California on January, 2015

Depth, m	pvsB (free-living)		pvsB (attached)		pvsB (Total)	
	cell#/L	STDEV	cell#/L	STDEV	cell#/L	STDEV
SF4 (0m)	1.12E+05	4.30E+03	1.12E+05	1.15E+04	1.92E+05	6.21E+03
SF7 (0m)	5.19E+04	7.82E+02	2.69E+05	5.88E+04	2.94E+05	5.78E+04
SF8 (0m)	2.03E+05	8.28E+03	1.92E+05	1.36E+04	3.19E+05	1.11E+04
SF8 (15m)	1.32E+05	1.47E+04	1.92E+05	3.82E+04	2.79E+05	4.61E+04

Depth, m	vibX (free-living)		vibX (attached)		vibX (Total)	
	cell#/L	STDEV	cell#/L	STDEV	cell#/L	STDEV
SF4 (0m)	8.00E+05	1.17E+05	1.85E+06	2.29E+05	2.25E+06	2.43E+05
SF7 (0m)	4.67E+05	1.15E+05	2.72E+06	5.47E+05	2.88E+06	5.50E+05
SF8 (0m)	2.23E+06	4.09E+05	2.55E+06	1.17E+05	3.93E+06	2.60E+05
SF8 (15m)	6.80E+05	2.44E+05	4.33E+06	1.62E+05	4.57E+06	2.15E+05

Depth, m	16S (free-lving)		16S (attached)		16S (Total)	
	cell#/L	STDEV	cell#/L	STDEV	cell#/L	STDEV
SF4 (0m)	6.46E+06	1.85E+06	3.76E+06	1.89E+06	8.53E+06	1.52E+06
SF7 (0m)	2.35E+06	5.46E+05	1.22E+07	1.59E+06	1.30E+07	1.39E+06
SF8 (0m)	1.68E+07	2.62E+06	5.39E+06	1.15E+06	1.91E+07	1.88E+06
SF8 (15m)	1.98E+07	0.00E+00	4.88E+06	3.99E+06	2.18E+07	2.17E+06

The primer designated pvsB was designed to hybridize the *pvsB* gene from *Marinobacter* species while the vibXII primer amplified the *pvsB* gene from non-*Marinobacter* species. Two separate degenerate primer sets were necessary as we could not find a single set that could adequately quantify both *Marinobacter* and non-*Marinobacter pvsB* (Gärdes et al., 2013). Nevertheless the PCR amplicons from both the pvsB and vibXII primer sets detect the same *pvsB* gene and hence report on the presence of vibrioferrin biosynthesis.

6.4.2 Gulf of California *G. catenatum* bloom of 2017

This study assayed water samples collected from Gulf of California in February 2017 during *G. catenatum* bloom to assess the relationship between phytoplankton and VF producing bacteria with total dissolve iron concentration $[Fe]_{diss}$. The *G. catenatum* was most bloomed in surface water of station S3 (52500 cells/L) followed by station S2 at 10 m depth (48679 cells/L). All seven points studied during this cruise were located in close proximity and thus clear difference was not seen between the stations with respect to algae-bacterial relationship. Instead of station based, the data were organized by the order of *G. catenatum* population to find a better pattern of algal-bacterial interaction with $[Fe]_{diss}$ (Figure 42). Inconsistent with the bloom in 2015, total bacteria cell count slightly increased along with *G. catenatum* in this study. Consistent with the bloom in 2015, the two highest bloomed stations (S3 0m and S2 10m) showed remarkably low abundance of non-*Marionobacter* VF producing bacteria in this study. The *Marinobacter* VF producing bacteria showed independent distribution from *G. catenatum* (Figure 42). The numbers of reasons for these observations with respect to alga-bacterial distribution can be thought, but one thing should be clearly stated is that the timing of sampling here was different from that of 2015. The water sample collection was delayed by two weeks from the peak of bloom in this study due to the storm while the collection was made on the maximum bloom day in 2015. Additionally, although both 2015 and 2017 *C. catenatum* blooms occurred in Gulf of California, the exact bloom location was different between these two events, San Felipe in 2015 and Puertecitos in 2017. The similarity of these two HAB events was the season of occurring, both during warm winter. However, the weather on the day of sampling was different, 2015 with sunny warm day and 2017 with right after the storm.

A positive attribute of this study was addition of analysis for $[Fe]_{diss}$. The total dissolved iron was decreased as *G. catenatum* increased. In general, it is difficult to see a clear pattern of $[Fe]_{diss}$ between closely located stations because iron is not only diluted to nM level in oceans but also the degree of dilution is even more pronounced at the surface water. Traditionally, a clear $[Fe]_{diss}$ trend seems to be seen only when compared between vertical water columns, higher $[Fe]_{diss}$ with deeper depths. This is explained by much more abundant phytoplankton biomass on surface water consuming available iron as their nutrient (Vraspir et al., 2009). Thus, it was a surprise that the closely located seven sites in this study showed a noticeable enough pattern, decreased $[Fe]_{diss}$ with increased *G. catenatum*. This was our first attempt on measuring $[Fe]_{diss}$ on the bloom water samples. The method may have a high potential use for $[Fe]_{diss}$ comparison even between closely located surface water samples.

Similar to the *G. catenatum* bloom in Gulf of California in 2015, this study also predominantly showed non-*Marinobacter* VF producers over *Marinobacter* (Figure 43). However, inconsistent with 2015 HAB, the samples from 2017 were abundant with free-living non-*Marinobacter* over attached. The observation of which more available non-*Marinobacter* over *Marinobacter* has been seen in three HAB events so far, the *G. catenatum* bloom in Gulf of California in 2015 and 2017 as well as *L. polyedrum* bloom in Scripps pier, San Diego in 2011 (Yarimizu et al., 2014). What this means to HABs is unclear at this point, but our speculation is that certain community of VF producer may be more involved in HAB events. The reason for the preference with free-living over attached VF producer in a HAB event is also not known but may involve timing of sampling such as before, during, after the bloom.

Being aware of the small sample size (n=7), the dataset was further analyzed statistically using the Regression analysis. The analysis showed a significant relationship between the

population of *G. catenatum* and free-living *Marinobacter* VF producer (p=0.030) as well as between *G. catenatum* and free-living total bacteria (p=0.033). The involvement of free-living bacteria in a phytoplankton bloom was a surprising outcome for us because numbers of studies have acknowledged the importance of attached bacteria as compared to free-living bacteria playing more important roles in bloom dyanmics (Rooney-Varga et al., 2005; Grossart et al., 2005). The relationship between $[Fe]_{diss}$ and *G. catenatum* was, while not statistically significant, appeared to have potentially weak associations (p=0.138). The effect of $[Fe]_{diss}$ on other variables may be difficult to see with statistical analysis due to the small variability in $[Fe]_{diss}$ between the seven sites (0.2 - 4 nM) unless $[Fe]_{diss}$ were transformed to have their large contributions on patterns (Clarke and Warwick, 2001). In a meantime, a strong correlation was found in between $[Fe]_{diss}$ and attached non-*Marinobacter* VF producer (p=0.081). Further studies need to be performed to make any concrete conclusions. However, this cruise collected additional information on *G. catenatum* and VF producer relation with respect to $[Fe]_{diss.}$

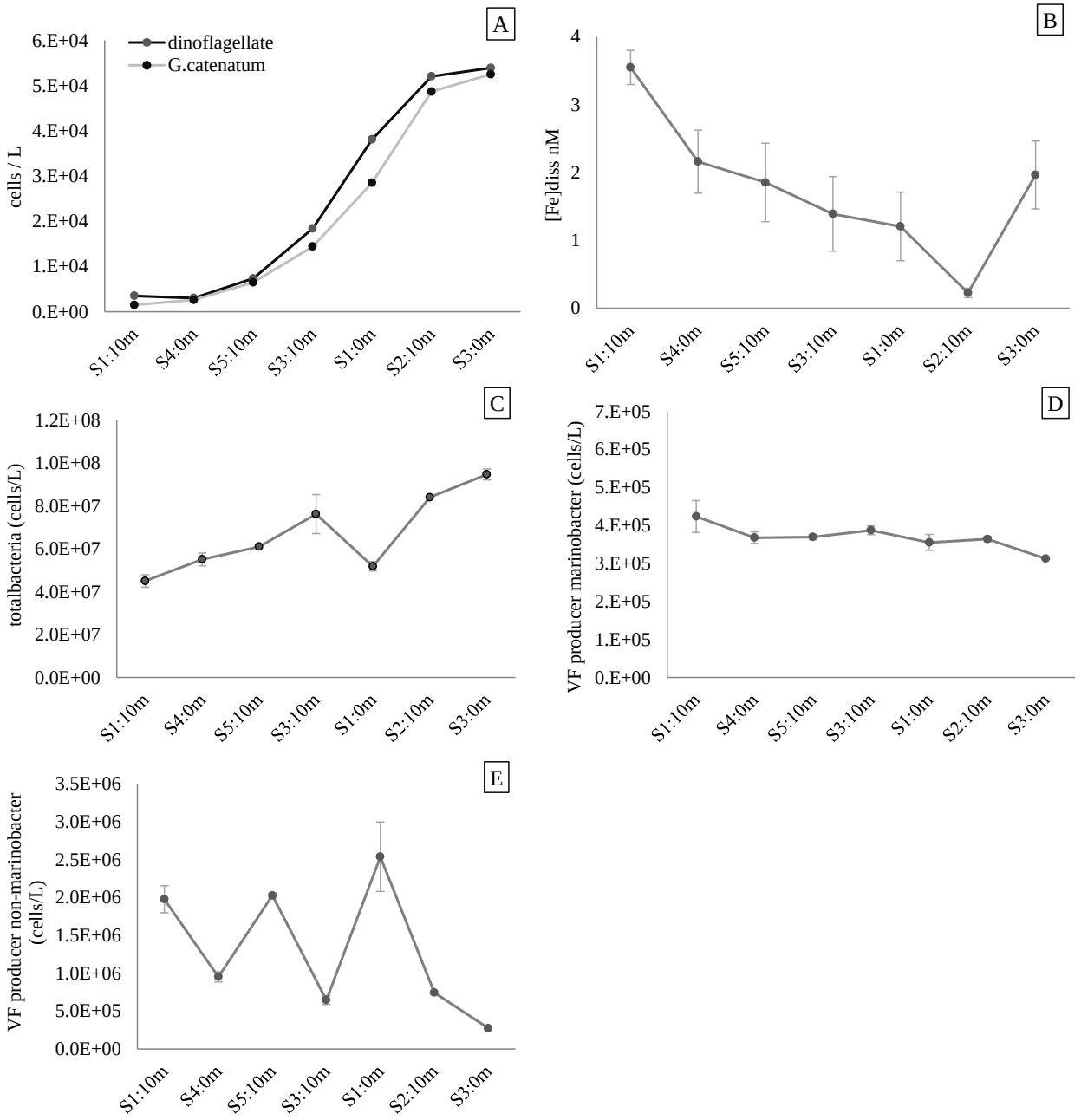

Figure 42 Concentration of Fe, G. catenatum, total bacteria, and vibrioferrin producing bacteria from Gulf of California on February, 2017

A: dinoflagellate and G. catenatum cell count, B: total dissolved iron, C: estimated total bacterial cell counts, D: estimated *Marinobacter* vibrioferrin producing bacteria count, E: estimated non-*Marinobacter* vibrioferrin producing bacteria count.

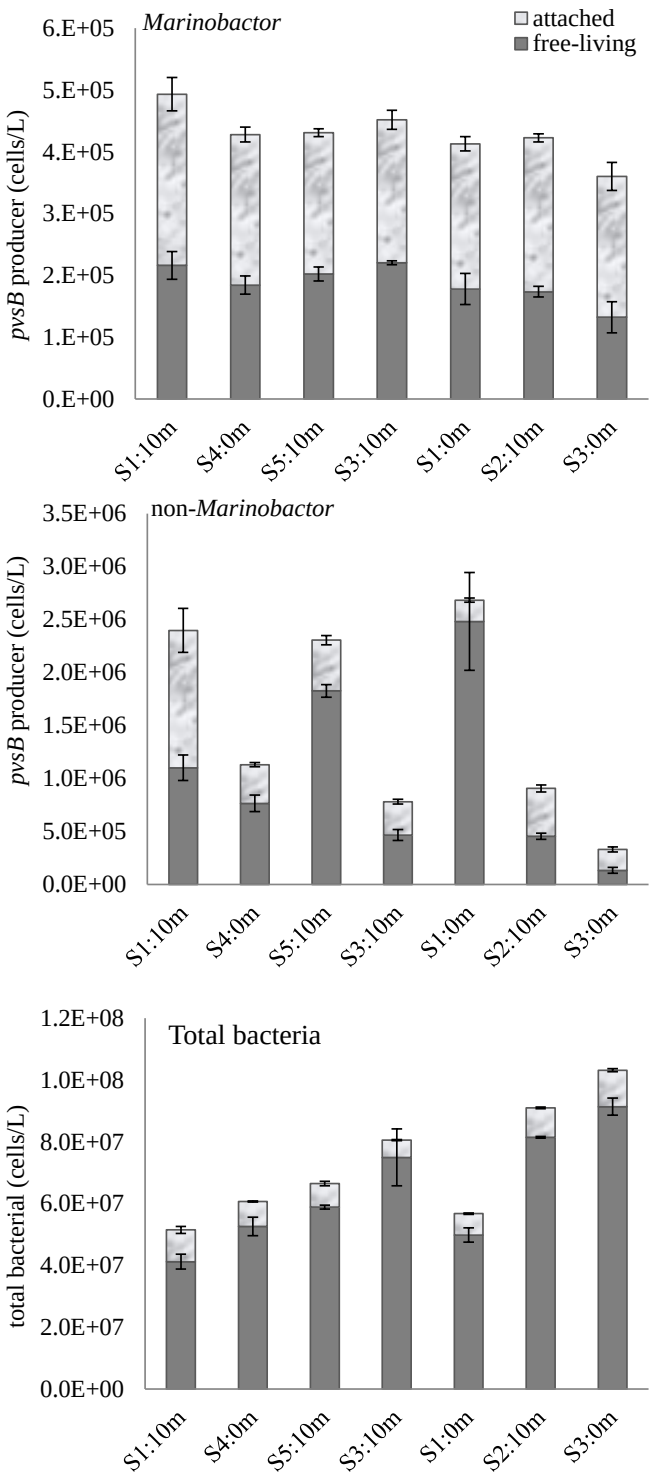

Figure 43 Distribution of free-living and attached bacteria during *G. catenatum* bloom at Gulf of California in February 2017

Table 18 Summary of cell number per liter of seawater collected from Gulf of California on February, 2017

	diatom cells/L	Dino cells/L	G.cat cells/L	Fe, nM	Stdev	VF Marinobacter cells/L	Stdev	VF non-Marino cells/L	Stdev
S1:0m	94600	38100	28500	1.2	0.5	4.1E+05	2.5E+04	2.7E+06	4.6E+05
S1:10m	15100	3500	1500	3.5	0.3	4.9E+05	4.9E+04	2.4E+06	2.1E+05
S2:0m	99200	23200	18400	11.0	2.2	3.2E+05	2.8E+04	2.8E+05	8.5E+03
S2:10m	26857	52036	48679	0.2	0.1	4.2E+05	8.9E+03	9.1E+05	2.5E+04
S3:0m	11200	53900	52500	2.0	0.5	3.6E+05	2.7E+03	3.3E+05	2.6E+04
S3:10m	26600	18400	14400	1.4	0.6	4.5E+05	1.4E+04	7.8E+05	6.9E+04
S4:0m	10378	3014	2616	2.2	0.5	4.3E+05	1.8E+04	1.1E+06	7.1E+04
S4:10m	8800	31360	30800	18.0	1.0	3.5E+05	1.7E+04	2.0E+05	3.8E+04
S5:0m	8560	17920	15560	0.2	0.2	4.1E+05	5.4E+03	1.7E+06	1.7E+05
S5:10m	34960	7360	6480	1.9	0.6	4.3E+05	8.3E+03	2.3E+06	1.7E+04

	marinobacter pvsB producer				non-marinobacter pvsB producer			
	0.2um	stdev	0.8um	stdev	0.2um	stdev	0.8um	stdev
S1:0m	1.8E+05	2.5E+04	2.4E+05	1.2E+04	2.5E+06	4.6E+05	2.0E+05	2.1E+04
S1:10m	2.2E+05	2.3E+04	2.8E+05	2.7E+04	1.1E+06	1.2E+05	1.3E+06	2.1E+05
S2:0m	1.2E+05	9.4E+03	2.0E+05	3.5E+04	1.7E+05	2.9E+03	1.1E+05	7.7E+03
S2:10m	1.7E+05	8.6E+03	2.5E+05	6.6E+03	4.5E+05	3.0E+04	4.5E+05	3.3E+04
S3:0m	1.3E+05	2.5E+04	2.3E+05	2.3E+04	1.3E+05	2.9E+04	2.0E+05	2.3E+04
S3:10m	2.2E+05	3.1E+03	2.3E+05	1.5E+04	4.7E+05	5.1E+04	3.1E+05	2.3E+04
S4:0m	1.8E+05	1.5E+04	2.4E+05	1.2E+04	7.6E+05	7.9E+04	3.7E+05	2.0E+04
S4:10m	1.2E+05	6.0E+03	2.2E+05	2.2E+04	3.0E+04	5.4E+03	1.7E+05	3.5E+04
S5:0m	1.7E+05	7.8E+03	2.4E+05	1.3E+04	1.3E+06	1.6E+05	4.5E+05	1.6E+04
S5:10m	2.0E+05	1.1E+04	2.3E+05	6.3E+03	1.8E+06	5.9E+04	4.8E+05	4.3E+04

total bacteria (cells/L)						
0.2um	stdev	0.8um	stdev	total	Stdev	total vibrioferrin
5.0E+07	2.3E+06	6.9E+06	2.6E+05	5.7E+07	2.2E+06	3.1E+06
4.1E+07	2.4E+06	1.0E+07	1.1E+06	5.1E+07	3.5E+06	2.9E+06
7.5E+07	1.7E+06	6.2E+06	2.3E+05	8.2E+07	1.5E+06	6.0E+05
8.1E+07	2.4E+05	9.5E+06	2.9E+05	9.1E+07	3.5E+05	1.3E+06
9.1E+07	2.8E+06	1.2E+07	5.3E+05	1.0E+08	2.4E+06	6.9E+05
7.5E+07	9.2E+06	5.6E+06	1.8E+05	8.1E+07	9.1E+06	1.2E+06
5.3E+07	3.0E+06	8.1E+06	1.5E+05	6.1E+07	3.1E+06	1.6E+06
7.2E+07	5.0E+06	9.4E+06	1.5E+05	8.1E+07	4.9E+06	5.4E+05
1.6E+08	5.3E+06	1.7E+07	1.3E+06	1.7E+08	4.2E+06	2.1E+06
5.9E+07	6.3E+05	7.6E+06	7.4E+05	6.6E+07	1.0E+06	2.7E+06

6.4.3 Baja California Pacific Ocean *Chattonella marina* bloom of 2017

This study analyzed the water samples collected from 22 stations with two depths (surface and DCM) in Pacific Ocean along the coast to offshore of northern Baja California in March 2017. Prior to this study, all California coast experienced a blob from a warm and dry El Ninõ followed by unusual rainy season. This cruise was performed right after a storm during the La Niña period. How El Ninõ and La Niña have effect on HABs is an on-going debate (Langlois, 2001; Kim et al., 2009), and thus how exactly this California blob influenced this study is not known at this moment. What known is that the blob caused the Pacific Ocean coast of northern California and Washington a long term Pseudo-nitzschia bloom with highly concentrated Domoic acid (Anderson, 2016). Interestingly, the Pseudo-nitzschia bloom widely spread in norther California but did not reach southern California, San Diego in particular, or any other phytoplankton species were hardly increased in San Diego coast during this period. The water temperature in San Diego may have been too warm for Pseudo-nizschia as the surface water temperature at Scripps Pier San Diego hit a record high over 25˚C in August 2016 (Southern California Coastal Ocean Observing System (SCCOOS): www.sccoos.org/data/habs/index.php). As expected, Pseudo-nitzschia bloom was not detected during this Pacific Ocean cruise in Baja California which is located even further south of San Diego. Instead, different phytoplankton species were seen during this cruise. For instance at station 31, a relatively higher *C. marina* cell count was observed within a small diameter of the station (1175 cells/L) and also relatively higher cell counts of dinoflagellate (19975 cells/L) and diatom (11536 cells/L) were detected (**Error! Reference source not found.**). The Chl *a* assay showed rather intermediate pigment concentration at station 31 (2.8 µg/L), however the water around the station 31 contained the higher pigment as seen in S29 at DCM (5.9 µg/L) and station S30 at DCM (3.2 µg/L). These

data indicated that the zone around station 31 was likely to be inhabited with various types of phytoplankton.

In terms of VF producing bacteria distribution, consistent with the previous cruises, non-*Marinobacter* was a few magnitude orders higher than *Marinobacter*. The distribution preference of free-living or attached VF producer depends on the station in this cruise (Figure 44). For instant, *Marinobacter* VF producer was dominant with free-living over attached at all stations while non-*Marinobacter* VF producer was predominantly particle associated in the southern stations (station 15 – station 28) and free-living in the northern stations (station 29 – station 34), the area around the *C. marina* bloom. This was consistent with the result form the *G. catenatum* bloom in Gulf of California in 2017 where the bloom water samples contained abundant free-living non-*Marinobacter* over attached.

As mentioned earlier, it is generally difficult to see clear difference of total dissolved iron in horizontal water samplings due to its highly diluted concentration in upper column of ocean. However, once again, the analytical method we used showed a sort of trend, relatively higher $[Fe]_{diss}$ in southern stations and lower $[Fe]_{diss}$ in norther stations around the *C. marina* bloom (Figure 44, Table 21). This was also consistent with the result form the *G. catenatum* bloom in Gulf of California in 2017 where the water from bloom core contained less concentrated $[Fe]_{diss}$.

It is difficult to find a correlation between alga-bacteria population with involvement of $[Fe]_{diss}$ by a simple plot for this cruise due to its larger sample size (n=42). Thus, the dataset was first examined graphically using one-way ANOVA through software Prism for correlations between Chl *a* and other variables as well as between $[Fe]_{diss}$ and other variables. The dataset was further analyzed for association between these variables using linear regression. No relationship was observed between $[Fe]_{diss}$ and Chl *a* ($p=0.286$) consistent with the result from

the *G. catenatum* bloom in Gulf of California in 2017. In both cases, the simple plot seemed to imply an inverse relationship between $[Fe]_{diss}$ and Chl *a* but they were statistically insignificant. In contrast, a strong relationship was observed between $[Fe]_{diss}$ and free-living non-*Marinobacter* VF producers (p=0.0331) and between $[Fe]_{diss}$ and free-living *Marinobacter* VF producers (p=0.0234) (Figure 45). Once again, significant involvement of free-living bacteria in phytoplankton dynamics was a surprising result because traditionally attached bacteria have been intensively studied for the purpose.

An additional attribute of this study was the nutrients other than iron such as NO_3/NO_2, NH_4, PO_4, SIO_2 were measured (Table 21) and thus relationship between these nutrients and $[Fe]_{diss}$ was able to be assessed. There was a significant relationship between $[Fe]_{diss}$ and NO_3/NO_2 (p=0.0006) and between $[Fe]_{diss}$ and NH_4 (p=0.0034) which is supported by a prior publication by Goldberg et al. (2017). This suggests that NO_3/NO_2 and NH_4 could be used as an orthogonal detection parameter to support algae-bacterial mutualism with involvement of iron.

Table 19 Phytoplankton detection during *C. marina* bloom at Baja California Pacific Ocean in March 2017

Station	Chl *a* fluorescence	Diatom cells/L	dinoflagellate cells/L	Chattonella cells/L	Cocholodinium cells/L	Phyto total cells/L
S4_0m	0.6227	1000	4500	23	2455	9205
S4_DCM	4.3895					
S9_0m	2.2589	4068	1318	0	136	7386
S10_0m	2.3199	3250	1432	0	409	6341
S10_DCM	4.3834					
S13_0m	1.7704	4000	1114	0	0	8068
S13_DCM	3.9683					
S14_0m	1.9963	6159	818	23	0	8750
S14_DCM	10.4520					
S15_DCM	1.5995	3023	1227	0	45	9137
S16_0m	0.9768	2955	1432	23	227	4978
S16_DCM	1.0745					
S17_0m	1.3859	0	0	0	0	0
S17_DCM	1.6056					
S18_0m	1.5568	7132	2193	0	75	17438
S18_DCM	1.6484					
S21_0m	0.4274	4370	6616	0	194	12960
S21_DCM	0.7021	1213	1766	85	64	6085
S22_0m	0.3785	4386	1955	23	23	7705
S23_0m	0.2930	7523	1114	0	68	9364
S23_DCM	0.5494					
S25_0m	0.1221	3446	1807	0	0	9687
S25_DCM	0.3419	0	0	0	0	0
S26_0m	0.1343	6727	3869	29	115	12098
S26_DCM	2.1734					
S27_0m	0.2564	0	0	0		0
S27_DCM	0.9890	0	0	0		0
S28_0m	0.6227	1795	1114	23	45	7478
S28_DCM	1.4835					
S29_0m	0.5372	3636	3477	114	0	9863
S29_DCM	5.9036	17472	1208	0	0	19623
S30_0m	0.6471	0	0	0		0
S30_DCM	3.1624					
S31_0m	2.7900	11536	19975	1175	0	57575
S31_DCM	2.3077					
S32_0m	2.8144	5083	2333	0	123	9896
S32_DCM	2.8632					
S33_0m	1.4042	2708	1143	0	0	10409
S33_DCM	1.0745					
S34_0m	0.9035	3540	4700	0	0	26002
S34_DCM	1.4896					
Tuna1_0m	0.4518	0	0	0	0	0

Table 20 Bacterial distribution during C. marina bloom at Baja California Pacific Ocean in March 2017 (mean of 3)

Station	VF marinobacter free-living cells/L	VF marinobacter attached cells/L	VF non-marinobacter free-living cells/L	VF non-marinobacter attached cells/L	total bacteria free-living cells/L	total bacteria attached cells/L
S4_0m	2.1E+05	4.9E+05	1.2E+06	4.1E+05	6.1E+07	3.9E+07
S4_DCM	1.7E+05	5.4E+05	7.8E+05	2.1E+06	5.6E+07	5.4E+07
S9_0m	3.3E+05	7.4E+04	8.7E+05	8.7E+05	5.8E+07	5.7E+07
S10_0m	1.8E+05	1.3E+05	1.1E+06	6.5E+05	7.1E+07	3.5E+06
S10_DCM	1.9E+05	1.5E+05	7.0E+05	2.7E+05	3.3E+07	2.8E+07
S13_0m	1.9E+05	1.1E+05	1.1E+06	9.9E+05	5.0E+07	6.1E+07
S13_DCM	1.7E+05	6.6E+04	7.0E+05	1.8E+05	2.8E+07	3.8E+07
S14_0m	2.2E+05	1.6E+04	1.6E+06	1.1E+04	6.3E+07	1.1E+07
S14_DCM	1.7E+05	7.5E+03	1.3E+06	3.1E+02	4.2E+07	7.3E+04
S15_DCM	1.7E+05	1.7E+05	4.5E+05	2.3E+06	1.9E+07	2.1E+07
S16_0m	1.5E+05	1.3E+05	8.8E+05	2.0E+06	4.2E+07	2.6E+07
S16_DCM	1.7E+05	9.8E+04	4.4E+05	2.2E+06	1.5E+07	9.2E+06
S17_0m	1.6E+05	1.2E+05	3.1E+05	3.9E+06	2.5E+06	3.1E+07
S17_DCM	1.7E+05	1.1E+05	3.0E+05	2.8E+06	2.6E+06	3.5E+07
S18_0m	1.6E+05	1.1E+05	3.4E+05	3.8E+06	2.6E+06	4.3E+07
S18_DCM	1.9E+05	7.2E+04	2.2E+06	2.2E+06	7.4E+07	5.3E+07
S21_0m	1.8E+05	1.4E+05	6.7E+05	2.9E+06	1.5E+07	4.1E+07
S21_DCM	1.6E+05	9.7E+04	6.2E+05	1.8E+06	2.6E+07	3.2E+07
S22_0m	2.2E+05	9.3E+04	1.0E+06	1.4E+06	3.1E+07	3.6E+07
S23_0m	1.8E+05	8.9E+04	8.5E+05	1.6E+06	3.8E+07	4.6E+07
S23_DCM	1.4E+05	9.9E+04	3.8E+05	1.6E+06	3.3E+07	2.7E+07
S25_0m	1.8E+05	1.1E+05	4.6E+05	2.5E+06	1.0E+07	2.1E+07
S25_DCM	1.6E+05	1.1E+05	3.5E+05	5.7E+06	1.3E+07	3.8E+07
S26_0m	2.5E+05	1.0E+05	1.6E+06	3.7E+06	3.5E+07	4.9E+07
S26_DCM	3.4E+05	1.1E+05	2.6E+06	2.1E+06	2.0E+07	2.8E+07
S27_0m	2.3E+05	1.4E+05	1.7E+06	4.4E+06	3.9E+07	4.8E+07
S27_DCM	3.5E+05	1.1E+05	1.9E+06	4.2E+06	3.1E+07	2.1E+07
S28_0m	2.7E+05	1.8E+05	2.5E+06	4.2E+06	4.6E+07	3.1E+07
S28_DCM	2.2E+05	1.3E+05	1.1E+06	4.5E+06	3.0E+07	2.8E+07
S29_0m	2.0E+05	1.5E+05	1.4E+06	3.7E+06	3.8E+07	2.8E+07
S29_DCM	3.0E+05	1.0E+05	1.8E+06	1.9E+05	5.8E+07	3.2E+07
S30_0m	2.2E+05	1.7E+05	6.3E+06	3.5E+05	3.5E+07	1.1E+06
S30_DCM	2.8E+05	1.7E+05	2.4E+06	1.3E+06	5.8E+07	3.4E+06
S31_0m	2.2E+05	3.3E+05	1.5E+06	1.1E+06	4.2E+07	1.6E+07
S31_DCM	2.3E+05	3.3E+05	2.0E+06	5.7E+05	5.6E+07	2.9E+06
S32_0m	7.8E+05	2.3E+05	1.4E+06	8.6E+05	6.7E+07	2.2E+07
S32_DCM	2.2E+05	1.6E+05	2.8E+05	1.9E+05	3.9E+05	7.6E+06
S33_0m	2.1E+05	1.7E+05	3.6E+06	9.9E+04	6.1E+07	1.0E+06
S33_DCM	2.5E+05	2.1E+05	8.5E+06	2.9E+06	6.5E+07	9.1E+06
S34_0m	3.5E+05	1.9E+05	6.1E+06	6.4E+05	4.5E+05	1.2E+07
S34_DCM	3.1E+05	1.6E+05	3.9E+06	2.2E+05	1.5E+07	8.6E+06
Tuna1_0m	4.6E+05	2.2E+05	1.1E+06	2.7E+06	7.0E+07	1.4E+07

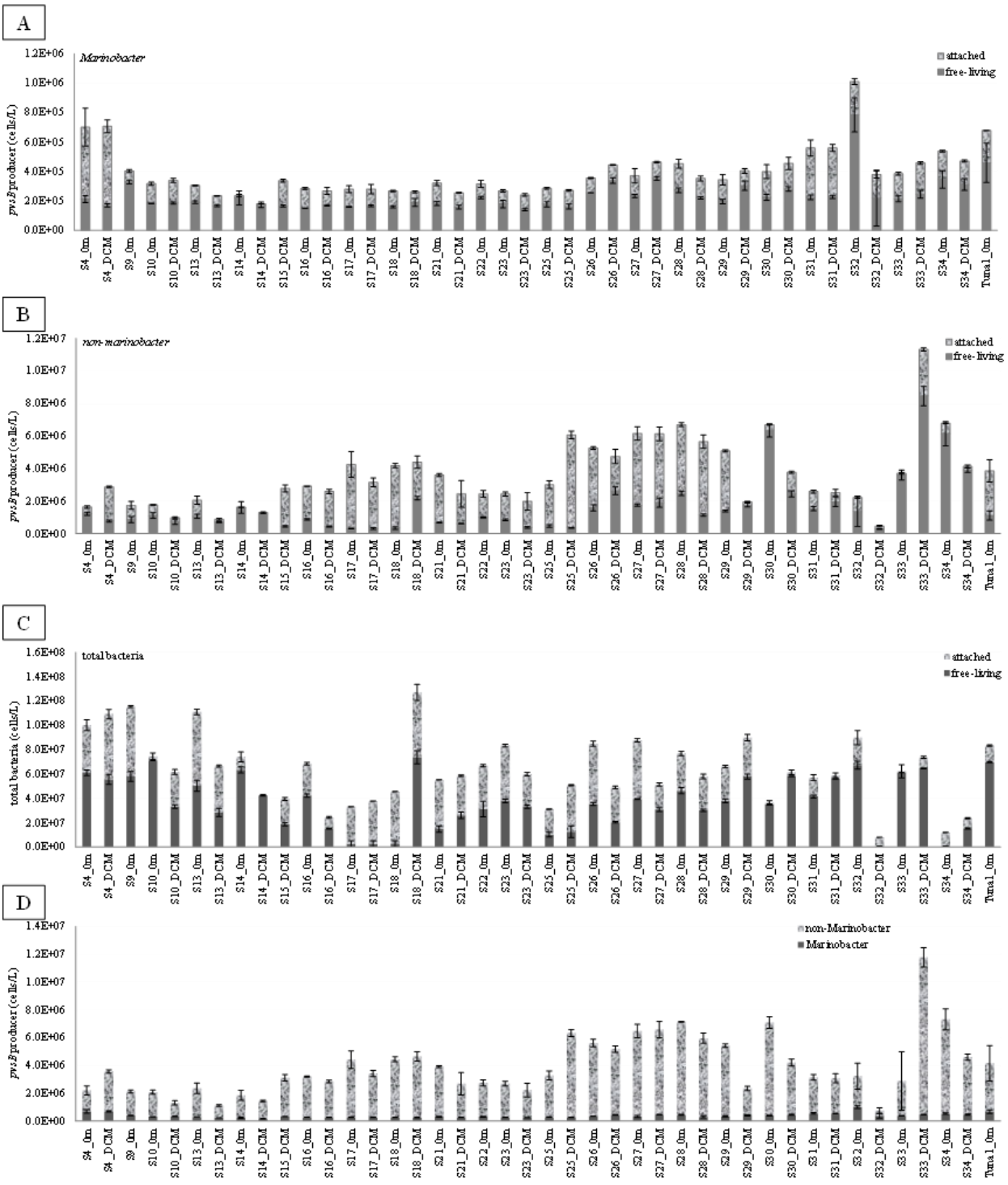

Figure 44 Distribution of phytoplankton, bacteria, total dissolved iron during *C. marina* bloom at Baja California Pacific Ocean in March 2017

The station "Tuna1" was located in between station 4 and station 5.

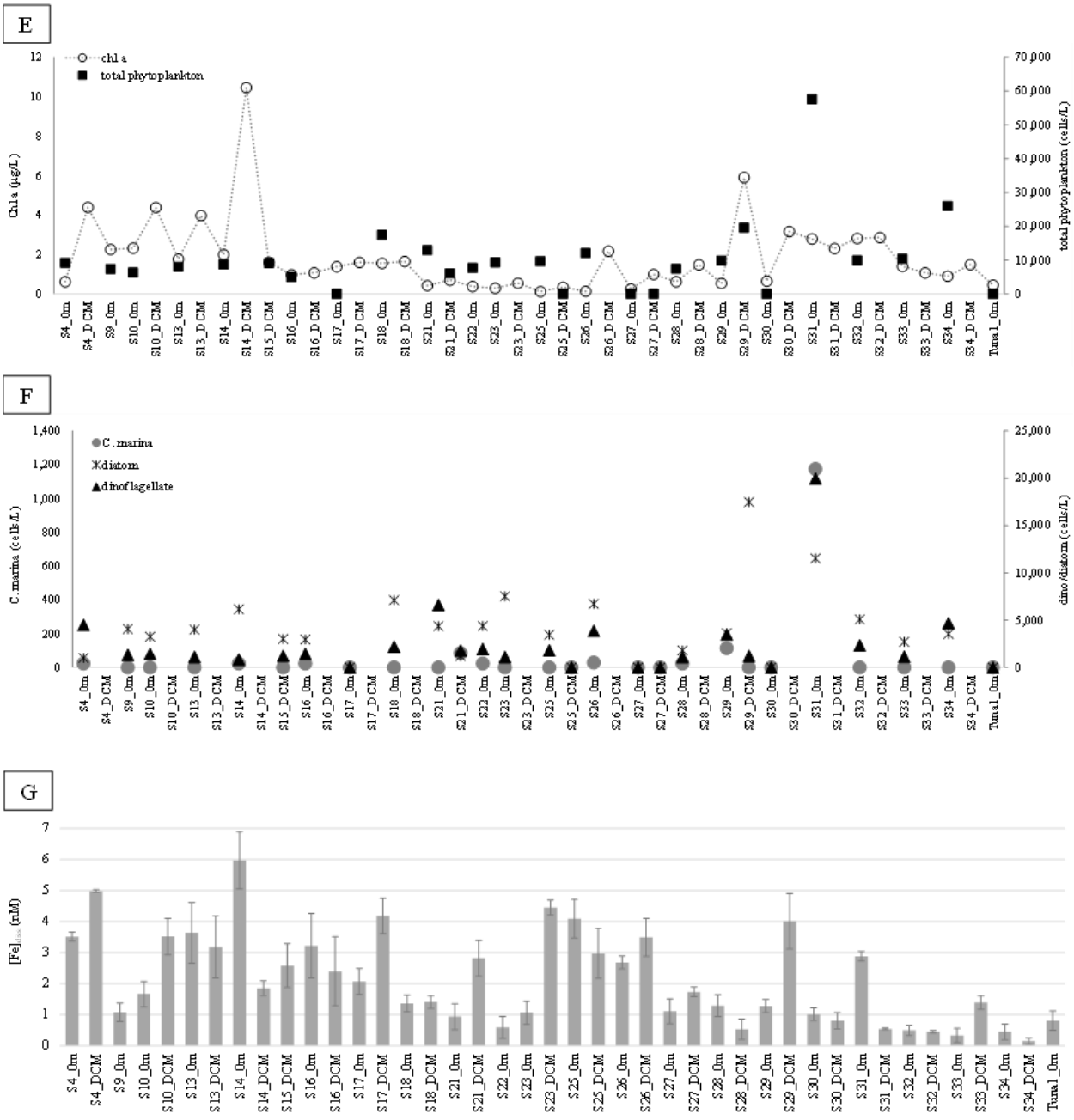

Figure 44 Continued

Table 21 Nutrient distribution during *C. marina* bloom at Baja California Pacific Ocean in March 2017

Station	NO_3+NO_2 (μM)	NH_4 (μM)	PO_4 (μM)	SiO_2 (μM)	Fe (nM)
S4_0m	4.3	0.1	0.7	5.2	3.5
S4_DCM					5.0
S9_0m	4.3	0.1	0.7	5.1	1.1
S10_0m	4.5	0.1	0.7	5.2	1.7
S10_DCM					3.5
S13_0m	4.6	0.1	1.0	5.3	3.6
S13_DCM					3.2
S14_0m	4.5	0.1	0.8	5.1	6.0
S14_DCM					1.9
S15_DCM	4.6	0.1	0.8	5.1	2.6
S16_0m	4.6	0.1	0.7	5.2	3.2
S16_DCM					2.4
S17_0m	4.6	0.1	0.8	5.2	2.1
S17_DCM					4.2
S18_0m	4.7	0.1	0.8	5.3	1.4
S18_DCM					1.4
S21_0m	4.8	0.1	0.8	5.4	0.9
S21_DCM	5.0	0.1	1.2	5.9	2.8
S22_0m	4.5	0.1	0.8	5.2	0.6
S23_0m	4.3	0.1	0.8	5.1	1.1
S23_DCM					4.5
S25_0m	4.2	0.1	0.8	5.1	4.1
S25_DCM	4.4	0.1	0.8	5.5	3.0
S26_0m	4.2	0.1	0.7	5.1	2.7
S26_DCM					3.5
S27_0m	4.1	0.1	0.2	5.1	1.1
S27_DCM	4.4	0.1	0.8	5.5	1.7
S28_0m	4.2	0.1	0.7	5.1	1.3
S28_DCM					0.5
S29_0m	4.2	0.1	0.7	5.1	1.3
S29_DCM	5.3	0.2	1.2	6.8	4.0
S30_0m	4.3	0.1	0.8	5.3	1.0
S30_DCM					0.8
S31_0m	4.4	0.1	0.8	5.4	2.9
S31_DCM					0.5
S32_0m	4.9	0.1	0.8	5.3	0.5
S32_DCM					0.5
S33_0m	4.9	0.1	0.8	5.3	0.3
S33_DCM					1.4
S34_0m	4.8	0.1	0.7	5.3	0.5
S34_DCM					0.1
Tuna1_0m	6.3	0.2	1.3	6.8	0.8

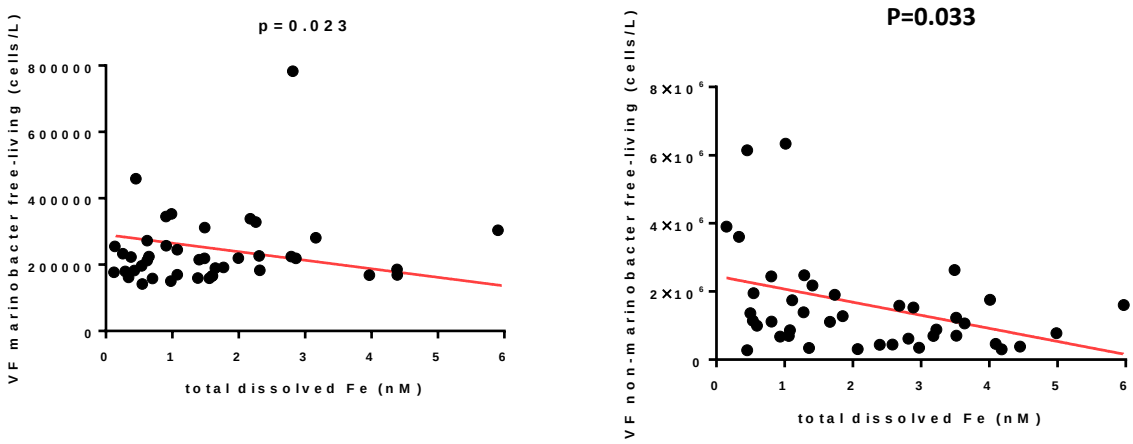

Figure 45 Regression analysis of VF producers and total dissolved iron from *C. marina* bloom at Baja California Pacific Ocean in March 2017

6.5 DISCUSSION

6.5.1 Distribution of *Marinobacter* and non-*Marinobacter* VF producers

VF producer from non-*Marinobacter* species outnumbered over that from *Marinobacter* species in all three blooms. The same phenomenon was observed in our prior study, *Lingulodinium polyedrum* bloom at the Scripps Pier in 2011 (Yarimizu et al., 2014). This is however contrast to what was seen in our other two environmental studies but performed during non-bloom seasons, a North Atlantic cruise (Gärdes, 2013) and a North Pacific cruise (unpublished data), where *Marinobacter* VF producers were greater contributors than the non-*Marinobacter's*. From these observations, we initially thought distribution of *Marinobacter* versus non-*Marinobacter* VF producer may be related to HAB events. This assumption was however proven to be unlikely. We have been monitoring local Scripps Pier water in San Diego monthly since September 2014 and no bloom has occurred during the time frame. These non-bloom water samples from Scripps pier has shown to contain greater non-*Marinobacter* VF producing bacteria (unpublished data). The distribution of *Marinobacter* and non-*Marinobacter*

could be rather location dependent. The North Atlantic cruise in particular targeted oligotrophic waters which may be a reason for preferring *Marinobacter* VF producers while the Pacific coast of San Diego and Baja California as well Gulf of California are abundant in nutrients. The purpose of measuring *Marinobacter* and non-*Marinobacter* VF producers separately is not only a logistics reason (single degenerate *pvsB* primer set could not adequately quantify both *Marinobacter* and non-*Marinobacter* pvsB, Gärdes et al., 2013) but also we believe certain group of VF producers may be more involved in bloom dynamics. For example, a PCA analysis with PCR amplicons from the *L. polyedrum* bloom study showed a statistically different community of VF producer involved in bloom initiation (Yarimizu et al., 2014). Measuring *Marinobacter* versus non-*Marinobacter* based VF producers separately may lead to such finding as bacterial community information when enough dataset are pooled.

6.5.2 Distribution of free-living and attached bacteria

The higher concentration of VF producers were found on 0.8 μm membranes during our first two HAB events studied, *L. polyedrum* bloom at Scripps pier in 2011 and *G. catenatum* bloom at Gulf of California in 2015. In contrast, the non-bloom water samples from the local Scripps pier San Diego has been monitored monthly showing that the opposite trend, the higher population of VF producers on 0.22 μm membranes (unpublished data). These data together initially made us think that VF producers were predominantly free-living during normal marine conditions and their association with phytoplankton were increased during HABs. Many prior publications support this assumption, the importance of attached bacteria in terms of phytoplankton growth. Reportedly, attached bacteria as compared to free-living bacteria have more influence on phytoplankton assemblages and their physiological status (Rooney-Varga et al., 2005; Grossart et al., 2005). However, our further studies with two later HAB events, *G.*

catenatum bloom at Gulf of California in 2017 and *C. marina* bloom at Baja California Pacific Ocean in 2017, discovered a contrast result. The free-living VF producers were equally or greatly dominated over attached during these two HAB events. A clear reason for the inconsistent distribution of free-living and attached VF producers is not clear at this point. However, these observations gave us a very important new insight, free-living bacteria may be much more involved in phytoplankton growth and bloom dynamics than traditionally expected.

To prove the importance of free-living bacteria to phytoplankton growth, we have performed a simple laboratory culture study. The model phytoplankton used was *L. polyedrum* as it was available in our lab. Axenic *L. polyedrum* culture was prepared by treating non-axenic *L. polyedrum* culture with 1% antibiotics (Penicillin/Streptomycin/Neomycin, P4083-100mL, sigma-Aldrich) for 24 hours. The cells were washed and resuspended with sterile growth media (seawater containing L1 nutrient). The sterility of the culture was tested with agar plate every day. The culture confirmed to be bacteria free on day 0 indicative of axenic *L. polyedrum* culture. However, bacterial growth was observed on day 2 by colony growth on agar plate (Figure 46). The bacteria in the culture were thereafter exponentially and continuously grown along with *L. polyedrum* up to at least for a week. These observations suggested that the attached bacteria which could be either symbiots of *L. polyedrum* or simply residing on *L. polyedrum* theca were somehow protected from antibiotics. The survived attached bacteria possibly become free-living as response to the elimination of free-living bacteria by antibiotics. The free-living and attached bacteria may present under a certain constant ratio. When small amount of antibiotics (0.1% v/v) was added every other day, the sterility of the *L. polyedrum* culture was maintained at all time and both bacteria and *L. polyedrum* growth were ceased (Figure 47). The free-living bacteria likely play an important role in algae growth.

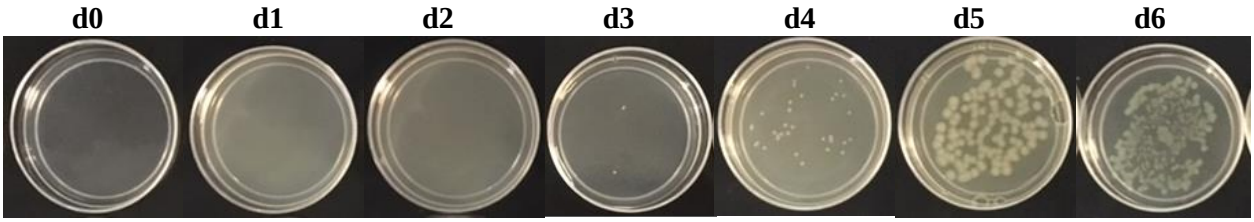

Figure 46 Sterility of Axenic *L. polyedrum* culture
To test the sterility of *L. polyedrum* cultures, a 10 μL sample culture was spread on a marine broth plate (5g/L peptone, 1g/L yeast extract, 15g/L agar in 75% seawater) and incubated at 25°C for 2-3 days. The absence of any visible bacterial colonies was considered indicative of bacteria free sample.

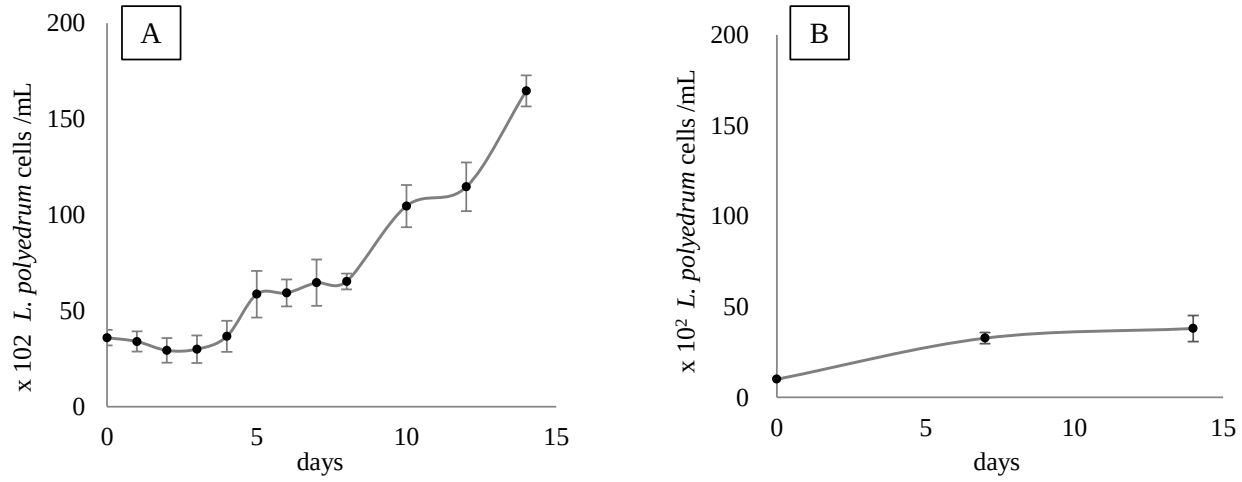

Figure 47 *L. polyedrum* growth in two "Axenic" conditions
A: treated with 1% (v/v) antibiotics (Penicillin/Streptomycin/Neomycin, P4083-100mL, Sigma-Aldrich) for 24 hours prior to cell count measurement, B: treated with 0.1% (v/v) antibiotics every other day over 15-days.

6.5.3 Phytoplankton and VF producer correlation

VF producer decreased as *G. catenatum* increased in the Gulf of California cruise in 2015. Consistently, the two highest bloomed stations during the Gulf of California cruise in 2017 showed remarkably low abundance of non-*Marionobacter* VF producer. Further, this cruise found a statistically significant correlation in between the population of *G. catenatum* and free-living *Marinobacter* VF producers which are predominantly found in the northern stations

around the *C. marina* bloom. In our first bloom study, L. polyedrum in Scripps Pier in 2011, VF and bloom species were simultaneously increased and decreased together. The mechanism of how bloom species and VF producing bacteria is related is not known at this point. However, these data showed a possible population correlation between VF producing bacteria and three bloom species, *L. polyedrum*, *G. catenatum*, and *C. marina*. More field studies to be performed of course, but these data have a potential to support our hypothesis, theoretically VF producers can reduce Fe(III) to Fe(II) and provide the free iron to pairing phytoplankton.

6.5.4 Total dissolved iron

A pattern was seen in increased bloom species with decreased $[Fe]_{diss}$ from the two cruises studied although the two variables were shown statistically insignificant. From the Baja Pacific Ocean cruise in 2017, a significant correlation was found in between $[Fe]_{diss}$ and free-living non-*Marinobacter* vibfiorerrin producers and between $[Fe]_{diss}$ and free-living *Marinobacter* vibfiorerrin producers. This was a surprising result for two reasons, generally $[Fe]_{diss}$ is a difficult parameter to find differences in horizontal water sampling as it is too diluted across the surface water, and once again that free-living VF producing bacteria showed a significant involvement.

6.6 CONCLUSIONS

This report summarized the studies performed with three cruises carried out in northern Baja California during phytoplankton blooms in 2015 and 2017. The studies measured population of phytoplankton, VF producing bacteria, and iron concentration from each station to seek for their correlation. The trend of correlation between these variables is not a concrete but rather case dependent. This may be because multiple factors are involved in one HAB event and each HAB event may have a unique combination of factors causing the case. Therefore, it cannot

simply summarize the three HABs studied here in one word. However, certain factors associated with HAB events became clearer through these studies. This report made a progress to support algae-bacterial interaction with involvement of iron in HABs.

6.7 ACKNOWLEDGMENTS

We would like to acknowledge the members of the Marine Ficotoxins Laboratory at CICESE for helping us sampling and providing us the hydrographic data. We would like to thank Professor Helmut Maske from the Marine Microbes Laboratory at CICESE for allowing us to use his facilities. We specially acknowledge Baja Aqua Farms for sponsoring the entire Pacific Ocean research cruise. Special thanks to Avery Tatters for providing us isolated *L. polyedrum* species from Venice Beach (University of Southern California) for our culture studies.

CHAPTER 7. OTHER ENVIRONMENTAL DATA FROM NORTH PACIFIC OCEAN CRUISES

7.1 ABSTRACT

Iron is an essential nutrient for both phytoplankton and bacteria, however bioavailability of iron in the marine environment is restricted because of its poor solubility in the oceanic regimes. Marine microorganisms face a challenge to acquire iron from low iron concentrated marine environment. Bacteria overcome this issue by evolving to produce iron chelating organic molecules called siderophores which bind exclusively insoluble form of iron (Fe^{+3}) and reduce them to soluble forms. Bacteria then utilize the reduced iron for their nutrient. On the other hand, little are known for phytoplankton's iron acquisition and there is no evidence for them to produce an iron chelator like siderophore. Our hypothesis is that certain bacteria and phytoplankton have a mutualistic relationship, and siderophores produced by marine bacteria may provide phytoplankton bioavailable iron. Siderophore producing bacteria may play an important role in algae-bacterial mutualism in our hypothetic context, however how such bacteria are distributed in oceanic environment is so far unknown. This chapter summarizes the distribution of bacteria containing gene encoded for vibrioferrin siderophore, a photo-active marine siderophore, in three oceanic regimes in North Pacific Ocean. One hypothesis was that vibrioferrin producers would avoid the photic zone as increased light intensity would lead to destruction of the native siderophore. Other hypothesis was vibrioferrin producers would

preferentially occupy the photic zone to maximize the efficiency of iron uptake via photoactive siderophores. The study found that vibrioferrin producing bacteria are in general more abundant near the surface to shallow marine water than in the deeper depths as well as near coastal than at open-ocean.

7.2 MATERIALS AND METHODS

7.2.1 Cruise 1: CCE P1106 (California Current Ecosystem P1106)

The cruise CCE P1106 was carried out between June 18th and July 17th, 2011 on the R/V Melville along the southwest of Point Conception (California, 33.2ºN - 34.1ºN and 121.1ºW - 121.7˚W) organized by the chief scientist Michael R. Landry from Scripps Institution of Oceanography, University of California San Diego. The area is known to be a good study site for phytoplankton growth and regional biogeochemistry as it has an alternating geography with iron replete and limiting waters (Hutchins, et al., 1998). This cruise was conducted for the purpose of investigating how this unique oceanic geography was effecting on chemical composition, biomass diversity, and activity of biota. The study site was divided into six Lagrangian-style referred as cycles encompassing three regions as described in Figure 48: oceanic (cycle 2 and cycle 5), front (cycle 1 and cycle 6), coastal (cycle 3 and cycle 4). The oceanic cycles were associated with an anticyclonic eddy, the coastal cycles were associated with two distinct cyclonic eddies, and the frontal cycles were interacting regions between the anticyclone and both cyclones. For our study purpose, water samples were collected from the six cycles with various depths covering from surface to approximately 250 m depth.

7.2.2 Cruise 2: UNOLS (University-National Oceanographic Laboratory System)

The UNOLS cruise was carried out between November 7th and November 17th, 2011 on the R/V New Horizon NH1212 along the Southern California borderland basins (California,

32.3ºN - 33.0ºN and 117.3ºW - 119.2˚W) organized by the chief scientist Clare Reimers from Oregon State University (NSF grant OCE-1041068). The primary goal of this cruise was to train early career chief scientists and the participants with different disciplines and regional interests were on board. The cruise covered the five regions of California coastal continental shelf, the Santa Monica Basin, the Santa Barbara Basin, the CalCOFI line, the San Nicolas Basin, and La Jolla canyon. Our focus was coast to open-ocean of CalCOFI line with four stations namely BC1, BC2, BC3, and BC4 with various depths covering approximately 250 m below the sea surface (Figure 49). CalCOFI line is a good site for studying phytoplankton diversity as the area has experienced numbers of phytoplankton blooms in the past (Kim, et al., 2009). Additionally, this transect spans deep oligotrophic waters, the transition zone, and a near shore coastal over which a steep iron gradient can be expected.

7.2.3 Cruise 3: GeoMICS (Global scale Microbial Interactions across Chemical Surveys)

The GeoMICS cruise was carried out between May 17th and May 20th, 2012 on the R/V Thompson along a subset of Line P (Washington, 48.2ºN – 49.5ºN and 125.6ºW - 129.3˚W) organized by the principle investigators, E. Virginia Armbrust and Anitra E. Ingalls from University of Washington (NSF grant OCE-1205232 and OCE-1205233). The goal of this cruise was to examine potential biological repercussions of changes in ocean chemistry and physics in the region which may create a distinctive biome. For our study purpose, water samples were collected from seven stations namely P1, P2, P3, P4, P5, P6, and P8 with various depths covering from surface to approximately 300 m depth (Figure 50).

7.2.4 Sampling

The details of sampling during CCE P1106 cruise are described in Krause, et al. (2015) and Brzezinski, et al. (2015). The sampling for the other two cruises, UNOLS and GeoMICS, were also conducted with the similar manner. Briefly, the location was determined by real-time monitoring using a Sea Soar and Moving Vessel Profiler and sampling depths were determined based on pressure triggered by an auto-fire module mounted on the rosette for the Niskin casts. The water samples were collected using a trace metal rosette with Teflon-coated Niskin bottles deployed on non-metallic hydroline. For analysis of siderophore producing bacteria, one liter of seawater was collected from each station at different depths in an acid washed plastic container and kept in a freezer equipped on the research ships until transferred to our laboratory. The samples were thawed out in our lab and filtered sequentially through 0.8 μm and 0.2 μm pore size polyvinylidene fluoride membranes using a pressure less than 3.3 kPa to avoid cell disintegration. The membranes were stored in -20°C until DNA extraction was performed. In theory, 0.8 μm and 0.2 μm pore-size membranes separate bacteria associating with eukaryotic phytoplankton from free-living bacteria. For GeoMICS cruise samples, 0.2 μm pore-size membrane alone was used to collect free-living and particle associated bacteria together.

7.2.5 Analytical assays

DNA extraction and qPCR were performed as described in Appendix A and Appendix B.

7.2.6 Chlorophyll a

The Chlorophyll *a* (Chl *a*) was measured during CCE P1106 and GeoMICS cruises to estimate phytoplankton abundance of each station. The details of sampling and measurement procedure for Chl *a* assay during CCE P1106 are described in Krause, et al. (2015). The measurement procedure for GeoMICS has not been published.

7.2.7 Statistical analysis

The dataset on vibrioferrin gene copy number from CCE P1106 and UNOLS cruises were statistically assessed for significant differences and similarity in areas. All statistical analyses were done in PRIMER ver. 6 and SYSTAT ver. 12. For UNOLS dataset, the vibrioferrin gene copy number at each station and each depth was calculated separately for *Marinobacter* and non-*Marinobacter* as well as summation of both. Then, the data on vibrioferrin gene copies were 4th root transformed to down weight the effects of overly abundant sites and account for the importance of rarely abundant sites, thereby integrating their contributions and focusing attention on patterns within the whole assemblage (Clarke and Warwick, 2001). The data were then normalized and a resemblance matrix of similarities in vibrioferrin gene copy abundance among all sample sites was created based on Euclidean distances on the transformed data. The quantitative differences in vibrioferrin gene copy among the four stations and the different depths were examined with a two-factor nested PERMANOVA, with station considered as fixed factor and depth considered as a random factor. The overall relationships between the 54 measured site characters and on vibrioferrin gene copy number were evaluated by principle component analysis (PCA) across the four geographic regions to identify the similarity in vibrioferrin abundance.

For CCE P1106 dataset, the vibrioferrin gene copy numbers from the stations were initially assessed by PCA, however, a clear pattern was not obtained from the analysis. The data were thus reorganized by two variables (Fe condition and depth) by categorizing them into iron condition of limited area (cycle 1, cycle 6, and cycle 3), unlimited area (cycle 2, and cycle 5), and intermediate area (cycle 4) as well as depth condition of surface, shallow, mid, and deep. The categorized data were then analyzed by Distribution-free analysis of variance (PERMANOVA – permutational analysis of variance).

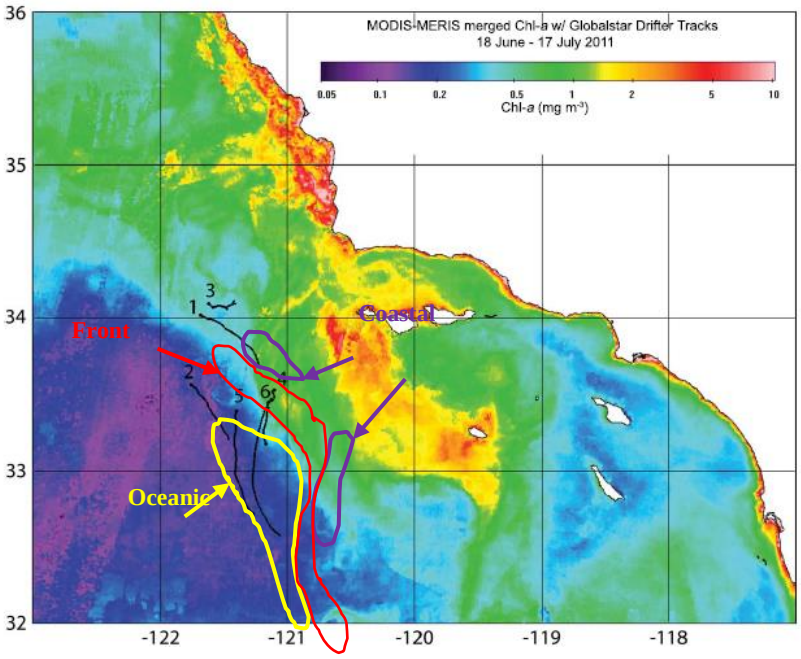

Figure 48 CCE P1106 cruise map

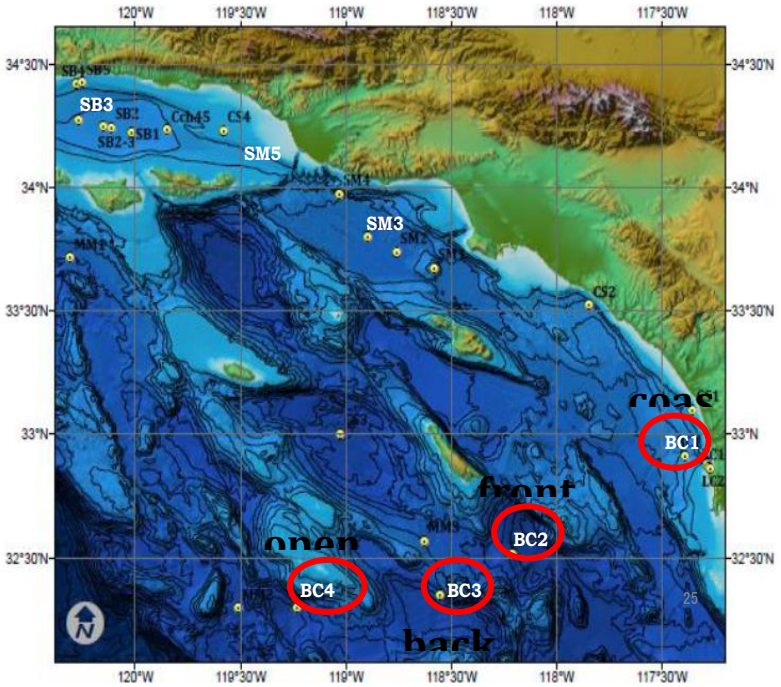

Figure 49 UNOLS cruise map

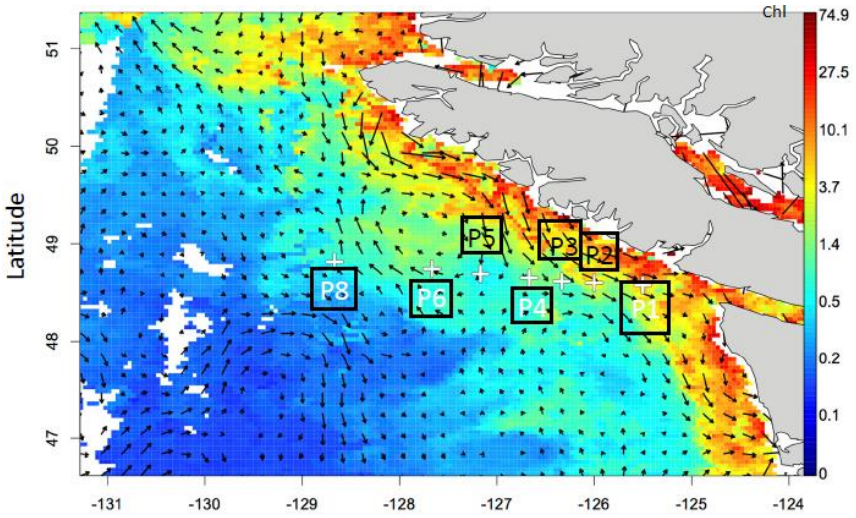

Figure 50 GeoMICS cruise map

7.3 RESULTS

7.3.1 CCE P1106

This cruise targeted the southwest of Point Conception and the area was divided into six cycles: open ocean (cycle 2 and cycle 5), front (cycle 1 and cycle 6), coastal (cycle 3 and cycle 4). For each station, data were collected for Chl *a*, total dissolved Fe, and total vibrioferrin producer cell count and plotted in Figure 51, Figure 52, and Figure 53, respectively. Then, statistical analysis with ANOVA was performed to test if bacteria distribution differed between stations and depth. The vibrioferrin producer from attached non-*Marinobacter* showed significant correlation with depth (Figure 54 A, p=0.0444). Further, regression was looked to search relationship between bacteria and total dissolved Fe as well as between bacteria and fluorescence. No statistically significant correlation was found from this analysis. As can be seen in Figure 1, this is probably due to the fact that the six Lagrangian-style cycles studied during this cruise were located relatively close proximity, although the site was categorized in open-ocean, frontal, and coastal, and it is difficult to fully distinguish pattern of variables. Lastly, the cycles were re-categorized by total iron concentration as limited (cycle 1, cycle 3, and cycle 6),

unlimited (cycle 2 and cycle 5), and intermediate (cycle 4) based on the reports, Krause, et al. (2015) and Brzezinski, et al. (2015). Then distribution-free analysis of variance PERMANOVA was performed to find correlation between vibrioferrin producer, iron concentration, and depth (Figure 54 B). This analysis found that vibrioferrin producers were abundant in the surface to shallow water with limited iron.

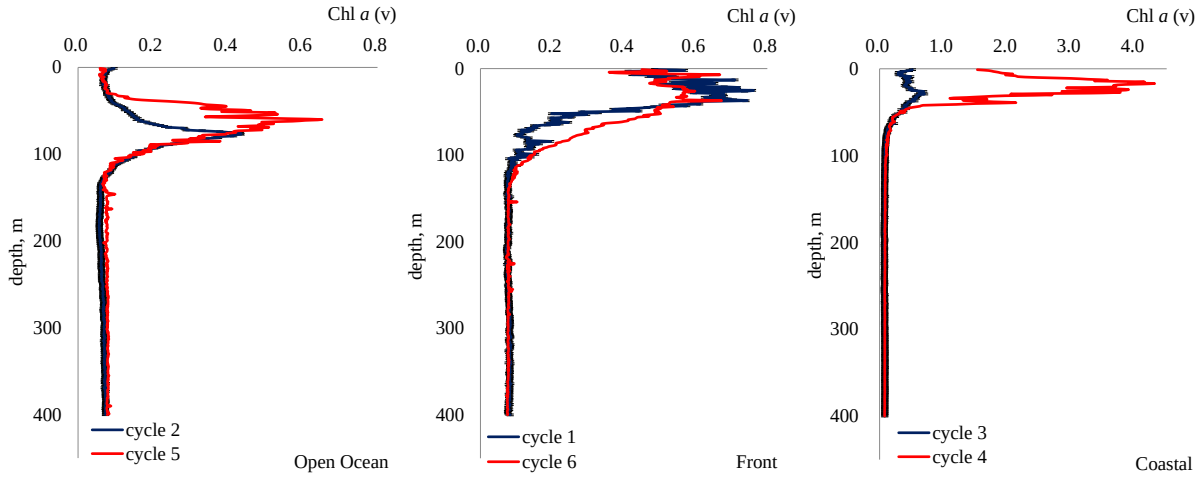

Figure 51 Concentration of Chl *a* at CCE P1106 cruise

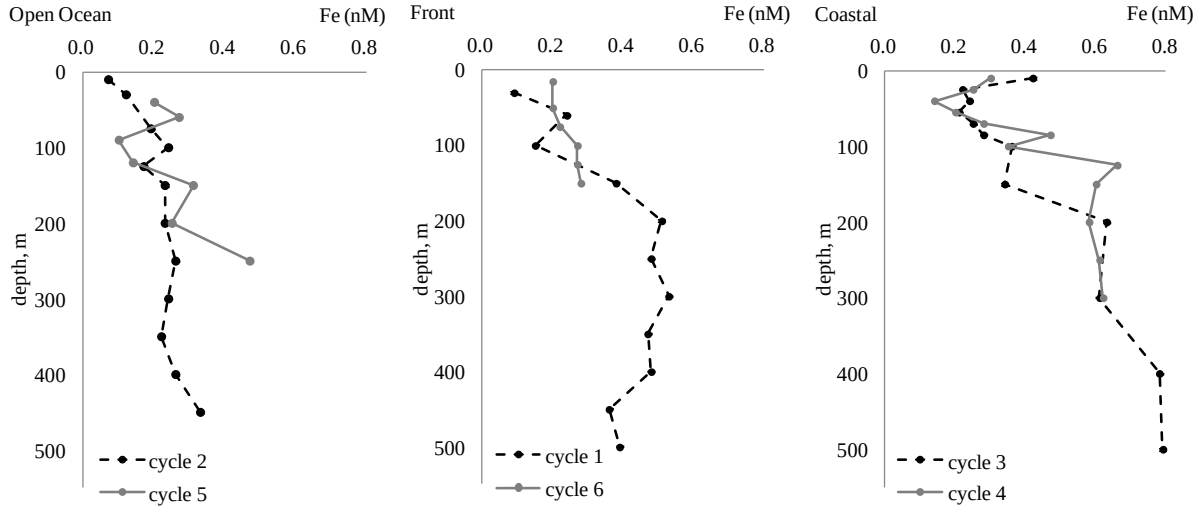

Figure 52 Concentration of total dissolved Fe at CCE P1106 cruise

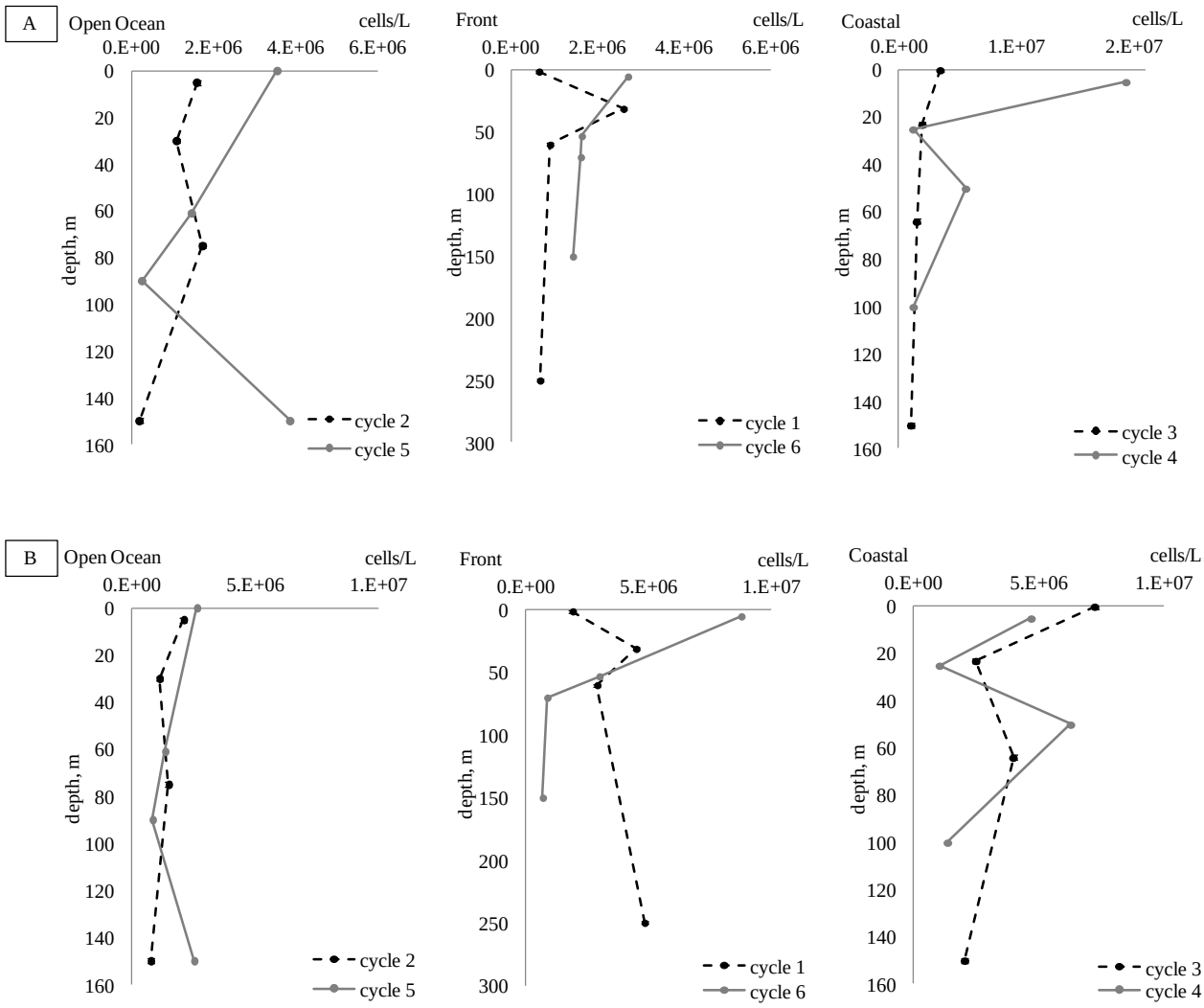

Figure 53 Estimated total bacteria cell count at CCE P1106 cruise
A: The top panel shows estimated total bacterial cell count. B: The bottom panel shows estimated total vibrioferrin producer.

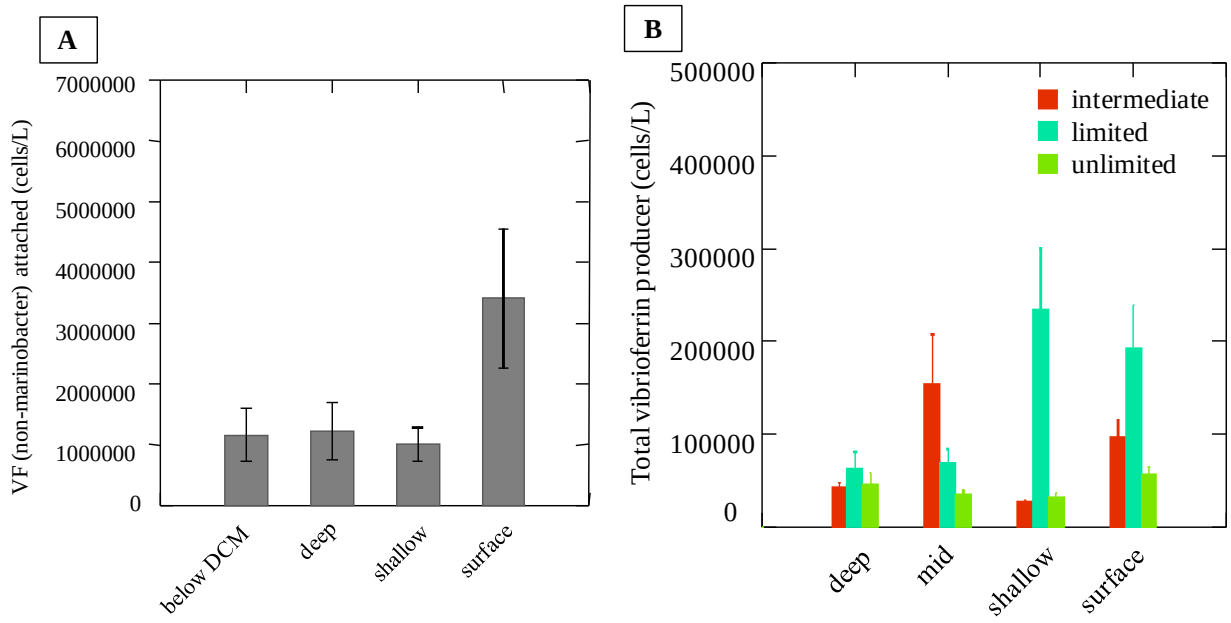

Figure 54 Statistical analysis for CCE P1106
A: ANOVA was performed to test if bacteria differ between stations and depth (Surface: ≈ 0-5m depth, shallow: ≈15-30m depth, below DCM: ≈ 50-75m depth, deep: ≈100-250m depth). B: PERMANOVA was performed to find correlation between vibrioferrin gene copies, iron concentration, and depth.

7.3.2 UNOLS

Four stations (BC1 through BC4) with various depths near the coast of northern San Diego to the open-ocean were studied with respect to the population of vibrioferrin producer. These four stations were much more distant with each other unlike the sites studied on CCE P1106 where six cycles were located closely. The assay results showed that vibrioferrin producer was in general more concentrated near the surface to shallow water than in the deep seawaters as well as at coastal than at open-ocean (Figure 55). In this cruise, *Marinobacter* vibrioferrin producers were generally greater contributors than the non-*Marinobacter's*. There was no distinct difference between the amount of attached and free-living vibrioferrin producers in this study (Figure 56). A statistical analysis by principle coordination analysis presented that the farthest open ocean station BC4 was clearly different from other stations in terms of distribution of

vibrioferrin producer (Figure 57). Further analysis by block ANOVA showed correlation between station and free-living *Marinobacter* vibrioferrin producer (p=0.0056), station and attached *Marinobacter* vibrioferrin producer (p=0.0002), and depth and total bacterial cell count (p=0.0031).

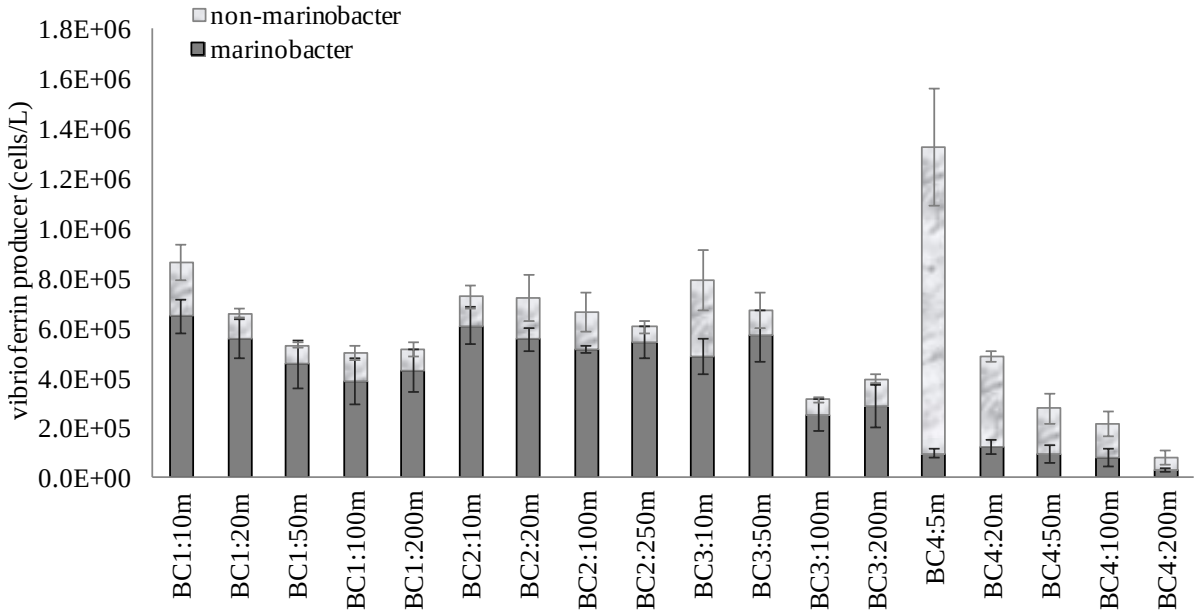

Figure 55 Distribution of vibrioferrin producer for UNOLS cruise

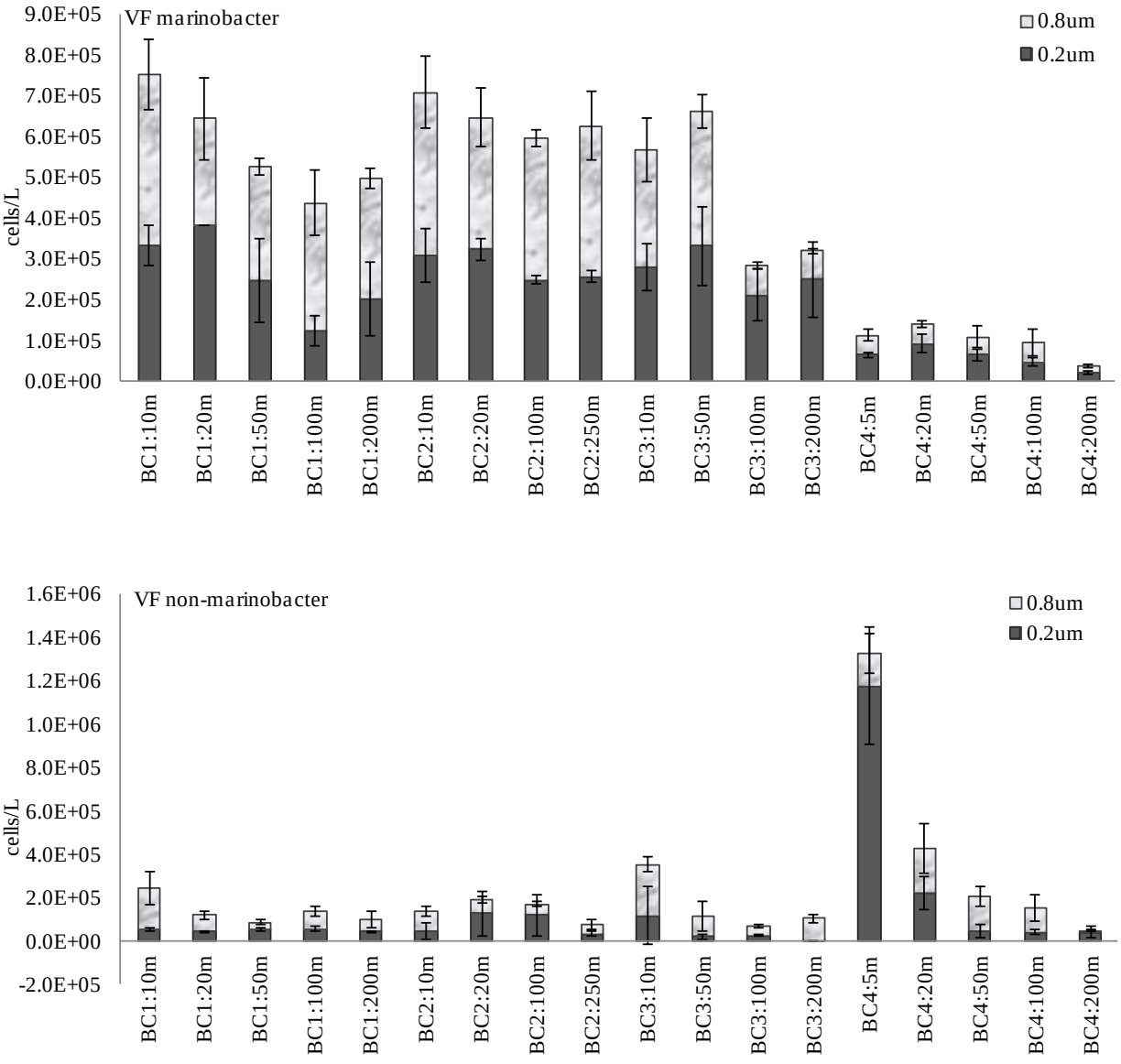

Figure 56 Distribution of free-living and attached vibrioferrin producer for UNOLS cruise

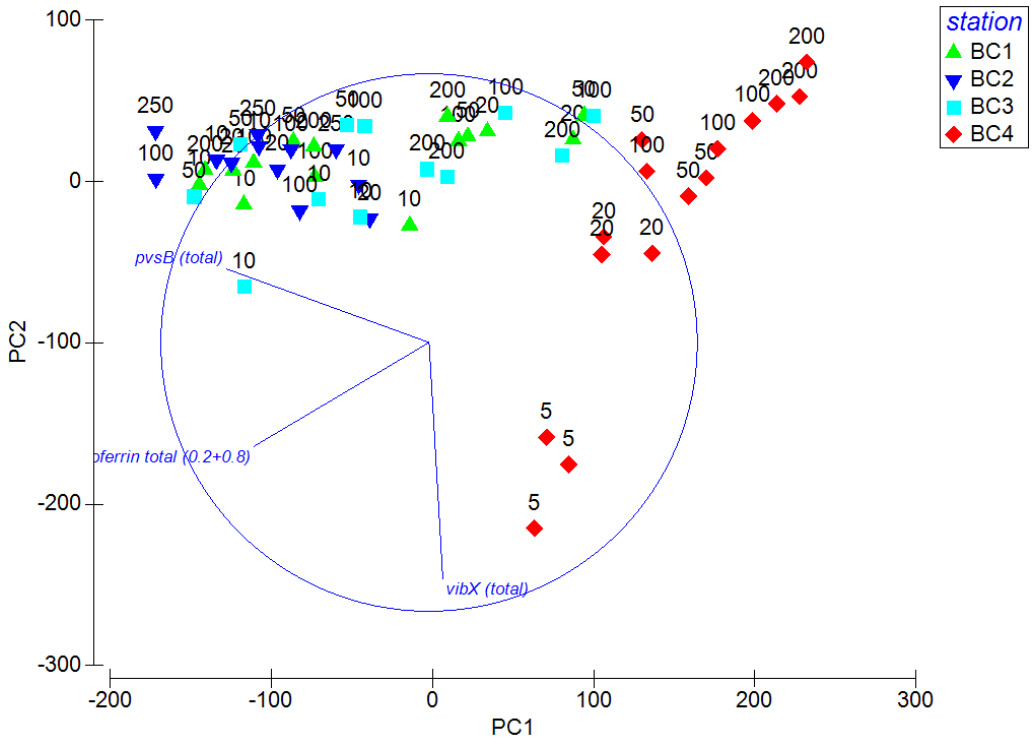

Figure 57 Principle Component Analysis of UNOLS cruise

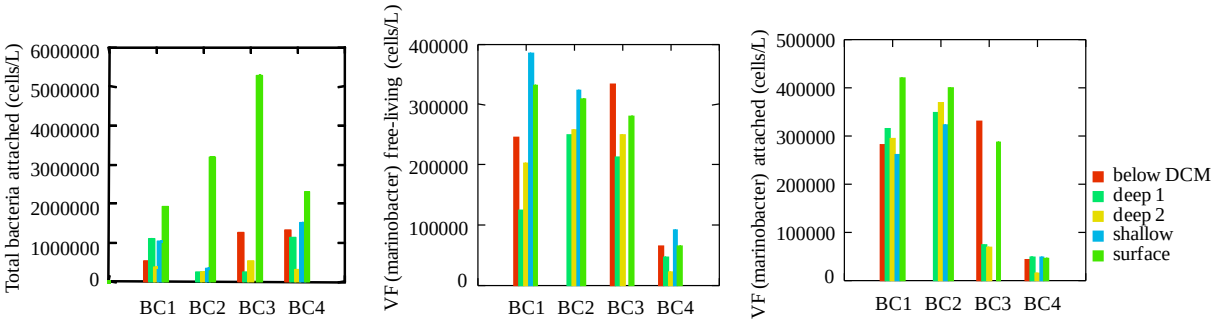

Figure 58 Statistical analysis of UNOLS cruise by blocked ANOVA
Surface: ≈ 10m depth, shallow: 20m depth, below DCM: 50m depth,
deep 1: 100m depth, deep 2: 200m

7.3.3 GeoMICS

Seven stations near the coast to open-ocean of Washington State were studied with respect to vibrioferrin producing bacterial population. In this cruise, the water sample was not separated by filter membrane size but all filtered through 0.2 μm. The statistical analysis showed (Figure 59) significant correlation between station and non-*Marinobacter* vibrioferrin producer (p=0.0189), depth and non-*Marinobacter* vibrioferrin producer (p=0.001), depth and total bacterial cell count (p=0.0051).

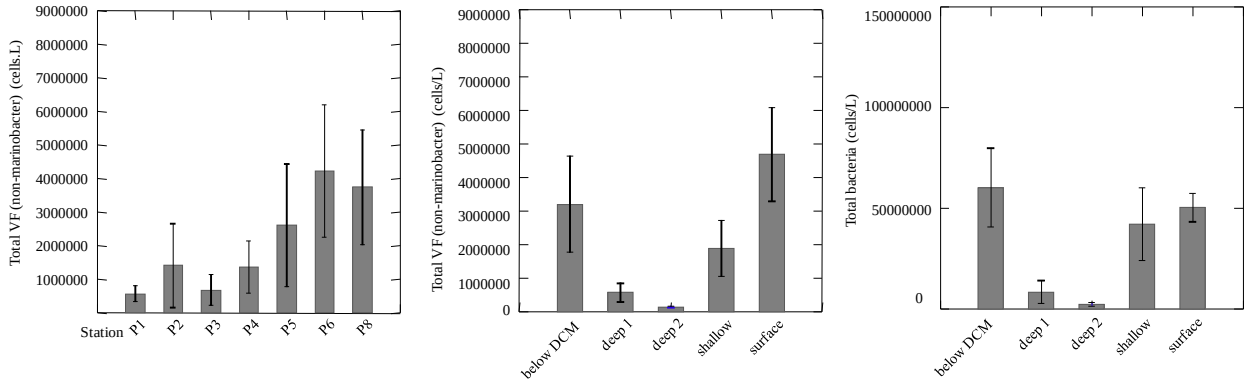

Figure 59 Statistical analysis of GeoMICS cruise by ANOVA
Surface: ≈ 0-5m depth, shallow: ≈15-25m depth, below DCM: ≈ 50-60m depth,
deep 1: ≈100-150m depth, deep 2: ≈250-300m depth

7.4 DISCUSSION

CCEP1106: The Chl *a* concentration during the cruise was exceptionally high at coastal cycle 4 above 50 m depth, approximately 10-fold more concentrated compared to that at the other cycles of the same depths suggesting that that cycle 4 may be a geochemically unique site. Chl *a* are generally more concentrated at surface to shallow water than at deeper depth as phytoplankton reside in photic zone for their photosynthesis. This was true for all six cycles during this cruise. Also in general, Chl *a* are more concentrated near the coast than at open-ocean as nutrients for phytoplankton are more available at coastal. This cruise however did not show a

distinct difference in Chl *a* concentration at between open-ocean, front, and coastal with exception of cycle 4. This is probably due to the fact that the six Lagrangian-style cycles studied during this cruise were located relatively close proximity regardless of how the site was categorized in open-ocean, frontal, and coastal.

The total dissolved iron concentration is generally higher at deeper water than at surface water as the majority of iron in aquatic regimes is chelated or insoluble form which tends to settle in sediment. This was true for the six cycles studied for this cruise. Also in general, the total dissolved iron concentration is generally higher near the coast than at open-ocean. However, the difference in Fe concentration between open-ocean and coastal during this cruise was a subtle. Because iron is diluted to pM level in ocean, it is generally difficult to see a clear trend between locations.

In general, both total bacteria and vibrioferrin producer were more abundant at surface to shallow waters as well as coastal region. The vibrioferrin gene copy numbers obtained from all the stations were further assessed by statistical analysis. The data set was reorganized by two variables, iron condition and depth. The iron condition was categorized by Fe-limited area (cycle 1, cycle 6, cycle 3), Fe-unlimited area (cycle 2, cycle 5), and Fe-intermediate area (cycle 4) while the depth was categorized by surface, shallow, mid, and deep ocean. The data were then analyzed by distribution-free analysis of variance (PERMANOVA – permutational analysis of variance). The iron limited region at shallow to surface water showed remarkably high abundance of vibrioferrin producer indicating that bacteria containing vibrioferrin gene were relatively populated in the iron limited sites during this study possibly suggesting that there is a potential importance of vibrioferrin producer in iron deficient regions.

UNOLS: The assay results from this cruise more clearly showed that vibrioferrin producer was more concentrated near the surface to shallow water than in the deep seawaters as well as at coastal than at open-ocean. Prior to this study, we had two hypotheses regarding the distribution of vibrioferrin producers; One hypothesis was since vibrioferrin is a photo-active siderophore, the bacteria containing vibrioferrin gene would avoid the photic zone as increased light intensity would lead to destruction of the native siderophore. The other hypothesis was vibrioferrin producers would preferentially occupy the photic zone to maximize the efficiency of iron uptake via photoactive siderophores. After analyzing the samples from the two cruises, CCEP 1106 and UNOLS, the later hypothesis seemed more likely to be true.

A further statistical analysis by principle coordination analysis presented that the farthest open ocean station BC4 was clearly different from other stations in terms of distribution of vibrioferrin producer. BC4 is a unique station, in addition to the fact that vibrioferrin was remarkably low yield, as it is known as an oligotrophic zone representing an iron deficient water. Although iron concentration was not measured for this cruise, the iron deficient condition seemed to affect bacterial population (both total bacteria and vibrioferrin producers were remarkably low yield at BC4). The Chl *a* was measured by U.S. Naval research center, however, the database was crashed and lost shortly after the cruise. Thus, the correlation of Chl *a* and vibrioferrin producers was not assessed for this cruise.

GeoMICS: Once again, the population of vibrioferrin producing bacteria during this cruise was generally higher at the surface to shallow waters (at and above 100 m depth) than that at the deeper waters. The unusual observation from this cruise was that both total bacterial and vibrioferrin producer were slightly more populated at the farthest open-ocean station P8 above 100 m than at other stations closer to the coast for unknown reasons. The assay result also

showed once again that both estimated total bacteria cell number and vibrioferrin producers were decreased remarkably below 100 m depth at all stations.

7.5 CONCLUSIONS

Iron acquisition is a challenge for marine organisms due to the poor solubility of iron in ocean. Bacteria overcome this issue by evolving to produce siderophores which chelate insoluble iron Fe(III) from marine environment, reduce them to bioavailable iron Fe(II), and to utilize them for their needs. Iron acquisition of phytoplankton on the other hand are not well understood at this point. We postulate that certain bacteria and phytoplankton have a mutualistic relationship, and photoactive siderophores produced by marine bacteria may play an important role in providing phytoplankton bioavailable iron. This study was conducted to have an idea of how widely the bacteria producing such siderophores (we focused on studying vibrioferrin siderophores) are distributed in North Pacific Ocean. With exception of a very few cases, vibrioferrin producing bacteria are more abundant near the surface to shallow marine water (above 100 m depth) than in the deeper depths as well as near coastal than at open-ocean in North Pacific Ocean. This observation suggests that vibrioferrin producing bacteria are preferentially occupied the photic zone to maximize the efficiency of iron uptake via photoactive siderophores. The number of both vibrioferrin producers and phytoplankton are definitely decreased at non-photic zones. The correlation between distribution of vibrioferrin producers, phytoplankton, and total dissolved iron in North Pacific Ocean must be further monitored to make any conclusions.

It should be noted that RT-qPCR was used for this study as an analytical tool to quantify vibrioferrin producers because direct quantification of photoactive siderophore in seawater has been very difficult due to their low concentration in the marine environment and their rapid

degradation by photochemical reactions. Vibrioferrin was isolated in the past however not from a field sample but from highly concentrated *Marinobacter* cell culture grown in a dark and cold room to slow their degradation (Amin et al., 2007). The purification process was labor intensive as the supernatant from the culture was purified through ESI-MS followed by two times RT-HPLC in dark and cold room (Amin, et al., 2007) as the half-life of vibrioferrin was found to be approximately 6 minutes under sunlight (Amin et al., 2009). It is logistically impossible to collect large volume of field sample that meets LC detection limit of vibrioferrin. Even if the large volume collection is overcome somehow, vibrioferrin will be degraded by the time above described purification process is completed which hampers their accurate quantification. For above reasons, quantify photo-active siderophores from field samples has been an on-going challenge. Our lab is using RT-qPCR to search for siderophore biosynthesis genes involved in the production of the photo-active siderophores. RT-qPCR can detect lowest as 20 gene copies (Bach et al., 2002; Labrenz, et al., 2004) which is thousands fold lower detection limit obtained by HPLC. This test method overcomes the quantification issue caused by the nature of photo active marine siderophores, low concentration and rapid photo degradation. However, we are aware of the limit of this method. Measuring selected gene copy does not represent siderophore quantity in marine environment but only quantifies the density of bacteria that carry siderophore genes. Johnson et al. argues that siderophore biosynthesis is typically turned on and bacterial derived siderophore production should be highly active in most oceanic regimes where iron level is so low (Johnson et al., 1994). It is our future assignment to verify the siderophore gene expression level of field samples by measuring its gene copy from mRNA.

7.6 ACKNOWLEDGEMENTS

We thank the following members for providing us opportunities to join the research cruises and necessary data and advice.

- Katherine A. Barbeau, Scripps Institution of Oceanography, University of California San Diego
- Randie Bundy, Scripps Institution of Oceanography, University of California San Diego
- Mark D. Ohman, Scripps Institution of Oceanography, University of California San Diego
- Magan Schatz, University of Washington
- Astrid Gärdes, Leibniz Centre for Tropical Marine Research
- Matthew Edwards, San Diego State University
- Clare Reimers, Oregon State University (UNOLS cruise chief, map)
- Jake Bailey, University of Minnesota (UNOLS cruise sub-chief, map)
- Michael R. Landry, Scripps Institution of Oceanography, University of California San Diego (CCE P1106 cruise chief, map)
- E. Virginia Armbrust, University of Washington (GeoMICS cruise chief)
- Anitra E. Ingalls, University of Washington (GeoMICS cruise chief)
- Francois Ribalet, University of Washington (GeoMICS map)

Table 22 Total dissolved iron concentration from CCE P1106 cruise

Datetime GMT	Latitude (º)	Longitude (º)	Cycle	Depth (m)	Dissolved Fe Mean (nM/L)	Dissolved Fe Standard Deviation (nM/L)
2011-06-25 13:05:00	33.89753	-121.4239	Cycle 1	30	0.09	0.01
2011-06-25 13:05:00	33.89753	-121.4239	Cycle 1	60	0.24	0.04
2011-06-25 13:05:00	33.89753	-121.4239	Cycle 1	100	0.15	0.01
2011-06-25 13:05:00	33.89753	-121.4239	Cycle 1	150	0.38	0.01
2011-06-25 13:05:00	33.89753	-121.4239	Cycle 1	200	0.51	0.03
2011-06-25 13:05:00	33.89753	-121.4239	Cycle 1	250	0.48	0.02
2011-06-25 13:05:00	33.89753	-121.4239	Cycle 1	300	0.53	0.06
2011-06-25 13:05:00	33.89753	-121.4239	Cycle 1	350	0.47	0.02
2011-06-25 13:05:00	33.89753	-121.4239	Cycle 1	400	0.48	0.01
2011-06-25 13:05:00	33.89753	-121.4239	Cycle 1	450	0.36	0.01
2011-06-25 13:05:00	33.89753	-121.4239	Cycle 1	500	0.39	0.00
2011-06-28 10:03:00	33.41495	-121.6212	Cycle 2	10	0.07	0.06
2011-06-28 10:03:00	33.41495	-121.6212	Cycle 2	30	0.12	0.02
2011-06-28 10:03:00	33.41495	-121.6212	Cycle 2	75	0.19	0.01
2011-06-28 10:03:00	33.41495	-121.6212	Cycle 2	100	0.24	0.02
2011-06-28 10:03:00	33.41495	-121.6212	Cycle 2	125	0.17	0.01
2011-06-28 10:03:00	33.41495	-121.6212	Cycle 2	150	0.23	0.05
2011-06-28 10:03:00	33.41495	-121.6212	Cycle 2	200	0.23	0.01
2011-06-28 10:03:00	33.41495	-121.6212	Cycle 2	250	0.26	0.05
2011-06-28 10:03:00	33.41495	-121.6212	Cycle 2	300	0.24	0.05
2011-06-28 10:03:00	33.41495	-121.6212	Cycle 2	350	0.22	0.01
2011-06-28 10:03:00	33.41495	-121.6212	Cycle 2	400	0.26	0.01
2011-06-28 10:03:00	33.41495	-121.6212	Cycle 2	450	0.33	0.03
2011-07-01 10:04:00	34.05727	-121.4760	Cycle 3	10	0.42	0.03
2011-07-01 10:04:00	34.05727	-121.4760	Cycle 3	25	0.22	0.01
2011-07-01 10:04:00	34.05727	-121.4760	Cycle 3	40	0.24	0.02
2011-07-01 10:04:00	34.05727	-121.4760	Cycle 3	55	0.21	0.01
2011-07-01 10:04:00	34.05727	-121.4760	Cycle 3	70	0.25	0.00
2011-07-01 10:04:00	34.05727	-121.4760	Cycle 3	85	0.28	0.08
2011-07-01 10:04:00	34.05727	-121.4760	Cycle 3	100	0.36	0.03
2011-07-01 10:04:00	34.05727	-121.4760	Cycle 3	150	0.34	0.12
2011-07-01 10:04:00	34.05727	-121.4760	Cycle 3	200	0.63	0.01
2011-07-01 10:04:00	34.05727	-121.4760	Cycle 3	300	0.61	0.18
2011-07-01 10:04:00	34.05727	-121.4760	Cycle 3	400	0.78	0.03
2011-07-01 10:04:00	34.05727	-121.4760	Cycle 3	500	0.79	0.17

Table 22 continued

Datetime GMT	Latitude (º)	Longitude (º)	Cycle	Depth (m)	Dissolved Fe Mean (nM/L)	Dissolved Fe Standard Deviation (nM/L)
2011-07-08 09:58:00	33.38195	-121.1576	Cycle 4	10	0.30	0.01
2011-07-08 09:58:00	33.38195	-121.1576	Cycle 4	25	0.25	0.01
2011-07-08 09:58:00	33.38195	-121.1576	Cycle 4	40	0.14	0.01
2011-07-08 09:58:00	33.38195	-121.1576	Cycle 4	55	0.20	0.01
2011-07-08 09:58:00	33.38195	-121.1576	Cycle 4	70	0.28	0.01
2011-07-08 09:58:00	33.38195	-121.1576	Cycle 4	85	0.47	0.02
2011-07-08 09:58:00	33.38195	-121.1576	Cycle 4	100	0.35	0.04
2011-07-08 09:58:00	33.38195	-121.1576	Cycle 4	125	0.66	0.08
2011-07-08 09:58:00	33.38195	-121.1576	Cycle 4	150	0.60	0.08
2011-07-08 09:58:00	33.38195	-121.1576	Cycle 4	200	0.58	0.04
2011-07-08 09:58:00	33.38195	-121.1576	Cycle 4	250	0.61	0.01
2011-07-08 09:58:00	33.38195	-121.1576	Cycle 4	300	0.62	0.04
2011-07-11 09:57:00	33.0675	-121.4093	Cycle 5	40	0.20	0.05
2011-07-11 09:57:00	33.0675	-121.4093	Cycle 5	60	0.27	0.01
2011-07-11 09:57:00	33.0675	-121.4093	Cycle 5	90	0.10	0.01
2011-07-11 12:54:00	33.0152	-121.4108	Cycle 5	120	0.14	0.03
2011-07-11 12:54:00	33.0152	-121.4108	Cycle 5	150	0.31	0.02
2011-07-11 12:54:00	33.0152	-121.4108	Cycle 5	200	0.25	0.03
2011-07-11 12:54:00	33.0152	-121.4108	Cycle 5	250	0.47	0.00
2011-07-13 11:58:00	33.50187	-121.1175	Cycle 6	15	0.20	0.01
2011-07-13 11:58:00	33.50187	-121.1175	Cycle 6	50	0.20	0.00
2011-07-13 11:58:00	33.50187	-121.1175	Cycle 6	75	0.22	0.00
2011-07-13 11:58:00	33.50187	-121.1175	Cycle 6	100	0.27	0.00
2011-07-13 11:58:00	33.50187	-121.1175	Cycle 6	125	0.27	0.00
2011-07-13 11:58:00	33.50187	-121.1175	Cycle 6	150	0.28	0.00

Table 23 Vibrioferrin gene copy number and total bacteria cell count from CCE P1106 cruise

cycle	dep. m	*pvsB* (0.2µm filter)		*pvsB* (0.8µm filter)		*vibX* (0.2µm filter)		*vibX* (0.8µm filter)	
		mean cell/ L	STDEV	mean cell/ L	STDEV	mean cell/ L	STDEV	mean cell/ L	STDEV
1	1	7.5E+04	6.4E+04	3.5E+04	5.4E+03	1.1E+05	6.5E+04	9.4E+05	9.0E+05
	31	3.9E+05	5.9E+04	1.2E+06	5.7E+04	2.1E+06	1.1E+05	2.2E+06	6.4E+05
	60	4.8E+04	9.5E+03	1.5E+05	1.4E+04	2.7E+05	2.7E+04	5.0E+05	2.4E+05
	250	3.9E+05	5.9E+04	1.7E+05	6.6E+04	5.7E+05	7.6E+04	2.1E+06	2.7E+06
2	5	6.6E+04	7.4E+03	2.2E+04	1.8E+02	8.7E+04	6.7E+03	1.8E+06	9.1E+05
	30	4.0E+04	7.8E+03	1.9E+04	6.3E+03	6.1E+04	1.5E+04	8.8E+05	3.5E+05
	75	3.6E+04	8.0E+03	8.7E+04	1.9E+04	1.6E+05	2.5E+04	9.3E+05	3.8E+05
	150	8.7E+04	2.4E+04	1.9E+04	1.2E+04	1.0E+05	3.3E+04	3.0E+05	1.5E+05
3	0	6.3E+05	6.9E+04	4.3E+05	1.1E+04	1.1E+06	7.4E+04	1.5E+06	5.6E+05
	23	5.6E+05	2.0E+04	2.4E+05	1.3E+04	8.1E+05	2.0E+04	4.5E+05	3.1E+04
	64	2.6E+05	9.5E+04	5.8E+04	5.5E+03	3.1E+05	8.6E+04	3.4E+06	2.7E+06
	150	1.6E+05	1.7E+04	3.2E+04	1.1E+04	1.9E+05	1.7E+04	1.7E+06	1.2E+06
4	5	4.8E+04	1.3E+04	4.5E+04	2.7E+04	1.0E+05	2.9E+04	7.2E+05	8.5E+04
	25	4.6E+04	2.3E+04	2.3E+04	4.1E+02	7.1E+04	2.1E+04	4.7E+05	4.0E+04
	50	3.1E+05	1.3E+05	1.0E+05	9.3E+04	4.2E+05	1.3E+05	4.4E+06	9.2E+05
	100	1.2E+05	9.2E+04	5.8E+04	2.0E+03	1.9E+05	7.7E+04	1.5E+05	2.8E+04
5	0	7.1E+04	2.4E+04	9.6E+04	8.9E+03	2.0E+05	1.5E+04	8.5E+05	2.6E+05
	61	8.9E+04	7.4E+04	3.2E+04	2.3E+03	1.2E+05	6.6E+04	3.8E+05	1.4E+05
	90	7.1E+04	2.8E+04	1.7E+04	5.6E+03	8.7E+04	3.2E+04	4.5E+05	9.3E+04
	150	7.1E+04	1.4E+04	1.1E+05	2.7E+04	2.1E+05	5.0E+04	6.8E+05	2.5E+05
6	5	2.3E+05	1.2E+05	2.6E+05	1.3E+05	5.5E+05	2.9E+05	2.8E+06	1.3E+06
	53	5.2E+04	1.9E+04	4.5E+04	1.7E+04	1.1E+05	3.9E+04	1.5E+06	2.5E+05
	70	5.7E+04	4.6E+04	4.2E+04	7.2E+03	1.1E+05	4.9E+04	4.6E+05	3.8E+04
	150	5.9E+04	1.6E+04	4.7E+04	4.6E+03	1.1E+05	1.9E+04	2.4E+05	5.6E+04

Table 24 Vibrioferrin gene copy number and total bacteria cell count from UNOLS cruise

		pvsB (0.2μm filter)		*pvsB* (0.8μm filter)		*vibX* (0.2μm filter)		*vibX* (0.8μm filter)	
		Mean cells/L	STDEV	Mean cells/L	STDEV	Mean cells/L	STDEV	Mean cells/L	STDEV
BC1	10	3.3E+05	4.9E+04	4.2E+05	8.7E+04	5.8E+04	6.7E+03	1.9E+05	7.5E+04
	20	3.8E+05	0.0E+00	2.6E+05	1.0E+05	4.7E+04	4.6E+03	7.6E+04	2.0E+04
	50	2.5E+05	1.0E+05	2.8E+05	2.0E+04	5.3E+04	7.6E+03	3.8E+04	1.4E+04
	100	1.2E+05	3.8E+04	3.2E+05	8.2E+04	5.8E+04	1.3E+04	8.2E+04	2.1E+04
	200	2.0E+05	9.0E+04	3.0E+05	2.4E+04	4.5E+04	3.9E+03	5.5E+04	3.7E+04
BC2	10	3.1E+05	6.6E+04	4.0E+05	8.9E+04	5.1E+04	3.8E+04	8.7E+04	2.4E+04
	20	3.2E+05	2.6E+04	3.2E+05	7.3E+04	1.3E+05	1.0E+05	6.2E+04	1.8E+04
	100	2.5E+05	9.1E+03	3.5E+05	2.0E+04	1.2E+05	9.4E+04	5.0E+04	1.4E+04
	250	2.6E+05	1.4E+04	3.7E+05	8.4E+04	3.6E+04	9.7E+03	4.1E+04	2.4E+04
BC3	10	2.8E+05	5.6E+04	2.9E+05	7.8E+04	1.2E+05	1.3E+05	2.4E+05	3.4E+04
	50	3.3E+05	9.8E+04	3.3E+05	4.3E+04	2.2E+04	1.0E+04	9.4E+04	7.0E+04
	100	2.1E+05	6.3E+04	7.3E+04	7.0E+03	2.8E+04	4.6E+03	4.4E+04	5.9E+03
	200	2.5E+05	9.4E+04	7.0E+04	6.2E+03	4.5E+02	7.6E+02	1.1E+05	1.8E+04
BC4	5	6.4E+04	7.3E+03	4.8E+04	1.5E+04	1.2E+06	2.7E+05	1.5E+05	9.0E+04
	20	9.2E+04	2.4E+04	4.9E+04	9.2E+03	2.2E+05	7.7E+04	2.1E+05	1.1E+05
	50	6.5E+04	1.5E+04	4.4E+04	2.6E+04	4.7E+04	3.0E+04	1.6E+05	4.4E+04
	100	4.6E+04	1.1E+04	4.8E+04	3.4E+04	4.4E+04	1.2E+04	1.1E+05	6.2E+04
	200	2.2E+04	4.2E+03	1.6E+04	3.7E+03	4.5E+04	2.9E+04	5.9E+03	2.2E+03

Table 25 Vibrioferrin gene copy number and total bacteria cell count from GeoMICS cruise

location	depth, m	total bacteria (0.2µm)		*pvsB* (0.2µm filter)		*vibX* (0.2µm filter)	
		Mean cell/ L	STDEV	Mean cell/ L	STDEV	Mean cell/ L	STDEV
P1	5	1.2E+05	2.9E+04	4.7E+05	8.1E+04	2.6E+07	6.8E+06
	15	2.5E+05	2.2E+04	1.1E+05	2.6E+04	4.9E+07	2.9E+06
	40	5.8E+04	8.4E+03	6.7E+05	2.6E+05	3.3E+06	1.4E+05
	100	2.9E+05	4.4E+03	1.0E+06	1.3E+05	3.9E+07	8.5E+06
P2	5	9.2E+04	4.6E+03	3.3E+06	1.2E+05	5.6E+07	5.3E+06
	22	5.0E+04	4.6E+03	8.7E+05	1.4E+05	1.1E+07	6.9E+05
	100	5.4E+04	6.9E+03	1.2E+05	5.9E+03	5.7E+06	8.3E+05
P3	5	7.5E+04	1.0E+04	2.2E+06	6.2E+05	6.7E+07	8.2E+06
	20	5.6E+04	7.0E+03	2.3E+05	4.5E+04	1.1E+07	4.5E+06
	55	1.5E+05	2.1E+04	6.5E+05	2.5E+04	4.8E+07	1.7E+06
	150	5.3E+04	5.6E+03	1.1E+05	2.1E+04	1.0E+07	3.1E+06
	300	4.3E+04	6.2E+03	2.1E+05	5.3E+04	4.2E+05	3.2E+04
P4	5	8.4E+04	4.1E+03	2.3E+06	7.9E+04	2.6E+07	3.0E+06
	20	3.5E+05	5.3E+04	3.6E+06	1.8E+05	6.7E+07	3.6E+06
	45	1.9E+05	6.0E+04	8.2E+05	1.5E+05	9.5E+07	4.8E+06
	150	4.1E+04	2.9E+03	7.3E+04	4.8E+03	7.8E+05	8.0E+04
	300	5.6E+04	8.4E+03	9.7E+04	1.3E+04	1.4E+06	4.7E+05
P5	5	1.9E+05	8.8E+03	8.5E+06	4.9E+05	5.2E+07	6.8E+06
	20	9.2E+04	3.8E+03	5.3E+05	1.3E+05	9.4E+06	1.3E+06
	55	1.8E+05	2.7E+04	3.5E+06	1.8E+06	3.2E+07	9.2E+06
	150	4.7E+04	9.5E+03	4.1E+05	6.2E+04	1.1E+06	5.0E+05
	300	7.4E+04	8.1E+03	1.2E+05	2.2E+04	5.2E+06	4.6E+05
P6	5	1.6E+05	1.6E+04	8.3E+06	1.8E+06	6.5E+07	3.4E+06
	15	5.7E+04	3.4E+03	2.5E+06	2.6E+05	2.0E+07	1.5E+06
	20	1.1E+05	1.8E+04	8.5E+06	1.4E+06	6.0E+07	3.8E+06
	150	2.7E+05	1.7E+04	1.9E+06	3.4E+05	1.3E+06	5.7E+05
	300	6.9E+04	2.3E+03	1.2E+05	1.3E+04	2.9E+06	4.7E+05
P8	5	1.5E+05	1.5E+04	7.7E+06	1.7E+06	6.1E+07	3.2E+06
	20	2.2E+06	1.7E+05	5.4E+06	8.3E+05	1.3E+08	4.5E+07
	33	9.2E+05	1.1E+05	5.2E+06	2.5E+05	1.2E+08	1.2E+07
	150	6.7E+04	1.2E+04	3.1E+05	5.4E+04	1.5E+06	4.1E+05
	300	6.8E+04	2.2E+04	1.9E+05	5.1E+04	1.5E+06	8.4E+05

REFERENCES

Abergel, R. J., Zawadzka, A. M., & Raymond, K. N. (2008). Petrobactin-mediated Iron transport in pathogenic bacteria: Coordination chemistry of an unusual 3,4-catecholate/citrate siderophore. *Journal of American Chemical Society, 130,* 2124-2125.

Abualhaija, M. M., & Berg, C. M. G. v. d. (2014). Chemical speciation of iron in seawater using catalytic cathodic stripping voltammetry with ligand competition against salicylaldoxime. *Marine Chemistry, 164*, 60-74.

Alexander, D. B., & Zuberer, D. A. (1991). Use of chrome azurol S reagents to evaluate siderophore production by rhizosphere bacteria. *Biology and Fertility of Soils, 12*, 39-45.

Allen, W. E. (1938). "Red water" Along the west coast of the United States in 1938. *Science, 88*(2272), 55-56.

Allen, W. E. (1941). Twenty years' statistical studies of marine plankton dinoflagellates of Southern California. *The American Midland Naturalist, 26*(3), 603-635.

Almazán-Becerril, & García-Mendoza. (2008). Maximum efficiency of charge separation of photosystem II of the phytoplankton community in the Eastern Tropical North Pacific off Mexico: A nutrient stress diagnostic tool? *Ciencias Marinas, 34*(1), 29-43.

Amin, S. A., Kupper, F. C., Green, D. H., Harris, W. R., & Carrano, C. J. (2007). Boron binding by a siderophore isolated from marine bacteria associated with the toxic dinoflagellate *Gymnodinium catenatum*. *Journal of American Chemical Society, 129*(3), 478-479.

Amin, S. A., Green, D. H., Hart, M. C., Kupper, F. C., Sunda, W. G., & Carrano, C. J. (2009). Photolysis of iron–siderophore chelates promotes bacterial–algal mutualism. *Proceedings of the National Academy of Sciences of the United States, 106*(40), 17071-17076.

Amin, S. A., Green, D. H., Kupper, F. C., & Carrano, C. J. (2009). Vibrioferrin, an unusual marine siderophore: Iron binding, photochemistry, and biological implications. *Inorganic Chemistry, 48*, 11451-11458.

Amin, S. A., Green, D. H., Gardes, A., Romano, A., Trimble, L., & Carrano, C. J. (2012). Siderophore-mediated iron uptake in two clades of *Marinobacter spp.* associated with phytoplankton: the role of light. *Biometals, 25*, 181-192.

Amin, S. A., Green, D. H., Waheeb, D. A., Gardes, A., & Carrano, C. J. (2012). Iron transport in the genus Marinobacter. *Biometals, 25*, 135-147.

Amin, S. A., Hmelo, L. R., Tol, H. M. v., Durham, B. P., Carlson, L. T., Heal, K. R., . . . Armbrust, E. V. (2015). Interaction and signaling between a cosmopolitan phytoplankton and associated bacteria. *Nature, 522*, 98-101.

Anderson, D. M. (1994). Red Tides. *Scientific American, 271*(2), 52-58.

Anderson, D. M., Cembella, A. D., & Hallegraeff, G. M. (2012). Progress in Understanding Harmful Algal Blooms: Paradigm Shifts and New Technologies for Research, Monitoring, and Management. *Annual Review of Marine Science, 4*, 143-176.

Azam, F., & Worden, A. Z. (2004). Microbes, molecules, and marine ecosystems. *Science, 303*(5664), 1622-1624.

Azam, F., & Malfatti, F. (2007). Microbial structuring of marine ecosystems. *Nature Reviews Microbiology, 5*(12), 782-791.

Bach, H. J., Toman, J., Schloter, M., & Munch, J. C. (2002). Enumeration of total bacteria and bacteria with genes for proteolytic activity in pure cultures and in environmental samples by quantitative PCR mediated amplification. *Journal of Microbiological Methods, 49*(3), 235-245.

Baden, D. G., & Adams, D. J. (2000). Brevetoxins: Chemistry, mechanism of action, and methods of detection. In L. M. Botana (Ed.), *Seafood and Freshwater Toxins: Pharmacology, Physiology, and Detection* (1st ed., pp. 505-532). New York: Marcel Dekker, Inc.

Barbeau, K., Rue, E. L., Bruland, K. W., & Butler, A. (2001). Photochemical cycling of iron in the surface ocean mediated by microbial iron(iii)-binding ligands. *Nature, 413*, 409-413.

Barbeau, K., Zhang, G., Live, D. H., & Butler, A. (2002). Petrobactin, a photoreactive siderophore produced by the oil-degrading marine bacterium Marinobacter hydrocarbonoclasticus. *Journal of American Chemical Society, 124*(3), 378-379.

Barbeau, K., Rue, E. L., Trick, C. G., Bruland, K. W., & Butler, A. (2003). Photochemical reactivity of siderophores produced by marine heterotrophic bacteria and cyanobacteria based on characteristic Fe(III) binding groups. *Limnology & Oceanography, 48*(3), 1069-1078.

Bell, W., & Mitchell, R. (1972). Chemotactic and Growth Responses of Marine Bacteria to Algal Extracellular Products. *Biological Bulletin, 143*(2), 265-277.

Bell, W. H., & Lang, J. M. (1974). Selective stimulation of marine bacteria by algal extracellular products. *Limnology & Oceanography, 19*(5), 833-839.

Benderliev, K. M., & Ivanova, N. (1994). High-affinity siderophore-mediated iron-transport system in the green alga *Scenedesmus incrassatulus*. *Planta, 193*(2), 163-166.

Bertranda, E. M., McCrowa, J. P., Moustafaa, A., Zhenga, H., McQuaida, J. B., Delmontd, T.

O., . . . Allena, A. E. (2015). Phytoplankton-bacterial interactions mediate micronutrient colimitation at the coastal Antarctic sea ice edge. *PNAS, 112*(32), 9938-9943.

Biers, E. J., Sun, S., & Howard, E. C. (2009). Prokaryotic genomes and diversity in surface ocean waters: Interrogating the global ocean sampling metagenome. *Applied and Environmental Microbiology, 75*(7), 2221-2229.

Bolch, C. J. S., Subramanian, T. A., & Green, D. H. (2011). The toxic dinoflagellate Gymnodinium catenatum (Dinophyceae) requires marine bacteria for growth. *J. Phycol, 47*, 1009-1022.

Böttger, L. H., Miller, E. P., Andresen, C., Matzanke, B. F., Küpper, F. C., & Carrano, C. J. (2012). Atypical iron storage in marine brown algae: a multidisciplinary study of iron transport and storage in Ectocarpus siliculosus. *Journal of Experimental Botany, 63*(16), 5763-5772.

Boyd, P. W., Watson, A. J., Law, C. S., Abraham, E. R., Trull, T., Murdoch, R., . . . Zeldis, J. (2000). A mesoscale phytoplankton bloom in the polar Southern Ocean stimulated by iron fertilization. *Nature, 407,* 695-702.

Boye, M., vandenBerg, C. M. G., deJong, J. T. M., Leach, H., Croot, P., & deBaar, H. J. W. (2001). Organic complexation of iron in the Southern Ocean. *Deep-Sea Research I, 48*, 1477-1497.

Braun, V. (1995). Energy-coupled transport and signal transduction through the Gram-negative outer membrane via TonB-ExbB-ExbD-dependent receptor proteins. *FEMS Microbiology Reviews, 16*, 295-307.

Braun, V., Hantke, K., & Köster, W. (1998). Bacterial iron transport: mechanisms, genetics, and regulation. *Met Ions Biol Syst, 35*, 67-145.

Bruland, K. W., & Franks, R. P. (1979). Sampling and analytical methods for the determination of copper, cadmium, zinc, and nickel at the nanogram per liter level in sea water. *Analytica Chimica Acta, 105*, 233-245.

Bruland, K. W., Donat, J. R., & Hutchins, D. A. (1991). Interactive influences of bioactive trace metals on biological production in oceanic waters. *Limnology & Oceanography, 36*(8), 1555-1577.

Bruland, K. W., Rue, E. L., & Smit, G. J. (2001). Iron and macronutrients in California coastal upwelling regimes: Implications for diatom blooms. *Limnology and Oceanography, 46*(7), 1661-1674.

Brzezinski, M. A., Krause, J. W., Bundy, R. M., Barbeau, K. A., Franks, P., Goericke, R., . . . Stukel, M. R. (2015). Enhanced silica ballasting from iron stress sustains carbon export in a frontal zone within the California Current. *Journal of Geophysical Research, 120*, 4654-4668. doi:10.1002/2015JC010829

Buck, K. N., Moffett, J., Barbeau, K. A., Bundy, R. M., Kondo, Y., & Wu, J. (2012). The organic complexation of iron and copper: an intercomparison of competitive ligand exchange–adsorptive cathodic stripping voltammetry (CLE-ACSV) techniques. *Limnology and Oceanography: Methods, 10*, 496-515.

Burkholder, J. M. (1998). Implications of harmful microalgae and heterotrophic dinoflagellates in management of sustainable marine fisheries. *Ecological Applications, 8*(1), S37-S62.

Caruana, A. M. N., & Malin, G. (2014). The variability in DMSP content and DMSP lyase activity in marine dinoflagellates. Progress in oceanography, 120, 410-424.

Cendrowski, S., MacArthur, W., & Hanna, P. (2004). *Bacillus anthracis* requires siderophore biosynthesis for growth in macrophages and mouse virulence. *Molecular Microbiology, 51*(2), 407-417.

Challis, G. L., & Naismith, J. H. (2004). Structural aspects of non-ribosomal peptide biosynthesis. *Current Opinion in Structural Biology, 14*, 748.

Challis, G. L. (2005). A widely distributed bacterial pathway for siderophore biosynthesis independent of nonribosomal peptide synthetases. *ChemBioChem, 6*, 601-611.

Clarke, T. E., Tari, L. W., & Vogel, H. J. (2001). Structural biology of bacterial iron uptake systems. *Current Topics in Medicinal Chemistry, 1*(1), 7-30.

Coale, K. H., Johnson, K. S., Fitzwater, S. E., Gordon, R. M., Tanner, S., Chavez, F. P., . . . Kudela, R. (1996). A massive phytoplankton bloom induced by an ecosystem-scale iron fertilization experiment in the equatorial Pacific Ocean. *Nature, 383*, 495-501.

Croot, P. L., & Heller, M. I. (2012). The importance of kinetics and redox in the biogeochemical cycling of iron in the surface ocean. *Frontiers in Microbiology, 3*(219), 1-15.

Cruz-Lopez, R., & Maske, H. (2015). A non-amplified FISH protocol to identify simultaneously different bacterial groups attached to eukaryotic phytoplankton. J. Appl. Phycol., 27, 797.

Dominguez, H. J., Paz, B., Daranas, A. H., Norte, M., Franco, J. M., & Fernandez, J. J. (2010). Dinoflagellate polyether within the yessotoxin, pectenotoxin and okadaic acid toxin groups: Characterization, analysis and human health implications. *Toxicon, 56*, 191-217.

Dyson, K., & Huppert, D. D. (2010). Regional economic impacts of razor clam beach closures due to harmful algal blooms (HABs) on the Pacific coast of Washington. *Harmful Algae, 9*, 264–271.

EC. Regulation Nº 853/2004 of the European Parlamient and of the Council of 29 April 2004, laying down specific hygiene rules for food of animal origin. (2004). *L 226*, 22.

Eiki, K., Satake, M., Koike, K., Ogata, T., Mitsuya, T., & Oshima, Y. (2005). Confirmation of yessotoxin production by the dinoflagellate Protoceratium reticulatum in Mutsu Bay. *Fisheries Science, 71*, 633-638.

Epstein, P. R., Ford, T. E., & Colwell, R. R. (1993). Marine ecosystems. *The Lancet, 342*(8881), 1216-1219.

Fisher, M., Zamir, A., & Pick, U. (1998). Iron uptake by the halotolerant alga *Dunaliella* is mediated by a plasma membrane transferrin. *The journal of Biological Chemistry, 273*(28), 17553-17558.

Francis, J., Madinaveitia, J., Macturk, H. M., & Snow, G. A. (1949). Isolation form acid-fast bacteria of a growth-factor for *Mycobacterium johnei* and of a precursor of Phthiocol. *Nature, 163*, 365-366.

Fontaine, S. L., Quinn, J. M., Nakamoto, S. S., Page, M. D., Göhre, V., Moseley, J. L., . . . Merchant, S. (2002). Copper-dependent iron assimilation pathway in the model photosynthetic eukaryote *Chlamydomonas reinhardtii*. *Eukaryotic Cell, 1*(5), 736-757.

Fortuine, R. (1975). Paralytic shellfish poisoning in the North Pacific: Two historical accounts and implications for today. *The Alaskan Medicine, 17*, 71-76.

Gärdes, A., Triana, C., Amin, S. A., Green, D. H., Romano, A., Trimble, L., & Carrano, C. J. (2013). Detection of photoactive siderophore biosynthetic genes in the marine environment. *Biometals, 26*, 507-516.

Geider, R. J., & Roche, J. L. (1994). The role of iron in phytoplankton photosynthesis, and the potential for iron-limitation of primary productivity in the sea. *Photosynthesis Research, 39*, 275-301.

GEOHAB. (2001). Global Ecology and Oceanography of Harmful Algal Blooms. In P. Glibert & G. Pitcher (Eds.), *Science Plan* (pp. 1-88). Baltimore and Paris.

Gledhill, M., & Berg, C. M. G. v. d. (1994). Determination of complexation of iron (III) with natural organic complexing ligands in seawater using cathodic stripping voltammetry. *Marine Chemistry, 47*(1), 41-54.

Glibert, P. M., Anderson, D. M., Gentien, P., Graneli, E., & Sellner, K. G. (2005). The global complex phenomena of harmful algae blooms. *Oceanography, 18*(2), 130-141.

Goldberg, S. J., Nelson, C. E., Viviani, D. A., Shulse, C. N., & Church, M. J. (2017). Cascading influence of inorganic nitrogen sources on DOM production, composition, lability and microbial community structure in the open ocean. *Environmental Microbiology, 19*(9), 3450-3464.

Green, D. H., Llewellyn, L. E., Negri, A. P., Blackburn, S. I., & Bolch, C. J. S. (2004). Phylogenetic and functional diversity of the cultivable bacterial community associated with the paralytic shellfish poisoning dinoflagellate *Gymnodinium catenatum*. *FEMS Microbiology Ecology, 47*(3), 345-357.

Grossart, H.-P., Levold, F., Allgaier, M., Simon, M., & Brinkhoff, T. (2005). Marine diatom species harbour distinct bacterial communities. *Environmental Microbiology (2005), 7*(6),

860-873.

Guindon, S., & Gascuel, O. (2003). A simple, fast, and accurate algorithm to estimate large phylogenies by maximum likelihood. *Systematic Biology, 52*(5), 696-704.

Hallegraeff, G. M. (1993). A review of harmful algal blooms and their apparent global increase. *Phycologia, 32*(2), 79-99.

Hallegrae, G. M., & Fraga, S. (1998). Bloom dynamics of the toxic dinofagellate Gymnodinium catenatum, with emphasis on Tasmanian and Spanish coastal waters. In D. M. Anderson, A. D. Cembella, & G. M. Hallegrae (Eds.), *Physiological Ecology of Harmful Algal Blooms* (Vol. 41, pp. 59-80). Verlag Berlin Heidelberg: Springer.

Hallegraeff, G., & Gollasch, S. (2006). Ecological studies: Ecology of harmful algae. In L. M.M. Caldwell, M. G.Heldmaier, D. R.B. Jackson, W. O.L. Lange, S. H.A.Mooney, J. E.-D. Schulze, & K. U. Sommer (Eds.), *Anthropogenic Introductions of Microalgae* (Vol. 189, pp. 379-402). Netherlands: Springer.

Halstead, B. W. (1988). *Poisonous and Venomous Marine Animals of the World* (2nd ed.). Princeton, N.J. : Darwin Press.

Hartnett, A., Bottger, L. H., Matzanke, B. F., & Carrano, C. J. (2012). Iron transport and storage in the coccolithophore: *Emiliania huxleyi*. *Metallomics, 4*, 1160-1166.

Hartnett, A., Böttger, L. H., Matzanke, B. F., & Carrano, C. J. (2012). A multidisciplinary study of iron transport and storage in the marine green alga *Tetraselmis suecica*. *Journal of Inorganic Biochemistry, 116*, 188-194.

Heukelem, L. V., & Thomas, C. S. (2001). Computer-assisted high-performance liquid chromatography method development with applications to the isolation and analysis of phytoplankton pigments. *Journal of Chromatography A, 910*, 31-49.

Hoagland, P., & Scatasta, S. (2006). Ecological studies: Ecology of harmful algae. In L. M.M. Caldwell, M. G.Heldmaier, D. R.B. Jackson, W. O.L. Lange, S. H.A.Mooney, J. E.-D. Schulze, & K. U. Sommer (Eds.), *The Economic Effects of Harmful Algal Blooms* (Vol. 189, pp. 391-402). Netherlands: Springer.

Honner, S., Kudela, R. M., & Ethan Handler, M. (2012). Bilateral mastoiditis from red tide exposure. *The Journal of Emergency Medicine, 43*(4), 663-666.

Hopkinson, B. M., & Morel, F. M. M. (2009). The role of siderophores in iron acquisition by photosynthetic marine microorganisms. *Biometals, 22*, 659-669.

Horner, R. A., & Postel, J. R. (1993). Toxic diatoms in western Washington waters (U .S . west coast). *Hydrobiologia, 269/270*, 197-205.

Hudson, R. J. M., & Morel, F. M. M. (1989). Distinguishing between extra- and intracellular iron in marine phytoplankton. *Limnology & Oceanography, 34*(6), 1113-l 1120.

Hunter, K. A., & Boyd, P. W. (2007). Iron-binding ligands and their role in the ocean biogeochemistry of iron. *Environmental Chemistry, 4*, 221-232.

Hutchins, D. A., G. R. DiTullio, Y. Zhang, and K. W. Bruland. (1998). An iron limitation mosaic in the California upwelling regime. *Limnology and Oceanography, 43*(6), 1037-1054.

Ibisanmi, E., Sander, S. G., Boyd, P. W., Bowie, A. R., & Hunter, K. A. (2011). Vertical distributions of iron-(III) complexin gligands in the Southern Ocean. *Deep-Sea Research II, 58*, 2113–2125.

Javed, R., Yarimizu, K., Pelletier, N., Li, C., and Knowles, A.F. (2007). "Mutagenesis of lysine 62, asparagine 64, and conserved region 1 reduces the activity of human ecto-ATPase (NTPDase 2)." Biochemistry 46: 6617-6627.

Jin, D., Thunberg, E., & Hoagland, P. (2008). Economic impact of the 2005 red tide event on commercial shellfish fisheries in New England. *Ocean & Coastal management, 51*, 420-429.

Katoh, K., Misawa, K., Kuma, K., & Miyata, T. (2002). MAFFT: a novel method for rapid multiple sequence alignment based on fast Fourier transform. *Nucleic Acids Res., 30*(14), 3059-3066.

Khan, S., Arakawa, O., & Onoue, Y. (1997). Neurotoxins in a toxic red tide of *Heterosigma akashiwo* (Raphidophyceae) in Kagoshima Bay, Japan. *Aquaculture Research, 28*(1), 9-14.

Kim, H.-J., Miller, A. J., McGowan, J., & Carter, M. L. (2009). Coastal phytoplankton blooms in the Southern California Bight. *Progress in oceanography, 82*, 137-147.

Kirkpatrick, B., Fleming, L. E., Squicciarini, D., Backer, L. C., Clark, R., Abraham, W., . . . Baden, D. G. (2004). Literature review of Florida red tide: implications for human health effects. *Harmful Algae, 3*, 99-115.

Kranzler, C., Lis, H., Shaked, Y., & Keren, N. (2011). The role of reduction in iron uptake processes in a unicellular, planktonic cyanobacterium. *Environmental Microbiology, 13*(11), 2990-2999.

Krause, J. W., Brzezinski, M. A., Goericke, R., Landry, M. R., Ohman, M. D., Stukel, M. R., & Taylor, A. G. (2015). Variability in diatom contributions to biomass, organic matter production and export across a frontal gradient in the California Current Ecosystem. *Journal of Geophysical Research: Oceans, 120*(2), 1032-1042.

Küpper, F. C., Carrano, C. J., Kuhn, J.-U., & Butler, A. (2006). Photoreactivity of iron(III)-aerobactin: photoproduct structure and iron(III) coordination. *Inorganic Chemistry, 45*, 6028-6033.

Kustka, A. B., Allen, A. E., & Morel, F. M. M. (2007). Sequence analysis and transcriptional regulation of iron acquisition genes in two marine diatoms. *Journal of Phycology, 43*,

715-729.

Labrenz, M., Brettar, I., Christen, R., Flavier, S., Bötel, J., & Höfle, M. G. (2004). Development and application of a real-time PCR approach for quantification of uncultured bacteria in the central Baltic Sea. *Applied and Environmental Microbiology, 70*(8), 4971-4979.

Langlois, G. W., & Smith, P. (2000). Phytoplankton. In H. A. Karl, J. L. Chin, E. Ueber, P. H. Stauffer, & J. W. H. II (Eds.), *Beyond the Golden Gate Oceanography, Geology, Biology, and Environmental Issues in the Gulf of the Farallones* (Vol. Circular 1198, pp. 32-35). San Francisco, California: U.S. Department of the Interior & U.S. Geological Survey.

Langlois, G. (2001). Marine Biotoxin Monitoring in California, 1927-1999. In R. RaLonde (Ed.), *Harmful Algal Blooms on the North American West Coast* (Vol. AK-SG-01-05, pp. 31-34). Alaska: University of Alaska Sea Grant College Program.

Legrand, A. M. (1999). Ciguatera toxins: origin, transfer through the food chain and toxicity to humans. In B. Reguera, L. Blanco, M. Fernandez, & T. Wyatt (Eds.), *Harmful algae : proceedings of the VIII International conference on harmful algae, Vigo, Spain, 25-29 June 1997 = Algas nocivas* (pp. 39-43). Vigo, Spain: Xunta de Galicia Intergovernmental Oceanographic Commission of UNESCO.

Legaard, K. R., & Thomas, A. C. (2006). Spatial patterns in seasonal and interannual variability of chlorophyll and sea surface temperature in the California Current. *Journal of Geophysical Research, 111*(C06032), 1-21. doi:10.1029/2005JC003282

Lentz, S. J., Fewings, M., Howd, P., Fredericks, J., & Hathaway, K. (2008). Observations and a model of undertow over the inner continental shelf. *Journal of Physical Oceanography, 38*(C11), 2341-2357.

Lewis, J., & Hallet, R. (1997). *Lingulodinium polyedrum* (Gonyaulax polyedra) a blooming dinoflagellate. In A. D. Ansell, R. N. Gibson, & M. Barnes (Eds.), *Oceanography and Marine Biology: an annual review* (Vol. 35, pp. 97-161). London UK and Pennsylvania USA: UCL Press.

Lewis, R. J., Vernoux, J.-P., & Brereton, I. M. (1998). Structure of Caribbean Ciguatoxin Isolated from *Caranx latus*. *Journal of American Chemical Society, 120*(24), 5914-5920.

Lewis, R. J., Molgo, J., & Adams, D. J. (2000). Pharmacology of toxins involved in ciguatera and related fish poisonings. In L. M. Botana (Ed.), *Seafood and Freshwater Toxins: Pharmacology, Physiology, and Detection* (1st ed., pp. 419–447). New York: Marcel Dekker, Inc.

Lewitus, A. J., Horner, R. A., Caron, D. A., Garcia-Mendoza, E., Hickey, B. M., Hunter, M., . . . Tweddle, J. F. (2012). Harmful algal blooms along the North American west coast region: History, trends, causes, and impacts. *Harmful Algae, 19*, 133-159.

Lozupone, C., Hamady, M., & Knight, R. (2006). UniFrac – An online tool for comparing microbial community diversity in a phylogenetic context. *BMC Bioinformatics, 7*(371), 1-14.

Macrellis, H. M., Trick, C. G., Rue, E. L., Smith, G., & Bruland, K. W. (2001). Collection and detection of natural iron-binding ligands from seawater. *Marine Chemistry, 76*, 175-187.

Maldonado, M. T., Strzepek, R. F., Sander, S., & Boyd, P. W. (2005). Acquisition of iron bound to strong organic complexes, with different Fe binding groups and photochemical reactivities, by plankton communities in Fe-limited subantarctic waters. *Global Biogeochemical Cycles, 19*, GB4S23.

Martin, J. H., & Fitzwater, S. E. (1988). Iron deficiency limits phytoplankton growth in the north-east Pacific subarctic. *Nature, 331*, 341-343.

Martin, J. H., & Gordon, R. M. (1988). Northeast Pacific iron distributions in relation to phytoplankton productivity. *Deep Sea Research Part A. Oceanographic Research Papers, 35*(2), 177-196. doi:10.1016/0198-0149(88)90035-0

Martin, J. H., et al. (1994). Testing the iron hypothesis in ecosystems of the equatorial Pacific Ocean. *Nature, 371*, 123-129.

Mayali, X., & Azam, F. (2004). Algicidal bacteria in the sea and their impact on algal blooms. *J Eukaryot Microbiol. , 51*(2), 139-144.

Mayali, X., & Franks, P. J. S. (2008). Bacteria-induced motility reduction in *Lingulodinium polyedrum* (Dinophyceae). *Journal of Phycology, 44*, 923-928.

McQuaid, J. B., Kustka, A. B., Oborník, M., Horák, A., McCrow, J. P., Karas, B. J., . . . Allen, A. E. (2018). Carbonate-sensitive phytotransferrin controls high-affinity iron uptake in diatoms. Nature, 555, 534-537.

Miethke, M., & Marahiel, M. A. (2007). Siderophore-based iron acquisition and pathogen control. *Microbiology and Molecular Biology Reviews, 71*(3), 413-451.

Miles, C. O., Wilkins, A. L., Hawkes, A. D., Selwood, A. I., Jensen, D. J., Cooney, J. M., . . . MacKenzie, A. L. (2006). Identification of 45-hydroxy-46,47-dinoryessotoxin, 44-oxo-45,46, 47-trinoryessotoxin, and 9-methyl-42,43,44,45,46,47,55-heptanor-38-en-41-oxoyessotoxin, and partial characterization of some minor yessotoxins, from *Protoceratium reticulatum*. *Toxicon, 47*, 229-240.

Miller, E. P., Bottger, L. H., Weerasinghe, A. J., Crumbliss, A. L., Matzanke, B. F., Meyer-Klaucke, W., . . . Carrano, C. J. (2014). Surface-bound iron: a metal ion buffer in the marine brown alga Ectocarpus siliculosus? *Journal of Experimental Botany, 65*(2), 585-594.

Miller, E. P., Auerbach, H., Schünemann, V., Tymon, T., & Carrano, C. J. (2016). Surface binding, localization and storage of iron in the giant kelp Macrocystis pyrifera.

Metallomics, 8, 403-411.

Morrissey, J., & Guerinot, M. L. (2009). Iron uptake and transport in plants: The good, the bad, and the ionome. *Chemical Reviews, 109*(10), 4553–4567.

Moog, P. R., & Brtiggemann, W. (1994). Iron reductase systems on the plant plasma membrane-A review. *Plant and soil, 165*, 241-260.

Morel, F. M. M., Hudson, R. J. M., & Price, N. M. (1991). Limitation of productivity by trace metals in the sea. *Limnology & Oceanography, 36*(8), 1742-1755.

Morris, P. D., Campbell, D. S., Taylor, T. J., & Freeman, J. I. (1991). Clinical and epidemiological features of neurotoxic shellfish poisoning in North Carolina. *American Journal of Public Health, 81*(4), 471-474.

Murata, M., Kumagai, M., Lee, J. S., & Yasumoto, T. (1987). Isolation and structure of yessotoxin, a novel polyether compound implicated in diarrhetic shelfish poisoning. *Tetrahedron Letters, 28*(47), 5869-5872.

Murata, M., Legrand, A. M., Ishibashi, Y., Fukui, M., & Yasumoto, T. (1990). Structures and configurations of ciguatoxin from the moray eel *Gymnothorax javanicus* and its likely precursor from the dinoflagellate *Gambierdiscus toxicus*. *Journal of American Chemical Society, 112*(11), 4380-4386.

Naito, K., Imai, I., & Nakahara, H. (2008). Complexation of iron by microbial siderophores and effects of iron chelates on the growth of marine microalgae causing red tides. *Phycological Research, 56*, 58-67.

Nishio, T., Tanaka, N., Hiratake, J., Katsube, Y., Ishida, Y., & Oda, J. (1988). Isolation and structure of the novel dihydroxamate siderophore alcaligin. *J. Am. Chem. SOC, 110*, 8733-8734.

Ogino, H., Kumagai, M., & Yasumoto, T. (1997). Toxicologic evaluation of yessotoxin. *Natural toxins, 5*, 255-259.

Okaichi, T. (1989). Red tide problem in the Seto Inland Sea, Japan. In T. Okaichi, D. M. Anderson, & T. Nemoto (Eds.), *Red tides: biology, environmental science, and toxicology* (pp. 131-136). New York: Elsevier.

Paz, B., Daranas, A. H., Norte, M., Riobo, P., Franco, J. M., & Fernandez, J. J. (2008). Yessotoxins, a group of marine polyether toxins: an overview. *Marine Drugs, 6*, 73-102. doi:10.3390/md20080005

Price, D. W., Kizer, K. W., & Hansen, K. H. (1991). California's paralytic shellfish poisoning prevention program 1927–1989. *Journal of Shellfish Research, 10*, 119-145.

Pulido, O. M. (2008). Domoic acid toxicologic pathology: A review. *Mar. Drugs, 6*, 180-219.

Raven, J. A. (2013). Iron acquisition and allocation in stramenopile algae. *Journal of Experimental Botany, 64*(8), 2119-2127.

Ramanan, R., Kim, B.-H., Cho, D.-H., Oh, H.-M., & Kim, H.-S. (2016). Algae-bacteria interactions: evolution, ecology and emerging applications. *Biotechnology Advances, 34*, 14-29.

Raymond, K. N., Allred, B. E., & Sia, A. K. (2015). Coordination chemistry of microbial iron transport. *Acc. Chem. Res., 48*(9), 2496-2505.

Robinson, N. J., Procter, C. M., Connolly, E. L., & Guerinot, M. L. (1999). Aferric-chelate reductase for iron uptake fromsoils. *Nature, 397*, 694-697.

Roegner, G. C., Hickey, B. M., Newton, J. A., Shanks, A. L., & Armstrong, D. A. (2002). Wind-induced plume and bloom intrusions into Willapa Bay, Washington. *Limnology and Oceanography, 47*(4), 1033-1042.

Römheld, V., & Marschner, H. (1986). Evidence for a specific uptake system for iron phytosiderophores in roots of grasses. *Plant Physiology, 80*, 175-180.

Rooney-Varga, J., Giewat, M., Savin, M., Sood, S., LeGresley, M., & Martin, J. (2005). Links between phytoplankton and bacterial community dynamics in a coastal marine environment. *Microb Ecol. , 49*(1), 163-175.

Rue, E. L., & Bruland, K. W. (1995). Complexation of iron(III) by natural organic ligands in the Central North Pacific as determined by a new competitive ligand equilibration/adsorptive cathodic stripping voltammetric method. *Marine Chemistry, 50*, 117-138.

Rue, E. L., & Bruland, K. W. (1997). The role of organic complexation on ambient iron chemistry in the equatorial Pacific Ocean and the response of a mesoscale iron addition experiment. *Limnology and Oceanography, 42*, 901-910.

Sandy, M., & Butler, A. (2009). Microbial iron acquisition: Marine and terrestrial siderophores. *Chem. Rev., 109*, 4580-4595.

Scheuer, P. J., Takahashi, W., Tsutsumi, J., & Yoshida, T. (1967). Ciguatoxin: Isolation and chemical nature. *Science, 155*(3767), 1267-1268.

Seymour, J., Amin, S., Raina, J.-B., & Stocker, R. (2017). Zooming in on the phycosphere: the ecological interface for phytoplankton-bacteria relationships. *Nature Microbiology, 2*, 17065. doi:10.1038/nmicrobiol.2017.65

Shaked, Y., Kustka, A. B., Morel, F. M. M., & Erel, Y. (2004). Simultaneous determination of iron reduction and uptake by phytoplankton. *Limnology and Oceanography: Methods, 2*, 137-145.

Shumway, S. E. (1990). A review of the effects of algal blooms on shellfish and aquaculture. *Journal of the World Aquaculture Society, 21*(2), 65-104.

Smayda, T. J. (1998). Ecophysiology and bloom dynamics of *Heterosigma akashiwo Raphidophyceae*. In D. M. Anderson, A. D. Cemballa, & G. Hallegraeff (Eds.), *Physiological Ecology of Harmful Algae Blooms (Nato ASI subseries G)* (Vol. 41, pp. 113-131). Berlin, Germany: Springer; 1st edition.

Smil, V. (2001). *Enriching the Earth: Fritz Haber, Carl Bosch, and the Transformation of World Food Production*. Cambridge, MA, USA: The MIT Press.

Sonier, M. B., & Weger, H. G. (2010). Plasma membrane ferric reductase activity of iron-limited algal cells is inhibited by ferric chelators. *Biometals, 23*(6), 1029-1042.

Soria-Dengg, S., & Horstmann, U. (1995). Ferrioxamines B and E as iron sources for the marine diatom Phaeodactylum tricornutum. *Marine Ecology Progress Series, 127*, 269-277.

Sournia, A. (1978). *Phytoplankton Manual*. 7 Place de Fontenoy, 75700 Paris: The United Nations Educational, Scientific and Cultural Organization.

Steidinger, K. A., & Baden, D. G. (1984). 7 - Toxic Marine Dinoflagellates A2 - Spector, David L *Dinoflagellates* (pp. 201-261). San Diego: Academic Press.

Sutak, R., Botebol, H., Blaiseau, P.-L., Léger, T., Bouget, F.-Y., Camadro, J.-M., & Lesuisse, E. (2012). A comparative study of iron uptake mechanisms in marine microalgae: Iron binding at the cell surface is a critical step. *Plant Physiology, 160*, 2271-2284.

Symes, J. L., & Kester, D. R. (1985). The distribution of iron in the northwest Atlantic. *Marine Chemistry, 17*, 57-74.

Tachibana, K., Nukina, M., Joh, Y.-G., & Scheuer, P. J. (1987). Recent developments in the molecular structure of ciguatoxin. *Biological Bulletin, 172*(1), 122-127.

Tai, V., & Palenik, B. (2009). Temporal variation of Synechococcus clades at a coastal Pacific Ocean monitoring site. *The ISME Journal, 3*, 903-915.

Takai, A., Bialojan, C., Troschka, M., & Rüegg, J. C. (1987). Smooth muscle myosin phosphatase inhibition and force enhancement by black sponge toxin. *EFBS Letters, 217*(1), 81-84.

Tanabe, T., Funahashi, T., Nakao, H., Miyoshi, S., Shinoda, S., & Yamamoto, S. (2003). Identification and characterization of genes required for biosynthesis and transport of the siderophore vibrioferrin in *Vibrio parahaemolyticus*. *Journal of Bacteriology, 185*(23), 6938-6949.

Terao, K. (2000). Ciguatera toxins: toxicology. In L. M. Botana (Ed.), *Seafood and Freshwater Toxins: Pharmacology, Physiology, and Detection* (1st ed., pp. 449-472). New York: Marcel Dekker, Inc.

Tillett, D., & Neilan, B. A. (2000). Xanthogenate Nucleaic Acid Isolation from Cultured and Environmental Cyanobacteria. *J. Phycol., 36*.

Tortell, P. D., Maldonado, M. T., & Price, N. M. (1996). The role of heterotrophic bacteria in iron-limited ocean ecosystems. *Nature, 383*(330-332), 330.

Torrey, H. B. (1902). An unusual occurrence of dinoflagellata on the California coast. *The American Naturalist, 36*(423), 187-192.

Tubaro, A., Sosa, S., Bornancin, A., & Hungerford, J. (2008). Pharmacology and Toxicology of Diarrheic Shellfish Toxins. In L. M. Botana (Ed.), *Seafood and Freshwater Toxins: Pharmacology, Physiology, and Detection* (2nd ed., pp. 229-253). Boca Raton, FL, USA: CRC Press.

Tweddle, J. F., Strutton, P. G., Foley, D. G., O'Higgins, L., Wood, A. M., Scott, B., . . . Forster, Z. (2010). Relationships among upwelling, phytoplankton blooms, and phycotoxins in coastal Oregon shellfish. *Marine Ecology Progress Series, 405*, 131-145.

Uthermöl, H. (1958). Zur vervollkommung der quantitativen phytolankton-methodik. *Mitteilungen-Internationale Vereinigung für Theoretische und Angewandte Limnologie, 9*, 1-39.

Van den Berg, C. M. G. (1995). Evidence for organic complexation of iron in seawater. *Marine Chemistry, 50*, 139-157.

Venrick, E. L., & Hayward, T. L. (1984). *Determining chlorophyll on the 1984 CalCOFI surveys*. Retrieved from

Vraspir, J. M., & Butler, A. (2009). Chemistry of marine ligands and siderophores. *Annual Review of Marine Science, 1*, 43-63.

Wandersman, Ć., & Delepelaire, P. (2004). Bacterial iron sources: From Siderophores to Hemophores. *Annu. Rev. Microbiol, 58*, 611-647.

Wang, D.-Z. (2008). Neurotoxins from marine dinoflagellates: a brief review. *Marine Drugs, 6*, 349-371.

Weger, H. G., Lam, J., Wirtz, N. L., Walker, C. N., & Treble, R. G. (2009). High stability ferric chelates result in decreased iron uptake by the green alga Chlorella kessleri owing to decreased ferric reductase activity and chelation of ferrous iron. *Botany, 87*(10), 922-931.

Wong, C. S., Johnson, W. K., Sutherland, N., Nishioka, J., Timothy, D. A., Robert, M., & Takeda, S. (2006). Iron speciation and dynamics during SERIES, a mesoscale iron enrichment experiment in the NE Pacific. *Deep-Sea Research II, 53*, 2075-2094.

Wells, M. L. (1994). Pumping iron in the Pacific. *Nature, 368*(6469), 295-296.

Winant, C. D., & Dorman, C. E. (1997). Seasonal patterns of surface wind stress and heat flux over the Southern California Bight. *Journal of Geophysical Research, 102*(C3), 5641-5653.

Wu, J., & III, G. W. L. (1994). Size-fractionated iron concentrations in the water column of the western North Atlantic Ocean. *Limnology & Oceanography, 39*(5), 1119-1129.

Yasumoto, T., Nakajima, I., Bagnis, R., & Adachi, R. (1977). Finding of a dinoflagellate as a likely culprit of ciguatera. *Jpn. Soc. Sci. Fish, 43*, 1021-1026.

Yasumoto, T., Oshima, Y., & Yamaguchi, M. (1978). Occurrence of a new type of shellfish poisoning in the Tohoku district. *Bulletin of the Japanese Society of Scientific Fisheries, 44*(11), 1249-1255.

Yamamoto, S., Okujo, N., Yoshida, T., Matsuura, S., & Shinoda, S. (1994). Structure and iron transport activity of vibrioferrin, a new siderophore of Vibrio parahaemolyticus1. *Journal of Biochemistry, 115*, 868-874.

Yamamoto, S., Fujita, Y., Okujo, N., Minami, C., Matsuura, S., & Shinoda, S. (1992). Isolation and partial characterization of a compound with siderophore activity from *Vibrio parahaemolyticus*. *FEMS Microbiology Letters, 94*, 181-186.

Yarimizu, K., Cruz-López, R., & Carrano, C. J. (submitted 2018). Iron and Harmful Algae Blooms: Potential Algal-Bacterial Mutualism between *Lingulodinium polyedrum* and *Marinobacter algicola*. *Frontier.*

Yarimizu, K., Cruz-López, R., Auerbach, H., Heimann, L., Schűnemann, V., & Carrano, C. J. (2017). Iron uptake and storage in the HAB dinoflagellate *Lingulodinium polyedrum*. *Biometals, 30*, 945-953.

Yarimizu, K., Polido, G., Gardes, A., Carter, M. L., Hilbern, M., & Carrano, C. J. (2014). Evaluation of photo-reactive siderophore producing bacteria before, during and after a bloom of the dinoflagellate *Lingulodinium polyedrum*. *Metallomics, 6*, 1156-1163.

Yilmaz, M., & Phlips, E. J. (2009). Improved methods for the isolation of cyanobacterial DNA from environmental samples. *J. Phycol., 45*, 517.

APPENDIX

XANTHOGENATE DNA EXTRACTION

Prepare all solutions stated below. To extract DNA from bacterial colonies, first grow colonies in marine broth overnight. Then, harvest bacteria cells by centrifugation and re-suspend pellet in 50 µL TER buffer. Add 750 µL of XS buffer and vortex to mix. Incubate at 70°C for 30 min to break cell walls while vortex every 10 min. Then follow the below described procedure.

Table 26 TER (Tris, EDTA, RNaseA) buffer preparation

material*	mass/volume
Tris-HCl, pH7.4	10 mM
EDTA, pH7.4	1 mM
RNaseA	100 µg/mL

* Filter through 0.22 µm and store aliquots in -20ºC up to 2 years.

Table 27 Solutions required for DNA extraction

	EDTA	SDS	ammonium acetate	Tris-HCl
MW	416.20	288.38	77.08	121.14
final conc.	0.5M	10%	8M	1M
mass needed	20.81 g	10 g	15.39 g	12.11 g
final volume	100 mL	100 mL	25 mL	100 mL
pH	8.0	NA	NA	7.4
autoclave	yes	yes	no*	yes

Store all the solution in 5°C. *The solution needs to be filtered through 0.22 µm membrane.

Table 28 XS buffer (15 mL) preparation

material	mass/volume
Water	9.9 mL
1M Tris-HCl, pH7.4	1.5 mL
0.5M EDTA, pH8.0	0.6 mL
8M Ammonium Acetate	1.5 mL
10% SDS	1.5 mL
Potassium Ethyl Xanthenate	0.15 g

XS buffer must be prepared on the day of analysis.
Warm the solution in water bath to dissolve all the materials.

XS / TER buffer

- Mix 15mL of XS buffer and 1mL of TER buffer on the day of analysis.
- Detergent (SDS), protease (Potassium Ethyl Xanthte), and RNaseA is used to remove membrane lipids, proteins, and RNA in cells, respectively.

Cell Lysis

- Filter samples through membrane (0.8 μm and 0.2 μm).
- Place a membrane into an autoclaved eppendorf tube.
- Add 0.5 mL of XS/TER buffer to an eppendorf tube to soak a membrane.
- Incubate the eppendorf tube at 70ºC water bath for 30 minutes. Every 10 minutes, vortex vigorously.
- Wash the surface of the membrane with another 0.5 mL of XS/TER buffer. Collect all the solutions in the eppendorf tube and discard the membrane.
- Place the eppendorf tube on ice for 15 minutes to precipitate debris.
- Centrifuge the eppendorf tube at 13,000 rpm for 10 minutes.
- Transferred the supernatant into another eppendorf tube. Discard the pellet.

Precipitation of DNA

- Add 1 mL of isopropanol in the eppendorf tube containing supernatant.
- Incubate at room temperature for 10 minutes or store at -20C until next step is preceded.
- Centrifuge at 13,000 rpm for 10 minutes in cold room.
- Carefully remove supernatant by inverting the tube on paper towel. Keep pellet (not visible). This step removes alcohol soluble salt.

Washing DNA

- Add 0.5 mL of ice cold 70% Ethanol into the tube containing DNA pellet.
- Scrape the side of the tube using pipette tips.
- Centrifuge the eppindorf tube at 13,000 rpm for 10 minutes in cold room.
- Discard the ethanol by inverting the tube.
- Dry the pellet in 44ºC oven for 10 minutes.

Final Product

- Add 100 µL of nuclease free water.
- Dissolve the pellet using pipette and vortex.
- Label the sample and store in -20ºC.

QUANTITATIVE RT-PCR PROTOCOL

Ensure instrument (iQ5 coupled with iCycler, Bio-Rad) is calibrated with plates and lid to be used for assay per manufacture's instruction. 16S gene copies were initially estimated by TaqMan qPCR. After the 16S gene copies obtained by TaqMan and regular qPCR were confirmed to be equivalent, all the 16S assays were performed by regular qPCR method.

Standard DNA:

- Extract DNA from standard bacterial strain listed in Table 29.
- Prepare stock standard DNA at 200 μg/mL with sterile water. Adjust conc. by spectrophotometer OD_{260}.
- Serial dilution of the stock to 10^{-1}, 10^{-2}, 10^{-3}, 10^{-4}, 10^{-5}, and 10^{-6} with sterile water.
- Working standard conc. are 200, 20, 2, 0.2, 0.02, 0.002, and 0.0002 μg/mL.

Primers:

- Order primers in Table 30. Dilute them to 100 μM upon receipt and store at -80°C.
- Remove primer set from -80°C storage and thaw on ice.
- Dilute primers to 200 μg/mL with sterile water on the day of assay. Adjust conc. by spectrophotometer OD_{260}.

Table 29 List of standard bacterial strains

Speices	Genus	Gene cluster	Standard Name	Gen Bank Code
Marinobacter	*Marinobacter algicola*	*pvsB*	DG893	NZ_ABCP00000000.1
Vibrioferrin	*Vibrio splendidus*	*vibXII*	Vibrio	NZ_AJZL00000000.1
Petrobactin	*Marinobacter aquaeolei*	*asbE*	1381	NC_008740
Aerobactin	*Vibrio fisherii*	*iucC*	MJ11	NC_011184

Table 30 List of primer set and sequence

Gene name	Primer name	bp	MW	Primer sequence	μM at 20 μg/mL
Marinobacter vibrioferrin	pvsB1486m-f	25	7546.5	5'-ARATGTTYACCACCATYACCYTGCA-3	2.65
	pvsB1741m-r	28	8542.1	5'-CMMKYTTGCCRTAGAAYTTRTTRATRTC-3'	2.34
16S	FP16SrDNA-f	20	6135.0	5'-GGTAGTCYAYGCMSTAAACG-3'	3.26
	RP16SrDNA-r	19	5755.8	5'-GACARCCATGCASCACCTG-3'	3.47
Non-marinobacter vibrioferrin	vibXII-f	21	6425.8	5'-GARGCNTCNAAYCARCARAAY-3'	3.11
	vibXII-r	18	5457.7	5'-NGCNGCRTCRTTRTCYTT-3'	3.66
Petrobactin	asbEII-f			5'-CCNGARCGNGARAAYAARTTYCAY-3'	
	asbEII-r			5'-NCCYTCCCANCGRAARTCNGGRTC-3'	
Aerobactin	iucC-f			5'-ATHGCNCAYGGNCARAAY-3'	
	iucC-r			5'-RTCNACRAARTGNCCNTG-3'	

TaqMan probe:

- TaqMan probe is light sensitive. Treat the probe in dark at all time.
- Order TaqMan 16SrDNAprobe FAM-TKCGCGTTGCDTCGAATTAAWCCAC-TAMRA from Applied Biosystems (P/N 450025) in solid.
- For amount of probe containing 6000 pmol per Certificate of Analysis, for instance, add nuclease free water 60 μL to prepare 100 μM stock probe.
- Dilute the stock by 10-fold with nuclease free water to prepare 10 μM working solution.
- Store the stock and working probes in -20 °C. It can be freeze-thaw multiple times.
- TaqMan probe is light sensitive. Treat the probe in dark at all time.

Sample preparation:

- Clean a hood and pipettes with 70% ethanol and UV light.
- Place well plate on ice under hood.
- Prepare master mix per Table 31.
- Add 2 μL of standard DNA or sample DNA into each well.
- Add 23 μL of master mix into each well.
- Cover the plate with lid and centrifuge the plate for a second.

PCR program:

- Use qPCR program in Table 32. Enter sample and standard information. Ensure to select correct well type and lid type on the software.

- Chose “persistent well factors” for qPCR and “collect factor from experimental plate” with “FAM” as fluorophore for TaqMan assay. Click “Begin Run”

Table 31 qPCR master mix per well

qPCR	
Universal SYBR Green (172-5121, BioRad)	12.5 µL
Primer F	2.5 µL (20 µg/mL final conc.)
Primer R	2.5 µL (20 µg/mL final conc.)
Nuclease Free water	5.5 µL
Total (add 2µL DNA)	25 µL

TaqMan qPCR	
2x iQ Supermix* (170-8862, Bio-Rad)	12.5 µL
Primer F (16S)	2.5 µL (20 µg/mL final conc.)
Primer R (16S)	2.5 µL (20 µg/mL final conc.)
Nuclease Free water	4.25 µL
TaqMan Probe	1.25 µL (0.5 µM final conc.)
Total (add 2µL DNA)	25 µL

*Per user’s guide, 2x iQ Supermix should not be freeze-thaw. Once thawed out, store the tube in 5ºC with 6 months expiration date.

Table 32 qPCR and TaqMan-PCR cycles

	qPCR	
Cycle 1 (x1)	95ºC	5 min
Cycle 2 (x45)	95ºC	10 sec
Cycle 2	60ºC	1 min
Cycle 3 (x1)	60ºC	30 sec

TaqMan PCR	
95ºC	10 min
95ºC	20 sec
60ºC	1 min
4ºC	hold

Quantitative Analysis:

Open the qPCR result file. Correct baseline of each standard and sample. Record efficiency, linearity, slope, and intercept of the standard curve. Reference these values to the manufacturing specifications (efficiency of between 90% and 110 %, slope value from -3.6 to -3.1, and linearity of >0.980). Ensure the linear square regression for the standard to be 0.95 or above with at least three standard data points. For qPCR, the sample melting temperature (Tm) must present the sample of interest. If the area-under-curve of the non-specific Tm exceeds that of the sample of interest, these data are eliminated from analysis. Once the standard curve is corrected, archive the report by clicking “Reports”, “Select Report”, and “PCR Quant Detailed”. From the report,

obtain the SQ of each sample. Convert SQ values to gene copy number and estimated bacterial cell count using the equation:

$$gene\ copy\ per\ L = DNA\ conc.\left(\frac{ng}{\mu l}\right) \text{ x } \left(\frac{1\ g}{10^9\ ng}\right) \text{ x } \left(\frac{1\ mol\ bpDNA}{660\ g\ DNA}\right)$$
$$\text{x } \left(\frac{6.022 \text{ x } 10^{23}\ bp}{mol\ bp}\right) \text{ x } \left(\frac{1\ copy}{genome\ bp}\right) \text{ x } \left(\frac{number\ of\ target\ gene}{1\ genome\ of\ standard}\right) \text{x } CF$$

DNA conc. is starting quantity (SQ) of sample DNA containing gene of interest in ng/μL obtained by RT-qPCR. CF is concentration factor and genome bp is genome length of standard (i.e., DG893 has 4,413,003 bp). The average MW of one DNA base pair is assumed to be 660 g/ mol. The number of gene copies of interest, for instance, pvsB in DG893 genome is one. Estimation of bacterial cell number from gene copy number is obtained from the following equation where the average copy number of 16s rRNA genes is assumed to be 1.8 (Biers et al., 2009).

$$bacterial\ cell\ number\ in\ L = \left(\frac{gene\ copy\ number}{L}\right) \text{ x } \left(\frac{1\ genome}{number\ of\ target\ gene}\right)$$

MARINE BROTH, LYSOGENY BROTH (LB), AND PLATES PREPARATION

Mix materials in Table 33. Adjust pH if needed. For plates, add agar after pH is adjusted. Autoclave solution at 121°C for 20 minutes. Cool the solution to approximately 55°C. Add antibiotics as needed and stir solution using autoclaved stir bar. If you are preparing for plates, dispense solution into plates. Cool the plates to ambient, close the lid of the plates, label solution and plates and store at 5°C.

Table 33 Marine broth, lysogeny broth (LB), and plates prep

	Marine broth	Marin broth plates	LB	LB plates**
peptone	5g	5g	NA	NA
tryptone	NA	NA	10 g	10 g
yeast extract	1g	1g	5g	5g
NaCl	NA	NA	10 g	10 g
sea water	750 mL	750 mL	NA	NA
water	250 mL	250 mL	1L	1L
pH	8.0	don't adjust	7.5	7.5
agar	NA	15 g (add after pH)	NA	15 g (add after pH)
Kanamycin*	NA	NA 30 mg	NA	NA
Ampicillin*	NA	NA	NA 100 µg/mL	NA 100 µg/mL

CHROME AZUROL S (CAS) ASSAY

Soak all glassware with 6N HCl to remove any trace elements for 1hr, or with 1N HCl for 24 hours, or 0.1N HCl for 2 weeks. Rinse with nano pure water to remove HCl.

Fe(III) solution (1mM $FeCl_3$-$6H_2O$)

- Dissolve 1.3 g of $FeCl_3$-$6H_2O$ in 5 mL 0.01N HCl. This is stock Fe(III) containing 1M $FeCl_3$-$6H_2O$.
- Dilute 50 µL of the stock to 50 mL 0.01N HCl. This is working Fe(III) solution, 1mM Fe(III).

CAS solution (200 mL)

- Dissolve 43.7 mg HDTMA in 12 mL water. Put aside.
- Mix 18.2 mg CAS in 15 mL water. To this solution, add 3 mL of Fe(III) working solution.
- Slowly add CAS/Fe mixture to the HDTMA solution.
- Dissolve 4.31 g Piperazine anhydrous buffer in water approximately 50 mL. Adjust pH 5.6 with concentrated HCl. Cool the solution before adding it to other solutions.
- Add Piperazine solution to CAS/Fe/HDTMA solution.
- QS to 200 mL. Filter to sterilize.

CAS shuttle solution

- Prepare 0.2 M 5-sulfosalicylic acid.
- Mix 1mL of CAS solution and 20 µL of CAS shuttle. This is good only for 1 day.

Sample Test

- Centrifuge samples to collect supernatant.
- Mix 0.5 mL of supernatant and 0.5 mL of CAS shuttle solution. The color change from purple to clear red indicate siderophore production.

DNA CLEANING BY QIAAMP®DNA STOOL MINI KIT

(CAT# 51504)

This is used to clean DNA extracted from environmental samples. In many cases, environmental samples contain unknown materials to interfere with qPCR assay. Treating DNA of environmental samples with this protocol solves this problem. The procedure was adopted and modified slightly from the manufacturing instruction.

Before start:

- Prepare buffer AW1 and AW2 accord to manufacture's instruction.
- Warm up buffer ASL and AL at 70°C water bath to dissolve precipitate.

Procedure:

- For 100 µL DNA from environment sample, add 0.7 mL buffer ASL. Vortex for 1 min. Heat at 70°C for 5 min.
- Vortex for 15 sec and centrifuge for 1 min.
- Transfer the supernatant into 2 mL eppi tube. Discard the pellet.
- Add half cut InhibitEX tablet. Vortex immediately for 1 min. Incubate at room temp for 1min. Centrifuge for 3 min.
- Transfer all the supernatant into a new 1.5 mL eppi tube. Centrifuge for 3 min. Repeat two times to remove precipitate as much as possible.
- In a new 1.5 mL eppi tube, add 15 µL proteinase K. In this tube, add all the supernatant.
- Add 400 µL Buffer AL. Vortex for 15 sec. Incubate at 70°C for 10 min.
- Add 400 µL of absolute ethanol. Invert tube several times to mix well.
- Apply the sample solution into a QIAamp spin column which is place in a 2 mL collection eppi tube. Centrifuge for 1 min. Keep the spin column and discard the filtrate.
- Add 500 µL buffer AW1 to the spin column. Centrifuge for 1 min. Keep the spin column and discard the filtrate.
- Add 500 µL buffer AW2 to the spin column. Centrifuge for 3 min. Keep the spin column and discard the filtrate.
- Place the spin column in a new 2 mL collection eppi tube. Centrifuge for 1 min. Discard the filtrate.
- Transfer the spin column in a new 1.5 mL eppi tube.
- Add 100 µL buffer AE (or starting volume) in the center of the spin column. Centrifuge for 1 min to elute DNA.

DNA PURIFICATION BY QIAQUICK GEL EXTRACTION KIT (CAT# 28704)

This protocol is used to obtain purified qPCR products (amplicon). The method was adopted from the kit and modified slightly.

Materials required:

- Agarose (Fisher, BP160-100)
- GeneRulerTM, 1Kb DNA ladder, 0.5 μg/μL, Fermentas, P/N SM0311)
- 6x loading dye (Fermentas, P/N R0611)
- Ethidium Bromide (1% solution, Fisher, BP1302-10)
- QIAquick Gel Extraction Kit (P/N 28704)

Selecting qPCR Samples:

From qPCR results, select samples that showed a peak of melt temperature of interest. For instance, qPCR samples treated with pvsB primers should show a melt peak at around 85ºC.

TAE (Tris, Acetic acid, and EDTA) buffer:

Make x50 TAE buffer (1L) as in Table 34 and store at ambient temperature. The pH of this buffer is not adjusted but naturally should be around 8.5. On the day of use, dilute 1/50 with water.

Table 34 Tris, acetic acid, and EDTA (TAE) buffer x50

material	concentration	amount/ 1L
Tris base	2M	242 g
Glacial acetic acid	NA	57.1 mL
0.5M EDTA (pH8.0)	0.05M	100 mL
water	NA	QS to 1L

2% agarose gel:

Dissolve 1.5 g of agarose in 75 mL of x1 TAE buffer. Microwave the mixture for 90 sec to dissolve agarose completely. Cool the solution to approximately 60°C and add 4.5 μL of Ethidium Bromide. Mix and pour the solution into a gel shape with a 10-well comb. Wait 15 min to solidify the gel and remove the comb. Set up the gel apparatus and pour over 1x TAE buffer in the apparatus.

Sample, standard, and electrophoresis:

Mix 25 µL of qPCR product and 4.2 µL of 6x loading dye. For positive control, mix 25 µL of PCR product from standard DNA with 4.2 µL of 6x loading dye. Mix 10 µL of ladder and 2 µL of 6x loading dye to make a marker. Load whole volume in each well of the gel. Program constant voltage at 110 for 1 hour. Run gel until the fast dye passes at least middle of the gel. The sample amplicons run faster than the fast dye. In theory, the size of the DNA from the qPCR products should be between 100 bp and 250 bp. Expose the gel under UV light. The positive control and ladder will show a bright band. Using it as an indicator, cut out a band from samples and store the piece of the gel in an eppindorf tube. Freeze the piece of gel at -20°C until next step is performed.

QIAquick Gel Extraction Kit:

- Use QIAquick gel extraction kit (Qiagen, P/N 28704) to purify DNA from the gel pieces.
- Weigh out gel slice (allowed max mass is 400 mg). Add 3 volumes of Buffer QG.
- Incubate at 50°C water bath for 10 minutes to dissolve gel slice. Vortex 2-3 minutes. The color of mixture should be yellow.
- Add 1volume of isopropanol.
- Place a QIAquick spin column in a 2 mL collection tube. Apply the yellow sample solution into the column. Centrifuge for 1 min. Discard flow-through.
- Add 500 µL Buffer QG. Centrifuge for 1 min. Discard flow-through.
- Add 750 µL Buffer PE to wash the pellet. Let stand for 5 min at ambient temperature. Centrifuge for 1 min. Discard flow-through.
- Place the column into a clean 1.5 mL eppendofr tube. Add 30 µL Buffer EB. Let stand for 4 min. Centrifuge for 1 min.
- Store the purified DNA in -20°C

COMPETENT CELL PREPARATION

Making competent cells is a 3-day procedure.

Day 1: plate preparation

Prepare low salt LB plates without ampicillin, LB plates with ampcillin, and LB solution without ampicillin.

Day 1: *E. coli* streak on plate

Remove glycerol stock *E. coli* strain (Top10 or JM109) from -80°C and thaw on ice. Use fresh low salt LB plate without ampicillin. Streak *E. coli* stock on the plate with a sterilized metal stick. Incubate the plate in 37°C oven over night. For control, spread glycerol stock on LB/amp plate (*E. coli* strains should not grow on LB/amp plate).

Day 1: SOB media (Super Optimal Broth)

Mix all the ingredients in Table 35 and adjust pH to 7.5 with 10N NaOH. QS volume to 500 mL. Place 200 mL in 1-L flask, 100 mL in 500-mL flask (may not be used), 5 mL in 15-mL glass vial. Seal the top with sponge and autoclave for 15min.

Table 35 Super Optimal Broth (SOB) media 500 mL

material	concentration	mass/500mL
Yeast extract	0.5% w/v	2.5 g
Tryptone	2% w/v	10 g
Sodium Chloride (NaCl)	10 mM	0.3 g
Potassium Chloride (KCl)	2.5 mM	0.1 g
Magnesium Sulfide ($MgSO_4$)	20 mM	1.2 g

Day 1: SOC media (Super Optimal Broth with Catabolite Repression)

SOC is SOB plus 20 mM glucose. Prepare 1M glucose sterile filter. Mix the concentrated glucose 2 mL and 98 mL autoclaved SOB. Dispense and store in 5°C or -20°C.

Day 1: TFB I (Transformation Buffer I)

Mix ingredient in Table 36 and QS to 100 mL with water. DO NOT autoclave. Filter sterilize with 0.2 μm membrane. Keep solution at 5°C.

Table 36 Transformation Buffer I (TFB I)

	Final conc.	mg/100mL
Potassium Acetate	30 mM	294.5
Manganese Chloride	50 mM	989.6
Potassium chloride	100 mM	745.6
Calcium Chloride	10 mM	147.0
Glycerol (100%)	15 %	11.89 mL

Day 1: TFB II (Transformation buffer II)

Mix all the ingredients in Table 37 and QS to 50 mL. Sterile filter with 0.2 μm membrane (or autoclave). Keep the solution at 5°C.

Table 37 Transformation Buffer II (TFB II)

	Final conc.	mg/50mL
Sodium MOPS (pH 7.0)*	10 mM	104.65
Calcium Chloride	75 mM	551.3
Potassium Chloride	10 mM	37.3
Glycerol (100%)	15% (w/v)	6 mL

*Prepare 0.2M MOPS with pH adjusted to 7.0. Add 2.5 mL of this stock in 50 mL TFB(II).

Day 2: Preculture

Harvest a few *E. coli* colonies from the plate incubated at 37°C overnight. Transfer the colonies in 5 mL autoclaved SOB. Shake vigorously (225 rpm) for 4 hrs (overnight is okay too) at 37°C.

Day 2: Culture

Transfer 4 mL of preculture into 200 mL autoclaved SOB. Shake vigorously (225 rpm) at 37°C. Measure OD_{550} every 30 minutes using 1mL cuvette (Do not use nano drop UV spectrophotometer). Stop shaking when OD_{550} reaches 0.5 (OD_{600} should be around 3.7-4.0). It takes approximately 90 minutes for the culture to reach this turbidity.

Day 2: Competent cells

Dispense 200 mL *E. coli* culture into 4 tubes of 50 mL Falcon tubes. Centrifuge at 1600-g for 20 minutes at 4°C. Invert the tubes to discard the solution and keep pellet. Leave the tubes upside down on paper towel for 1-2 minutes. Resuspend each tube with 20 mL TFB(I) with pipetting ups and downs (will not become complete suspension). Keep the tubes on ice for 2 hours. Combine 2 tubes in one (2 total tubes remained). Spin down at 1200-g for 10 minutes. Remove supernatant by inverting and using paper towel. Resuspend the pellet with 4 mL TFB (II)/ tube (100 mL cells). Aliquot 100 µL of competent cells in autoclaved eppindorf tubes. Flash freeze and store at -80°C.

Day 3: Confirmation of competent cells

Thaw 50 µL of freshly made competent cell from -80°C. Add 1 µL pUC19 DNA. For negative control, use 50 µL competent cell without pUC19. Incubate on ice for 30 min. Perform transformation per Appendix H Ligation and Transformation. Premix 40 µL of 40 mg/mL X-gal and 100 µL of 100 µM IPTG per plate. Spread 140 µL of the premix on a LB/amp plate. Dry the plates for 30 minutes (no longer than 30 minutes). Spread 100 µL of transformation solution and 1/10 diluted transformation solution on the plates. Incubate plates at 37°C overnight. All colonies should be blue indicating pUC19 vector is transformed into *E. coli* cells producing ß-galactosidases. The negative control should not grow colonies as vector is not taken by *E. coli* cells meaning that *E. coli* is not ampicillin resistant. Calculate efficiency of competent cells by colony forming unit (cfu). A good competent cell should have efficiency of 1.5×10^8 to 6×10^8.

$$\text{Efficiency } \left(\frac{\text{cfu}}{\mu\text{g}}\right) = \text{colonies on plate } \left(\frac{1}{amount\ of\ DNA\ plated\ in\ ng}\right) \text{ x } 1000$$

For example, if a commercial pUC19 DNA is 10pg/µL, colonies obtained on a plate is 500, and 100 µL is spread on a plate, the efficiency is calculated:

$$\text{Efficiency } \left(\frac{\text{cfu}}{\mu\text{g}}\right) = 500 \text{ x } \left(1\mu\text{L x } \frac{10 \text{ pg}/\mu\text{L}}{1000} \text{ x } \frac{100\ \mu\text{L}}{1000\ \mu\text{L}}\right) \text{ x } 1000$$

LIGATION AND TRANSFORMATION

Purchase pGEM-T Easy Vector System I (P/N A1360, Promega). To link two ends of insert DNA into vector covalently, mix sample with DNA ligase in a small eppindor tube as in Table 38. For maximum ligation efficiency, store the mixture at 5ºC overnight. For qualitative assay, the mixture can be stored in ambient temperature for 1hour.

Table 38 Ligation with pGEM-T Easy Vector System I

Ligation Mixture	Sample	Positive Control	Negative Control
2x Ligation Buffer	5 µL	5 µL	5 µL
Vector (pGEM-T Easy Vector)	1 µL	1 µL	1 µL
Sample DNA	3 µL	0 µL	0 µL
Control DNA (from kit)	0 µL	3 µL	0 µL
T4 DNA ligase	1 µL	1 µL	1 µL
Water	0 µL	0 µL	3 µL

Bacteria transformation

- Prepare LB/amp plates, SOC media, X-gal (40 mg/mL in DMSO), and IPTG (100 µM in water).
- The water bath should be heated exactly to 42ºC. Warm SOC media to 37ºC. Thaw *E. coli* competent cells on ice.
- In each *E. coli* competent cell tube containing 50 µL cell), add all 10 µL of ligation mix. Mix by flicking gently. Incubate on ice for 30 minutes. Then, heat at 42 ºC for exactly 50 seconds. Immediately return on ice for 2 minutes.
- Add 950 µL of warmed SOC media to each tube. Incubated at 37ºC shaker for 90 minutes.
- Premix 40 µL of 40 mg/mL X-gal and 100 µL of 100 µM IPTG per plate. Spread 140 µL of the premix on a LB/amp plate. Dry the plate in 37ºC incubator for 30 minutes (no longer than 30 min) at upright position.
- Spread 100 µL of transformation mixture on a plate and 100 µL of 1/10 diluted transformation mixture on a plate.
- Incubate the plates in 37ºC oven overnight. The sample plates should contain white colonies (sign of transformation with insert DNA), pale blue colonies (sign of possible transformation with insert DNA), and blue colonies (sign of transformation without insert DNA). Positive control should be full of white colonies. Negative control should be full of blue colonies.

Second culture plate

- If the plate is too full with colonies and it is difficult to pick a white colony, second culture must be performed.
- Prepare LB/am plate with X-gal and IPTG as described above.
- From the 1st cultured plates, pick a white colony using a pipette tip and transfer on the plate. Repeat the procedure until 15-20 white colonies are transferred to one plate.
- Incubate the plates at 37ºC oven overnight. The plate should show nice size of grown colonies aligned on the plates.

DNA SEQUENCING

The sequencing can be performed by outsourcing company (GENWIZ). There are two ways to order sequencing, providing bacterial colony or DNA extracted from bacterial colony.

Sequence by bacterial colony:

- Mix 5 mL of LB broth and 5 μL of 100 mg/mL ampicillin in a sterile glass tube.
- Pick a white colony from a plate and grow in LB/amp media overnight at 37°C.
- Transfer 100 μL of the bacteria solution into a PCR tube or plate, add 10 μL of glycerol.
- Store in -80°C or dryice. Send it for sequencing service.

Sequence by DNA from bacterial colony:

- Mix 5 mL of LB broth and 5 μL of 100 mg/mL ampicillin in a sterile glass tube.
- Pick a white colony from a plate and grow in LB/amp media overnight at 37°C.
- Harvest bacterial cells by centrifugation. Keep pellet.
- Resuspend pellet in 150 μL Buffer P1 (Quiagen Plasmid Plus Midi kit, Cat# 12941: 50mM Tris-Cl, pH 8.0, 10mM EDTA, 100 μg/mL RNaseA, stored in 5°C). Vortex to mix.
- Add 150 μL of Buffer P2 (Lysis Buffer: 200mM NaOH, 1% SDS). Invert to mix.
- Add 150 μL of buffer P3 (Neutralization Buffer: 3.0M potassium acetate at pH 5.5). Invert to mix.
- Centrifuge for 10 min. In the new tubes, mix 50 μL of 3M sodium acetate (NaOAc, pH5.9) and 350 μL of isopropanol. Add the supernatant.
- Incubate on ice for 30 minutes and centrifuge at 5ºC for another 30 minutes to remove supernatant. Keep pellet.
- Add ice cold 70% ethanol to wash the pellet DNA.
- Centrifuge. Keep pellet.
- Dry pellet in oven. Resuspend the pellet with 30 μL of PCR water. Store in -20°C.
- Dilute DNA to 50 μg/mL with water. Prepare primer T7 at 5 μM. Mix 10 μL of DNA and 5 μL of T7 primer in a PCR tube. Send it for sequencing service.

Insert DNA sequence by FinchTV:

The inserted DNA is in between SacII and SpeI (Table 39, Figure 60). Find sequence of insert DNA using free software, FinchTV.

Table 39 SacII and SpeI sequence

Primer Name	Primer sequence
SacII	5'- TTCGATT -3'
SpeI	5'- ATCACTAGTG-3'

Figure 60 pGEM vector and insert map

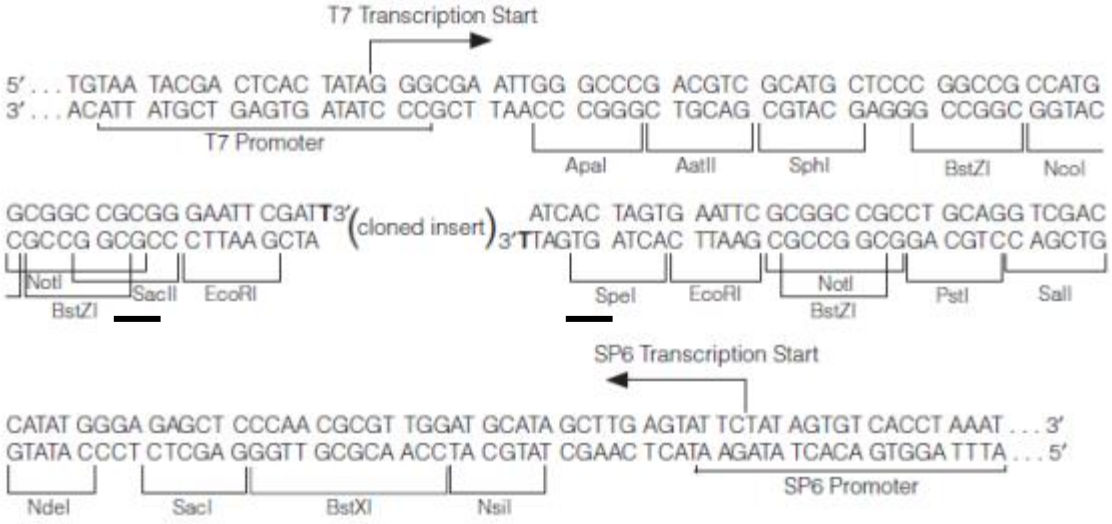

PROTEIN SEQUENCE LIBRARY

Conversion of DNA to protein sequence:

- Convert DNA sequences obtained by Finch TV to the protein sequences using BLAST website (http://blast.ncbi.nlm.nih.gov/Blast.cgi) with program "blastx" to search protein database using a translated nucleotide query.
- Enter DNA sequence in text format in the blank box of the screen, and hit "blast" icon.
- From the list of possible alignment, select the species likely to be marine bacteria.
- Copy the protein sequence shown in the "query" and save in a text file.
- The following sequence results should be eliminated from further analysis;
  - ✓ The sequence of "SpeI" is aligned immediately after the sequence of "SacII" meaning the sequence of inserted DNA sequence is not found. This indicated that *E.coli* competent cells successfully transformed the vector; however, the vector did not contain the DNA insert. It is a ligation failure.
  - ✓ The inserted DNA sequence is found in between "SpeI" and "SacII" using FinchTV. However, no close related protein sequence is found by BLAST.
  - ✓ The sequencing results show the overlapped peaks in spectra interfering the sequence reading. It indicates that multiple colonies were transferred into one spot of the 2nd cultured plate. As a result, the DNA from the multiple colonies were sequenced at the same time.
  - ✓ The DNA sequence of "SpeI" is not found, and the 3' end of the inserted DNA is not found. The cause is unknown.
  - ✓ The spectra intensity is too low and merged to the baseline meaning the sequence is not read accurately. This could be inefficiency of bacteria growth or inefficiency of DNA extraction during the sequencing process.

File alignment:

The protein sequences obtained are aligned in text file as exemplified below. Align references as the same way. The selected references are organisms containing conserved region of interested gene and closely related by phylogeny.

>AsbE_0.2um_B1

SNQQNAIIAFDEQGKMTLAMKDNDAA

Phylogenetic tree:

- Import text files of both samples and references to Geneious program by following the tutorial section “importing sequencing”.
- Select all the imported sequences in the program and click the icon “Tree”. This process provides the phylogenetic tree in the tab of “Tree view”. The tree file can be saved under PDF format.
- Under the “Text view” tab, Newick format is provided. Copy the Newick format and pasted in text file and save. A few commonly associated terms are described below.
  - ✓ Branch length: a measure of the amount of divergence between two nodes in a tree. Branch lengths are usually expressed in units of substitutions per site of the sequence alignment.
  - ✓ Nodes: represent the inferred common ancestors of the sequences that are grouped under them.
  - ✓ Tips or leaves: represent the sequences used to construct the tree.
  - ✓ Taxonomic units: can be species, genes or individuals associated with the tips of the tree

Statistical analysis:

- Convert text files of protein sequence into Nexus file and create environment file in text file as follows:
- Use website (http://www.phylogeny.fr/version2_cgi/data_converter.cgi).
- Copy the Newick format and paste on the website.
- From the dropdown menu of output format, select “NEXUS” and hit the icon “convert”.
- Copy the resulting nexus file in text file and save.
- Prepare environment file in text format as shown below. The environment file should contain all the sample information. If the names in the environment file do not match to the names in the sample files, the statistical analysis cannot be accurately performed.

AsbE_0.2um_B1 0.2um_B 1

AsbE_0.2um_M1 0.2um_M 1

AsbE_0.8um_E1 0.8um_E 1

AsbE_0.2um_B2 0.2um_B 1

AsbE_0.2um_M2 0.2um_M 1

- UniFrac Analysis: Use the website (http://bmf2.colorado.edu/unifrac/index.psp). Upload nexus format (in text file) and the environment file (in text file). Select tree as "Yes" and hit the icon "load tree". Follow the UniFrac manual to obtain statistical analysis results.

FE UPTAKE OF *L.POLYEDRUM* (FE SOURCES)

The following describes Fe uptake experiment procedure for *L.polyedrum* from various Fe sources.

- Gently centrifuge 30 mL of *L. polyedrum* stock. Wash the cells with sterile Scripps water three times. Re-suspend the cells with sterile Scripps water containing L1 media without Fe. Grow the cells in Fe-starved condition for 5 days.
- Prepare 10 mM $FeCl_3$ stock solution by mixing 27.03 mg $FeCl_3$ in 10 mL water (pH adjusted to between 6.5 and 8.5).
- Prepare FeEDTA (1 mM Fe and 10 mM EDTA) by mixing 20.81 mg EDTA and 0.5 mL stock 10 mM $FeCl_3$. QS to 5 mL water (pH adjusted to between 6.5 and 8.5).
- Prepare FeEDDHA (1 mM Fe and 10 mM EDDHA) by mixing 18.02 mg EDTA and 0.5 mL stock 10 mM $FeCl_3$. QS to 5 mL water (pH adjusted to between 6.5 and 8.5).
- Prepare FeCitrate (1 mM Fe and 10 mM citric acid) by mixing 9.61 mg citric acid and 0.5 mL stock 10 mM $FeCl_3$. QS to 5 mL water (pH adjusted to between 6.5 and 8.5).
- Prepare FeVF (1 mM Fe and 3 mM vibrioferrin) by mixing 6.52 mg VF and 0.5 mL stock 10 mM $FeCl_3$. QS to 5mL water (pH adjusted to between 6.5 and 8.5).
- Dilute 43 mM $^{55}FeCl_3$ (conc. of radioactive $FeCl_3$ at the time of our use) by mixing 1 µL of standard and 9 µL of water.
- Prepare $^{55/56}$FeEDTA containing ^{55}Fe: ^{56}Fe = 1: 140 by mixing 1 mL of ^{56}FeEDTA stock and 1.7 µL of $^{55}FeCl_3$ diluted solution. This solution contains 1 mM $^{55/56}$Fe and 10 mM EDTA, EDTA:Fe molar ratio = 10: 1, ^{56}Fe: ^{55}Fe molar ratio = 140 : 1
- Prepare $^{55/56}$FeEDDHA containing ^{55}Fe: ^{56}Fe = 1: 140 by mixing 1 mL of ^{56}FeEDDHA stock and 1.7 µL of $^{55}FeCl_3$ diluted solution. This solution contains 1 mM $^{55/56}$Fe and 10 mM EDDHA, EDDHA:Fe molar ratio = 10: 1, ^{56}Fe: ^{55}Fe molar ratio = 140 : 1
- Prepare $^{55/56}$FeCitrate containing ^{55}Fe: ^{56}Fe = 1: 140 by mixing 1 mL of ^{56}FeCitrate stock and 1.7 µL of $^{55}FeCl_3$ solution. This solution contains 1 mM $^{55/56}$Fe and 10 mM Citrate, Citrate:Fe molar ratio = 10: 1, ^{56}Fe: ^{55}Fe molar ratio = 140 : 1
- Prepare $^{55/56}$FeVibrioferrin containing ^{55}Fe: ^{56}Fe = 1: 140 by mixing 1 mL of ^{56}FeVF stock and 1.7 µL of $^{55}FeCl_3$ solution. This solution contains 1mM $^{55/56}$Fe and 3 mM VF, VF:Fe molar ratio = 3: 1, ^{56}Fe: ^{55}Fe molar ratio = 140 : 1
- In 22-mL starved *L. polyedrum* culture, add 220 µL of $^{55/56}$FeEDTA solution. This contains 10 µM Fe. Prepare 5 sets: Prepare samples: Fe starved *L. polyedrum* treated with FeEDTA, Fe sufficient *L. polyedrum* treated with FeEDTA, Fe starved *L. polyedrum* treated with FeEDTA on ice, Fe starved *L. polyedrum* treated with FeEDDHA, Fe starved *L. polyedrum* treated with FeCitrate, Fe starved *L. polyedrum* treated with FeVF light, Fe starved *L. polyledrum* treated with FeVF dark.
- Incubate at 20°C with 12 hours light-dark cycle.

- Remove 2 mL of the culture and filter through 0.6 μm membrane. Wash the membrane with 15 mL sterile seawater.
- Place the membrane in a scintillation vial. Add 15 mL of Hionic Fluor scintillation fluid. Mix well.
- Measure ^{55}Fe by scintillation counter using the tritium channel. Calculate Fe uptake/cell per protocol the following protocol.

FE UPTAKE CALCULATION EXAMPLE

The following describes an exemplified calculation to find amount of Fe taken by a cell.

Prepare stock ^{56}FeEDTA (^{56}Fe: EDTA= 1 mM: 10 mM) at pH6.5

Mix 416 mg EDTA (MW 416.20) and 27 mg $^{56}FeCl_3$ (MW 270.30) in water. Adjust pH 6.5. QS to 100 mL.

EDTA = 0.416 g/ 416.2 g/ 0.1 L x 1000 = 10 mM

^{56}Fe = 0.027 g/ 270.3 g/ 0.1 L x 1000 = 1 mM

Prepare Fe standard, $^{55/56}$FeEDTA ($^{55/56}$Fe: EDTA= 1 mM: 10 mM, ^{56}Fe: ^{55}Fe= 140: 1)

Mix 10 mL of stock ^{56}FeEDTA and 1.7 μL of ^{55}Fe (stock 43mM).

EDTA = 10 mM

^{56}Fe = 1 mM

^{56}Fe = 43 mM x (1.7 μL/1000/1000)/ 0.01 mL = 0.0073 mM

^{56}Fe/ ^{56}Fe = 1/ 0.0073 =137 (appx. 140)

Total activity in the 10 mL solution (Ci) = (21.64 Ci/L from C of A) x (1.7μL/1000/1000) = $3.6x10^{-5}$

Experiment set up (Fe: EDTA= 10 μM: 100 μM)

In 100 mL Fe starved *L. polyedrum* culture, add 1 mL of Fe standard.

EDTA = 10 mM x 0.00 1L / 0.1 L x 1000 = 100 μM

^{56}Fe = 1 mM x 0.001 L / 0.1 L x 1000 = 10 μM

^{55}Fe = 0.0073 mM x 0.001 L/0.1 L = 0.073 μM

Fe standard in a Scintillation vial as a standard

Add 40 μL Fe standard in a Scintillation vial. Add 15 mL fluid. Total Fe mass is calculated.

^{56}Fe = (10 mM/1000) x (40 μL/1000/1000) = $4x10^{-8}$ M: $4x10^{-8}$ M x 55.845 g/mole =$2.23x10^{-6}$ g

^{55}Fe = (0.0073 mM/1000) x (40 μL/1000/1000) = $3x10^{-10}$ M: $3x10^{-10}$ M x 55.845 g/mole = $1.63x10^{-8}$ g

Alternatively, total ^{55}Fe mass in the vial can be calculated

Total activity in a vial (Ci) = (3.6 x 10^{-5} Ci) x (40 μL/1000)/ 10 mL Fe standard) = 1.47 x 10^{-7}

^{55}Fe = ($1.47x10^{-7}$ Ci) / (4.81 Ci/g from C of A) = $3.0x10^{-8}$ g (close to $1.63x10^{-8}$ g)

Total DPM in the vial = (1.47 x 10^{-7} Ci) x (2.22 $x10^{12}$) = 3.2 x 10^5

DPM/ng Fe = (3.2 x 10^5) / ($3.0x10^{-8}$ g/ 1000/1000/1000) = $1.07x10^4$

CPM from Scintillation counter (i.e., on 1/23/17 I got 387454.5)

Efficiency (CPM/DMP) = 387454.5/ $1.07x10^4$ = 1.217 (121.7% efficiency)

Sample Fe uptake calculation

Fe-starved *L. polyedrum* 22000 cells in FeEDTA (see experiment set up) for 30 minutes showed CPM 40436.02.

Total DPM in sample = 40436.02 / (1.22 efficiency) = 33144.3

Total ^{55}Fe mass uptake = 33144.3 DPM /(1.07×10^{4} DPM/ngFe) = 3.1 ng ^{55}Fe

Total $^{55/56}$Fe mass uptake = 3.1 ngFe x (140 ratio of ^{56}Fe/^{55}Fe) = 435 ng ^{total}Fe

Fe uptake/cell = 435ng/ 22000 = 1.98×10^{-2} ng/cell

FE UPTAKE OF *L.POLYEDRUM* (INHIBITION)

The following describes Fe uptake experiment procedure for *L.polyedrum* in presence of various inhibitors.

- Gently centrifuge 30 mL of *L. polyedrum* stock. Wash the cells with sterile Scripps water three times. Re-suspend the cells with Scripps water containing L1 media without Fe. Grow the cells in Fe-starved condition for 5 days.
- Prepare ^{56}FeEDTA at molar ratio of EDTA: Fe= 10:1 by mixing 416 mg EDTA (MW 416.20) and 27 mg $FeCl_3.6H_2O$ (MW 270.30) in water. Adjust pH to 6.5 and QS to 100 mL with water. This solution contains 1 mM ^{56}Fe and 10 mM EDTA.
- Prepare $^{55/56}$FeEDTA by mixing 10 mL of ^{56}FeEDTA solution and 1.6 µL of 0.045 M radioactive Fe. At this point EDTA: Fe= 10: 1 and ^{56}Fe : ^{55}Fe molar ratio = 140 : 1
- In 22-mL starved culture, add 220 µL of $^{55/56}$FeEDTA solution. This contains 10 µM Fe. Prepare 5 sets: Starved, ice treated, NaN3 treated, CCCP treated, ascorbate treated.
  - ✓ The final conc of Na azide was 2.5 mM. A 20 µL of the stock Na azide (1.25 M) was added to 10 mL of L. polyedrum culture.
  - ✓ The final conc of CCCP was 25 µM. A 10 µL of the stock CCCP (25 mM in DMSO) was added to 10 mL of *L. polyedrum* culture.
  - ✓ The final conc of ascorbate was 100 µM. A 10 µL of the stock ascorbate (100 mM) was added to 10 mL of *L. polyedrum* culture.
- Incubate at 20°C with 12hr light-dark cycle.
- Remove 2 mL of the culture and filter through 0.6 µm membrane. Wash the membrane with 15 mL seawater.
- Remove another 2 mL of the culture and filter through 0.6 µm membrane. Wash the membrane with 15 mL seawater. Add 0.5 mL Ti(III) CitrateEDTA to the membrane surface and wash the membrane with 15 mL seawater.
- Place the membrane in a scintillation vial. Add 15 mL of Hionic Fluor scintillation fluid. Incubate in dark at room temp for 1 hour.
- Measure ^{55}Fe by scintillation counter using the tritium channel. Calculate Fe uptake/cell.

FE UPTAKE OF *L. POLYEDRUM* FROM FE-EDTA WITH DIFFERENT MOLAR RATIO

The following describes Fe uptake experiment procedure for *L.polyedrum* from FeEDTA with various Fe to EDTA ratio.

- Prepare 10 mM EDTA by dissolving 416.2 mg EDTA in 100 mL water (pH adjusted to 6.5).
- Prepare 10 mM $FeCl_3$ by mixing 27.03 mg $FeCl_3$ in 10 mL 0.01N HCl (pH < 2).
- Purchase $^{55}FeCl_3$ and record concentration (3 mM). Dilute 3 μL stock to 30 μL with water (at this point ^{55}Fe is 0.3 mM).
- Prepare various molar ratio of FeEDTA solution as in Table 40 (Fe: EDTA = 1: 0-9).
- In each 100 μL of FeEDTA solution, add 2 μL of 1/10 diluted $^{55}FeCl_3$ (at this point ^{55}Fe is 0.3 mM x 0.002 mL / 0.1 mL = 0.006 mM).
- In 5 mL of 5-day Fe starved *L. polyedrum* culture, add 50 μL of EDTA/^{56}Fe/^{55}Fe solution.

  At this point, ^{56}Fe is (10 mM x 0.1 mL /1 mL) x 0.05 mL / 5 mL = 0.01 mM =10 μM

  At this point, ^{55}Fe is 0.006 mM x 0.05 mL /5 mL x1000 = 0.06 μM

  Thus, ^{56}Fe: ^{55}Fe= 167: 1

  The final EDTA concentration and M ratio of EDTA : Fe is shown in Table 41.
- Incubate at room temp under grow light for 6 hours.
- Filter all 5 mL of sample through 0.8 μm membrane. Transfer the membranes into scintillation vials. Add 15 mL fluid and read ^{55}Fe.

Table 40 One mL FeEDTA buffer solution preparation

ID	EDTA, M_ratio	Fe, M_ratio	EDTA (stock 10mM), mL	Fe (stock 10mM), mL	water, mL
1	0.0	1	0.00	0.1	0.90
2	0.1	1	0.01	0.1	0.89
3	0.3	1	0.03	0.1	0.87
4	0.5	1	0.05	0.1	0.85
5	0.7	1	0.07	0.1	0.83
6	1.0	1	0.10	0.1	0.80
7	3.0	1	0.30	0.1	0.60
8	5.0	1	0.50	0.1	0.40
9	7.0	1	0.70	0.1	0.20
10	9.0	1	0.90	0.1	0.00

Table 41 Final molar ratio of EDTA and Fe

ID	working stock EDTA, mM	Final EDTA in LP culture, mM	Final Fe in LP culture, mM	EDTA/ Fe, M ratio
1	0.0	0.000	0.01	0.0
2	0.1	0.001	0.01	0.1
3	0.3	0.003	0.01	0.3
4	0.5	0.005	0.01	0.5
5	0.7	0.007	0.01	0.7
6	1.0	0.010	0.01	1.0
7	3.0	0.030	0.01	3.0
8	5.0	0.050	0.01	5.0
9	7.0	0.070	0.01	7.0
10	9.0	0.090	0.01	9.0

FE REDUCTASE REQUIREMENT OF *L. POLYEDRUM*

The following describes experiment procedure for *L.polyedrum* Fe reduction (Table 42).

- Prepare 10 mM EDTA by dissolving 416.2 mg EDTA in 100 mL water (pH adjusted to 6.5).
- Prepare 10 mM $FeCl_3$ by mixing 27.03 mg $FeCl_3$ in 10 mL 0.01N HCl (pH < 2).
- Purchase $^{55}FeCl_3$ and record concentration (3 mM). Dilute 2 μL stock to 18 μL with water (at this point ^{55}Fe is 0.3 mM).
- Prepare FeEDTA solution by mixing 300 μL of 10 mM EDTA, 100 μL of 10 mM Fe, and 600 μL of water (final Fe: EDTA = 1 mM: 3 mM).
- In each 100 μL of FeEDTA solution, add 2 μL of 1/10 diluted $^{55}FeCl_3$ (at this point ^{55}Fe is 0.3 mM x 0.002 mL / 0.1 mL = 0.006 mM).
- Prepare 20 mM Ferrozine by dissolving 10 mg in 1mL water (0.01 g/ 514.45 MW /0.001 L x 1000 =20 mM).
- In 5 mL of 10-day Fe starved *L. polyedrum* culture (antibiotics treated), add 25 μL of 20 mM Ferrozine (final conc: 0.02 M x 0.000025 L /0.005 x1000000= 100 μM). Incubate at RT for 1hr. Do the same for Fe sufficient *L. polyedrum* culture.
- In 5 mL of L. polyedrum /Ferrozine, add 50 μL of $^{55/56}FeEDTA$ solution.

  At this point, ^{56}Fe is (10 mM x 0.1 mL /1 mL) x 0.05 mL / 5 mL = 0.01 mM =10 μM

  At this point, ^{55}Fe is 0.006 mM x 0.05 mL /5 mL x1000 = 0.06 μM

  Thus, ^{56}Fe: ^{55}Fe= 167: 1
- The final EDTA concentration is ((10 mM x 0.3 mL /1 mL) x 0.05 /5 mL x 1000 = 30 μM), and the molar ratio of EDTA: Fe is 30 μM : 10 μM = 3: 1.
- Negative control: 5 mL of seawater with 30 μM $^{55/56}FeEDTA$, 100 μM Ferrozine.
- Positive control: 5 mL of seawater with 30 μM $^{55/56}FeEDTA$, 1 mM L-ascorbate, 100 μM Ferrozine
- Incubate at room temp under grow light for 7 hours.
- Wash C18 Sep-Pak with 5 mL methanol followed by 10 mL water (place the column into a 15-mL conica tube, add methanol or water to the column, centrifuge).
- Filter all 5 mL of each sample through 5um membrane. Keep filtrate (contains FeFZ).
- Add 4 mL of filtrate (1 mL increment) to the wetted C18 column. Centrifuge.
- Wash the column with 3 mL of 0.5 M NaCl/ 0.005 M HCl (alternatively sterile seawater with 0.005 M HCl) by centrifugation. Repeat the wash process two more times.
- Elute the retained material by 5 mL of methanol (1 mL increment) by centrifugation. Transfer the eluent in scintillation vial.
- Dry the methanol by placing the scintillation vials in 44°C oven for overnight.

- Add 15mL of scintillation fluid and mixed vigorously. Read CPM.

Table 42 Material concentration used for reductase experiment

	(-) control	(+) control	Fe-starved	Fe-sufficient
Sterile seawater (+AB)	5mL	5mL	NA	NA
Fe-starved LP (+AB)	NA	NA	5mL	NA
Fe-sufficient LP (+AB)	NA	NA	NA	5mL
Ferrozine	100μM	100μM	100μM	100μM
L-ascorbate	NA	1mM	NA	NA
$^{55/56}Fe$	10μM	10μM	10μM	10μM
EDTA	30μM	30μM	30μM	30μM

AB stands for antibiotics